

Electron-phonon interaction in strongly correlated materials

Von der Fakultät für Mathematik und Physik
der Universität Stuttgart
zur Erlangung der Würde eines
Doktors der Naturwissenschaften (Dr. rer. nat.)
genehmigte Abhandlung

vorgelegt von

Oliver Rösch

aus Bietigheim-Bissingen

Hauptberichter: Prof. Dr. Ole Krogh Andersen

Mitberichter: Prof. Dr. Alejandro Muramatsu

Tag der mündlichen Prüfung: 5. Dezember 2005

Max-Planck-Institut für Festkörperforschung
Stuttgart

2005

Für Sabine

Contents

Abstract	9
Introduction	11
1 Electron-phonon interaction in the t-J model	15
1.1 Introduction	15
1.2 Three-band model	16
1.2.1 Definition	16
1.2.2 Transformation of O- p orbitals	17
1.2.3 Modulation of parameters	20
1.3 Effective low-energy model	22
1.4 t - J model for the undistorted lattice	24
1.4.1 Undoped system	24
1.4.2 Doped system	26
1.5 t - J model with phonons	31
1.6 Summary	38

2	Anomalous softening of the half-breathing phonon	39
2.1	Introduction	39
2.2	Numerical results for t - J model with phonons	41
2.2.1	Half-breathing and breathing modes	44
2.2.2	Doping dependence	47
2.3	Three-band model in Hartree-Fock approximation	49
2.3.1	Model	51
2.3.2	Results for phonon softening	54
2.3.3	Comparison with results from t - J model	56
2.4	Discussion	63
2.4.1	Relative importance of coupling mechanisms	63
2.4.2	Comparison with other approaches	67
2.4.3	Non-linear contributions to electron-phonon coupling	69
2.4.4	Coupling to other phonon modes	71
2.5	Summary	73
3	Polaronic effects in undoped cuprates	75
3.1	Introduction	75
3.2	Electron-phonon coupling in undoped cuprates	78
3.3	Adiabatic approximation	84
3.3.1	Dispersion of incoherent spectral features	86
3.3.2	Extension to finite temperatures	88
3.3.3	Computational method	89

3.4	ARPES spectra for undoped La_2CuO_4	91
3.5	Summary and discussion	96
4	Property-dependent apparent electron-phonon interaction	99
4.1	Introduction	99
4.2	Definition of models	101
4.3	Sum rule for phonon self-energy	102
4.3.1	Interacting electrons	104
4.3.2	Non-interacting electrons	104
4.3.3	Discussion	105
4.4	Sum rule for electron self-energy	105
4.4.1	Interacting electrons	105
4.4.2	Non-interacting electrons	108
4.4.3	Discussion	109
4.5	Apparent coupling strengths	110
4.6	Numerical results	111
4.7	Effect of vertex corrections	114
4.7.1	Electron self-energy	115
4.7.2	Phonon self-energy and charge response function	118
4.7.3	Example: two-site Hubbard model	119
4.7.4	Discussion	122
4.8	Summary	122

Conclusions	125
Zusammenfassung	129
A Exact diagonalization	135
A.1 Calculation of ground state	135
A.2 Calculation of spectral functions	136
A.3 Calculation of self-energies	137
B Adiabatic approximation revisited	139
B.1 Improved version	139
B.2 Core hole problem	141
B.3 Holstein model	143
B.4 t - J model with phonons	150
B.5 Comparison with diagrammatic Monte Carlo method	153
C Green's function formalism	157
D Vertex function in the two-site Hubbard model with phonons	159
Bibliography	170
List of publications	171
Curriculum vitae	173
Acknowledgements	175

Abstract

We study electron-phonon interaction in strongly correlated systems where the interplay with electron-electron interactions needs to be taken into account explicitly. We specifically consider cuprate high-temperature superconductors but also investigate in more general terms the influence of strong correlations.

We first develop a model framework by deriving an effective low-energy model from a three-band model of the copper oxide planes in the cuprates allowing for the modulation of its parameters by lattice distortions. The electron-phonon interaction in the resulting t - J model with phonons is dominated by the on-site coupling due to phonon-induced changes in the large energy gain of Zhang-Rice singlets.

Using exact diagonalization of finite clusters, we find that this model successfully describes the anomalous softening upon doping of the oxygen half-breathing mode in these compounds. Both the dependence on doping and the phonon wavevector are in good agreement with experiment. A comparison with results from a Hartree-Fock mean-field approximation of the three-band model shows the importance of treating strong correlations directly.

After deriving the additional electron-phonon interaction that arises in undoped cuprates from the modulation of the electrostatic potential, we conclude that the coupling is strong enough to lead to the polaronic behavior seen in photoemission from these systems. Based on an adiabatic approximation, we explain the dispersion of the phonon side band according to predictions from purely electronic models and develop an efficient method for calculating spectra. Applying it to our model yields results that agree well with experiment.

Finally, we use sum rules for the phonon and the electron self-energy to show generally that due to strong correlations the effect of electron-phonon interaction can be at variance from what is expected for non-interacting electrons. Electronic and phononic properties are affected differently leading to a mismatch of the respective apparent electron-phonon couplings. We also discuss the importance of vertex corrections to the electron-phonon interaction in strongly correlated materials.

Introduction

In condensed matter, the electronic degrees of freedom are strongly influenced in their properties by the presence of an array of ions. Many properties of solids can be successfully understood by assuming the ionic lattice to be static. But there are also collective vibrational modes, commonly referred to as phonons, which can influence the electrons and vice versa. The resulting coupling between electronic and lattice degrees of freedom, i.e., the electron-phonon interaction, is often studied in models with no electron-electron interaction [1]. This approach of assuming (effectively) non-interacting electrons leads to the successful description of a variety of phenomena. A prominent example is superconductivity which can be understood in a lot of materials in terms of a phonon-mediated effective interaction between electrons using the Bardeen-Cooper-Schrieffer (BCS) theory [2] or its strong-coupling version, the Migdal-Eliashberg theory [3, 4, 5], which treat the electrons in a mean-field approximation.

In some systems, however, electrons are strongly correlated due to the Coulomb repulsion between them, especially when their kinetic energy is comparatively small. It is then not a good approximation to treat electrons as quasi-independent particles that are only subjected to an average field created by the other electrons. Instead, the description of such a strongly correlated system requires the solution of a true many-body problem which takes into account the electron-electron interaction explicitly. This implies that also the electron-phonon interaction in strongly correlated materials with strong electron-electron interaction cannot be discussed appropriately in the theoretical framework developed for non-interacting electrons. Rather, both interactions need to be treated on an equal footing to assess their interplay. For example, in alkali-doped fullerenes [6], there is strong Coulomb interaction between electrons on the same molecule and at the same time the electrons couple strongly to intra-molecular Jahn-Teller phonons. When both interactions are taken into account directly, e.g. using dynamical mean-field theory [7], the superconductivity in these compounds can be understood in terms of a local pairing [8] whereas the Migdal-

Eliashberg theory fails to give a proper description.

Another important example for strongly correlated systems are the cuprate high-temperature superconductors. Their discovery in 1986 by Bednorz and Müller [9] and the rapid advance to transition temperatures well above the boiling point of nitrogen [10] triggered enormous research activities that continue until today. High-temperature superconductivity has been found in a variety of different compounds which, however, all have in common that their structure is layered and consists of one or more copper-oxygen planes per unit cell. The electronic structure at low energies results mainly from the Cu- $3d_{x^2-y^2}$ and O- $2p_{x/y}$ orbitals in these planes with the electrons being strongly correlated due to strong Coulomb interaction between two electrons in the same Cu- d orbital. The strong correlations cause the undoped cuprates to be antiferromagnetic Mott insulators. Superconductivity appears upon doping in the range of about 5 to 25% doped charge carriers per Cu atom for hole-doped materials like $\text{La}_{2-x}\text{Sr}_x\text{CuO}_4$ or $\text{YBa}_2\text{Cu}_3\text{O}_{6+y}$ with the highest transition temperature occurring at the optimal doping of about 15%. Electron doping, e.g. in $\text{Nd}_{2-x}\text{Ce}_x\text{CuO}_4$, can also lead to superconductivity in a narrower range around approximately 15% doping.

The closeness of superconducting and antiferromagnetic phases is often seen as an indication that the pairing mechanism in the high-temperature superconductors is mainly originating from the strong electronic correlations. The observed d -wave symmetry of the superconducting gap can be understood quite naturally in such a scenario whereas it is generally believed that a phonon-mediated mechanism is more favorable to an s -wave symmetry. Among other things, also the fact that there is only a rather small oxygen isotope effect on the transition temperature in optimally doped samples [11] and the finding that the electron-phonon coupling from density-functional linear-response calculations is not sufficiently strong [12] led to the widespread view that electron-phonon interaction is not the main driving force for the high-temperature superconductivity in the cuprates. Instead, most research has focused on the electronic degrees of freedom alone, with the aim of understanding within a purely electronic picture not only the pairing mechanism of high-temperature superconductivity but also other peculiar features of the cuprates like e.g. the pseudogap [13] or the linear temperature dependence of the resistivity over a wide temperature range at optimal doping [14].

Nevertheless, there is considerable experimental evidence for strong electron-phonon coupling in the cuprates which we summarize in the following, with more details to some of the phenomena given later in the introductions to the individ-

ual chapters. Neutron scattering experiments, for example, show an anomalously strong softening of a phonon mode upon doping accompanied by a large line width [15, 16, 17, 18, 19] signaling strong coupling of doped charge carriers to lattice degrees of freedom. Phonon anomalies like e.g. superconductivity-induced softening and a Fano line shape have also been observed in Raman spectroscopy [20, 21, 22]. Although the oxygen isotope effect on the superconducting transition temperature is small around optimal doping, it becomes significantly larger for lower dopings [23]. Quasi-particle dispersions deduced from angle-resolved photoemission spectroscopy (ARPES) [24] show kink-like features that have been interpreted in terms of coupling to phonon modes [25]. In undoped compounds, the spectra indicate polaronic behavior [26, 27] pointing to even stronger electron-phonon interaction which leads to self-trapped polarons.

These findings suggest that the coupling to lattice degrees of freedom plays an important role in the cuprates, and they have recently attracted much interest. As the cuprate high-temperature superconductors are strongly correlated materials, the effects of electron-phonon interaction should be studied using analytical and numerical approaches that explicitly take into account the interplay between electron-phonon and electron-electron interactions. In this thesis, we address several of the aforementioned phenomena from this point of view. Although first of all we specifically consider cuprates, we also expect some general insight into how strong correlations affect the description of electron-phonon interaction developed for non-interacting electrons. The following outline of the thesis gives more details on our agenda.

- In Chapter 1, we develop a model framework by incorporating electron-phonon coupling into a three-band model that describes the electronic structure of the copper oxide (CuO_2) planes in the cuprates. Strong correlations are taken into account via the inclusion of a Hubbard-like Coulomb repulsion on the Cu sites. In order to obtain a simpler model which is more suitable for analytical and numerical approaches to the problem, degrees of freedom with high energy are projected out leaving an effective low-energy model. The resulting t - J model with phonons includes electron-phonon interaction which derives from physically reasonable mechanisms for the modulations of the parameters in the three-band model by lattice distortions. It forms the basis for the calculations and considerations in the following chapters.
- In Chapter 2, we study the softening of the planar oxygen half-breathing mode in cuprates using the model derived in the previous chapter. After an introduc-

tion to the main experimental results, we use exact diagonalization to calculate the effects of the electron-phonon coupling on phonon properties. In such an approach, both electron-electron and electron-phonon interactions are treated in an essentially exact way except for finite-size effects. Besides the softening, also the broadening of phonons can be calculated and compared to experiment. For comparison, we consider in addition the three-band model in a Hartree-Fock mean-field approximation. This allows us to draw conclusions about the importance of including strong correlations explicitly like in the t - J model.

- In Chapter 3, we focus on undoped cuprates and the polaronic behavior observed in these compounds with ARPES. We derive the additional electron-phonon coupling in the undoped system which arises from the modulation of the electrostatic potential due to a much weaker screening of the Coulomb interaction. We address not only the question whether there is strong enough coupling to lead to self-trapped polarons, but also the puzzling observation of phonon-related features dispersing according to predictions of purely electronic models. Using an adiabatic approximation, we develop a theory for ARPES spectra which facilitates the qualitative understanding of many features. In addition, it leads to an efficient method for the quantitative calculation of spectra from undoped systems that allows for the simultaneous consideration of many phonon modes at finite temperatures. Based on this approach and employing our calculated electron-phonon coupling, we compute realistic ARPES spectra of undoped cuprates that can be directly compared with experimental results.
- In Chapter 4, the interplay between electron-phonon coupling and electron-electron interaction in strongly correlated materials is discussed from a more general point of view. Using sum rules for the phonon self-energy and the electron-phonon contribution to the electron self-energy in the generic t - J model with on-site electron-phonon coupling and comparing to results obtained assuming non-interacting electrons, we assess the effect of strong correlations on phonon and electron properties. We focus on the resulting property dependence of apparent coupling constants and support our findings with numerical calculations. The sum rules are also useful to discuss the importance of vertex corrections in a diagrammatic treatment of electron-phonon interactions in strongly correlated systems.

Finally, we end by giving conclusions and append some supplementary material. The publications based on this thesis are listed on page 171.

Chapter 1

Electron-phonon interaction in the t - J model

1.1 Introduction

In order to study the interplay of strong electronic correlations and electron-phonon coupling in the high-temperature superconductors, we need a model that describes the relevant electronic and lattice degrees of freedom.

We take the widely accepted view that the two-dimensional CuO_2 planes common to all cuprate superconductors contain the essential physics of the electrons in these materials. The three-band model [28] is used to describe the electronic structure at low energies and includes the $\text{Cu-}3d_{x^2-y^2}$ and $\text{O-}2p_{x/y}$ orbitals which strongly hybridize. Strong correlations are incorporated by a Hubbard term taking into account the on-site Coulomb repulsion between two holes in the same d orbital.

Electron-phonon interaction can be introduced in a realistic way as the effect of lattice distortions on parameters of the three-band model (like the hopping amplitudes and the level energies) can be estimated or calculated quite directly.

The three-band model with electron-phonon interaction, however, is still a relatively complex model which makes it hard to obtain analytical or numerical results. Therefore, we derive an effective low-energy model where states with high energy are projected out and only indirectly influence the remaining degrees of freedom. The reduced size of the Hilbert space facilitates calculations and also allows for an easier interpretation of the results.

This leads to the t - J model [29] which now includes electron-phonon interaction. In this model, doped holes form so-called Zhang-Rice singlets which have binding

energies of several eV that give uninteresting contributions to the total energy in case of an undistorted lattice, but can lead to on-site electron-phonon coupling with large prefactors when modulated by lattice distortions. Similar models have already been derived before, see e.g. Refs. [30, 31, 32], but in a less general way and with differing conclusions about the importance of different coupling mechanisms.

In the beginning of this chapter we introduce the three-band model in a form suitable for the subsequent considerations and describe the modulation of its parameters due to lattice distortions. After presenting the general procedure for the derivation of an effective low-energy model we first consider the undistorted lattice and obtain the t - J model. Then, we generalize the derivation to include lattice distortions. This finally leads to the electron-phonon interaction in the t - J model.

1.2 Three-band model

1.2.1 Definition

The three-band model has been proposed by Emery [28] for the description of the relevant electronic degrees of freedom in the copper oxide planes of cuprates. It is defined by the following Hamiltonian:

$$H = \sum_{i\sigma} \varepsilon_i^d d_{i\sigma}^\dagger d_{i\sigma} + \sum_{i\delta\sigma} \varepsilon_{i\delta}^p p_{i\delta\sigma}^\dagger p_{i\delta\sigma} + U \sum_i d_{i\uparrow}^\dagger d_{i\uparrow} d_{i\downarrow}^\dagger d_{i\downarrow} + H_{\text{hop}}, \quad (1.1)$$

with

$$H_{\text{hop}} = \sum_{i\delta\sigma} \left(-t_{i\delta} d_{i\sigma}^\dagger p_{i\delta\sigma} + t_{i(-\delta)} d_{i\sigma}^\dagger p_{(i-2\delta)\delta\sigma} + \text{H.c.} \right). \quad (1.2)$$

The model describes a two-dimensional square lattice of N CuO_2 unit cells with the lattice constant a . There are N Cu- d orbitals labeled by i located on the nodes of the lattice at \mathbf{R}_i . Between each pair of neighboring Cu- d orbitals, there is one O- p orbital in the middle of the corresponding bond labeled by $i\delta$, where $\delta \in \{\hat{x}/2, \hat{y}/2\}$ indicates the offset to the Cu- d orbital at \mathbf{R}_i (see also Fig. 1.1). The operators for creating a hole with spin $\sigma \in \{\uparrow, \downarrow\}$ in these orbitals are $d_{i\sigma}^\dagger$ and $p_{i\delta\sigma}^\dagger$, respectively. The vacuum corresponds to all orbitals being completely filled, i.e., it contains no holes. The level energies ε_i^d and $\varepsilon_{i\delta}^p$ are site-dependent to allow for a modulation due to lattice distortions. A Hubbard term takes into account the Coulomb repulsion U of two holes in the same Cu- d orbital. H_{hop} describes nearest-neighbor hopping between Cu- d and O- p orbitals. The hopping amplitudes $t_{i(\pm\delta)}$ can also be modulated by lattice distortions. The signs reflect the symmetry of the orbitals (cf. Fig. 1.1). A

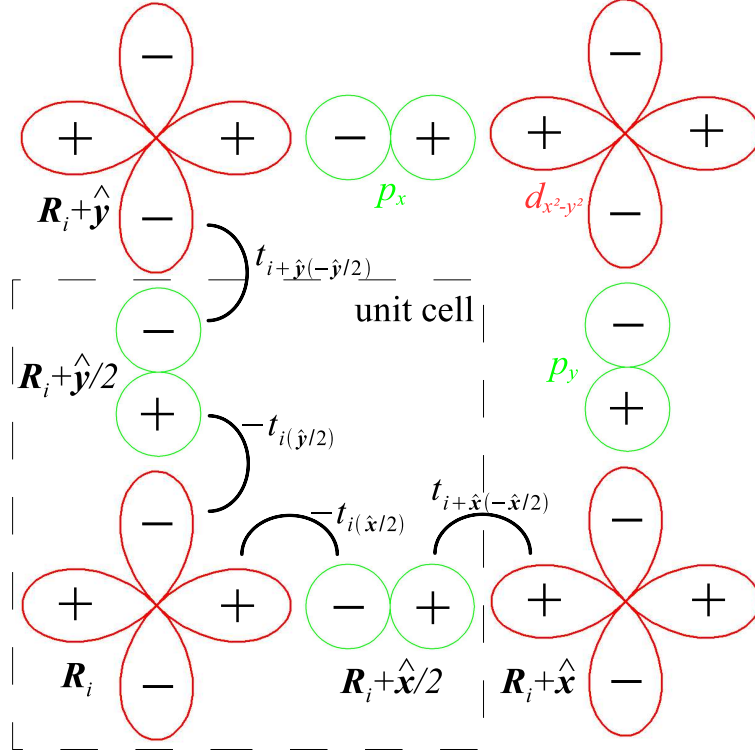


Figure 1.1: Schematic view of the Cu- d (red) and O- p (green) orbitals in a CuO_2 plane. The signs show the relative phases of the orbitals.

unit cell index like $(i - 2\delta)$ is to be understood as the index j of the unit cell with the Cu- d orbital located at $\mathbf{R}_j = \mathbf{R}_i - 2\delta$.

1.2.2 Transformation of O- p orbitals

We show in the following that, after choosing a new representation for the O- p orbitals, the three-band model can effectively be formulated using only half of the new operators if we consider an undistorted lattice. In this case, both level energies and hopping amplitudes are site-independent and ε_i^d , $\varepsilon_{i\delta}^p$, and $t_{i(\pm\delta)}$ can be replaced by the unmodulated values ε^d , ε^p , and t_{pd} . Introducing Fourier-transforms of the field operators in site representation which are labeled by the wavevector \mathbf{k} ,

$$d_{i\sigma} = \frac{1}{\sqrt{N}} \sum_{\mathbf{k}} d_{\mathbf{k}\sigma} e^{i\mathbf{k}\cdot\mathbf{R}_i}, \quad (1.3)$$

$$p_{i\delta\sigma} = \frac{1}{\sqrt{N}} \sum_{\mathbf{k}} p_{\mathbf{k}\delta\sigma} e^{i\mathbf{k}\cdot(\mathbf{R}_i+\delta)}, \quad (1.4)$$

the hopping part of the three-band model, Eq. (1.2), in the undistorted lattice takes the form

$$H_{\text{hop}}^{(0)} = 2it_{pd} \sum_{\mathbf{k}\delta\sigma} \sin(\mathbf{k} \cdot \boldsymbol{\delta}) \left(p_{\mathbf{k}\delta\sigma}^\dagger d_{\mathbf{k}\sigma} - d_{\mathbf{k}\sigma}^\dagger p_{\mathbf{k}\delta\sigma} \right). \quad (1.5)$$

Eq. (1.5) shows that d states hybridize only with a certain linear combination of p states with the same wavevector. This suggests to form new operators for $\mathbf{k} \neq (0, 0)$,

$$\phi_{\mathbf{k}\sigma} = -i\beta_{\mathbf{k}} \left(\sin(k_x a/2) p_{\mathbf{k}(\hat{x}/2)\sigma} + \sin(k_y a/2) p_{\mathbf{k}(\hat{y}/2)\sigma} \right), \quad (1.6)$$

$$\bar{\phi}_{\mathbf{k}\sigma} = -i\beta_{\mathbf{k}} \left(-\sin(k_y a/2) p_{\mathbf{k}(\hat{x}/2)\sigma} + \sin(k_x a/2) p_{\mathbf{k}(\hat{y}/2)\sigma} \right), \quad (1.7)$$

with the normalization factor

$$\beta_{\mathbf{k}} = \left([\sin(k_x a/2)]^2 + [\sin(k_y a/2)]^2 \right)^{-\frac{1}{2}}. \quad (1.8)$$

The original operators $p_{i\delta\sigma}$ fulfill standard fermionic anticommutation relations – all anticommutators vanish except for $[p_{i\delta\sigma}, p_{j\delta'\sigma'}^\dagger]_+ = \delta_{ij}\delta_{\delta\delta'}\delta_{\sigma\sigma'}$. We use the notation $[A, B]_+ = AB + BA$ for the anticommutator of two operators A and B . One finds that the new operators fulfill analogous relations: $[\phi_{\mathbf{k}\sigma}, \phi_{\mathbf{k}'\sigma'}^\dagger]_+ = \delta_{\mathbf{k}\mathbf{k}'}\delta_{\sigma\sigma'}$, $[\bar{\phi}_{\mathbf{k}\sigma}, \bar{\phi}_{\mathbf{k}'\sigma'}^\dagger]_+ = \delta_{\mathbf{k}\mathbf{k}'}\delta_{\sigma\sigma'}$, and all other anticommutators are zero. The hopping part of the Hamiltonian in the undistorted system, Eq. (1.5), can now be rewritten as

$$H_{\text{hop}}^{(0)} = 2t_{pd} \sum_{\mathbf{k} \neq (0,0) \sigma} \beta_{\mathbf{k}}^{-1} \left(d_{\mathbf{k}\sigma}^\dagger \phi_{\mathbf{k}\sigma} + \phi_{\mathbf{k}\sigma}^\dagger d_{\mathbf{k}\sigma} \right). \quad (1.9)$$

We see from Eq. (1.9) that only hopping between ϕ and d orbitals is possible. The $\bar{\phi}$ orbitals do not hybridize with the d orbitals. Using

$$\phi_{i\sigma} = \frac{1}{\sqrt{N}} \sum_{\mathbf{k}} \phi_{\mathbf{k}\sigma} e^{i\mathbf{k} \cdot \mathbf{R}_i}, \quad (1.10)$$

$$\bar{\phi}_{i\sigma} = \frac{1}{\sqrt{N}} \sum_{\mathbf{k}} \bar{\phi}_{\mathbf{k}\sigma} e^{i\mathbf{k} \cdot \mathbf{R}_i}, \quad (1.11)$$

we return to a site representation. As we consider the limit of infinite system size ($N \rightarrow \infty$), the $\mathbf{k} = (0, 0)$ contribution in Eqs. (1.10) and (1.11) can be neglected. The general three-band model, Eq. (1.1), can now be written as

$$H = H_0 + V, \quad (1.12)$$

where

$$H_0 = \varepsilon^d \sum_{i\sigma} d_{i\sigma}^\dagger d_{i\sigma} + \varepsilon^p \sum_{i\sigma} \left(\phi_{i\sigma}^\dagger \phi_{i\sigma} + \bar{\phi}_{i\sigma}^\dagger \bar{\phi}_{i\sigma} \right) + U \sum_i d_{i\uparrow}^\dagger d_{i\uparrow} d_{i\downarrow}^\dagger d_{i\downarrow} \quad (1.13)$$

and

$$V = V^{(0)} + V^{(t)} + V^{(\varepsilon)}, \quad (1.14)$$

with

$$V^{(0)} = 2t_{pd} \sum_{ij\sigma} \alpha(\Delta\mathbf{R}_{ij}) d_{i\sigma}^\dagger \phi_{j\sigma} + \text{H.c.}, \quad (1.15)$$

$$\begin{aligned} V^{(t)} = & \frac{1}{2} \sum_{ij\sigma\delta} \sum_{s=\pm} \Delta t_{i(s\delta)} [\gamma(\Delta\mathbf{R}_{ij}) - \gamma(\Delta\mathbf{R}_{ij} + 2s\delta)] d_{i\sigma}^\dagger \phi_{j\sigma} \\ & + \frac{1}{2} \sum_{ij\sigma\delta} \sum_{s=\pm} f(\delta) \Delta t_{i(s\delta)} s [\gamma(\Delta\mathbf{R}_{ij} + s(\delta - \bar{\delta})) - \gamma(\Delta\mathbf{R}_{ij} + s(\delta + \bar{\delta}))] d_{i\sigma}^\dagger \bar{\phi}_{j\sigma} \\ & + \text{H.c.}, \end{aligned} \quad (1.16)$$

and

$$\begin{aligned} V^{(\varepsilon)} = & \sum_{i\sigma} \Delta\varepsilon_i^d d_{i\sigma}^\dagger d_{i\sigma} \\ & + \sum_{i\delta\sigma jj'} \frac{\Delta\varepsilon_{i\delta}^p}{4} \left([\gamma(\Delta\mathbf{R}_{ji}) - \gamma(\Delta\mathbf{R}_{ji} - 2\delta)] \phi_{j\sigma}^\dagger \right. \\ & \quad \left. + f(\delta) [\gamma(\Delta\mathbf{R}_{ji} + \bar{\delta} - \delta) - \gamma(\Delta\mathbf{R}_{ji} - \delta - \bar{\delta})] \bar{\phi}_{j\sigma}^\dagger \right) \\ & \times \left([\gamma(\Delta\mathbf{R}_{ij'}) - \gamma(\Delta\mathbf{R}_{ij'} + 2\delta)] \phi_{j'\sigma} \right. \\ & \quad \left. + f(\delta) [\gamma(\Delta\mathbf{R}_{ij'} + \delta - \bar{\delta}) - \gamma(\Delta\mathbf{R}_{ij'} + \delta + \bar{\delta})] \bar{\phi}_{j'\sigma} \right). \end{aligned} \quad (1.17)$$

We have introduced the notation

$$\varepsilon_i^d = \varepsilon^d + \Delta\varepsilon_i^d, \quad (1.18)$$

$$\varepsilon_{i\delta}^p = \varepsilon^p + \Delta\varepsilon_{i\delta}^p, \quad (1.19)$$

$$t_{i(\pm\delta)} = t_{pd} + \Delta t_{i(\pm\delta)} \quad (1.20)$$

to describe the modulation of level energies and hopping amplitudes in a distorted lattice. H_0 contains the unmodulated d , ϕ , and $\bar{\phi}$ level energies as well as the Hubbard term whereas the remaining part V describes the unmodulated hopping ($V^{(0)}$), its modulation by lattice distortions ($V^{(t)}$), and the modulation of the level energies ($V^{(\varepsilon)}$). Furthermore, the following definitions are used.

$$\Delta\mathbf{R}_{ij} = \mathbf{R}_i - \mathbf{R}_j, \quad (1.21)$$

\mathbf{R}	$\mathbf{0}$	$\pm\hat{\mathbf{x}}, \pm\hat{\mathbf{y}}$	$\pm(\hat{\mathbf{x}} + \hat{\mathbf{y}}), \pm(\hat{\mathbf{x}} - \hat{\mathbf{y}})$	$\pm 2\hat{\mathbf{x}}, \pm 2\hat{\mathbf{y}}$
$\alpha(\mathbf{R})$	$\lambda = 0.958$	-0.140	-0.024	-0.014
$\gamma(\mathbf{R})$	$\gamma_0 = 1.286$	$\gamma_1 = 0.328$	$\gamma_{11} = 0.210$	$\gamma_2 = 0.165$

Table 1.1: Numerical values of $\alpha(\mathbf{R})$ (Eq. (1.22)) and $\gamma(\mathbf{R})$ (Eq. (1.23)) for $N \rightarrow \infty$ together with the definition of abbreviations for often used values.

$$\alpha(\mathbf{R}) = \frac{1}{N} \sum_{\mathbf{k} \neq (0,0)} \beta_{\mathbf{k}}^{-1} e^{i\mathbf{k} \cdot \mathbf{R}}, \quad (1.22)$$

$$\gamma(\mathbf{R}) = \frac{1}{N} \sum_{\mathbf{k} \neq (0,0)} \beta_{\mathbf{k}} e^{i\mathbf{k} \cdot \mathbf{R}}, \quad (1.23)$$

$$f(\boldsymbol{\delta}) = \begin{cases} -1 & \text{if } \boldsymbol{\delta} = \frac{\hat{\mathbf{x}}}{2}, \\ +1 & \text{if } \boldsymbol{\delta} = \frac{\hat{\mathbf{y}}}{2} \end{cases}, \quad (1.24)$$

$$\bar{\boldsymbol{\delta}} = \begin{cases} \frac{\hat{\mathbf{y}}}{2} & \text{if } \boldsymbol{\delta} = \frac{\hat{\mathbf{x}}}{2}, \\ \frac{\hat{\mathbf{x}}}{2} & \text{if } \boldsymbol{\delta} = \frac{\hat{\mathbf{y}}}{2} \end{cases}. \quad (1.25)$$

In Tab. 1.1, some numerical values of $\alpha(\mathbf{R})$ and $\gamma(\mathbf{R})$ are given for $N \rightarrow \infty$.

In the undistorted lattice, the model defined in Eqs. (1.12)-(1.17) reduces to $H = H_0 + V^{(0)}$ and there is no interaction between the $\bar{\phi}$ orbitals on the one hand and the other orbitals on the other hand. For the description of the d and ϕ orbitals, one could therefore omit the $\bar{\phi}$ orbitals. Once we allow for site-dependent hopping amplitudes and level energies, however, the model contains the additional terms $V^{(t)}$ and $V^{(\epsilon)}$. They lead to coupling between the $\bar{\phi}$ orbitals and the other orbitals, and all orbitals must be taken into account.

1.2.3 Modulation of parameters

We now discuss how the modulations of hopping and level energies are assumed to depend on the displacements of the atoms from their equilibrium positions.

Band structure calculations within the local density approximation (LDA) for La_2CuO_4 [33] show that, upon variation of the lattice constant a , the bandwidth (splitting between bonding and anti-bonding $d_{x^2-y^2} - p_{x/y(\sigma)}$ bands) is proportional to a^{-n} , with n between about 3.1 and 3.7. Therefore, for our calculations we assume the following dependence of the hopping amplitude in the three-band model on the actual distance r between two nearest-neighbor Cu and O atoms:

$$t_{pd}(r) = t_{pd} \left(\frac{a/2}{r} \right)^{3.5}. \quad (1.26)$$

An $r^{-3.5}$ dependence was also used in Refs. [30,34,35,36]. We denote the displacement of a Cu atom from its equilibrium position at \mathbf{R}_i by $\mathbf{u}_{\text{Cu},i} = (u_{\text{Cu},i}^{\hat{x}/2}, u_{\text{Cu},i}^{\hat{y}/2})$. The displacement of an O atom from its equilibrium position at $\mathbf{R}_i + \boldsymbol{\delta}$ is given by $\mathbf{u}_{\text{O},i\boldsymbol{\delta}}$, analogously. Working to linear order in the displacements, we then obtain

$$\Delta t_{i(\pm\boldsymbol{\delta})} \approx \pm \left. \frac{dt_{pd}}{dr} \right|_0 (u_{\text{O},i(\pm\boldsymbol{\delta})}^{\boldsymbol{\delta}} - u_{\text{Cu},i}^{\boldsymbol{\delta}}). \quad (1.27)$$

$|_0$ indicates that the expression to the left is to be evaluated for the undistorted lattice where $r = a/2$.

The dependence of the level energies on the atomic displacements is obtained by assuming that the energy of a hole in a certain orbital is also influenced by the Coulomb interaction with the ionic charges in its surrounding which depends on the distance between the ions. We further assume that because of screening only the nearest-neighbor ions need to be taken into account. The effective level energies entering the three-band model from Eq. (1.1) are then given by

$$\varepsilon_i^d = \varepsilon_{\text{bare}}^d + (-2) \sum_{\boldsymbol{\delta}} \sum_{s=\pm} U_{pd}(|s\boldsymbol{\delta} + \mathbf{u}_{\text{O},i(s\boldsymbol{\delta})} - \mathbf{u}_{\text{Cu},i}|) \quad (1.28)$$

and

$$\varepsilon_{i\boldsymbol{\delta}}^p = \varepsilon_{\text{bare}}^p + 2 [U_{pd}(|\boldsymbol{\delta} + \mathbf{u}_{\text{O},i\boldsymbol{\delta}} - \mathbf{u}_{\text{Cu},i}|) + U_{pd}(|-\boldsymbol{\delta} + \mathbf{u}_{\text{O},i\boldsymbol{\delta}} - \mathbf{u}_{\text{Cu},i+2\boldsymbol{\delta}}|)]. \quad (1.29)$$

The bare level energies $\varepsilon_{\text{bare}}^d$ and $\varepsilon_{\text{bare}}^p$ are modified by the screened Coulomb interaction

$$U_{pd}(r) = U_{pd} \frac{a/2}{r} \quad (1.30)$$

with the surrounding ions assuming a $1/r$ dependence on the interionic distance. We use the nominal ionic charges from the undoped system of -2 and $+2$ for O and Cu ions, respectively, neglecting any effect of charge fluctuations or doping. Expanding to first order in the displacements, we find the following modulations of the level energies:

$$\Delta \varepsilon_i^d \approx -2 \left. \frac{dU_{pd}}{dr} \right|_0 \sum_{\boldsymbol{\delta}} \sum_{s=\pm} s u_{\text{O},i(s\boldsymbol{\delta})}^{\boldsymbol{\delta}}, \quad (1.31)$$

$$\Delta \varepsilon_{i\boldsymbol{\delta}}^p \approx 2 \left. \frac{dU_{pd}}{dr} \right|_0 (u_{\text{Cu},i+2\boldsymbol{\delta}}^{\boldsymbol{\delta}} - u_{\text{Cu},i}^{\boldsymbol{\delta}}). \quad (1.32)$$

1.3 Effective low-energy model

In this section we derive an expression for an effective low-energy model of the three-band model using degenerate perturbation theory derived with the help of Löwdin's partitioning technique [37].

Treating both hopping and the effect of lattice modulations as a perturbation, in zeroth order the three-band model is given by H_0 from Eq. (1.13). Undoped cuprates have one hole per CuO_2 unit cell. As for these materials $U > \varepsilon^p - \varepsilon^d > 0$, the ground state of H_0 of the undoped system has exactly one hole in each of the N d orbitals. It has a degeneracy due to the equivalence of all spin configurations. If the system is doped with \tilde{N} additional holes, the set of degenerate ground states of H_0 is given by all states that have all N d orbitals singly occupied and \tilde{N} holes in ϕ or $\bar{\phi}$ orbitals.

We divide the Hilbert space for a given doping into two subsets by defining the projection operator P that projects onto the subset of degenerate ground states of H_0 with the eigenenergy

$$E_0 = PH_0P = N\varepsilon^d + \tilde{N}\varepsilon^p. \quad (1.33)$$

All other states which are in the second subset projected onto by the orthogonal operator $Q = 1 - P$ have eigenenergies with respect to H_0 that are higher than E_0 by at least

$$\Delta_{pd} = \varepsilon^p - \varepsilon^d. \quad (1.34)$$

The resolvent operator $(z - H)^{-1}$ has poles in the complex z -plane at the eigenenergies of the full three-band model H from Eq. (1.12). It has the following block form with respect to the two previously defined subspaces of the Hilbert space:

$$(z - H)^{-1} = \begin{pmatrix} z - PHP & PHQ \\ QHP & z - QHQ \end{pmatrix}^{-1}. \quad (1.35)$$

Coupling between these two subspaces is only provided by the perturbation V from Eq. (1.14), so we have $PHQ = PVQ$ and $QHP = QVP$ in the off-diagonal elements in Eq. (1.35). We want to obtain an effective low-energy model where the higher-energy states from the Q subspace are projected out. But their effect on the states in the P subspace through V must still be taken into account. This can be achieved by downfolding Eq. (1.35) to a resolvent operator confined to the P subspace that still has the same poles as $(z - H)^{-1}$:

$$\begin{aligned} P(z - H)^{-1}P &= P(z - PHP - PHQ(z - QHQ)^{-1}QHP)^{-1}P \\ &= P(z - \tilde{H}(z))^{-1}P. \end{aligned} \quad (1.36)$$

This defines an energy-dependent Hamiltonian $\tilde{H}(z)$ in the P subspace. We have

$$\begin{aligned} P\tilde{H}(E)P &= PHP + PHT(E)HP \\ &= E_0 + PVP + PVT(E)VP, \end{aligned} \quad (1.37)$$

where

$$T(E) = Q(E - QHQ)^{-1}Q. \quad (1.38)$$

Introducing the abbreviations

$$R_0 = Q(E_0 - QH_0Q)^{-1}Q \quad (1.39)$$

and

$$V'(E) = QVQ + E_0 - E \quad (1.40)$$

and using the operator identity [37]

$$(A - B)^{-1} = A^{-1} + A^{-1}B(A - B)^{-1}, \quad (1.41)$$

we can rewrite Eq. (1.38) as

$$T(E) = R_0 + R_0V'(E)T(E). \quad (1.42)$$

Solving for $T(E)$ we obtain

$$\begin{aligned} T(E) &= (1 - R_0V'(E))^{-1}R_0 \\ &= R_0 + R_0V'(E)R_0 + R_0V'(E)R_0V'(E)R_0 + \dots \end{aligned} \quad (1.43)$$

From Eqs. (1.14)-(1.17) and (1.27)-(1.32), it follows that V has terms proportional to t_{pd} (in $V^{(0)}$), t_{pdu} (in $V^{(t)}$), and u (in $V^{(\varepsilon)}$) where u stands for an atomic displacement. If we want to obtain an effective Hamiltonian that is correct to order t_{pd}^2u , we need to include in $\tilde{H}(z)$ only terms up to third order in the perturbation V . It suffices then to take into account just the first two terms in the second line of Eq. (1.43) when substituting for $T(E)$ in Eq. (1.37). An eigenstate $|\Phi\rangle$ (from the P subspace) of the resulting – still energy-dependent – Hamiltonian fulfills the eigenvalue equation

$$(E_0 + PVP + PVR_0VP + PVR_0(V + E_0 - E)R_0VP)|\Phi\rangle = E|\Phi\rangle. \quad (1.44)$$

Transferring the E -dependent term in Eq. (1.44) to the right one obtains

$$(E_0 + PVP + PVR_0VP + PVR_0(V + E_0)R_0VP)|\Phi\rangle = E(1 + PVR_0^2VP)|\Phi\rangle. \quad (1.45)$$

Now, we introduce

$$|\chi\rangle = \xi^{-1}|\Phi\rangle = (1 + PVR_0^2VP)^{1/2}|\Phi\rangle, \quad (1.46)$$

substitute in Eq. (1.45), left multiply by ξ , and then expand the square root to obtain the desired accuracy up to order t_{pd}^2u . This leads to the Schrödinger equation $H_{\text{eff}}|\chi\rangle = E|\chi\rangle$ with the energy-independent effective Hamiltonian

$$H_{\text{eff}} = E_0 + PVP + PVR_0VP + PVR_0VR_0VP - \frac{1}{2}PV(PVR_0^2 + R_0^2VP)VP. \quad (1.47)$$

For the special case of an undistorted lattice, we also give an effective Hamiltonian $H_{\text{eff},4}$ which is correct to order t_{pd}^4 . Then, $V = V^{(0)}$ and terms containing an odd number of V^0 operators vanish. With an analogous procedure like the one leading to Eq. (1.47), one obtains

$$\begin{aligned} H_{\text{eff},4} = & E_0 + PV^{(0)}R_0V^{(0)}P + PV^{(0)}R_0V^{(0)}R_0V^{(0)}R_0V^{(0)}P \\ & - \frac{1}{2}PVR_0(R_0VPV + VPVR_0)R_0VP. \end{aligned} \quad (1.48)$$

1.4 t - J model for the undistorted lattice

As was first shown by Zhang and Rice [29], the t - J model can be derived as an effective low-energy model of the three-band model. In this section, we give a derivation for the undistorted lattice using the effective Hamiltonian from Eq. (1.48).

1.4.1 Undoped system

In the undoped system, the P subspace is spanned by the eigenstates $|n\rangle$ of H_0 with exactly one hole per Cu- d orbital which we label by n to distinguish the different spin configurations. They have the eigenenergy $E_0 = N\varepsilon^d$ with respect to H_0 .

The matrix elements of the second term in Eq. (1.48) can be rewritten in the usual second-order perturbation theory form

$$\langle n|V^{(0)}R_0V^{(0)}|n'\rangle = \sum_{\{w\}} \frac{\langle n|V^{(0)}|w\rangle\langle w|V^{(0)}|n'\rangle}{E_0 - E_w}, \quad (1.49)$$

where $\sum_{\{w\}}$ denotes the sum over all eigenstates $|w\rangle$ of H_0 in the Q subspace with the eigenenergy E_w with respect to H_0 . Due to $V^{(0)}$, each Cu- d hole in the state $|n\rangle$ can virtually hop from its site i to a ϕ orbital on any site j , and back again. The

corresponding intermediate states are higher in energy by $E_w - E_0 = \Delta_{pd}$, and the respective matrix elements are $|\langle w|V^{(0)}|n\rangle|^2 = 4t_{pd}^2|\alpha(\Delta\mathbf{R}_{ij})|^2$. There are no other contributions to Eq. (1.49). Therefore, only the diagonal matrix elements are non-zero:

$$\langle n|V^{(0)}R_0V^{(0)}|n'\rangle = -\frac{4t_{pd}^2}{\Delta_{pd}}\sum_{ij}|\alpha(\Delta\mathbf{R}_{ij})|^2\delta_{n,n'} = -N\frac{4t_{pd}^2}{\Delta_{pd}}\delta_{n,n'}. \quad (1.50)$$

Here, we use the sum rule

$$\begin{aligned} \sum_j|\alpha(\Delta\mathbf{R}_{ij})|^2 &= \frac{1}{N^2}\sum_j\sum_{\mathbf{k},\mathbf{k}'}\beta_{\mathbf{k}}^{-1}\beta_{\mathbf{k}'}^{-1}e^{i(\mathbf{k}-\mathbf{k}')(\mathbf{R}_i-\mathbf{R}_j)} \\ &= \frac{1}{N}\sum_{\mathbf{k}}([\sin(k_x a/2)]^2 + [\sin(k_y a/2)]^2) \\ &= 1. \end{aligned} \quad (1.51)$$

In the first line of Eq. (1.51), the definitions (1.21) and (1.22) are used. Because of $\sum_j e^{i(\mathbf{k}-\mathbf{k}')\mathbf{R}_j} = N\delta_{\mathbf{k},\mathbf{k}'}$, we can simplify the expression as shown in the second line where Eq. (1.8) has been inserted. Finally, it is easy to show that $\sum_{\mathbf{k}}[\sin(\mathbf{k}\mathbf{R})]^2 = N/2$ for any $\mathbf{R} \neq 0$, and we obtain the result in the last line. As the sum rule is almost exhausted already by the local contribution for $j = i$ ($|\alpha(\mathbf{0})|^2 = \lambda^2 \approx 0.92$ for $N \rightarrow \infty$, cf. Tab. 1.1), we only introduce a small error of order $1 - \lambda^2$ if we neglect all intermediate states where a Cu- d hole hops to any non-local ϕ orbital. Also, in the following, we will always restrict ourselves to the leading contribution proportional to a power of λ when calculating diagonal elements of the effective Hamiltonian.

$$\langle n|V^{(0)}R_0V^{(0)}|n'\rangle \approx -N\frac{4\lambda^2 t_{pd}^2}{\Delta_{pd}}\delta_{n,n'} = NE^{\text{Cu-}d}\delta_{n,n'}. \quad (1.52)$$

The result is used to define the Cu- d self-energy

$$E^{\text{Cu-}d} = -\frac{4\lambda^2 t_{pd}^2}{\Delta_{pd}}, \quad (1.53)$$

the energy correction per one Cu- d hole.

Finally, we consider the remaining terms in Eq. (1.48) which are of order t_{pd}^4 . We neglect constant energy shifts and keep only the super-exchange interaction H_J derived from these terms [38]:

$$H_J = J\sum_{\langle i,j\rangle}\left(\mathbf{S}_i \cdot \mathbf{S}_j - \frac{1}{4}n_i n_j\right), \quad (1.54)$$

with

$$J = 4t_{pd}^4 \left(\frac{1}{\Delta_{pd}^2 U} + \frac{1}{\Delta_{pd}^3} \right). \quad (1.55)$$

This is a spin- $\frac{1}{2}$ Heisenberg model with antiferromagnetic coupling ($J > 0$). $\langle i, j \rangle$ denotes nearest-neighbor pairs of copper sites, and the spin operator \mathbf{S}_i refers to the spin of a hole in the Cu- d orbital at site i . $n_i = \sum_{\sigma} d_{i\sigma}^{\dagger} d_{i\sigma}$ measures the hole occupancy on copper site i .

1.4.2 Doped system

We now turn to the doped system. We first consider the case of one additional hole compared to the undoped system and later generalize to higher dopings. In the one-hole sector, the P subspace is spanned by the eigenstates of H_0 with all Cu- d orbitals singly occupied and one hole in an oxygen orbital which have the lowest eigenenergy $E_0 = N\varepsilon^d + \varepsilon^p$ with respect to H_0 . Those states can be further distinguished as to whether the additional hole occupies a ϕ or a $\bar{\phi}$ orbital and whether its spin forms a singlet or a triplet combination with the spin of the local Cu- d hole. We will see that the second-order energy correction is largest for ϕ - d singlets which separates them from the other combinations by an energy of the order of Δ_{pd} . This will allow us to consider only the ϕ - d singlets in the final effective low-energy model.

ϕ - d singlets

We begin by considering basis states with a local singlet formed by a Cu- d hole and a ϕ hole on the same site. These states are denoted by

$$|i, \alpha\rangle = \Psi_i^{\dagger} R_{i\alpha}^{\dagger} |0\rangle, \quad (1.56)$$

where

$$\Psi_i = \frac{1}{\sqrt{2}} (\phi_{i\uparrow} d_{i\downarrow} - \phi_{i\downarrow} d_{i\uparrow}) \quad (1.57)$$

and

$$R_{i\alpha} = \prod_{j \neq i} d_{j\tilde{\sigma}(i,\alpha,j)}. \quad (1.58)$$

$|0\rangle$ describes a system with no holes. Individual states are labeled by the site i where the singlet is located and by the configuration α of the Cu- d holes on all other sites which is fixed by the spin orientations $\tilde{\sigma}(i, \alpha, j)$. We tacitly assume the operators in Eq. (1.58) to be in a defined order, e.g. based on a consecutive numbering of all sites.

The diagonal elements of the second-order contribution to the effective Hamiltonian with respect to these basis states are

$$\langle i, \alpha | V^{(0)} R_0 V^{(0)} | i, \alpha \rangle = \sum_{\{w\}} \frac{|\langle w | V^{(0)} | i, \alpha \rangle|^2}{E_0 - E_w}. \quad (1.59)$$

We use the same notation as in Eq. (1.49). The intermediate states $|w\rangle$ leading to a non-vanishing contribution in Eq. (1.59) are listed in the following together with a description of the corresponding virtual process, the energy difference to the ground-state energy, and the required matrix element.

- A Cu- d hole from site $j \neq i$ hops into the ϕ orbital at site $l \neq i$:

$$|w_{1jl}\rangle = \phi_{l\bar{\sigma}(i,\alpha,j)}^\dagger d_{j\bar{\sigma}(i,\alpha,j)} |i, \alpha\rangle \quad (1.60)$$

$$\text{with } E_{w_{1jl}} - E_0 = \Delta_{pd}, \quad |\langle w_{1jl} | V^{(0)} | i, \alpha \rangle|^2 = 4t_{pd}^2 |\alpha(\Delta\mathbf{R}_{jl})|^2. \quad (1.61)$$

- A Cu- d hole from site $j \neq i$ hops into the ϕ orbital at site i :

$$|w_{2j}\rangle = \phi_{i\uparrow}^\dagger \phi_{i\downarrow}^\dagger d_{i\bar{\sigma}(i,\alpha,j)}^\dagger d_{j\bar{\sigma}(i,\alpha,j)} R_{i\alpha}^\dagger |0\rangle, \quad (1.62)$$

$$\text{with } E_{w_{2j}} - E_0 = \Delta_{pd}, \quad |\langle w_{2j} | V^{(0)} | i, \alpha \rangle|^2 = 2t_{pd}^2 |\alpha(\Delta\mathbf{R}_{ji})|^2. \quad (1.63)$$

- The Cu- d hole on site i hops into the local ϕ orbital:

$$|w_3\rangle = \phi_{i\uparrow}^\dagger \phi_{i\downarrow}^\dagger R_{i\alpha}^\dagger |0\rangle, \quad (1.64)$$

$$\text{with } E_{w_3} - E_0 = \Delta_{pd}, \quad |\langle w_3 | V^{(0)} | i, \alpha \rangle|^2 = 8t_{pd}^2 |\alpha(\Delta\mathbf{R}_{ii})|^2. \quad (1.65)$$

- The Cu- d hole from site i hops into the ϕ orbital on site $j \neq i$:

$$|w_{4j}\rangle = \frac{1}{\sqrt{2}} (\phi_{i\uparrow}^\dagger \phi_{j\downarrow}^\dagger - \phi_{i\downarrow}^\dagger \phi_{j\uparrow}^\dagger) R_{i\alpha}^\dagger |0\rangle, \quad (1.66)$$

$$\text{with } E_{w_{4j}} - E_0 = \Delta_{pd}, \quad |\langle w_{4j} | V^{(0)} | i, \alpha \rangle|^2 = 4t_{pd}^2 |\alpha(\Delta\mathbf{R}_{ij})|^2. \quad (1.67)$$

- The ϕ hole on site i hops into the local Cu- d orbital:

$$|w_5\rangle = d_{i\uparrow}^\dagger d_{i\downarrow}^\dagger R_{i\alpha}^\dagger |0\rangle, \quad (1.68)$$

$$\text{with } E_{w_5} - E_0 = U - \Delta_{pd}, \quad |\langle w_5 | V^{(0)} | i, \alpha \rangle|^2 = 8t_{pd}^2 |\alpha(\Delta\mathbf{R}_{ii})|^2. \quad (1.69)$$

- The ϕ hole on site i hops into the Cu- d orbital on site $j \neq i$:

$$|w_{6j}\rangle = d_{i\bar{\sigma}(i,\alpha,j)}^\dagger d_{j-\bar{\sigma}(i,\alpha,j)}^\dagger R_{i\alpha}^\dagger |0\rangle, \quad (1.70)$$

$$\text{with } E_{w_{6j}} - E_0 = U - \Delta_{pd}, \quad |\langle w_{6j} | V^{(0)} | i, \alpha \rangle|^2 = 2t_{pd}^2 |\alpha(\Delta \mathbf{R}_{ij})|^2. \quad (1.71)$$

We use only the intermediate states $|w_{1jj}\rangle$, $|w_3\rangle$, and $|w_5\rangle$ in Eq. (1.59) because they give the leading contribution $\propto \lambda^2$. The corresponding virtual processes involve only local hopping of a hole between orbitals on the same site.

$$\begin{aligned} \langle i, \alpha | V^{(0)} R_0 V^{(0)} | i, \alpha \rangle &\approx -(N-1) \frac{4\lambda^2 t_{pd}^2}{\Delta_{pd}} - \left(\frac{8\lambda^2 t_{pd}^2}{\Delta_{pd}} + \frac{8\lambda^2 t_{pd}^2}{U - \Delta_{pd}} \right) \\ &= (N-1) E^{\text{Cu-}d} + E^{\text{singlet}}, \end{aligned} \quad (1.72)$$

where the singlet self-energy

$$E^{\text{singlet}} = -8\lambda^2 t_{pd}^2 \left(\frac{1}{\Delta_{pd}} + \frac{1}{U - \Delta_{pd}} \right) \quad (1.73)$$

was defined by the remaining energy correction after subtracting $N - 1$ Cu- d self-energies defined by Eq. (1.53).

Looking at off-diagonal elements of the second-order term in H_{eff} , we focus on those which correspond to an effective hopping of a singlet from site i to site j with the simultaneous transfer of the Cu- d hole from site j to site i , i.e., at elements between $|i, \alpha\rangle$ and $|j, \alpha'\rangle = \Psi_j^\dagger R_{j\alpha'}^\dagger |0\rangle$ with

$$R_{j\alpha'}^\dagger = s(i, \alpha, j) d_{i\bar{\sigma}(i,\alpha,j)}^\dagger d_{j\bar{\sigma}(i,\alpha,j)}^\dagger R_{i\alpha}^\dagger \quad (1.74)$$

and $s(i, \alpha, j)$ being (-1) raised to the power of the number of occupied sites between sites i and j in the state $|i, \alpha\rangle$ for the chosen site order. In

$$\langle j, \alpha' | V^{(0)} R_0 V^{(0)} | i, \alpha \rangle = \sum_{\{\tilde{w}\}} \frac{\langle j, \alpha' | V^{(0)} | \tilde{w} \rangle \langle \tilde{w} | V^{(0)} | i, \alpha \rangle}{E_0 - E_{\tilde{w}}} \quad (1.75)$$

we have non-vanishing contributions from the following intermediate states:

$$|\tilde{w}_1\rangle = d_{i\bar{\sigma}(i,\alpha,j)}^\dagger d_{j-\bar{\sigma}(i,\alpha,j)}^\dagger R_{i\alpha}^\dagger |0\rangle \quad \text{with } E_{\tilde{w}_1} - E_0 = U - \Delta_{pd}, \quad (1.76)$$

$$|\tilde{w}_2\rangle = d_{i\uparrow}^\dagger d_{i\downarrow}^\dagger R_{i\alpha}^\dagger |0\rangle \quad \text{with } E_{\tilde{w}_2} - E_0 = U - \Delta_{pd}, \quad (1.77)$$

$$|\tilde{w}_3\rangle = \phi_{j\bar{\sigma}(i,\alpha,j)}^\dagger d_{j\bar{\sigma}(i,\alpha,j)}^\dagger |i, \alpha\rangle \quad \text{with } E_{\tilde{w}_3} - E_0 = \Delta_{pd}, \quad (1.78)$$

$$|\tilde{w}_4\rangle = \frac{1}{\sqrt{2}} (\phi_{i\uparrow}^\dagger \phi_{j\downarrow}^\dagger - \phi_{i\downarrow}^\dagger \phi_{j\uparrow}^\dagger) R_{i\alpha}^\dagger |0\rangle \quad \text{with } E_{\tilde{w}_4} - E_0 = \Delta_{pd}, \quad (1.79)$$

for $l \neq i, j$ and $\tilde{\sigma}(i, \alpha, l) = \tilde{\sigma}(i, \alpha, j)$

$$|\tilde{w}_{5l}\rangle = d_{i\tilde{\sigma}(i,\alpha,l)}^\dagger d_{l-\tilde{\sigma}(i,\alpha,l)}^\dagger R_{i\alpha}^\dagger |0\rangle \quad \text{with} \quad E_{\tilde{w}_{5l}} - E_0 = U - \Delta_{pd}, \quad (1.80)$$

and for $l \neq i, j$ and $\tilde{\sigma}(i, \alpha, l) = -\tilde{\sigma}(i, \alpha, j)$

$$|\tilde{w}_{6l}\rangle = \phi_{j\tilde{\sigma}(i,\alpha,l)}^\dagger d_{l\tilde{\sigma}(i,\alpha,l)} |i, \alpha\rangle \quad \text{with} \quad E_{\tilde{w}_{6l}} - E_0 = \Delta_{pd}. \quad (1.81)$$

The corresponding matrix elements are

$$\langle j, \alpha' | V^{(0)} |\tilde{w}_{1/2}\rangle \langle \tilde{w}_{1/2} | V^{(0)} | i, \alpha \rangle = -s(i, \alpha, j) 4t_{pd}^2 \lambda \alpha(\Delta \mathbf{R}_{ij}), \quad (1.82)$$

$$\langle j, \alpha' | V^{(0)} |\tilde{w}_{3/4}\rangle \langle \tilde{w}_{3/4} | V^{(0)} | i, \alpha \rangle = -s(i, \alpha, j) 2t_{pd}^2 \lambda \alpha(\Delta \mathbf{R}_{ij}), \quad (1.83)$$

$$\langle j, \alpha' | V^{(0)} |\tilde{w}_{5l/6l}\rangle \langle \tilde{w}_{5l/6l} | V^{(0)} | i, \alpha \rangle = -s(i, \alpha, j) 2t_{pd}^2 \alpha(\Delta \mathbf{R}_{il}) \alpha(\Delta \mathbf{R}_{lj}). \quad (1.84)$$

We neglect the contributions from the intermediate states $|\tilde{w}_{5l}\rangle$ and $|\tilde{w}_{6l}\rangle$ involving third sites $l \neq i, j$ and keep only the leading contribution that contains a factor of λ :

$$\langle j, \alpha' | V^{(0)} R_0 V^{(0)} | i, \alpha \rangle \approx s(i, \alpha, j) 4t_{pd}^2 \lambda \alpha(\Delta \mathbf{R}_{ij}) \left(\frac{2}{U - \Delta_{pd}} + \frac{1}{\Delta_{pd}} \right). \quad (1.85)$$

Other off-diagonal elements of $PV^{(0)}R_0V^{(0)}P$ between singlet states in the P subspace, e.g. such that involve a spin flip in addition to the singlet hopping, are neglected as their leading term is at most proportional to $\alpha(\hat{\mathbf{x}})$ instead of λ .

ϕ - d triplets

Next, we consider analogously basis states in the P subspace with the ϕ hole forming a triplet instead of a singlet with the local d hole. The calculation of the diagonal elements of the second-order terms in the effective Hamiltonian is analogous to the one presented for the singlets. But the matrix elements involving the intermediate states $|w_3\rangle$ (Eq. (1.64)) and $|w_5\rangle$ (Eq. (1.68)) now vanish. There is only the contribution $(N-1)E^{\text{Cu-}d}$ from the intermediate states $|w_{1jl}\rangle$ (Eq. (1.60)) if we neglect again terms of order $1 - \lambda^2$. We therefore find a vanishing triplet self-energy $E^{\text{triplet}} = 0$. Off-diagonal elements of $PV^{(0)}R_0V^{(0)}P$ between the ϕ - d triplet states are at most comparable in size to those found for singlet states in Eq. (1.85).

$\bar{\phi}$ holes

All remaining basis states in the P subspace have the additional hole in a $\bar{\phi}$ orbital which does not couple to other orbitals. Therefore, the diagonal elements of $PV^{(0)}R_0V^{(0)}P$ between these states equal $NE^{\text{Cu-}d}$ as if the system was undoped. All off-diagonal elements vanish.

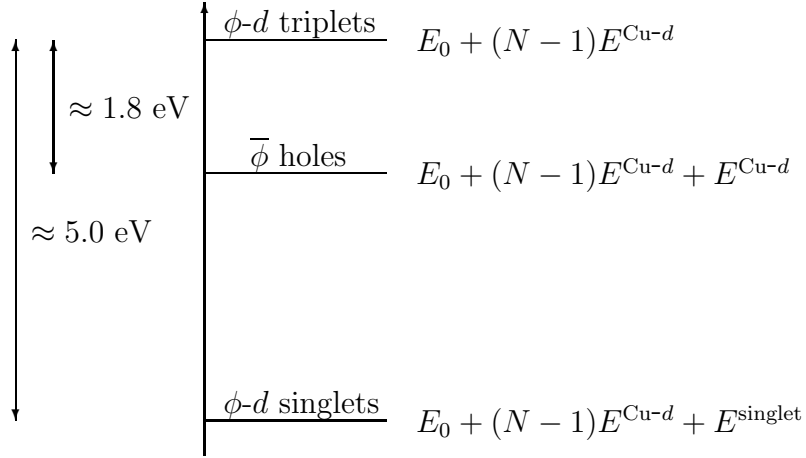


Figure 1.2: Schematic comparison of the diagonal matrix elements of the effective Hamiltonian for different states. The energy separations are calculated using $t_{pd} = 1.2$ eV, $U = 10$ eV, $\Delta_{pd} = 3$ eV.

Discussion

The second-order energy correction is largest for the ϕ - d singlets as can be seen in Fig. 1.2 where we compare the diagonal elements of the effective Hamiltonian for the different states using typical parameters ($t_{pd} = 1.2$ eV, $U = 10$ eV, $\Delta_{pd} = 3$ eV). The singlet states are separated by at least $|E^{\text{singlet}} - E^{\text{Cu-d}}| \approx 3.3$ eV from all other states. This energy is comparable to Δ_{pd} , the energy separation between the P and Q subspaces. But as there is no coupling between singlets and $\bar{\phi}$ holes, the relevant energy difference $|E^{\text{singlet}}| \approx 5.0$ eV between singlets and triplets is even larger. Together with the fact that matrix elements between the two spin combinations are small (second order in the perturbation), this allows us to neglect states with triplets or $\bar{\phi}$ holes and to consider only singlet states in the effective low-energy model.

The hopping of a singlet from site i to site j as described by Eq. (1.85) is always accompanied by the simultaneous hopping of the Cu- d hole on site j to site i . This allows us to formulate everything in terms of Cu- d holes only, with singlets corresponding to empty sites, i.e., the states $|i, \alpha\rangle$ are translated into $R_{i\alpha}^\dagger |0\rangle$. With respect to this new set of states the Hamiltonian

$$4t_{pd}^2 \lambda \left(\frac{2}{U - \Delta_{pd}} + \frac{1}{\Delta_{pd}} \right) \sum_{ij\sigma} \alpha(\Delta \mathbf{R}_{ij}) \tilde{c}_{i\sigma}^\dagger \tilde{c}_{j\sigma} \quad (1.86)$$

has off-diagonal matrix elements equivalent to those found for the effective model in Eq. (1.85) within the old formulation. By using constrained fermion operators

$\tilde{c}_{i\sigma}^\dagger = d_{i\sigma}^\dagger(1 - d_{i-\sigma}^\dagger d_{i-\sigma})$, we ensure that the Cu- d holes can only hop to empty sites as the states $R_{i\alpha}^\dagger|0\rangle$ do not contain doubly occupied sites. As $|\alpha(\mathbf{R})|$ decreases quickly with increasing $|\mathbf{R}|$ (e.g. $|\alpha(\hat{\mathbf{x}} + \hat{\mathbf{y}})/\alpha(\hat{\mathbf{x}})| = 0.17$), it is a good approximation to consider only terms in Eq. (1.86) that describe hopping between nearest-neighbor sites. If we incorporate our other results for the effective Hamiltonian, we arrive at the so-called t - J model [29]

$$H_{t-J} = -t \sum_{\langle i,j \rangle \sigma} \left(\tilde{c}_{i\sigma}^\dagger \tilde{c}_{j\sigma} + \tilde{c}_{j\sigma}^\dagger \tilde{c}_{i\sigma} \right) + J \sum_{\langle i,j \rangle} \left(\mathbf{S}_i \cdot \mathbf{S}_j - \frac{1}{4} n_i n_j \right) \quad (1.87)$$

$$+ \sum_i \left(E^{\text{Cu-}d} n_i + E^{\text{singlet}} (1 - n_i) \right) + E_0,$$

where

$$t = -4t_{pd}^2 \lambda \alpha(\hat{\mathbf{x}}) \left(\frac{2}{U - \Delta_{pd}} + \frac{1}{\Delta_{pd}} \right). \quad (1.88)$$

With our usual parameters, one finds $t \approx 0.5$ eV. The smallness of the off-diagonal elements in the effective Hamiltonian justifies that we only considered the diagonal elements in discussing the energy separation of the singlet states from all other states. The second term in Eq. (1.87) is the antiferromagnetic interaction between the spins of the Cu- d holes from Eq. (1.54) that is obtained in fourth order perturbation theory. In the second line of Eq. (1.87), the contributions to the total energy in zeroth and second order in the perturbation are included. For a fixed number of holes, they only give a constant energy shift and could also be left away. But when the on-site energies of the order of several eV (cf. Fig. 1.2) are modulated by lattice distortions, they can become an important source for electron-phonon coupling as we will see in the following. The model in Eq. (1.87) is defined for an arbitrary number of doped holes although the terms were derived explicitly only for the undoped system or the system with one additional hole. So, possible interactions between doped charge carriers are neglected.

1.5 t - J model with phonons

We now include the effects of lattice distortions into the effective low-energy model of the three-band model. We work to linear order in the atomic displacements u and up to second order in t_{pd} , the parameter treated as a perturbation already in the case of an undistorted lattice. Therefore, we derive an effective Hamiltonian in the form of Eq. (1.47) which includes all terms up to order $t_{pd}^2 u$.

As before, we consider a system doped with one additional hole and later generalize to arbitrary dopings. We restrict ourselves to states in the P subspace with a ϕ - d singlet. It was shown in the previous section that these are the relevant low-energy states in the undistorted lattice, and we assume that the effect of lattice distortions does not lead to a qualitative change of this picture.¹ In the following, we therefore calculate the matrix elements of the different terms in H_{eff} with respect to the states $|i, \alpha\rangle$ introduced in Eq. (1.56).

In the term in Eq. (1.47) which is linear in the perturbation V ,

$$PVP = PV^{(\varepsilon)}P, \quad (1.89)$$

only the modulation of the level energies $V^{(\varepsilon)}$ contributes as $V^{(0)}$ and $V^{(t)}$ do not connect states within the P subspace. The diagonal elements of Eq. (1.89) are given by

$$\langle i, \alpha | V^{(\varepsilon)} | i, \alpha \rangle = \sum_j \Delta\varepsilon_j^d + \sum_{j\delta} \frac{\Delta\varepsilon_{j\delta}^p}{4} |\gamma(\Delta\mathbf{R}_{ij}) - \gamma(\Delta\mathbf{R}_{ij} - 2\delta)|^2 \quad (1.90)$$

when we use Eq. (1.17). The first term on the right hand side of Eq. (1.90) vanishes as we assume that there is no ($\mathbf{q} = \mathbf{0}$)-contribution to the modulation of the level energies which would merely amount to a global renormalization of ε^d and ε^p . In the second term, the modulations of the level energies of the four nearest-neighbor p orbitals with respect to the Cu- d orbital at site i are multiplied by $(\gamma_0 - \gamma_1)^2/4 = \alpha(\mathbf{0})^2/4 = \lambda^2/4$. The importance of all remaining terms can be estimated as follows.

$$\begin{aligned} \sum'_{j\delta} \frac{\Delta\varepsilon_{j\delta}^p}{4} |\gamma(\Delta\mathbf{R}_{ij}) - \gamma(\Delta\mathbf{R}_{ij} - 2\delta)|^2 &\leq \frac{\Delta\varepsilon_{\text{max}}^p}{4} \sum'_{j\delta} |\gamma(\Delta\mathbf{R}_{ij}) - \gamma(\Delta\mathbf{R}_{ij} - 2\delta)|^2 \\ &= \Delta\varepsilon_{\text{max}}^p (1 - \lambda^2). \end{aligned} \quad (1.91)$$

The prime on the summation symbol indicates that the four p orbitals which are nearest neighbors to the Cu- d orbital at site i are not included in the sum. The individual p level modulations are replaced by the maximum amplitude of the modulation, $\Delta\varepsilon_{\text{max}}^p$. In the second line of Eq. (1.91) we used that

$$\begin{aligned} \sum_{j\delta} |\gamma(\Delta\mathbf{R}_{ij}) - \gamma(\Delta\mathbf{R}_{ij} - 2\delta)|^2 & \quad (1.92) \\ &= \frac{1}{N^2} \sum_{j\delta} \sum_{\mathbf{k} \neq \mathbf{0}} \sum_{\mathbf{k}' \neq \mathbf{0}} \beta_{\mathbf{k}} \beta_{\mathbf{k}'} e^{i(\mathbf{k}-\mathbf{k}')(\mathbf{R}_i - \mathbf{R}_j)} (1 - e^{-i2\mathbf{k}\delta}) (1 - e^{i2\mathbf{k}'\delta}) \end{aligned}$$

¹Our later results for the electron-phonon coupling justify this assumption. One finds from a simple estimate that the amplitude of the modulation of the effective level energies in the t - J model is only about 10% of the singlet-triplet splitting when parameters typical for the cuprates are used.

$$\begin{aligned}
&= \frac{4}{N} \sum_{\boldsymbol{\delta}} \sum_{\mathbf{k} \neq \mathbf{0}} \frac{[\sin(\mathbf{k}\boldsymbol{\delta})]^2}{[\sin(k_x a/2)]^2 + [\sin(k_y a/2)]^2} \\
&= 4 \frac{N-1}{N} \rightarrow 4 \quad \text{for } N \rightarrow \infty.
\end{aligned}$$

According to Eq. (1.91), we only make an error of order $1 - \lambda^2$ by approximating

$$\langle i, \alpha | V^{(\varepsilon)} | i, \alpha \rangle \approx \frac{\lambda^2}{4} \sum_{\boldsymbol{\delta}} \left(\Delta \varepsilon_{i\boldsymbol{\delta}}^p + \Delta \varepsilon_{(i-2\boldsymbol{\delta})\boldsymbol{\delta}}^p \right). \quad (1.93)$$

Non-vanishing off-diagonal elements of Eq. (1.89) are given by

$$\begin{aligned}
\langle j, \alpha' | V^{(\varepsilon)} | i, \alpha \rangle &= \sum_{l\boldsymbol{\delta}\sigma} \frac{\Delta \varepsilon_{l\boldsymbol{\delta}}^p}{4} \langle j, \alpha' | \phi_{j\sigma}^\dagger \phi_{i\sigma} | i, \alpha \rangle \times \\
&\times (\gamma(\Delta \mathbf{R}_{jl}) - \gamma(\Delta \mathbf{R}_{jl} - 2\boldsymbol{\delta})) (\gamma(\Delta \mathbf{R}_{li}) - \gamma(\Delta \mathbf{R}_{li} + 2\boldsymbol{\delta})).
\end{aligned} \quad (1.94)$$

As before, we consider only nearest-neighbor hopping ($j = i \pm 2\boldsymbol{\delta}$) where the singlet and a Cu- d hole swap their sites. The state $|j, \alpha'\rangle$ is defined as in Eq. (1.74), and with

$$\langle j, \alpha' | \sum_{\sigma} \phi_{j\sigma}^\dagger \phi_{i\sigma} | i, \alpha \rangle = -s(i, \alpha, j) \frac{1}{2} \quad (1.95)$$

one obtains for instance

$$\begin{aligned}
\langle i + 2\boldsymbol{\delta}, \alpha' | V^{(\varepsilon)} | i, \alpha \rangle &\approx \frac{s(i, \alpha, j)}{8} \lambda \left[\lambda \Delta \varepsilon_{i\boldsymbol{\delta}}^p \right. \\
&+ (\gamma_2 - \gamma_1) (\Delta \varepsilon_{(i-2\boldsymbol{\delta})\boldsymbol{\delta}}^p + \Delta \varepsilon_{(i+2\boldsymbol{\delta})\boldsymbol{\delta}}^p) \\
&\left. + (\gamma_{11} - \gamma_1) (\Delta \varepsilon_{i\bar{\boldsymbol{\delta}}}^p + \Delta \varepsilon_{(i-2\bar{\boldsymbol{\delta})}\bar{\boldsymbol{\delta}}}^p + \Delta \varepsilon_{(i+2\boldsymbol{\delta})\bar{\boldsymbol{\delta}}}^p + \Delta \varepsilon_{(i+2\boldsymbol{\delta}-2\bar{\boldsymbol{\delta})}\bar{\boldsymbol{\delta}}}^p) \right].
\end{aligned} \quad (1.96)$$

We include only the leading term $\propto \lambda$ from the modulation of the seven p orbitals which are nearest neighbors to the d orbitals at sites i and j .

Next, we consider terms in H_{eff} which are of second order in V .

$$\begin{aligned}
PVR_0VP &= P(V^{(0)} + V^{(t)})R_0(V^{(0)} + V^{(t)})P \\
&\approx PV^{(0)}R_0V^{(0)}P + PV^{(0)}R_0V^{(t)}P + PV^{(t)}R_0V^{(0)}P.
\end{aligned} \quad (1.97)$$

In the second line of Eq. (1.97), the term containing twice $V^{(t)}$ is neglected as we only work up to linear order in the displacements. The first of the remaining three terms was already discussed when the undistorted lattice was considered. Terms containing $\bar{\phi}$ in $V^{(t)}$ can be neglected since $V^{(0)}$ does not connect states from the P subspace to intermediate states with holes in $\bar{\phi}$ orbitals. Like $V^{(0)}$, the remaining part of $V^{(t)}$ is proportional to $d_{i\sigma}^\dagger \phi_{j\sigma} + \phi_{j\sigma}^\dagger d_{i\sigma}$. Therefore, the two other terms in the second line of

Eq. (1.97) can be evaluated using the same intermediate states that were considered for $PV^{(0)}R_0V^{(0)}P$ in the undistorted lattice, only the matrix elements differ. For the diagonal elements, one finds as the leading contribution

$$\begin{aligned} & \langle i, \alpha | V^{(0)}R_0V^{(t)} + V^{(t)}R_0V^{(0)} | i, \alpha \rangle \\ & \approx \sum_j \left[-(1 - \delta_{j,i}) \frac{2\lambda^2 t_{pd}}{\Delta_{pd}} - \delta_{j,i} \left(\frac{4\lambda^2 t_{pd}}{\Delta_{pd}} + \frac{4\lambda^2 t_{pd}}{U - \Delta_{pd}} \right) \right] \sum_{\delta} \sum_{s=\pm} \Delta t_{j(s\delta)}. \end{aligned} \quad (1.98)$$

The corresponding result for the off-diagonal elements in case of nearest-neighbor hopping is

$$\begin{aligned} & \langle i \pm 2\delta, \alpha' | V^{(0)}R_0V^{(t)} + V^{(t)}R_0V^{(0)} | i, \alpha \rangle \\ & \approx s(i, \alpha, j) \frac{\lambda t_{pd}}{2} \left(\frac{2}{U - \Delta_{pd}} + \frac{1}{\Delta_{pd}} \right) \left[\alpha(\hat{\mathbf{x}}) \sum_{\delta'} \sum_{s=\pm} (\Delta t_{i(s\delta')} + \Delta t_{j(s\delta')}) \right. \\ & \quad - \lambda (\Delta t_{i(\pm\delta)} + \Delta t_{j(\mp\delta)}) + (\gamma_1 - \gamma_2) (\Delta t_{i(\mp\delta)} + \Delta t_{j(\pm\delta)}) \\ & \quad \left. + (\gamma_1 - \gamma_{11}) (\Delta t_{i(+\bar{\delta})} + \Delta t_{i(-\bar{\delta})} + \Delta t_{j(+\bar{\delta})} + \Delta t_{j(-\bar{\delta})}) \right] \end{aligned} \quad (1.99)$$

which includes all leading terms proportional to λ .

Finally, we discuss contributions to the effective model which are of third order in the perturbation:

$$\begin{aligned} & PV R_0 V R_0 V P - \frac{1}{2} PV (P V R_0^2 + R_0^2 V P) V P \\ & \approx PV^{(0)} R_0 V^{(\varepsilon)} R_0 V^{(0)} P - \frac{1}{2} PV^{(\varepsilon)} P V^{(0)} R_0^2 V^{(0)} P - \frac{1}{2} P V^{(0)} R_0^2 V^{(0)} P V^{(\varepsilon)} P. \end{aligned} \quad (1.100)$$

In the second line of Eq. (1.100), only terms are kept that are of first order in the atomic displacements. Terms in $V^{(\varepsilon)}$ that contain $\bar{\phi}$ do not contribute to them and can be neglected. For the diagonal elements of Eq. (1.100), analogous to the treatment of corresponding lower order terms, we only include intermediate states where holes hop between orbitals localized on the same site. Therefore, only terms in $V^{(\varepsilon)}$ contribute that are proportional to $\phi_{j\sigma}^\dagger \phi_{j\sigma}$ or $d_{j\sigma}^\dagger d_{j\sigma}$. They do not alter states to which they are applied to. For this reason, the same intermediate states can be used that were considered already for the diagonal elements of the second-order terms in the effective Hamiltonian, and we find as the leading contribution (proportional to powers of λ)

$$\begin{aligned} & \langle i, \alpha | (V^{(0)}R_0V^{(\varepsilon)}R_0V^{(0)} - \frac{1}{2}V(PVR_0^2 + R_0^2VP)V) | i, \alpha \rangle \\ & \approx \sum_j \left[(1 - \delta_{j,i}) \frac{4\lambda^2 t_{pd}^2}{\Delta_{pd}^2} + \delta_{j,i} \left(\frac{8\lambda^2 t_{pd}^2}{\Delta_{pd}^2} - \frac{8\lambda^2 t_{pd}^2}{(U - \Delta_{pd})^2} \right) \right] \times \\ & \quad \times \left[\frac{\lambda^2}{4} \sum_{\delta} (\Delta \varepsilon_{j\delta}^p + \Delta \varepsilon_{(j-2\delta)\delta}^p) - \Delta \varepsilon_j^d \right]. \end{aligned} \quad (1.101)$$

The off-diagonal elements for nearest-neighbor hopping are given by

$$\begin{aligned}
& \langle i + 2\boldsymbol{\delta}, \alpha' | (V^{(0)} R_0 V^{(\varepsilon)} R_0 V^{(0)} - \frac{1}{2} V (P V R_0^2 + R_0^2 V P) V) | i, \alpha \rangle \\
& \approx s(i, \alpha, j) 2\lambda t_{pd}^2 \left(\frac{2}{(U - \Delta_{pd})^2} - \frac{1}{\Delta_{pd}^2} \right) \times \\
& \times \left\{ \alpha(\hat{\mathbf{x}}) \left[\frac{\lambda^2}{4} \sum_{\boldsymbol{\delta}} (\Delta\varepsilon_{i\boldsymbol{\delta}}^p - \Delta\varepsilon_{(i-2\boldsymbol{\delta})\boldsymbol{\delta}}^p + \Delta\varepsilon_{j\boldsymbol{\delta}}^p - \Delta\varepsilon_{(j-2\boldsymbol{\delta})\boldsymbol{\delta}}^p) - \Delta\varepsilon_i^d - \Delta\varepsilon_{i+2\boldsymbol{\delta}}^d \right] \right. \\
& \quad - \frac{1}{4} \left[\lambda^3 \Delta\varepsilon_{i\boldsymbol{\delta}}^p + \lambda^2 (\gamma_2 - \gamma_1) (\Delta\varepsilon_{(i-2\boldsymbol{\delta})\boldsymbol{\delta}}^p + \Delta\varepsilon_{(i+2\boldsymbol{\delta})\boldsymbol{\delta}}^p) \right. \\
& \quad \left. \left. + \lambda^2 (\gamma_{11} - \gamma_1) (\Delta\varepsilon_{i\bar{\boldsymbol{\delta}}}^p + \Delta\varepsilon_{(i-2\bar{\boldsymbol{\delta}})\bar{\boldsymbol{\delta}}}^p + \Delta\varepsilon_{(i+2\boldsymbol{\delta})\bar{\boldsymbol{\delta}}}^p + \Delta\varepsilon_{(i+2\boldsymbol{\delta}-2\bar{\boldsymbol{\delta}})\bar{\boldsymbol{\delta}}}^p) \right] \right\}.
\end{aligned} \tag{1.102}$$

The first term within the curly brackets in Eq. (1.102) is due to the site-diagonal terms (proportional to $\phi_i^\dagger \phi_i$ or $d_i^\dagger d_i$) in $V^{(\varepsilon)}$. As they do not change the states to which they are applied to, we can use the same intermediate states that were employed for the off-diagonal elements of the second-order contributions to H_{eff} . The remaining part of Eq. (1.102) is obtained from the site-off-diagonal terms in $V^{(\varepsilon)}$ proportional to $\phi_i^\dagger \phi_j$. We only consider the modulation of the seven p orbitals which are nearest neighbors to the d orbitals on sites i and j thereby keeping only the leading contributions which contain at most one geometrical prefactor (like $\alpha(\hat{\mathbf{x}})$ or combinations of $\gamma(\mathbf{R})$) other than powers of λ .

So far, we considered the effect of static lattice distortions on the effective low-energy model. We now assume that these distortions are caused by the vibrations of the atoms around their equilibrium positions, i.e., by phonons. By adding

$$H_{\text{ph}} = \sum_{\mathbf{q}\nu} \hbar \omega_{\mathbf{q}\nu} b_{\mathbf{q}\nu}^\dagger b_{\mathbf{q}\nu} \tag{1.103}$$

to the effective low-energy Hamiltonian, their kinetic and potential energy is included (except for the zero-point energy which we neglect as an unimportant constant energy shift). The phonon operator $b_{\mathbf{q}\nu}^\dagger$ creates a phonon from branch ν with wavevector \mathbf{q} and eigenfrequency $\omega_{\mathbf{q}\nu}$. The atomic displacements are then given by

$$\mathbf{u}_{\text{Cu},i} = \frac{1}{\sqrt{N}} \sum_{\mathbf{q}\nu} \sqrt{\frac{\hbar}{2\omega_{\mathbf{q}\nu}}} (b_{\mathbf{q}\nu} + b_{-\mathbf{q}\nu}^\dagger) \frac{\boldsymbol{\epsilon}_{\text{Cu}}(\mathbf{q}, \nu)}{\sqrt{M_{\text{Cu}}}} e^{i\mathbf{q}\cdot\mathbf{R}_i}, \tag{1.104}$$

$$\mathbf{u}_{\text{O},i\boldsymbol{\delta}} = \frac{1}{\sqrt{N}} \sum_{\mathbf{q}\nu} \sqrt{\frac{\hbar}{2\omega_{\mathbf{q}\nu}}} (b_{\mathbf{q}\nu} + b_{-\mathbf{q}\nu}^\dagger) \frac{\boldsymbol{\epsilon}_{\text{O}\boldsymbol{\delta}}(\mathbf{q}, \nu)}{\sqrt{M_{\text{O}}}} e^{i\mathbf{q}\cdot(\mathbf{R}_i + \boldsymbol{\delta})}, \tag{1.105}$$

with the polarization vectors $\boldsymbol{\epsilon}_{(i)}(\mathbf{q}, \nu) = (\epsilon_{(i)}^{\hat{x}/2}, \epsilon_{(i)}^{\hat{y}/2})$ for $(i) \in \{\text{Cu}, \text{O}_{\hat{x}/2}, \text{O}_{\hat{y}/2}\}$ and the atom masses M_{Cu} and M_{O} . The matrix elements of the effective Hamiltonian depend on the lattice distortions through $\Delta t_{i(\pm\delta)}$, ϵ_i^d , and $\epsilon_{i\delta}^p$. By expressing these modulations first in terms of the atomic displacements as in Eqs. (1.27), (1.31), and (1.32), we can then make the transition to second quantization using Eqs. (1.104) and (1.105).

Considering again sites with singlets as empty sites, we arrive at the following t - J model with electron-phonon interaction as an effective low-energy model:

$$H = H_{t-J} + H_{\text{ph}} + H_{\text{ep}}, \quad (1.106)$$

where H_{t-J} is the effective Hamiltonian for the undistorted lattice from Eq. (1.87), and H_{ph} from Eq. (1.103) describes the non-interacting phonon modes in the system. The interaction between electronic and lattice degrees of freedom is given by

$$H_{\text{ep}} = \frac{1}{\sqrt{N}} \sum_{ij\sigma} \tilde{c}_{i\sigma}^\dagger \tilde{c}_{j\sigma} \sum_{\mathbf{q}\nu} g_{ij}(\mathbf{q}, \nu) (b_{\mathbf{q}\nu} + b_{-\mathbf{q}\nu}^\dagger) \quad (1.107)$$

with the coupling constant

$$g_{ij}(\mathbf{q}, \nu) = i \sqrt{\frac{\hbar}{2\omega_{\mathbf{q}\nu}}} e^{i\mathbf{q}\cdot(\mathbf{R}_i + \mathbf{R}_j)/2} [A(\mathbf{q}, \nu) \delta_{i,j} + \sum_{\boldsymbol{\delta}} \sum_{s=\pm} B^{\boldsymbol{\delta}}(\mathbf{q}, \nu) \delta_{i,j+s2\boldsymbol{\delta}}]. \quad (1.108)$$

On the one hand, the phonons couple to the on-site energies in the t - J model with the coefficient

$$A(\mathbf{q}, \nu) = A^{(t)}(\mathbf{q}, \nu) + A^{(\epsilon)}(\mathbf{q}, \nu), \quad (1.109)$$

where we further distinguish between contributions arising from the modulation of the p - d hopping in the three-band model,

$$A^{(t)}(\mathbf{q}, \nu) = 4\lambda^2 t_{pd} \left. \frac{dt_{pd}}{dr} \right|_0 \left(\frac{2}{U - \Delta_{pd}} + \frac{1}{\Delta_{pd}} \right) \sum_{\boldsymbol{\delta}'} \frac{\epsilon_{\text{O}\boldsymbol{\delta}'}^{\boldsymbol{\delta}'}}{\sqrt{M_{\text{O}}}} s_{\boldsymbol{\delta}'}, \quad (1.110)$$

and those due to the modulation of the level energies in the three-band model,

$$\begin{aligned} A^{(\epsilon)}(\mathbf{q}, \nu) &= -2\lambda^2 \left. \frac{dU_{pd}}{dr} \right|_0 \sum_{\boldsymbol{\delta}'} \frac{\epsilon_{\text{Cu}}^{\boldsymbol{\delta}'}}{\sqrt{M_{\text{Cu}}}} s_{\boldsymbol{\delta}'} c_{\boldsymbol{\delta}'} + 8\lambda^2 t_{pd}^2 \left. \frac{dU_{pd}}{dr} \right|_0 \times \\ &\times \left(\frac{2}{(U - \Delta_{pd})^2} - \frac{1}{\Delta_{pd}^2} \right) \left[2 \sum_{\boldsymbol{\delta}'} \frac{\epsilon_{\text{O}\boldsymbol{\delta}'}^{\boldsymbol{\delta}'}}{\sqrt{M_{\text{O}}}} s_{\boldsymbol{\delta}'} + \lambda^2 \sum_{\boldsymbol{\delta}'} \frac{\epsilon_{\text{Cu}}^{\boldsymbol{\delta}'}}{\sqrt{M_{\text{Cu}}}} s_{\boldsymbol{\delta}'} c_{\boldsymbol{\delta}'} \right], \end{aligned} \quad (1.111)$$

using the abbreviation $s_{\boldsymbol{\delta}} = \sin(\mathbf{q} \cdot \boldsymbol{\delta})$. $A^{(t)}(\mathbf{q}, \nu)$ is derived from the diagonal matrix elements from Eq. (1.98) whereas $A^{(\epsilon)}(\mathbf{q}, \nu)$ is obtained from those in Eqs. (1.93) and

(1.98). In these matrix elements, terms proportional to $1 - \delta_{j,i}$ describe modulation of the Cu- d self-energy and therefore coupling to the d hole density n_i . Those proportional to $\delta_{j,i}$ and the contribution from Eq. (1.93) enter with the opposite sign as they are due to the modulation of the singlet self-energy and couple to empty sites measured by $1 - n_i$.

On the other hand, the phonons modulate also the effective hopping in the t - J model with the coefficient

$$B^\delta(\mathbf{q}, \nu) = B^{\delta,(t)}(\mathbf{q}, \nu) + B^{\delta,(\varepsilon)}(\mathbf{q}, \nu) \quad (1.112)$$

which we split analogously into

$$\begin{aligned} B^{\delta,(t)}(\mathbf{q}, \nu) &= \lambda t_{pd} \left. \frac{dt_{pd}}{dr} \right|_0 \left(\frac{2}{U - \Delta_{pd}} + \frac{1}{\Delta_{pd}} \right) \times \\ &\times \left[2\alpha(\hat{\mathbf{x}}) \sum_{\delta'} \frac{\epsilon_{O\delta'}^{\delta'}}{\sqrt{M_O}} s_{\delta'} c_\delta - \lambda \frac{\epsilon_{Cu}^\delta}{\sqrt{M_{Cu}}} s_\delta \right. \\ &\left. + (\gamma_1 - \gamma_2) \left(2 \frac{\epsilon_{O\delta}^\delta}{\sqrt{M_O}} c_\delta - \frac{\epsilon_{Cu}^\delta}{\sqrt{M_{Cu}}} \right) s_\delta + 2(\gamma_1 - \gamma_{11}) \frac{\epsilon_{O\bar{\delta}}^{\bar{\delta}}}{\sqrt{M_O}} s_{\bar{\delta}} c_\delta \right] \end{aligned} \quad (1.113)$$

from Eq. (1.99) and

$$\begin{aligned} B^{\delta,(\varepsilon)}(\mathbf{q}, \nu) &= 8\lambda\alpha(\hat{\mathbf{x}}) t_{pd}^2 \left. \frac{dU_{pd}}{dr} \right|_0 \left(\frac{2}{(U - \Delta_{pd})^2} - \frac{1}{\Delta_{pd}^2} \right) \times \\ &\times \left(2 \sum_{\delta'} \frac{\epsilon_{O\delta'}^{\delta'}}{\sqrt{M_O}} s_{\delta'} + \lambda^2 \sum_{\delta'} \frac{\epsilon_{Cu}^{\delta'}}{\sqrt{M_{Cu}}} s_{\delta'} c_{\delta'} \right) c_\delta \\ &+ \lambda \left. \frac{dU_{pd}}{dr} \right|_0 \left[\frac{1}{2} - 2\lambda^2 t_{pd}^2 \left(\frac{2}{(U - \Delta_{pd})^2} - \frac{1}{\Delta_{pd}^2} \right) \right] \times \\ &\times \left(\lambda \frac{\epsilon_{Cu}^\delta}{\sqrt{M_{Cu}}} s_\delta + 2(\gamma_2 - \gamma_1) \frac{\epsilon_{Cu}^\delta}{\sqrt{M_{Cu}}} (s_\delta - 2s_\delta^3) + 4(\gamma_{11} - \gamma_1) \frac{\epsilon_{Cu}^{\bar{\delta}}}{\sqrt{M_{Cu}}} s_{\bar{\delta}} c_{\bar{\delta}} c_\delta \right) \end{aligned} \quad (1.114)$$

from Eqs. (1.96) and (1.102).

This coupling differs slightly from the one given in Ref. [39]. In the present derivation, contributions to the second-order Cu- d self-energy of order $1 - \lambda^2$ were neglected which were explicitly considered previously. In the treatment of the modulation of the O - p level energies, the prefactor λ^2 was approximated by 1 in Ref. [39] where also the direct hopping between ϕ levels induced by this modulation was neglected. Finally, in Eq. (6) in Ref. [39], there is a misprint. In the second-last term, s_y ($= \sin(q_y a/2)$) must be replaced by $\sin(q_y a)$.

1.6 Summary

To summarize, with Eqs. (1.106)-(1.114) we have obtained an effective low-energy model for the description of electron-phonon interaction in (doped) cuprates. In order to achieve this, we started out from the three-band model for the CuO_2 planes. The effects of lattice distortions on its parameters can be quite directly estimated in a physically reasonable way. We take into account not only the modulation of the p - d hopping, but also the change in level energies due to the screened Coulomb interaction. After changing to a suitable representation of the O- p orbitals, an effective low-energy model can be derived by projecting out high-energy states. The general formalism is first applied to the three-band model for the undistorted lattice. At low energies, doped holes are found to lead to Zhang-Rice singlets whose hopping in a background of antiferromagnetically interacting spins is described by the resulting effective model, the t - J model. By generalizing the derivation to the distorted lattice, the interaction with phonons is included into the effective low-energy model. Both the effective hopping and the on-site energies in the t - J model are modulated by phonons.

The thus obtained model forms the basis for the discussion of the strong softening of certain phonon modes upon doping in the next chapter. In this context, we will also discuss the importance of different coupling mechanisms and compare with other approaches. In Chap. 3, we modify the coupling to allow for an appropriate description of electron-phonon coupling in the undoped cuprates where the screening of the Coulomb interaction is less effective. Finally, a generic form of the model is used in Chap. 4 to discuss in general electron-phonon interaction in the presence of strong electronic correlations.

Chapter 2

Anomalous softening of the half-breathing phonon

2.1 Introduction

Phonons in the high- T_c cuprates have been studied extensively by neutron scattering. See e.g. Refs. [17, 40] for reviews of the results. Experimental phonon dispersions for $\text{La}_{2-\delta}\text{Sr}_\delta\text{CuO}_4$ (filled circles) as well as results from a shell model calculation [16] (lines) are shown in Fig. 2.1 for the undoped and a 10% doped system (left and right panel, respectively). The shell model describes almost all phonon branches rather accurately in both the undoped and the doped compound.

The highest mode of Δ_1 symmetry, however, shows an anomalously strong softening upon doping. This softening is anomalous in the sense that it is not captured by the shell model. Whereas the phonon is quite well described in the undoped system, the calculations do not reproduce the strong softening seen experimentally half way along the $(1,0,0)$ direction. This mode is the so-called oxygen half-breathing phonon that describes an out-of-phase bond-stretching vibration of half of the oxygen atoms in the CuO_2 plane. The displacement pattern is shown schematically in the upper right corner of Fig. 2.3. Anomalies of such bond-stretching phonons have been observed not only in high- T_c cuprates [15, 41, 42, 18, 19, 43, 44, 45, 46] but also in other compounds [47, 48, 49]. This phonon mode also shows a large broadening in the doped system as illustrated in Fig. 2.2. The intrinsic broadening of the peak's full width at half maximum (FWHM) is about 1.2 THz or 5 meV for $\mathbf{q} = (\pi/a, 0, 0)$ in the 15% doped system. Both the softening and the width indicate that the half-breathing couples strongly to doped holes.

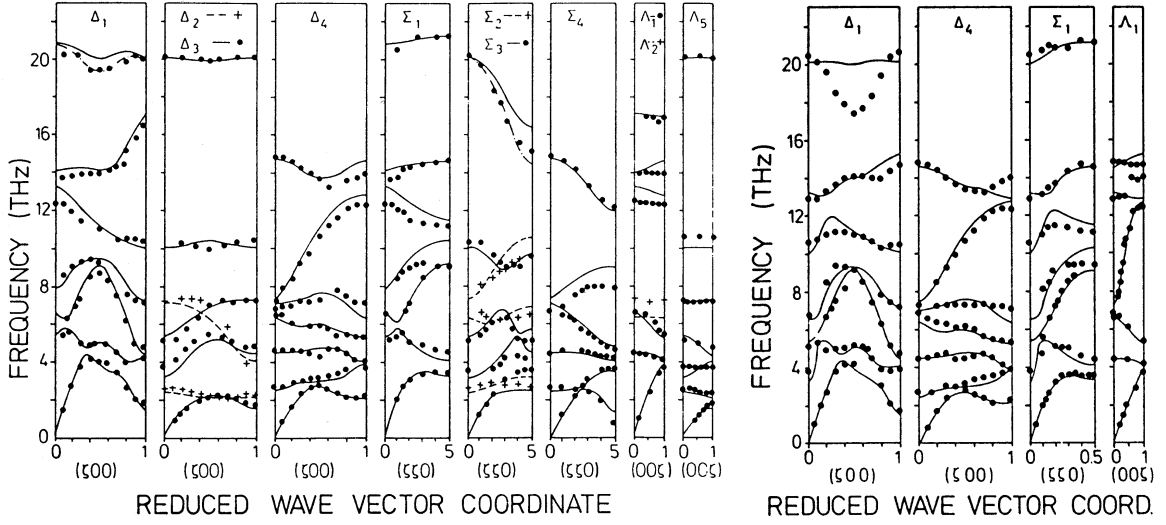


Figure 2.1: Phonon dispersions for La_2CuO_4 (left panel) and $\text{La}_{1.9}\text{Sr}_{0.1}\text{CuO}_4$ (right panel) calculated in a shell model [16] (lines) together with experimental results from neutron scattering (filled circles). The figure illustrates that the half-breathing mode in the Δ_1 symmetry at 20 THz and several apical oxygen modes in the Λ_1 symmetry at 12-16 THz are strongly softened upon doping.

Some phonons of Λ_1 symmetry also show a strong softening upon doping. These are modes which involve mainly the displacement of apical O atoms. One example is the so-called O_2^Z mode with the reduced wavevector $(0, 0, 1)$ that has an energy of about 17 THz in the undoped system (see Fig. 2.1). In the 15% doped system it softens by about 30% and has a large width of about 17 meV [17]. The softening is, however, well described by the shell model that takes into account the effect of doping only via the screening due to free carriers. In this sense, the softening of these phonons is not anomalous. But still a strong coupling to doped holes is suggested, and we will show in Chap. 3 that apical oxygen modes indeed couple strongly via the modulation of the electrostatic potential in the undoped system.

In this chapter, we focus on exploring the anomalous softening of the half-breathing mode within the effective low-energy model of the phonon-modulated CuO_2 plane derived in Chap. 1. First, we describe the numerical methods used to solve this model. Then, we discuss the results for softening and broadening of the half-breathing mode addressing also the dependences on the phonon wavevector and doping. We find a rather good correspondence between our calculations and experimental results. In order to judge the importance of strong correlations in this context, we also compare to results obtained in the Hartree-Fock mean-field approximation of the three-band

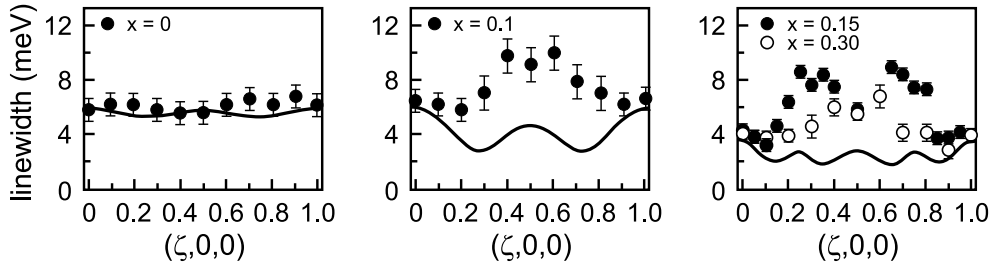


Figure 2.2: Width of the half-breathing phonon for $\text{La}_{2-x}\text{Sr}_x\text{CuO}_4$ as function of the reduced wavevector $(\xi, 0, 0)$ for the dopings $x = 0$ (left), $x = 0.1$ (middle), and $x = 0.15, 0.3$ (right). The full line shows the experimental resolution including focusing effects. The figure illustrates the large broadening for the doped system and the very small intrinsic broadening for the undoped system (after Pintschovius [40]).

model. Finally, we discuss various other aspects like the role of different coupling mechanisms, the importance of non-linear contributions to the electron-phonon interaction, and the coupling to other modes.

2.2 Numerical results for t - J model with phonons

For the electron-phonon interaction in the t - J model that we derived in the previous chapter, we want to evaluate the effect on phonon properties, especially the renormalization of the phonon frequencies.

We solve the t - J model with electron-phonon interaction from Eqs. (1.106)-(1.114) on finite clusters using exact diagonalization. This method is described in App. A and allows for an exact calculation of the ground state and dynamical correlation functions at zero temperature.

If we consider a system with N sites and K phonon modes, its Hilbert space is spanned by the basis $\{\otimes_{i=1}^N |\mu_i\rangle \otimes_{j=1}^K |\nu_j\rangle\}$. There is an electronic degree of freedom $|\mu_i\rangle$ on each site i which can be a fermion with spin up or down or an empty site. The total number of fermions with spin σ , N_σ , is conserved by our model. For fixed N_\uparrow and N_\downarrow corresponding to a doping $\delta = (N - \sum_\sigma N_\sigma)/N$, it then suffices to consider only the appropriate subset of all electronic configurations $\otimes_{i=1}^N |\mu_i\rangle$ which has the dimension $D_{\text{el}} = \binom{N}{N_\uparrow + N_\downarrow} \binom{N_\uparrow + N_\downarrow}{N_\uparrow}$. The phonon degrees of freedom $|\nu_j\rangle$ give the occupation number $\nu_j = 0, 1, \dots, \infty$ of each phonon mode j . There is infinitely many phonon configurations $\otimes_{j=1}^K |\nu_j\rangle$, but numerical calculations require a finite-dimensional Hilbert space, and only a finite subset can be included in the basis.

We choose to allow only for states with at most P phonons excited, i.e., $\sum_{i=1}^K \nu_i \leq P$. The dimension of the phonon Hilbert space is then given by $D_{\text{ph}} = \binom{K+P}{K}$ [50]. Thinking of the states $\otimes_{j=1}^K |\nu_j\rangle$ as eigenstates of the free phonon Hamiltonian $H_{\text{ph}} = \sum_j \hbar\omega_j b_j^\dagger b_j$, this corresponds to an energy cut-off if all modes have the same frequency. We typically consider modes corresponding to different wavevectors of the same optical phonon branch for which this is approximately true and the truncation scheme therefore seems physically reasonable. The results of the calculation in general depend on P , but converge to the results for the untruncated infinite Hilbert space for large enough P . The total dimension of the truncated Hilbert space is $D = D_{\text{el}} D_{\text{ph}}$.

We consider finite clusters that tile the infinite square lattice when translated by integer multiples of the vectors \mathbf{R}_a and \mathbf{R}_b which span the cluster. If $\mathbf{R}_a = a_x \hat{\mathbf{x}} + a_y \hat{\mathbf{y}}$ and $\mathbf{R}_b = b_x \hat{\mathbf{x}} + b_y \hat{\mathbf{y}}$ with $a_{x/y}, b_{x/y}$ being integers, the corresponding cluster has $N = |\mathbf{R}_a \times \mathbf{R}_b| = |a_x b_y - a_y b_x|$ sites. The choice $b_x = -a_y$ and $b_y = a_x$ gives (tilted) square clusters whereas for $a_y = b_x = 0$ one has rectangular clusters (later referred to as $a_x \times b_y$ clusters). For periodic boundary conditions, the allowed single-particle momenta are $\mathbf{k} = (b_y n_1 + a_y n_2)(2\pi/N)\hat{\mathbf{x}} + (b_x n_1 + a_x n_2)(2\pi/N)\hat{\mathbf{y}}$ for n_1, n_2 being integers which give N momenta in the first Brillouin zone. In general, we use twisted boundary conditions [51, 52] that amount to the conditions $\tilde{c}_{(i+\mathbf{R}_{a/b})\sigma} = e^{i\phi_{a/b}} \tilde{c}_{i\sigma}$ with arbitrary phases ϕ_a and ϕ_b . Periodic (anti-periodic) boundary conditions correspond to $\phi_a = \phi_b = 0$ (π). Twisted boundary conditions can be imposed by replacing $\tilde{c}_{i\sigma}^\dagger \tilde{c}_{j\sigma}$ by $e^{i\boldsymbol{\kappa}(\mathbf{R}_j - \mathbf{R}_i)} \tilde{c}_{i\sigma}^\dagger \tilde{c}_{j\sigma}$ in the site-off-diagonal terms of the Hamiltonian from Eq. (1.106) where $\boldsymbol{\kappa}$ is defined by $\phi_{a/b} = \boldsymbol{\kappa} \cdot \mathbf{R}_{a/b}$. The on-site terms as well as the exchange interaction remain unchanged. The discrete single-particle momenta are shifted by $\boldsymbol{\kappa}$, but bosonic correlation functions like the phonon Green's function are defined for momenta corresponding to difference vectors \mathbf{q} between these momenta. Therefore, irrespective of the chosen boundary conditions, the allowed \mathbf{q} values always equal those of the single-particle momenta \mathbf{k} for periodic boundary conditions.

We calculate the phonon spectral function

$$B_\nu(\mathbf{q}, \omega) = -\frac{1}{\pi} \text{Im} \langle\langle \hat{O}^\dagger; \hat{O} \rangle\rangle_\omega^{\text{ret}} \quad (2.1)$$

with $\hat{O} = b_{\mathbf{q}\nu} + b_{-\mathbf{q}\nu}^\dagger$ using exact diagonalization as described in appendix A.2. For the small finite clusters used in our calculations, we typically find spectra basically consisting of a single δ -function at the renormalized phonon frequency. In some cases, there is a split-up into a few peaks due to coupling to an electronic excitation with an energy close to the phonon frequency. In order to quantify the phonon softening in all cases, we use the center of gravity of the phonon spectrum for positive frequencies

$\omega > 0$ to define the renormalized phonon frequency:

$$\bar{\omega}_{\mathbf{q}\nu} = \frac{\int_0^\infty d\omega \omega B_\nu(\mathbf{q}, \omega)}{\int_0^\infty d\omega B_\nu(\mathbf{q}, \omega)} = \frac{\omega_{\mathbf{q}\nu}}{\langle 0 | \hat{O}^\dagger \hat{O} | 0 \rangle}. \quad (2.2)$$

The last term in Eq. (2.2) was obtained using

$$\int_0^\infty d\omega \omega B_\nu(\mathbf{q}, \omega) = \frac{1}{2} \int_{-\infty}^\infty d\omega \omega B_\nu(\mathbf{q}, \omega) = \frac{1}{2} \langle [[\hat{O}^\dagger, H]_-, \hat{O}]_- \rangle = \omega_{\mathbf{q}\nu}. \quad (2.3)$$

Therefore, the calculation of $\bar{\omega}_{\mathbf{q}\nu}$ only requires the expectation value of the operator $\hat{O}^\dagger \hat{O}$ in the ground state but not the full phonon spectral function.

We use realistic estimates for the parameters in the three-band model that enter the electron-phonon coupling in the effective low-energy model: $a = 3.8 \text{ \AA}$, $t_{pd} = 1.2 \text{ eV}$, $\Delta_{pd} = 3 \text{ eV}$, $U = 10 \text{ eV}$, and $U_{pd} = 1 \text{ eV}$ [53, 54, 55, 56, 57, 58]. The somewhat small value for t_{pd} partly compensates for the use of perturbation theory in obtaining the electron-phonon interaction in the t - J model and leads to a reasonable [59] $t = 0.47 \text{ eV}$ from Eq. (1.88) which will be used in the following. The expression for J from perturbation theory in Eq. (1.55) has an even smaller radius of convergence as function of t_{pd} [38]. We will therefore use the widely accepted value $J/t = 0.3$ instead of evaluating Eq. (1.55) for our parameters.

In the undoped system, the electron-phonon coupling is zero and the bare phonon frequencies $\omega_{\mathbf{q}\nu}$ are unrenormalized. Therefore, for our calculations, we determine the $\omega_{\mathbf{q}\nu}$ from the phonon dispersions of undoped La_2CuO_4 obtained in neutron scattering experiments [16, 15].

We fit a simple two-spring model of the CuO_2 plane with two different spring constants $\kappa_{\text{Cu-O}}$ and $\kappa_{\text{O-O}}$ for springs between nearest-neighbor Cu-O and O-O pairs, respectively, to the experimental dispersion of the (half-)breathing mode in undoped La_2CuO_4 in order to obtain the phonon polarization vectors for this mode. We used the values $\kappa_{\text{Cu-O}} = 7.86 \text{ eV/\AA}^2$ and $\kappa_{\text{O-O}} = 3.815 \text{ eV/\AA}^2$. The thus obtained polarization vectors are in good agreement with those found in a more realistic shell model calculation [53].

Both for obtaining the ground state and the phonon spectra, we use 160 iterations each in the Lanczos algorithm to ensure convergence of the exact diagonalization calculations. We find that the calculation of the phonon spectral function $B_\nu(\mathbf{q}, \omega)$ can be done for our model with sufficient accuracy by only including the modes from the ν -branch with wavevectors \mathbf{q} and $-\mathbf{q}$. Including more modes simultaneously only leads to very small changes, typically of the order of 0.1 meV for the renormalized phonon energies. All results in the following were obtained with only the pair of

modes included for which the phonon spectrum is calculated. For zone boundary modes like $\mathbf{q} = (\pi/a, \pi/a)$, only the single mode in question is considered. If there are degenerate modes like e.g. $\pm(\pi/(2a), 0)$ and $\pm(0, \pi/(2a))$ in the 4×4 cluster, all of them are included. The calculations were always done using all basis states with up to $P = 5$ excited phonons. This leads to converged results with an error of less than 0.1 meV for $\bar{\omega}_{\mathbf{q}\nu}$.

The calculations are done for different twisted boundary conditions. Both ϕ_a and ϕ_b are chosen out of the interval $[0; \pi[$. In order to reduce finite-size effects [52], we average $\bar{\omega}_{\mathbf{q}\nu}$ over the boundary conditions corresponding to this square in the ϕ_a - ϕ_b plane. We find that already averaging over the four corners, i.e., periodic, anti-periodic, and the two mixed boundary conditions ($\phi_a = 0$ (π), $\phi_b = \pi$ (0)), results in a value quite close to the one obtained from averaging over finer meshes. We therefore use only these four boundary conditions in the following.

2.2.1 Half-breathing and breathing modes

As discussed in the introduction to this chapter, anomalously strong softening upon doping is found in experiment for the optical phonon branch with the highest energy in $\text{La}_{2-\delta}\text{Sr}_\delta\text{CuO}_4$ (LSCO). Figure 2.3 shows the experimental dispersion of this branch for two different directions in the Brillouin zone ($\mathbf{q} = (\xi, \xi)$ and $\mathbf{q} = (\xi, 0)$, $\xi \in [0; \pi/a]$) and two different dopings ($\delta = 0$ and $\delta = 0.15$). The softening is largest towards the zone boundaries ($(\pi/a, \pi/a)$ and $(\pi/a, 0)$, respectively), and the half-breathing modes with $\mathbf{q} = (\xi, 0)$ are softened more strongly than the breathing modes with $\mathbf{q} = (\xi, \xi)$.

We now compare with results for our model obtained on a 4×4 cluster doped with 2 holes ($\delta = 0.125$, $N_\uparrow = N_\downarrow = 7$). The renormalized phonon frequencies for the five available wavevectors along the two \mathbf{q} directions are shown in Fig. 2.3. We average over periodic, anti-periodic and the two mixed boundary conditions. The error bars show the range of the results for the different boundary conditions. Despite the fairly large sensitivity on boundary conditions, the trends are clear. As the electron-phonon coupling in our model is zero for $\mathbf{q} = (0, 0)$, the frequency of this mode is unchanged compared to the undoped system. For the other wavevectors, we find a softening of the right order of magnitude when compared with experiment. We also reproduce the stronger softening of the half-breathing modes in agreement with experimental results.

We now specifically consider the half-breathing and the breathing mode at the

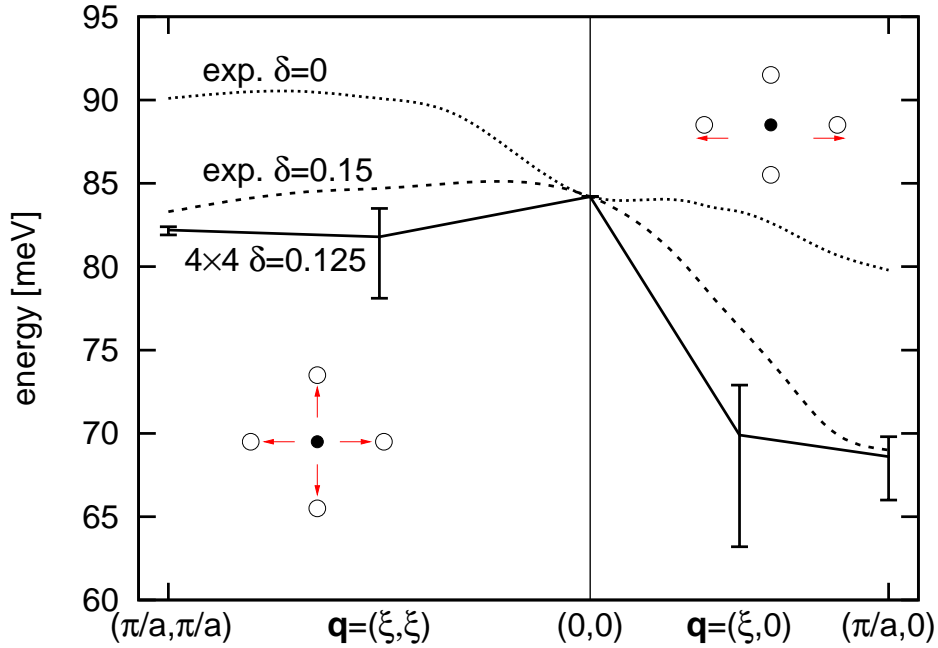


Figure 2.3: Phonon dispersions in the $(\xi, 0)$ and (ξ, ξ) directions. Experimental results (dotted line) are shown for $\text{La}_{2-\delta}\text{Sr}_\delta\text{CuO}_4$ with $\delta = 0$ and $\delta = 0.15$ [18]. Theoretical results (full line) for $\delta = 0.125$ show the calculated softening from the experimental $\delta = 0$ results. The average over boundary conditions is shown, and the bars show the spread due to different boundary conditions. There is a strong softening in the $(\xi, 0)$ direction, while the softening in the (ξ, ξ) direction is weaker. The insets show schematically the movements of oxygen atoms (open circles) in the CuO_2 plane in relation to Cu atoms (filled circles) for the two \mathbf{q} directions.

respective zone boundary. Figure 2.4 shows the corresponding phonon spectral functions. To obtain smooth spectra, a Lorentzian broadening is used. It is basically impossible to extract an intrinsic width of the phonon peak from the spectral function. Whereas for $\mathbf{q} = (1, 1)\pi/a$, the spectrum consists of virtually only a single pole, there are a few separate contributions to the $\mathbf{q} = (1, 0)\pi/a$ spectrum as indicated by the vertical lines. This might hint that the half-breathing mode is broadened more strongly, but no reliable quantitative prediction can be made.

Therefore, we calculate the phonon self-energy from the spectral function as described in App. A.3. First, a Hilbert transform can be used to obtain the phonon Green's function $D(\mathbf{q}, \omega)$ from the phonon spectral function $B(\mathbf{q}, \omega)$. The phonon

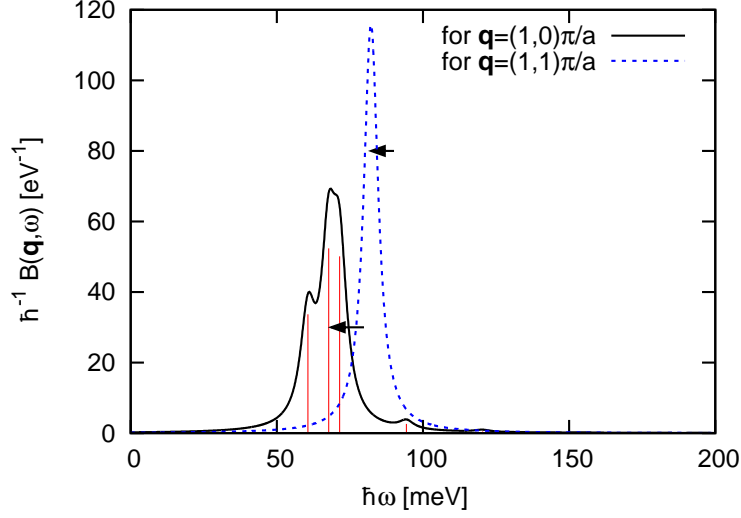


Figure 2.4: Phonon spectral functions for the half-breathing (full line) and the breathing mode (dashed line) for a 4×4 cluster, $\delta = 0.125$, and averaged over boundary conditions. A Lorentzian broadening with FWHM=6 meV was used. The arrows indicate the phonon softening ($\omega_{\mathbf{q}} \rightarrow \bar{\omega}_{\mathbf{q}}$). The vertical lines indicate energy and weight of the poles in the spectral function for the half-breathing phonon.

self-energy $\Pi(\mathbf{q}, \omega)$ is then calculated by inverting

$$D^{-1}(\mathbf{q}, \omega) = D_0^{-1}(\mathbf{q}, \omega) - \Pi(\mathbf{q}, \omega), \quad (2.4)$$

where $D_0(\mathbf{q}, \omega)$ is the non-interacting phonon Green's function. The result is shown in Fig. 2.5. Clearly, the self-energies for the half-breathing and the breathing mode have very different ω dependences. For $\mathbf{q} = (1, 0)\pi/a$, the spectral function of the self-energy is non-zero over an energy range of several eV. As expected from phase space arguments, it is linearly increasing with ω at low frequencies. Fitting $\alpha\hbar\omega$ to $\hbar \text{Im} \Pi(\mathbf{q}, \omega)$ within the range $[0; 0.5]$ eV gives $\alpha = 0.0107$ (independent of the broadening used). Then, for $\bar{\omega}_{\mathbf{q}} = 68.5$ meV one expects a phonon broadening with FWHM= $2\alpha\bar{\omega}_{\mathbf{q}} = 1.5$ meV. Although this is smaller than the experimental value of about 5 meV for 15% doped LSCO [18], we obtain the right order of magnitude. This result could not have been obtained from the phonon spectral function directly. For $\mathbf{q} = (1, 1)\pi/a$ on the other hand, the self-energy has only one dominant feature at high energies of several eV. At low frequencies, the self-energy is virtually zero. One expects therefore basically no contribution to the broadening of this mode from the electron-phonon interaction considered here. Also experimentally, the broadening of the breathing mode is found to be smaller than for the half-breathing mode [17].

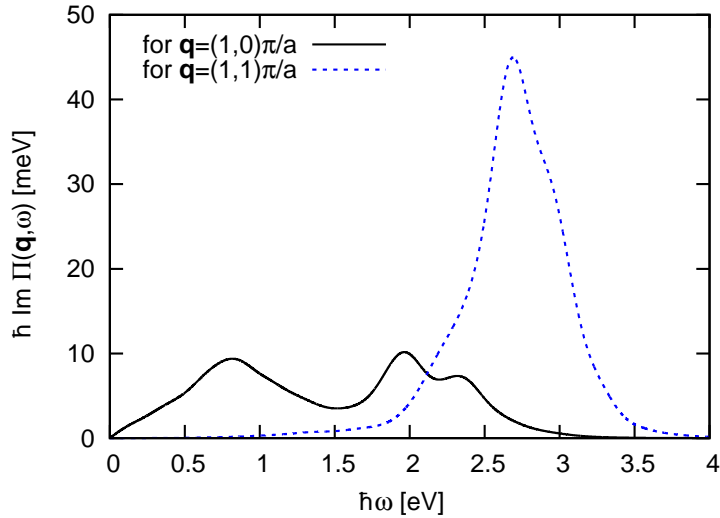


Figure 2.5: Imaginary part of the phonon self-energies for the half-breathing (full line) the and breathing mode (dashed line) for a 4×4 cluster, $\delta = 0.125$, and calculated from phonon spectra averaged over boundary conditions. A Gaussian broadening with FWHM=0.24 eV was used.

2.2.2 Doping dependence

We now study the doping dependence of the phonon softening in our model. First, we consider the dispersion of the half-breathing mode for \mathbf{q} along the $(\xi, 0)$ direction. We use all $a_x \times b_y$ rectangular clusters with an even number of (up to 20) sites and $a_x, b_y > 2$ that allow for \mathbf{q} points along $(0, 0) - (\pi/a, 0)$. These are the 4×4 square cluster and three rectangular clusters (4×3 , 6×3 , and 5×4). All clusters are doped with two holes keeping $N_\uparrow = N_\downarrow$. Therefore, the doping δ varies between 0.1 and 0.167 for the different cluster sizes. Figure 2.6 shows the corresponding renormalized phonon frequencies averaged over our four standard boundary conditions. For comparison, also the experimental dispersion for undoped La_2CuO_4 is shown which is used to define the bare phonon frequencies in our model. The softening increases with doping δ , e.g. at the zone boundary, the softening is 11% for $\delta = 0.1$ and 21% for $\delta = 0.167$. This is also observed experimentally, e.g. for $\text{La}_{2-\delta}\text{Sr}_\delta\text{CuO}_4$, the softening is about 11% for $\delta = 0.10$ [16, 15] and about 15.5% for $\delta = 0.15$ [18]. As a trend, we find for the few \mathbf{q} points available that the softening increases with \mathbf{q} approaching the zone boundary with irregularities probably due to finite-size effects.

To compare the doping dependence of the half-breathing and the breathing mode, we consider the respective zone boundary wavevector only. In addition to the pre-

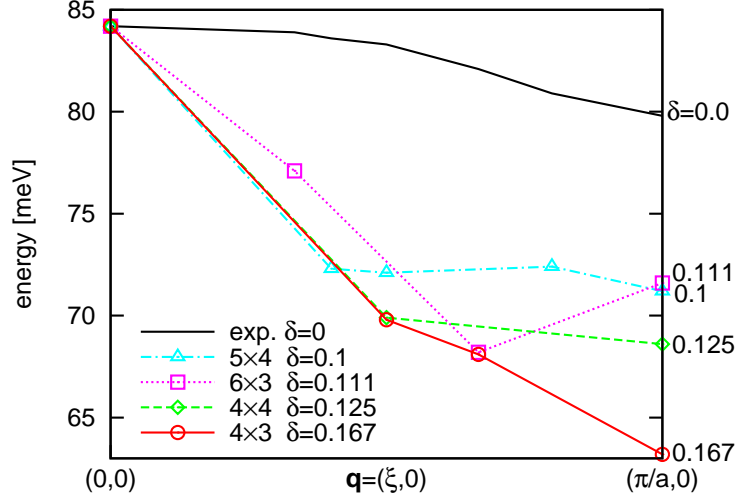


Figure 2.6: Phonon dispersion of the half-breathing mode in the $(\xi, 0)$ direction averaged over boundary conditions for clusters of different sizes. The corresponding doping δ is indicated. The figure shows that the softening increases with doping.

viously used clusters, we also use several tilted clusters that have been found [60] to be particularly useful for calculating estimates of properties of the infinite square lattice. We consider the bipartite clusters 10B, 12A/D, 14B, 16A, 4×4 (16B), 18A, 20A and the non-bipartite clusters 10A, 12B, 4×3 , 14A, 6×3 , 5×4 (employing the notation of Ref. [60] for the tilted clusters). The clusters are doped with two or (as far as computationally feasible) four holes, thereby extending the doping range up to $\delta = 0.333$. The renormalized frequencies of the two phonon modes averaged over boundary conditions and relative to the frequencies in the undoped system are shown in the left panel of Fig. 2.7. These results together with details on the used clusters are also listed in Tab. 2.1. One observes that also the softening of the breathing mode increases upon doping in agreement with experiment. For example, we obtain the relative phonon frequency 0.92 for $\delta = 0.125$, compared with the experimental results 0.97 ($\delta = 0.1$) and 0.92 ($\delta = 0.15$) [17]. In comparison with the half-breathing mode, however, the softening is weaker except for very large dopings. Whereas the softening of the breathing mode increases almost linearly with doping, one finds that the renormalization of the half-breathing mode increases more slowly towards higher doping. These trends agree with experimental results from neutron scattering [40] (reproduced in the left panel of Fig. 2.7) and inelastic x-ray scattering [61] where data for up to $\delta = 0.3$ also indicates some saturation of the softening of the half-breathing

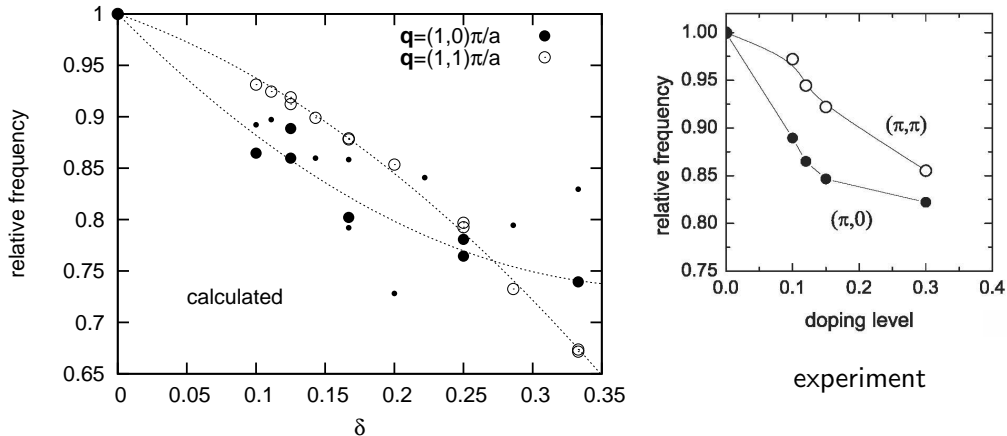


Figure 2.7: In the left panel, numerical results for the doping dependence of the softened phonon frequencies (relative to the frequencies in the undoped system) of the half-breathing ($\mathbf{q} = (1,0)\pi/a$, full circles, smaller diameter for non-bipartite clusters) and the breathing mode ($\mathbf{q} = (1,1)\pi/a$, empty circles) are shown. The dotted lines are second-order polynomials fitted to the results for bipartite clusters and serve to guide the eye. The right panel shows the corresponding experimental results for LSCO [40].

mode in overdoped samples. A similar trend has also been predicted by Ref. [62] using a slave-boson approach.

2.3 Three-band model in Hartree-Fock approximation

In this section, we study the three-band model with phonons in the Hartree-Fock (HF) mean-field approximation in contrast to the explicit treatment of strong electronic correlations in the derivation of an effective low-energy model in Chap. 1. We then compare the effects of the electron-phonon interaction in the two approaches in order to investigate the importance of strong correlations.

This is also motivated by extensive studies [63, 12, 64, 65] of phonons and electron-phonon interaction within the local density approximation (LDA) [66]. Bohnen *et al.* [65] found phonon frequencies in good agreement with experiment for $\text{YBa}_2\text{Cu}_3\text{O}_7$. In particular, the frequency of the half-breathing mode along the $(\xi, 0, 0)$ direction was correctly found to be anomalously soft. Since the LDA does not describe antifer-

cluster	$\mathbf{R}_a, \mathbf{R}_b$ [a]	bipartite	δ	\mathbf{q} [π/a]	rel. frequency
10A	(2, 3), (-2, 2)	no	0.2	(1, 0)	0.728
10B	(3, 1), (-1, 3)	yes	0.2	(1, 1)	0.853
12A	(2, 2), (-4, 2)	yes	0.167	(1, 0) & (0, 1)	0.802
				(1, 1)	0.879
			0.333	(1, 0) & (0, 1)	0.739
				(1, 1)	0.674
12B	(2, 3), (-2, 3)	no	0.167	(1, 0)	0.858
			0.333	(1, 0)	0.830
12D	(1, 3), (4, 0)	yes	0.167	(1, 1)	0.878
			0.333	(1, 1)	0.671
14A	(3, 2), (-1, 4)	no	0.143	(0, 1)	0.860
			0.286	(0, 1)	0.794
14B	(4, 2), (-1, 3)	yes	0.143	(1, 1)	0.899
			0.286	(1, 1)	0.733
16A	(4, 2), (0, 4)	yes	0.125	(1, 0) & (0, 1)	0.888
				(1, 1)	0.912
			0.25	(1, 0) & (0, 1)	0.764
				(1, 1)	0.792
16B	(4, 0), (0, 4)	yes	0.125	(1, 0) & (0, 1)	0.860
				(1, 1)	91.9
			0.25	(1, 0) & (0, 1)	0.781
				(1, 1)	0.797
18A	(3, 3), (-3, 3)	yes	0.111	(1, 1)	0.925
6×3	(6, 0), (0, 3)	no	0.111	(1, 0)	0.897
			0.222	(1, 0)	0.841
20A	(4, 2), (-2, 4)	yes	0.1	(1, 0) & (0, 1)	0.865
				(1, 1)	0.931
5×4	(5, 0), (0, 4)	no	0.1	(0, 1)	0.892

Table 2.1: This table lists more details to the results displayed in Fig. 2.7. For each cluster used, it gives the basic translation vectors and shows whether the cluster is bipartite. The dopings and phonon wavevectors which were considered are then listed together with the corresponding softened frequency (averaged over boundary conditions) relative to the frequency in the undoped system.

romagnetism in the undoped system, however, it cannot properly describe phonons in the undoped case. It is therefore not clear how much the phonon is softened upon doping in the LDA. Furthermore, LDA calculations show a weak electron-phonon coupling to the half-breathing phonon, with λ at the zone boundary being ≈ 0.01 [65]. This is in disagreement with the large width of the half-breathing phonon, which is believed to be due to a rather strong electron-phonon coupling. The weak coupling raises questions about the reasons for the low frequency of the half-breathing phonon in the LDA calculation for the doped system.

The HF mean-field approximation of the three-band model may be expected to simulate features of the LDA for the doped system. For instance, we find a similarly small width of the half-breathing phonon like in LDA. In contrast to LDA, however, this approximation gives an antiferromagnetic solution for the undoped system. We can therefore obtain the softening upon doping within this framework. The softening of the half-breathing phonon is indeed found to be of the same order of magnitude as the experimental result, supporting the idea that the LDA can describe the softening.

We find that the HF solution of the three-band model and the t - J model give a comparable softening of the half-breathing phonon. This happens, however, in a very different way in the two approaches. Furthermore, we find that the dependence on doping and phonon wavevector is rather different in the two approaches. In the t - J model, the softening is $\propto \delta$ for small δ , while the doping dependence is weaker in the HF solution. The t - J model gives a smaller softening for the $\mathbf{q} = (1, 1)\pi/a$ breathing mode than for the $\mathbf{q} = (1, 0)\pi/a$ half-breathing mode, while the opposite is found in the HF approximation. In both cases, t - J results are in better agreement with experiment.

2.3.1 Model

We consider the three-band model from Eq. (1.1) in the Hartree-Fock (HF) mean-field approximation,

$$H_{\text{HF}} = \sum_{i\sigma} (\varepsilon^d + U \langle n_{i-\sigma}^d \rangle) n_{i\sigma}^d + \varepsilon^p \sum_{j\sigma} n_{j\sigma}^p - U \sum_i \langle n_{i\uparrow}^d \rangle \langle n_{i\downarrow}^d \rangle + \sum_{\langle i,j \rangle \sigma} \left[t_{ij}^{pd} d_{i\sigma}^\dagger p_{j\sigma} + \text{H.c.} \right], \quad (2.5)$$

where $\langle n_{i\sigma}^d \rangle$ is the expectation value of $n_{i\sigma}^d$. Compared to Eq. (1.1), p orbitals are now simply labeled by j and the hopping amplitude t_{ij}^{pd} includes the signs due to the relative phases of the orbitals involved. We also introduce the effective level

$$\varepsilon_{i\sigma}^{d,\text{eff}} = \varepsilon^d + U \langle n_{i-\sigma}^d \rangle \quad (2.6)$$

that includes screening effects. We assume that the hopping integrals depend on the atomic separations as in Eq. (1.26). We neglect that the displacement of atoms also leads to changes in the electrostatic potentials (Eqs. (1.28) and (1.29)) that are found to be less important for the electron-phonon coupling in the t - J model (cf. Sec. 2.4.1).

A static distortion is built into the lattice, and the change of the total energy is calculated. From this, the interaction with the electrons and the softening of the phonon can be deduced. The displacements of the atoms (with masses M_i) in the lattice (N unit cells) are denoted by $\{\mathbf{u}_i\}$ with $\mathbf{u}_i = u/\sqrt{N} \text{Re}[\boldsymbol{\epsilon}_i/\sqrt{M_i} \exp(i\mathbf{q} \cdot \mathbf{R}_i)]$ for a phonon with wavevector \mathbf{q} , polarization vector $\boldsymbol{\epsilon}_i$, and amplitude u . The energy of the electronic system is then

$$E[\{\mathbf{u}_i\}] = \text{Tr}(H[\{\mathbf{u}_i\}]\rho[\{\mathbf{u}_i\}]), \quad (2.7)$$

where $\rho[\{\mathbf{u}_i\}]$ is the density matrix, in this case obtained in the HF approximation by solving Eq. (2.5). Using the Hellmann-Feynman theorem, it follows that

$$\frac{\partial^2 E}{\partial u^2} = \text{Tr} \left(\frac{\partial H}{\partial u} \frac{\partial \rho}{\partial u} \right) + \text{Tr} \left(\frac{\partial^2 H}{\partial u^2} \rho \right) \equiv \left(\frac{\partial^2 E}{\partial u^2} \right)^{(1)} + \left(\frac{\partial^2 E}{\partial u^2} \right)^{(2)}. \quad (2.8)$$

It is understood that the derivatives are evaluated in the undistorted lattice. The electron-phonon coupling adds $(\partial^2 E/\partial u^2)u^2/2$ to the bare phonon potential energy $\omega_{\mathbf{q}}^2 u^2/2$ where $\omega_{\mathbf{q}}$ is the bare phonon frequency. Writing the sum as $\bar{\omega}_{\mathbf{q}}^2 u^2/2$ defines the renormalized phonon frequency $\bar{\omega}_{\mathbf{q}}$. Therefore, Eq. (2.8) directly relates to the phonon softening:

$$\frac{\partial^2 E}{\partial u^2} = \bar{\omega}_{\mathbf{q}}^2 - \omega_{\mathbf{q}}^2 = 2\omega_{\mathbf{q}}\Pi(\mathbf{q}), \quad (2.9)$$

where in the last equality it was used that in the adiabatic limit considered here $\partial^2 E/\partial u^2$ can also be expressed in terms of the static phonon self-energy $\Pi(\mathbf{q})$.

From total energy calculations for the undistorted and distorted lattice, $\partial^2 E/\partial u^2$ can be deduced. If, in the modulated hopping amplitudes, we take into account only terms up to linear order in u , we obtain just the contribution $(\partial^2 E/\partial u^2)^{(1)}$. It describes how a first-order change in the external Hamiltonian leads to a first-order change in the density matrix which acts back at the Hamiltonian. This contribution can be calculated in linear response. Schematically, we write the three-band model from Eq. (1.1) as

$$H = \sum_{ij\sigma} T_{ij\sigma} c_{i\sigma}^\dagger c_{j\sigma} + H_U, \quad (2.10)$$

where i and j run over both Cu- d and O- p orbitals and the $c_{i\sigma}^\dagger$ equal the corresponding creation operators ($d_{i\sigma}^\dagger$ and $p_{i\sigma}^\dagger$, respectively). $T_{ij\sigma}$ comprises level energies and

hopping integrals whereas H_U describes the Coulomb interaction between two holes in the same d orbital. Then,

$$\begin{aligned}
\left(\frac{\partial^2 E}{\partial u^2}\right)^{(1)} &= \text{Tr} \left(\frac{\partial H}{\partial u} \frac{\partial \rho}{\partial u} \right) = \sum_{ij\sigma} \frac{\partial T_{ij\sigma}}{\partial u} \text{Tr} \left(c_{i\sigma}^\dagger c_{j\sigma} \frac{\partial \rho}{\partial u} \right) = \sum_{ij\sigma} \frac{\partial T_{ij\sigma}}{\partial u} \frac{\partial}{\partial u} \text{Tr} \left(c_{i\sigma}^\dagger c_{j\sigma} \rho \right) \\
&= \sum_{ij\sigma} \frac{\partial T_{ij\sigma}}{\partial u} \frac{\partial \langle c_{i\sigma}^\dagger c_{j\sigma} \rangle}{\partial u} = \sum_{ij\sigma} \frac{\partial T_{ij\sigma}}{\partial u} \sum_{mn\sigma'} \hbar^{-1} \chi_{ij\sigma mn\sigma'}^{(0)} \frac{\partial T_{mn\sigma'}^{\text{eff}}}{\partial u} \\
&= 2\omega_{\mathbf{q}} g_{\mathbf{q}} \chi^{(0)}(\mathbf{q}) g_{\mathbf{q}}^{\text{eff}} / (\hbar^2 N) = 2\omega_{\mathbf{q}} \Pi^{(1)}(\mathbf{q}), \tag{2.11}
\end{aligned}$$

where in the second line we calculate the first-order change of the expectation value $\langle c_{i\sigma}^\dagger c_{j\sigma} \rangle$ in linear response from the changes in the effective level energies and hopping integrals in Eq. (2.5) when written as

$$H_{\text{HF}} = \sum_{ij\sigma} T_{ij\sigma}^{\text{eff}} c_{i\sigma}^\dagger c_{j\sigma} - U \sum_i \langle n_{i\uparrow}^d \rangle \langle n_{i\downarrow}^d \rangle \tag{2.12}$$

by using the static response function $\chi_{ij\sigma mn\sigma'}^{(0)} = \langle\langle c_{i\sigma}^\dagger c_{j\sigma}; c_{m\sigma'}^\dagger c_{n\sigma'} \rangle\rangle_{\omega=0}$ for non-interacting electrons. In the third line of Eq. (2.11), we express $\partial T_{ij\sigma} / \partial u$ in terms of the coupling constant $g_{\mathbf{q}}$ by comparing the term in H which is linear in u with the standard expression for the electron-phonon interaction,

$$H_{\text{ep}} = \frac{\partial H}{\partial u} u = \sum_{ij\sigma} \frac{\partial T_{ij\sigma}}{\partial u} u c_{i\sigma}^\dagger c_{j\sigma} = \frac{g_{\mathbf{q}}}{\sqrt{N}} \sum_{ij\sigma} e^{i\mathbf{q} \cdot (\mathbf{R}_i + \mathbf{R}_j) / 2} \sqrt{\frac{2\omega_{\mathbf{q}}}{\hbar}} u c_{i\sigma}^\dagger c_{j\sigma}. \tag{2.13}$$

Analogously, the screened coupling constant $g_{\mathbf{q}}^{\text{eff}}$ is calculated from $\partial T_{ij\sigma}^{\text{eff}} / \partial u$. To quantify the screening, we introduce a dielectric function

$$\epsilon(\mathbf{q}) = g_{\mathbf{q}} / g_{\mathbf{q}}^{\text{eff}}. \tag{2.14}$$

Using the Fourier transform of the response function,

$$\chi^{(0)}(\mathbf{q}) = \sum_{ij\sigma} \sum_{mn\sigma'} \chi_{ij\sigma mn\sigma'}^{(0)} e^{i\mathbf{q} \cdot (\mathbf{R}_i + \mathbf{R}_j - \mathbf{R}_m - \mathbf{R}_n)}, \tag{2.15}$$

we are then led to the compact result in the third line of Eq. (2.11). This result can also be obtained from a diagrammatic technique for $\Pi^{(1)}$. It is described by the static contribution from a bubble diagram as shown in Fig. 2.8. This is the only diagram which enters in the HF approximation. We observe that the screening of the perturbation, described by $g_{\mathbf{q}}^{\text{eff}}$, enters only at one of the vertices. Using $g_{\mathbf{q}}^{\text{eff}}$ at both vertices would lead to double counting. By using the diagrammatic approach, we can

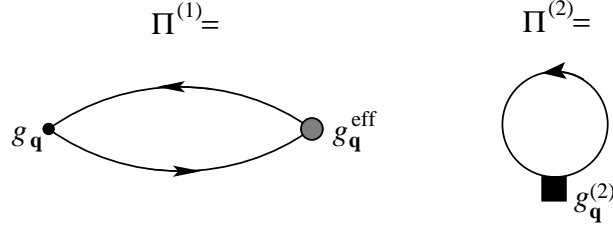


Figure 2.8: Diagrams representing the phonon softening in the HF approximation. $\Pi^{(1)}$ describes the linear response where $g_{\mathbf{q}}$ and $g_{\mathbf{q}}^{\text{eff}}$ describe the bare and screened perturbations due to a phonon. $\Pi^{(2)}$ gives the non-linear contribution.

obtain not only a contribution to the energy but also the width of the phonon as the phonon self-energy can be calculated for finite frequencies.

The non-linear contribution to the phonon softening,

$$\left(\frac{\partial^2 E}{\partial u^2}\right)^{(2)} = \text{Tr} \left(\frac{\partial^2 H}{\partial u^2} \rho \right) = \sum_{ij\sigma} \frac{\partial^2 T_{ij\sigma}}{\partial u^2} \langle c_{i\sigma}^\dagger c_{j\sigma} \rangle = 2\omega_{\mathbf{q}} \Pi^{(2)}(\mathbf{q}), \quad (2.16)$$

is described by the static part of the diagram for $\Pi^{(2)}$ shown in Fig. 2.8. It corresponds to a fermion line starting and ending at the vertex $g_{\mathbf{q}}^{(2)} \propto \partial^2 T_{ij\sigma} / \partial u^2$ which connects two fermion and two phonon lines. This diagram does not obtain an imaginary part even for finite frequencies and therefore makes no contribution to the width of the phonon.

2.3.2 Results for phonon softening

Here we present results for the three-band model in the Hartree-Fock approximation, using the parameters $t_{pd} = 1.6$ eV and $U = 8$ eV. The lattice parameter is $a = 3.8$ Å. We have adjusted ε^p so that the separation between the effective d levels and the p levels

$$\varepsilon^p - \varepsilon^{d,\text{eff}} = \varepsilon^p - \varepsilon^d - U \langle n_\sigma^d \rangle = 3 \text{ eV}, \quad (2.17)$$

where $\langle n_\sigma^d \rangle$ is the average occupation of the d levels per spin. This is a typical LDA estimate for $\varepsilon^p - \varepsilon^{d,\text{eff}}$ in a three-band model [58]. We perform two calculations, one for the undistorted lattice and one for a lattice where a phonon has been built in. This gives the second derivative, $\partial^2 E / \partial u^2$. From this derivative, we obtain the softening of the phonon due to the interaction with the electrons in the model, reducing the frequency $\omega_{\mathbf{q}}$ to $\bar{\omega}_{\mathbf{q}}$. Here, $\omega_{\mathbf{q}}$ is assumed to be due to forces not included in the model in Eq. (1.1), e.g. electrostatic forces and core-core overlap effects. The calculations

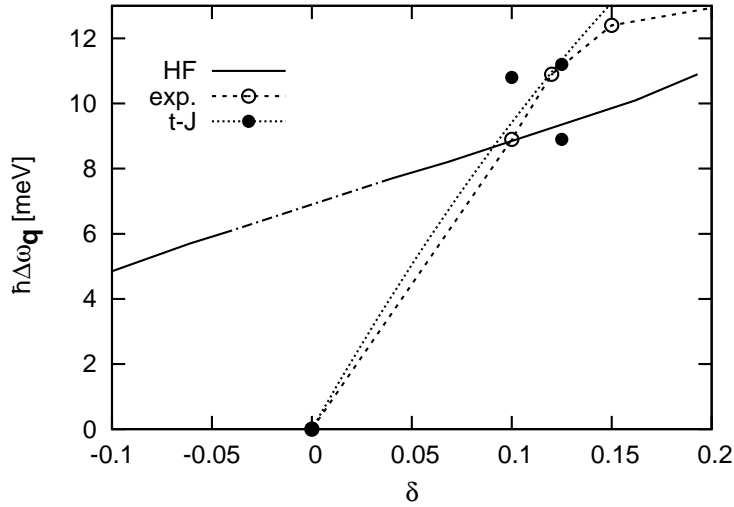


Figure 2.9: Softening $\hbar\Delta\omega_{\mathbf{q}}$ for the zone boundary half-breathing phonon. Results are given for the HF approximation (full line), the t - J model (full circles, dotted line), and according to experiment (open circles, dashed line) as a function of the hole doping δ . The lines serve to guide the eye between the few points in the t - J model from bipartite clusters (cf. Tab. 2.1) and experimental data for LSCO [40]. The HF approximation refers to results for the shift in a paramagnetic calculation for doping δ relative to an antiferromagnetic calculation for $\delta = 0$. The dash-dotted part of the HF line indicates schematically that the systems becomes antiferromagnetic for small dopings.

were performed for a cluster of 32×32 CuO_2 units and periodic boundary conditions. The doping was chosen in such a way that degenerate levels were either completely full or completely empty, i.e. all “shells” were either full or empty.

We first consider the half-breathing phonon for $\mathbf{q} = (1, 0)\pi/a$. We perform a calculation for the undoped system, having five electrons per unit cell and allowing for spin-polarization. We adjust $\omega_{\mathbf{q}}$ so that the softened energy $\hbar\bar{\omega}_{\mathbf{q}}$ equals the experimental value 80 meV for the zone boundary half-breathing phonon.

The result as a function of the hole doping δ ($\delta < 0$ means electron doping) is shown in Fig. 2.9. The doping dependence is relatively weak. Since the undoped system is antiferromagnetic, but the doped system is (assumed to be) paramagnetic, as found experimentally, the softening is not necessarily small for small dopings. The spin-polarized system has a large gap of about 4.6 eV. Due to this gap, the response of the system to a phonon is substantially weaker than for the paramagnetic state.

For instance, $(\partial^2 E/\partial u^2)^{(1)}$ contributes a softening of only about 4 meV for the spin-polarized system but 6 meV for a non-spin-polarized system with a similar number of electrons. Similarly, the contributions of $(\partial^2 E/\partial u^2)^{(2)}$ are about 8 and 13 meV, respectively.

We find that screening reduces the quantity $(\partial^2 E/\partial u^2)^{(1)}$ by about a factor of two, i.e., $\epsilon(\mathbf{q}) \approx 2$ in Eq. (2.14). By evaluating the diagram for $\Pi^{(1)}$ in Fig. 2.8, we find that the zone boundary half-breathing phonon is broadened by about 0.4 meV for $\delta = 0.16$. This is similar to what Bohnen *et al.* [65] found in an LDA calculation.

It is interesting to compare the half-breathing phonon and the $\mathbf{q} = (1, 1)\pi/a$ breathing phonon. In the model considered above, there is nesting for $\mathbf{q} = (1, 1)\pi/a$ in case of $\delta = 0$. As a result of this, there would be a very strong response for small δ , making the calculation rather meaningless. To avoid this unrealistically strong nesting, we change the Fermi surface by adding to the model hopping between O atoms which are nearest neighbors of a particular Cu atom,

$$H_{pp} = \sum_{\langle j, j' \rangle \sigma} \left[t_{jj'}^{pp} p_{j\sigma}^\dagger p_{j'\sigma} + \text{H.c.} \right], \quad (2.18)$$

where the sum is over all such pairs of oxygen sites j . The corresponding hopping integrals $t_{jj'}^{pp}$ have the absolute value t_{pp} with the signs determined by the relative orientations of the orbitals involved. We neglect the phonon modulation of t_{pp} and consider $t_{pp} = 1.1$ eV [58]. In this case, we adjust $\omega_{\mathbf{q}}$ so that $\hbar\bar{\omega}_{\mathbf{q}} = 90$ meV in the spin-polarized calculation for the undoped system, as found experimentally. For the doping $\delta = 0.096$, we find that the $\mathbf{q} = (1, 1)\pi/a$ breathing phonon is softened by 11 meV. This is a larger softening than what was found in Fig. 2.9 for this doping. We have also performed a calculation for the $\mathbf{q} = (1, 0)\pi/a$ half-breathing phonon in this model and for this doping. The softening is 7 meV which is again smaller than for the breathing phonon. This is contrary to experiment where a larger softening is found for the half-breathing phonon. Finally, we observe that the softening of the half-breathing phonon is only changed from about 9 meV for $t_{pp} = 0$ to 7 meV for $t_{pp} = 1.1$ eV. This justifies the neglect of t_{pp} for the qualitative analysis of the half-breathing phonon.

2.3.3 Comparison with results from t - J model

To make contact with the t - J model, we transform the non-interacting ($U = 0$) three-band model to an effective one-band model. The effect of U is later included by its screening effect derived in the HF approximation of the three-band model. We

assume that the O- p levels are far above the Cu- d levels (in the hole picture). We can then project out the O- p levels and obtain a model only with effective Cu- d levels. This model can be compared with the t - J model since both models have one band. Here, we focus on the linear-response term $(\partial^2 E/\partial u^2)^{(1)}$ in Eq. (2.11) which is of the same order of magnitude in the t - J model and in the HF approximation for a typical $\delta \approx 0.1$.

We introduce a projection operator P , which projects onto the Cu- d levels, and its complement $Q = 1 - P$. We consider the resolvent operator in the P -subspace as in Eq. (1.36) which defines the effective one-band Hamiltonian

$$P\tilde{H}(z)P = P(H + HQ\frac{1}{z - QHQ}QH)P, \quad (2.19)$$

where z is some typical energy. We then obtain the effective one-band level energies and hopping amplitudes

$$\varepsilon_{i\sigma}^{d,\text{One}} = \varepsilon^d + \sum_{\langle j \rangle} \frac{(t_{ij}^{pd})^2}{z - \varepsilon^p}, \quad (2.20)$$

$$t_{ii'}^{\text{One}} = \frac{t_{ij}^{pd} t_{ji'}^{pd}}{z - \varepsilon^p}, \quad (2.21)$$

where the sum for $\varepsilon_{i\sigma}^{d,\text{One}}$ runs over the nearest O neighbors of Cu and j for $t_{ii'}^{\text{One}}$ refers to the common nearest-neighbor O atom of the Cu atoms i and i' . We first consider the unperturbed (no phonon) system. We choose z to be in the middle of the band and solve the self-consistent equations

$$\varepsilon_{i\sigma}^{d,\text{One}} = \varepsilon^d + \frac{4(t_{pd})^2}{\varepsilon_{i\sigma}^{d,\text{One}} - \varepsilon^p}, \quad (2.22)$$

$$t_{ii'}^{\text{One}} = -\frac{(t_{pd})^2}{\varepsilon_{i\sigma}^{d,\text{One}} - \varepsilon^p}, \quad (2.23)$$

where the factor 4 for $\varepsilon_{i\sigma}^{d,\text{One}}$ comes from the four O neighbors of a Cu atom.

We then introduce a phonon in the system and ask for the linear response of the electronic system. A perturbation term is introduced in the one-band Hamiltonian

$$\delta\varepsilon_{i\sigma}^{d,\text{One}} = \sum_{\langle j \rangle} 2 \frac{t_{ij}^{pd} \delta t_{ij}^{pd}}{\varepsilon_{i\sigma}^{d,\text{One}} - \varepsilon^p}, \quad (2.24)$$

where δt_{ij}^{pd} are the changes in the Cu-O hopping integrals.

For a half-breathing phonon at the zone boundary, the on-site perturbation is

$$\frac{\partial \varepsilon_{i\sigma}^{d,\text{One}}}{\partial u} u = \pm 4t_{pd} \frac{\partial t_{pd}}{\partial u} \frac{1}{\varepsilon_{i\sigma}^{d,\text{One}} - \varepsilon^p} u, \quad (2.25)$$

source	t - J	HF	ratio
coupling	$[(2-1)\lambda^2/\Delta + 2\lambda^2/(U-\Delta)]^2$	$(1/\Delta)^2$	≈ 3
sum rule	$\approx 2\delta\pi N$	$\approx \pi N$	$\approx 2\delta$
screening	1	≈ 0.5	≈ 2
denominator			≈ 1
product			12δ

Table 2.2: Contributions to the phonon softening in the t - J model and in the HF approximation. Here $\Delta \equiv \varepsilon^p - \varepsilon^{d,\text{One}} = \varepsilon^p - \varepsilon^d$.

where u is the absolute value of the phonon amplitude. The quantity $\partial\varepsilon_{i\sigma}^{d,\text{One}}/\partial u$ enters as $\partial T_{ii\sigma}/\partial u$ in the calculation of $(\partial^2 E/\partial u^2)^{(1)}$ in Eq. (2.11) which by analogy can be used also for the effective one-band model. To linear order, there is no change in $t_{ii'}^{\text{One}}$ and therefore $\partial T_{ij\sigma}/\partial u = 0$ for $i \neq j$.

In the t - J model, the corresponding on-site perturbation is

$$\pm 4\lambda^2 t_{pd} \frac{\partial t_{pd}}{\partial u} \left(\frac{2-1}{\varepsilon^p - \varepsilon^d} + \frac{2}{U - (\varepsilon^p - \varepsilon^d)} \right) u, \quad (2.26)$$

according to Eq. (1.110). The first term comes from the hopping of a d hole into the O- p orbitals and the second term from the hopping of a O- p hole into the Cu- d orbital. The second term has no correspondence in Eq. (2.25). Equation (2.26) has an additional factor 2 coming from a phase coherence factor in the Zhang-Rice singlet. This results from the singlet being explicitly written as a sum of two terms. Both these effects are genuine many-body effects. The -1 in the first term in Eq. (2.26) results from taking the difference in the energy gain of a Zhang-Rice singlet and a single d hole. Also in the t - J model, the off-site coupling vanishes, cf. Eq. (1.113).

One can show that the phonon self-energy in the t - J model is approximately proportional to the charge response function χ^{t-J} for not too strong coupling like for the parameters used here (cf. Eq. (4.18)). This result can then be directly compared with the result in Eq. (2.11) for $\Pi^{(1)}$ if applied to the one-band model. In both cases, the response function is multiplied by the appropriate coupling constant squared, given by Eq. (2.25) and Eq. (2.26), respectively.

The phonon softening from linear response for the HF approximation is

$$\hbar\Delta\omega_{\mathbf{q}}^{(1)} \approx \text{Re } \Pi^{(1)}(\mathbf{q}) = -\frac{1}{\pi} \mathcal{P} \int d\omega \frac{g_{\mathbf{q}} g_{\mathbf{q}}^{\text{eff}} / (\hbar^2 N) |\text{Im } \chi^{(0)}(\mathbf{q}, \omega)|}{|\omega|}$$

$$= \underbrace{\frac{g_{\mathbf{q}}^2}{\hbar^2 N}}_{\text{coupling}} \underbrace{\frac{1}{\epsilon(\mathbf{q})}}_{\text{screening}} \underbrace{\left\langle \frac{\mathcal{P}}{|\omega|} \right\rangle_{|\text{Im } \chi^{(0)}(\mathbf{q}, \omega)|/\pi}}_{\text{denominator}} \underbrace{\frac{1}{\pi} \int d\omega |\text{Im } \chi^{(0)}(\mathbf{q}, \omega)|}_{\text{sum rule}}. \quad (2.27)$$

We assume that the phonon energy is small compared to electronic energies so that the softening is approximately given by the real part of the static phonon self-energy which we calculate using a Kramers-Kronig relation and obtaining the self-energy from a bubble diagram (cf. left part of Fig. 2.8). With Eq. (2.14) and after some rearranging of terms, it then follows that the softening on the one hand is proportional to the squared coupling constant which due to screening is divided by the dielectric constant. On the other hand, it depends on the average denominator with respect to the spectral function of the response function and the total weight of this spectrum (sum rule). We use the notation $\langle f(\omega) \rangle_{A(\omega)} = \int d\omega f(\omega) A(\omega) / [\int d\omega A(\omega)]$.

To compare the t - J model with the one-band model, we consider for both models the four contributions to the phonon softening in Eq. (2.27). We put $\varepsilon^p - \varepsilon^{d, \text{One}} = \varepsilon^p - \varepsilon^d \equiv \Delta = 3$ eV and $U = 8$ eV and find that the square of Eq. (2.26) is about a factor of three larger than the square of Eq. (2.25). This difference in the coupling constants is shown in Tab. 2.2. The two approaches further differ by the screening in the HF approach discussed in Eq. (2.14). This reduces the HF result by roughly a factor of two.

The linear response of the one-band model is given by

$$\chi^{(0)}(\mathbf{q}, z) = 2 \sum_{\mathbf{k}} [1 - f(\mathbf{k} + \mathbf{q})] f(\mathbf{k}) \left(\frac{1}{z - \omega(\mathbf{k}, \mathbf{q})} - \frac{1}{z + \omega(\mathbf{k}, \mathbf{q})} \right), \quad (2.28)$$

where $f(\mathbf{k})$ is the Fermi function for a state with wavevector \mathbf{k} and energy $\varepsilon(\mathbf{k})$ and $\omega(\mathbf{k}, \mathbf{q}) = \hbar^{-1}(\varepsilon(\mathbf{k} + \mathbf{q}) - \varepsilon(\mathbf{k}))$. We have the sum-rule

$$\frac{1}{N} \sum_{\mathbf{q} \neq 0} \int_{-\infty}^{\infty} d\omega |\text{Im } \chi^{(0)}(\mathbf{q}, \omega + i0^+)| = 4\pi n(1 - n)N \approx \pi N, \quad (2.29)$$

where N is the number of sites and n is the fractional filling of the band. Typically, we are interested in a system with $n = (1 + \delta)/2 \approx 0.5$ holes per site and spin which leads to the right hand side of Eq. (2.29). For the t - J model, we ask for the charge response function

$$\chi^{t-J}(\mathbf{q}, z) = \sum_{\nu} |\langle \nu | \rho_{\mathbf{q}} | 0 \rangle|^2 \left(\frac{1}{z - \omega_{\nu}} - \frac{1}{z + \omega_{\nu}} \right), \quad (2.30)$$

where $|\nu\rangle$ is an excited many-electron state with the excitation energy $\hbar\omega_{\nu}$ and $\rho_{\mathbf{q}}$ is

the charge density operator defined by

$$\rho_{\mathbf{q}} = \sum_i n_i e^{-i\mathbf{q}\cdot\mathbf{R}_i}. \quad (2.31)$$

One finds [34, 35, 36]

$$\frac{1}{N} \sum_{\mathbf{q} \neq 0} \int_{-\infty}^{\infty} d\omega |\text{Im} \chi^{t-J}(\mathbf{q}, \omega + i0^+)| = 2\pi N \delta(1 - \delta). \quad (2.32)$$

Eqs. (2.29) and (2.32) differ by approximately a factor of 2δ for small δ (see Tab. 2.2). This strong reduction at low doping of the charge response in the t - J model compared to that for effectively non-interacting electrons in the HF approximation is a consequence of strong correlations and will be discussed in detail in Chap. 4.

Finally, we have to consider that typical energy denominators in Eq. (2.28) and Eq. (2.30) could be different. Calculating the average denominator, we find comparable results for the two models. As can be seen from Tab. 2.2, the difference between the two approaches results in a ratio of about 12δ . For $\delta \approx 0.1$, the two results are then similar. This indicates why the t - J model and the HF solution of the three-band model can give similar softening of the half-breathing mode although the physics is quite different.

We next consider the imaginary part of the (retarded) phonon self-energy Π which determines the phonon width. As an orientation, we first consider a simple model. Since $\text{Im} \chi(\omega) \propto \omega$ for small ω , we assume

$$|\text{Im} \Pi(\mathbf{q}, \omega)| = \begin{cases} A\omega, & \text{if } |\omega| \leq W, \\ 0, & \text{otherwise,} \end{cases} \quad (2.33)$$

where A is some constant. From the Kramers-Kronig relation, we can then derive

$$\frac{\gamma}{-\hbar\Delta\omega_{\mathbf{q}}} = \pi \frac{\hbar\bar{\omega}_{\mathbf{q}}}{W}, \quad (2.34)$$

where $\gamma = 2\hbar \text{Im} \Pi(\mathbf{q}, \bar{\omega}_{\mathbf{q}})$ is the full width at half maximum of the phonon and $\Delta\omega_{\mathbf{q}}$ is its shift.

Figure 2.10 compares $\text{Im} \Pi(\mathbf{q}, \omega)$ for the half-breathing phonon in the one- and three-band models and the breathing phonon in the three-band model. The one-band model was constructed to describe what happens close to E_F , and therefore the one- and three-band models agree very well for small ω . For $|\omega| \gg 0$, the one-band model gives a larger $|\text{Im} \Pi(\mathbf{q}, \omega)|$ than the three-band model, and $|\text{Re} \Pi(\mathbf{q}, \omega)|$ is overestimated correspondingly in the one-band model. Appropriate numbers for the

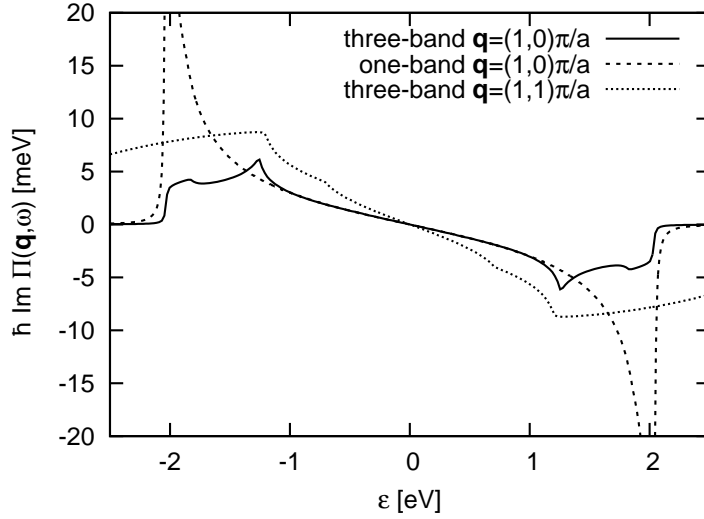


Figure 2.10: $\text{Im } \Pi(\mathbf{q}, \omega)$ for the $\mathbf{q} = (1, 0)\pi/a$ half-breathing mode in the three-band model (full line) and the one-band model (dashed line) and for the $\mathbf{q} = (1, 1)\pi/a$ breathing mode (dotted line). The doping is $\delta = 0.1$.

the half-breathing phonon and the one-band model are $W = 2$ eV, $\hbar\bar{\omega}_{\mathbf{q}} = 70$ meV, $\hbar\Delta\omega_{\mathbf{q}} = -7$ meV. Inserting this in Eq. (2.34) leads to $\gamma = 0.8$ meV. This is about twice the width calculated directly from $\text{Im } \Pi(\mathbf{q}, \omega)$. The reason for this overestimate is that, for small ω , $\text{Im } \Pi(\mathbf{q}, \omega)$ is actually smaller than assumed in Eq. (2.33).

Figure 2.10 also shows the HF result for the $\mathbf{q} = (1, 1)\pi/a$ breathing phonon. These results were obtained for $t_{pp} = 1.1$ eV. There is then no strong nesting of the Fermi surface. The HF approximation, nevertheless, gives a larger broadening for the $\mathbf{q} = (1, 1)\pi/a$ breathing phonon than for the $\mathbf{q} = (1, 0)\pi/a$ half-breathing phonon, irrespective of whether the latter is calculated for $t_{pp} = 0$ or $t_{pp} = 1.1$ eV. As is well-known [63], this is due to the fact that the wavevector $\mathbf{q} = (1, 1)\pi/a$ fits better to the traces of nesting left over for $t_{pp} = 1.1$ eV.

To study the phonon width in the t - J model, we calculate the phonon self-energy as described in App. A.3. As pointed out earlier, this approach has important advantages for small systems. The phonon spectral function $B(\mathbf{q}, \omega)$ has too few poles to determine the phonon width. A broadened version of $\Pi(\mathbf{q}, \omega)$, however, can give such information [67]. Results for $\Pi(\mathbf{q}, \omega)$ are shown in Fig. 2.11.

In the view of Eq. (2.34), one might have expected the width of the half-breathing phonon to be similar in the HF approximation and the t - J model since the shifts are similar. This is not true, however, since the frequency dependence differs strongly

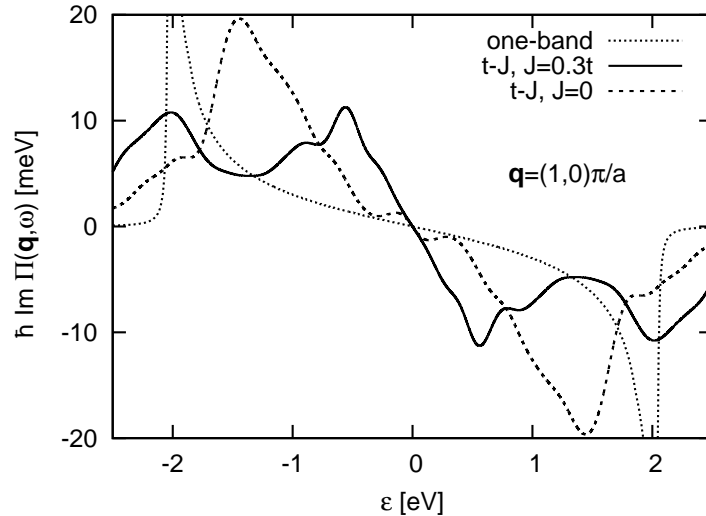


Figure 2.11: $\text{Im } \Pi(\mathbf{q}, \omega)$ for the $\mathbf{q} = (1, 0)\pi/a$ half-breathing mode in the t - J model for $J/t = 0.3$ (full line) and $J/t = 0$ (dashed line) and in the one-band model (dotted line). The results for the t - J model were obtained for a 4×4 cluster. The doping is $\delta = 0.125$.

from the linear dependence assumed in Eq. (2.33). This is illustrated in Fig. 2.11. The figure shows that for the t - J model with $J = 0$ some spectral weight has been moved to small frequencies due to the hopping constraint which creates low-energy excitations. This is even more true if J is finite (here, $J/t = 0.3$). The present clusters are too small to give reliable results, in particular for the low-lying excitations, and the results above should be considered as qualitative. They illustrate, however, the general trend of transferring some spectral weight to small frequencies which tends to lead to a substantially increased width of the half-breathing phonon.

To summarize, we have studied the properties of the (half-)breathing phonon in the three-band model comparing results for the t - J model with phonons and the HF approximation of the three-band model. Although the two approaches give similar softenings at typical dopings, the underlying physics is quite different. The hopping constraint in the t - J model, resulting from the strong Coulomb repulsion, leads to a strong reduction of the response to a phonon. This reduction is, however, partly compensated by several other effects. In particular, many-body effects in the energy of the Zhang-Rice singlet tend to increase the coupling in the t - J model. We find that the dependences on doping and phonon wavevector for the (half-)breathing mode are quite different in the two approaches, with the t - J model giving better agreement with experiment. The HF approximation also gives a too small width for the half-

breathing phonon. We therefore conclude that many-body effects play an important role for the interactions of the half-breathing phonon with the electrons.

2.4 Discussion

2.4.1 Relative importance of coupling mechanisms

The electron-phonon coupling in the t - J model derived in Chap. 1 describes the modulation of both the effective on-site energies and the effective hopping amplitudes. Besides this division into site-diagonal and site-off-diagonal coupling, one can also distinguish between the contributions that are due to the modulation of the p - d hopping amplitude in the three-band model and those arising from the modulation of the level energies in the original model.

We start our discussion of the relative importance of the different coupling mechanisms by showing that the phonon induced modulation of a parameter in the t - J model is basically proportional to the value of this parameter in the undistorted system. First, we consider contributions to the site-diagonal coupling. In a system without phonons, the on-site energy of sites without an extra doped hole is given by the Cu- d self-energy (Eq. (1.53)). Defining the average modulations of hopping amplitudes and p level energies around a Cu site,

$$\overline{\Delta t_i} = \frac{1}{4} \sum_{\delta} \sum_{s=\pm} \Delta t_{i(s\delta)}, \quad (2.35)$$

$$\overline{\Delta \varepsilon_i^p} = \frac{1}{4} \sum_{\delta} \left(\Delta \varepsilon_{i\delta}^p + \Delta \varepsilon_{(i-2\delta)\delta}^p \right), \quad (2.36)$$

it follows from Eqs. (1.98) and (1.101) that the modulation of $E^{\text{Cu-}d}$ at site i can be written as

$$\Delta E_i^{\text{Cu-}d} = E^{\text{Cu-}d} \left[2 \frac{\overline{\Delta t_i}}{t_{pd}} - \frac{\lambda^2 \overline{\Delta \varepsilon_i^p} - \Delta \varepsilon_i^d}{\Delta_{pd}} \right] \quad (2.37)$$

which is indeed proportional to $E^{\text{Cu-}d}$. An analogous result can be obtained for the on-site energy of sites with a Zhang-Rice singlet which consists of two contributions. On the one hand, it contains the singlet self-energy whose modulation can be expressed as

$$\Delta E_i^{\text{singlet}} = E^{\text{singlet}} \left[2 \frac{\overline{\Delta t_i}}{t_{pd}} - (\lambda^2 \overline{\Delta \varepsilon_i^p} - \Delta \varepsilon_i^d) \left(\frac{1}{\Delta_{pd}} - \frac{1}{U - \Delta_{pd}} \right) \right]. \quad (2.38)$$

On the other hand, it is also increased by Δ_{pd} compared to the Cu- d hole on-site energy due to the fact that the extra hole basically goes into a p orbital. According

to Eq. (1.93), the modulation of this contribution is

$$\Delta(\Delta_{pd})_i = \Delta_{pd} \frac{\lambda^2 \overline{\Delta \varepsilon_i^p}}{\Delta_{pd}}. \quad (2.39)$$

With these results, the site-diagonal contribution to the electron-phonon coupling in the t - J model can be written as $H_{\text{ep}}^{(\text{diag})} = \sum_i (\Delta E_i^{\text{Cu-d}} - \Delta E_i^{\text{singlet}} - \Delta(\Delta_{pd})_i) n_i$.

Correspondingly, the site-off-diagonal coupling is determined by the modulation of the effective hopping in the t - J model (Eq. (1.88)). In order to obtain a relatively simple expression, we now specifically consider the half-breathing mode at the zone boundary and assume $U - \Delta_{pd} \gg \Delta_{pd}$. Then, the modulation of the effective nearest-neighbor hopping perpendicular to the direction of \mathbf{q} is given by

$$\Delta t_{ij}^{\perp \mathbf{q}} = -t \frac{1}{2} \left[\left(1 + \frac{\gamma_1 - \gamma_{11}}{\alpha(\hat{\mathbf{x}})} \right) \frac{\overline{\Delta t_i} + \overline{\Delta t_j}}{t_{pd}} + \frac{\overline{\Delta \varepsilon_i^d} + \overline{\Delta \varepsilon_j^d}}{\Delta_{pd}} \right] \quad (2.40)$$

using Eqs. (1.96), (1.99), and (1.102). It is proportional to t as expected. The hopping parallel to \mathbf{q} is not modulated by the half-breathing mode.¹

Based on these results, we expect the site-diagonal coupling to dominate over the site-off-diagonal one because it has a much larger prefactor. For our usual parameters for the three-band model ($t_{pd} = 1.2$ eV, $\Delta_{pd} = 3$ eV, $U = 10$ eV) and considering the half-breathing mode at the zone boundary, the modulation of the on-site energy is proportional to $|E^{\text{singlet}} - E^{\text{Cu-d}}| \approx 3.3$ eV whereas the prefactor $t \approx 0.5$ eV in the modulation of the effective hopping is almost an order of magnitude smaller. This is confirmed by the numerical values of the coupling constants obtained from evaluating

¹This can be understood as follows. When the O atom inbetween sites i and j moves towards one of the sites, the hopping amplitude from the O atom to the nearer Cu atom is increased while that to the more distant site is decreased. To linear order in the displacements, these two effects cancel out in the effective hopping between the two sites which is proportional to the product of these two amplitudes when derived from a perturbation theory in t_{pd} . For the effective hopping perpendicular to \mathbf{q} , one would also expect no effect from the modulation of t_{pd} as the intermediate O atom does not move. Because of the non-local components in our Wannier-like p orbitals, however, there is a small contribution (proportional to $1 + (\gamma_1 - \gamma_{11})/\alpha(\hat{\mathbf{x}}) \approx 0.16$) in Eq. (2.40). The half-breathing mode also leads to an increase of the d level energies at half of all sites and a decrease at the other half. This modulates the effective hopping via the change of energy denominators in the corresponding expression from perturbation theory. For hopping along the direction of \mathbf{q} , the d level energies of the sites involved change in the opposite way leading to a cancelation to linear order in the displacements. In the perpendicular direction, the two changes work together causing the modulation described by the second term in Eq. (2.40).

Eqs. (1.109)-(1.114) for $\hbar\omega_{\mathbf{q}\nu} = 80$ meV. One finds

$$\sqrt{\frac{\hbar}{2\omega_{\mathbf{q}\nu}}}A^{(t)} = -0.24 \text{ eV}, \quad \sqrt{\frac{\hbar}{2\omega_{\mathbf{q}\nu}}}B^{\hat{\mathbf{y}}/2,(t)} = 0.0028 \text{ eV} \quad (2.41)$$

due to the modulation of t_{pd} and

$$\sqrt{\frac{\hbar}{2\omega_{\mathbf{q}\nu}}}A^{(\varepsilon)} = 0.032 \text{ eV}, \quad \sqrt{\frac{\hbar}{2\omega_{\mathbf{q}\nu}}}B^{\hat{\mathbf{y}}/2,(\varepsilon)} = -0.0046 \text{ eV} \quad (2.42)$$

due to the modulation of ε^d and ε^p . $B^{\hat{\mathbf{x}}/2,(t)} = B^{\hat{\mathbf{x}}/2,(\varepsilon)} = 0$ because the effective hopping in the t - J model is only modulated perpendicular to \mathbf{q} . As expected, the site-diagonal coupling ($\propto A$) is much stronger than the site-off-diagonal one ($\propto B$). Furthermore, the strong on-site coupling is mainly due to the modulation of the hopping in the three-band model whereas the modulation of the level energies gives only a minor contribution. The greater importance of the coupling from the modulation of t_{pd} mainly originates in the different power laws of the r dependence of t_{pd} ($\propto r^{-3.5}$) and U_{pd} ($\propto r^{-1}$), cf. Sec. 1.2.3. The respective powers enter the coupling as proportionality factors via $(dt_{pd}/dr)|_0$ and $(dU_{pd}/dr)|_0$. In addition, in the coupling due to the modulation of ε^d and ε^p there is a partial cancelation of terms proportional to $1/(U - \Delta_{pd})$ and $1/\Delta_{pd}$. In order to check the sensitivity of the strength of the different coupling mechanisms on the choice of parameters, we show in Fig. 2.12 the dependence on Δ_{pd} keeping all other parameters fixed to their usual values. One finds that our choice of $\Delta_{pd} = 3$ eV does not constitute a fine tuning to a peculiar coupling. Rather, irrespective of the exact value of Δ_{pd} , the relative importance of the different couplings remains unchanged and also their absolute magnitude does not depend very strongly on Δ_{pd} in the range of physically reasonable values.

It is interesting to reconsider our results for the softening of the half-breathing and full-breathing modes shown in Fig. 2.3 in terms of our finding that the site-diagonal terms (Eq. (1.109)) dominate the electron-phonon coupling. For the half-breathing modes, they are mainly proportional to $\sin(q_x a/2)$, suggesting a softening $\propto \sin^2(q_x a/2)$. This behavior is essentially found in our calculations, although the softening for $q_x = \pi/(2a)$ is stronger than expected from this argument. The prefactor, however, is a factor $\sqrt{2}$ larger for the breathing mode ($\mathbf{q} = (\pi/a, \pi/a)$) than for the half-breathing mode ($\mathbf{q} = (\pi/a, 0)$), suggesting twice as large a softening for the breathing mode. But the softening is actually stronger for the half-breathing mode. This can be understood by an analysis of the contributions to the softening similar to that given in Eq. (2.27) which can be used also for the t - J model if the screening

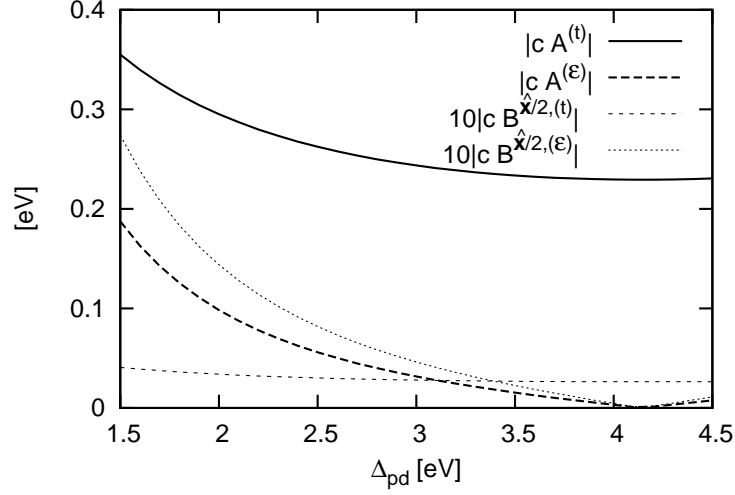


Figure 2.12: Dependence of different contributions to the electron-phonon coupling of the half-breathing mode at the zone boundary ($\hbar\omega_{\mathbf{q}\nu} = 80$ meV, $\mathbf{q} = (\pi/a, 0)$) on the charge transfer energy Δ_{pd} . All other parameters are fixed to their usual values ($t_{pd} = 1.2$ eV, $U = 10$ eV). We distinguish between site-diagonal (A) and site-off-diagonal (B , multiplied by a factor 10) coupling and between coupling from hopping ($^{(t)}$) and level energies ($^{(\varepsilon)}$) in the three-band model. We use the definition $c = \sqrt{\frac{\hbar}{2\omega_{\mathbf{q}\nu}}}$.

factor is put equal to one and the coupling is not too strong. Then, the imaginary part of the phonon self-energies for the half-breathing and breathing mode shown in Fig. 2.5 is approximately proportional to $g_{\mathbf{q}}^2 \text{Im} \chi^{t-J}(\mathbf{q}, \omega)$ from which we can deduce that with the coupling being twice as strong for the breathing mode the sum rule factor in Eq. (2.27) is similar for the two modes. But the self-energy for the half-breathing mode has much more spectral weight at lower energies. The contribution from the average energy denominator in Eq. (2.27) therefore is much larger for this mode compared to the breathing mode. This overcompensates the stronger coupling found for the latter one and explains why the softening is larger for the half-breathing mode. We explicitly discussed the modes at the zone boundary but a similar analysis applies for modes with \mathbf{q} within the Brillouin zone. One consistently finds that the modes along the $(\xi, 0)$ direction couple to excitations lower in energy than those along the (ξ, ξ) direction.

2.4.2 Comparison with other approaches

Electron-phonon interaction in the t - J model has been derived from the three-band model with phonons also by other authors. They come, however, to different conclusions on which coupling mechanism is most important. In this section, we discuss the different approaches in the light of our results.

In their derivation of a t - J model with electron-phonon coupling, von Szczepanski and Becker [30] take into account only the modulation of the p - d hopping amplitude in the original three-band model. An exact derivation is given only for the $\mathbf{q} = (1, 1)\pi/a$ oxygen breathing mode. The coupling for other phonon wavevectors is estimated from a linear interpolation between this result and the vanishing coupling for $\mathbf{q} = (0, 0)$. They consider solely coupling to the on-site energies in the t - J model whereas coupling to the effective hopping and to the exchange interaction is neglected. Their coupling mechanism (on-site coupling from modulation of t_{pd}) therefore effectively agrees with the one we found in Sec. 2.4.1 to be most important. To investigate the effect on phonons, the phonon self-energy is calculated in second-order perturbation theory using exact diagonalization of systems without phonons. The softening and broadening for a few \mathbf{q} points is shown but no systematic discussion of the dependence on wavevector and doping is given.

Horsch and Khaliullin [34, 35, 62] study the density response of the t - J model without phonons using a slave-boson approach. They then also consider only on-site electron-phonon coupling which they roughly estimate from the change of the Zhang-Rice singlet energy due to the modulation of t_{pd} in the three-band model. This is done for the (half-)breathing mode with the simplifying assumption that for any \mathbf{q} only O atoms move. Working to lowest order in the coupling, they relate the softening and broadening of the breathing mode to the density response. In their analysis, the increase of the softening upon doping is due to the scaling of the density response proportional to the doping δ . A low-energy (spin-)polaron peak which is only present for the $\mathbf{q} = (\xi, 0)$ direction gives rise to an extra contribution to the softening of the half-breathing mode when its energy is close to the phonon frequency around optimal doping. They use these results to explain differences of the half-breathing and breathing mode in softening and broadening. Similar studies have also been made using the complementary slave-fermion method [36].

In their derivation of electron-phonon coupling in the t - J model, Ishihara and Nagaosa [31] include also the modulation of the level energies in the three-band model in addition to the modulation of the hopping amplitudes. They argue that vertex

corrections would suppress site-diagonal coupling in the resulting low-energy model at large phonon momenta relevant for the (half-)breathing mode and concentrate entirely on the effect of the site-off-diagonal coupling. Our results do not support this view. As discussed in Sec. 2.4.1, it follows from our more detailed derivation that already the bare site-off-diagonal coupling is about an order of magnitude smaller than the site-diagonal one. Our calculations using exact diagonalization of finite clusters which fully include the effect of vertex corrections show that there is no suppression of the on-site coupling which basically determines the phonon softening and broadening. Switching on or off the site-off-diagonal coupling leads only to small changes.

Ishihara and Nagaosa also argue that the electron-phonon interaction arising from the modulation of the super-exchange interaction by the phonons would give an important contribution to the site-off-diagonal coupling. Ohkawa [32] even takes the view that this coupling mechanism is the most relevant one. In contrast, by working only up to order $t_{pd}^2 u$ in deriving the electron-phonon interaction we have neglected the coupling via the modulation of J in the Heisenberg term (Eq. (1.54)). The following arguments, however, show that this was justified. As can be seen from Eq. (1.55), the modulation of J is caused by its dependence on the phonon-modulated parameters t_{pd} and Δ_{pd} . Redoing the derivation leading to Eq. (1.55) for a distorted lattice gives the following variation of J [32]:

$$\Delta J_{ij} = 2J(\Delta t_{i[ij]} + \Delta t_{j[ij]})/t_{pd} + \underbrace{\frac{2t_{pd}^4}{\Delta_{pd}^2} \left(\frac{3}{\Delta_{pd}} + \frac{2}{U} \right)}_{< 3/2J} (\Delta \varepsilon_i^d + \Delta \varepsilon_j^d - 2\Delta \varepsilon_{[ij]}^p)/\Delta_{pd}. \quad (2.43)$$

Here, i and j are nearest-neighbor Cu sites, $[ij]$ denotes the O site in-between. Equation (2.43) shows that the corresponding electron-phonon coupling has a prefactor of order J in agreement with our finding in Sec. 2.4.1 that the modulation of a parameter is roughly proportional to its unperturbed value. But as J is small compared to t or the singlet-triplet splitting, the coupling derived from its modulation can be neglected compared to the other coupling mechanisms. In addition, one finds [30] that the contribution to Eq. (2.43) from the modulation of t_{pd} is only proportional to displacements of Cu atoms. This is also true for the contribution from the modulation of ε^p . Only the modulation of ε^d leads to a coupling proportional to the displacements of O atoms. This should be the dominant term because of the much smaller mass of the O atoms compared to the Cu atoms. But the \mathbf{q} dependence is such that e.g. the half-breathing mode does not couple at all via J at the zone boundary as

$\Delta\varepsilon_i^d = -\Delta\varepsilon_j^d$ in that case.

2.4.3 Non-linear contributions to electron-phonon coupling

The electron-phonon interaction in the t - J model has been derived in Chap. 1 up to linear order in the atomic displacements. In this section, we estimate the importance of the neglected non-linear contributions to the electron-phonon coupling. The results in Sec. 2.3 obtained for the HF solution of the three-band model, where second-order terms were included by the term $(\partial^2 E/\partial u^2)^{(2)}$ in Eq. (2.8), indicate that they might lead to non-negligible effects.

Instead of starting out from the three-band model (1.1) of the CuO_2 plane, we first consider an isolated CuO_4 plaquette consisting of only one Cu - d orbital and the four nearest-neighbor O - p orbitals. If we assume that distortions of the plaquette only lead to modulation of the p - d hopping amplitudes, it is described by the Hamiltonian

$$H_{\text{plaqu.}} = \varepsilon^d n^d + \varepsilon^p \sum_{j=1}^4 n_j^p + U n_{\uparrow}^d n_{\downarrow}^d + \sum_{\sigma=\uparrow,\downarrow} \sum_{j=1}^4 [(-1)^j t_j d_{\sigma}^{\dagger} p_{j\sigma} + \text{H.c.}]. \quad (2.44)$$

We treat the hopping amplitudes t_j between the d orbital and the four p orbitals (labeled by j) as a perturbation and calculate the ground-state energy of the plaquette with either one or two holes in second-order perturbation theory.

To zeroth order in the hopping, a single hole occupies the d orbital and lowers its energy by virtually hopping in and out of the p orbitals:

$$E_{\text{plaqu.}}^{\text{Cu-}d} = \varepsilon^d - \frac{1}{\Delta_{pd}} \sum_{j=1}^4 t_j^2. \quad (2.45)$$

In case of two holes in the plaquette, the second hole will go into the p orbitals in the atomic limit. The operator

$$\tilde{\phi}_{\sigma}^{\dagger} = \frac{\sum_{j=1}^4 (-1)^j t_j p_{j\sigma}^{\dagger}}{\sqrt{\sum_{j=1}^4 t_j^2}} \quad (2.46)$$

creates a hole in a linear combination of the p orbitals that maximizes the transition amplitude to the d orbital, $\langle \tilde{\phi}_{\sigma} | H_{\text{plaqu.}} | d_{\sigma} \rangle = \sqrt{\sum_{j=1}^4 t_j^2}$. One finds that the energy gain in second-order perturbation theory is largest for a singlet combination of a d hole and a $\tilde{\phi}$ hole leading to the following ground-state energy of plaquette with two holes:

$$E_{\text{plaqu.}}^{\text{singlet}} = \varepsilon^d + \varepsilon^d - 2 \left(\frac{1}{\Delta_{pd}} + \frac{1}{U - \Delta_{pd}} \right) \sum_{j=1}^4 t_j^2. \quad (2.47)$$

We expand the sum of the squared hopping amplitudes that occurs in Eqs. (2.45) and (2.47) up to second order in the atomic displacements assuming that t_{pd} depends only on the interatomic distance r :

$$\sum_{j=1}^4 t_j^2 = 4t_{pd}^2 - 2t_{pd} \left. \frac{dt_{pd}}{dr} \right|_0 \sum_{j=1}^4 (-1)^j u_j + \left[\left(\left. \frac{dt_{pd}}{dr} \right|_0 \right)^2 + t_{pd} \left. \frac{d^2 t_{pd}}{dr^2} \right|_0 \right] \sum_{j=1}^4 u_j^2 + \mathcal{O}(u^3), \quad (2.48)$$

where u_j denotes the displacement of the j th O atom and the Cu atom is assumed to remain at its equilibrium position.

If we think of the CuO_2 plane as being composed of individual plaquettes and neglect any effects arising from the fact that each plaquette actually couples to the four neighboring ones via the shared p orbitals, we can make the following low-energy (rather ground-state) approximation of the three-band model:

$$H_{\text{approx.}} = \sum_i \left(E_{\text{plaqu.}}^{\text{Cu-}d} n_i + E_{\text{plaqu.}}^{\text{singlet}} (1 - n_i) \right). \quad (2.49)$$

Like in the t - J model, a singlet is interpreted as the absence of a Cu- d hole and n_i measures the corresponding occupancy on the plaquette labeled by i . Using Eqs. (2.45), (2.47), and (2.48) we obtain the dependence of $H_{\text{approx.}}$ on the atomic displacements up to order u^2 . If we compare with the results of Chap. 1 for the on-site energies (second line of Eq. (1.87)) and the linear on-site electron-phonon interaction (Eq. (1.110)) in the t - J model due to the modulation of the t_{pd} , we find that they are already obtained from $H_{\text{approx.}}$ except for a factor λ^2 . This difference is due to neglecting intermediate states from hopping into orbitals on other sites in the derivation of the effective model for the lattice using perturbation theory.

By considering the terms in $H_{\text{approx.}}$ which are quadratic in the displacements, we can then estimate the effect of the non-linear electron-phonon interaction. As an example, we consider the O half-breathing phonon ($\mathbf{q} = (1, 0)\pi/a$) with amplitude u . One finds the following doping-dependent energy shift per site proportional to u^2 when the system is doped with δN holes:

$$\Delta E^{(2)} = - \left(\frac{1}{\Delta_{pd}} + \frac{2}{U - \Delta_{pd}} \right) \left[\left(\left. \frac{dt_{pd}}{dr} \right|_0 \right)^2 + t_{pd} \left. \frac{d^2 t_{pd}}{dr^2} \right|_0 \right] 2u^2 \delta. \quad (2.50)$$

This directly adds to the bare phonon potential energy per site $2 \cdot M_{\text{O}} \omega_{\text{bare}}^2 u^2 / 2$ and leads to the following estimate for the softening of the half-breathing mode due to the quadratic electron-phonon coupling:

$$\hbar \Delta \omega^{(2)} \approx \frac{\hbar}{2M_{\text{O}} \omega_{\text{bare}}} \frac{\Delta E^{(2)}}{u^2} \approx -0.044 \text{ eV } \delta. \quad (2.51)$$

The numerical value has been calculated for $\hbar\omega_{\text{bare}} = 80$ meV using our standard parameters for the three-band model and Eq. (1.26) for the distance dependence of t_{pd} . For a doping $\delta = 0.1$, one therefore expects roughly 4 meV softening compared to the undoped system. If $H_{\text{approx.}}$ is rederived taking into account also non-linear coupling from the modulation of the level energies using Eqs. (1.28-1.30), one finds a reduction of the softening effect by about 5%. As we have calculated a softening of about 10 meV for this doping from the linear electron-phonon interaction (cf. Tab. 2.1), the non-linear coupling could contribute with up to 30% to the total softening. Although we can expect only a crude estimate from the plaquette calculation, this result indicates the possible importance of non-linear contributions to the electron-phonon coupling. It is very difficult to consistently derive it for an effective model on the lattice as many approximations that could be made in Chap. 1 lead to errors of the order u^2 and therefore are no longer possible in this context. For this reason, we have explicitly derived only the linear electron-phonon interaction and neglected non-linear contributions in all related calculations as is customary in the field. Our estimate in this section, however, shows that non-linear electron-phonon coupling does not necessarily need to give negligibly small effects and should not be discarded from the start.

2.4.4 Coupling to other phonon modes

In this section, we consider the electron-phonon coupling to phonons other than the (half-)breathing mode. We found in Sec. 2.4.1 that the main contribution to the coupling derived in Chap. 1 comes from the modulation of the on-site energies in the t - J model due to the modulation of the p - d hopping in the three-band model. The corresponding coupling is proportional to the expression in Eq. (1.110) which shows that strong coupling requires the oxygen atoms in the CuO_2 plane to be displaced along the bond directions. This is true for the (half-)breathing mode which at the zone boundary involves only oxygen displacements along the bonds with an optimal relative phase shift. Towards the zone center, however, there is an increasing displacement of Cu atoms, too. Normalization of the phonon polarization vectors then leads to a reduction of the O polarization vectors. Completeness requires that the missing O weight is transferred to other modes. In a two-spring model, the weight goes to an acoustic mode for which the electron-phonon coupling therefore becomes non-negligible away from the zone boundary. Because of its small frequency, this mode is then softened far more (almost 50% for $\mathbf{q} = (\pi/(2a), 0)$) than observed experimentally.

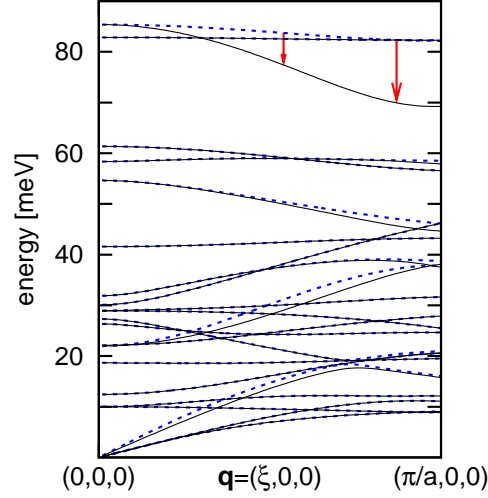


Figure 2.13: Phonon dispersion in the $(\xi, 0, 0)$ direction for a shell model. The dashed curves show results with the extra O-O spring describing the O atoms' coupling to the Zhang-Rice singlets. The arrows indicate the strong softening of the half-breathing mode, while other modes are not changed very much.

To address this, we have used a more realistic shell model [16, 15] for obtaining polarization vectors. This model gives almost exactly the same eigenvectors for the half-breathing mode as our two-spring model. The missing O weight towards the zone center, however, is now distributed over several modes, and the softening of a given mode is weaker. For instance, the longitudinal acoustic $\mathbf{q} = (\pi/(2a), 0)$ phonon is softened by about 25%. Although smaller than in the two-spring model, the softening is still too large. It is, however, further reduced by the repulsion from lower-lying modes of the same symmetry.

To study this, we have modified the shell model to take the electron-phonon interaction into account. The movement of two O atoms towards a Cu atom leads to a lowering of the Zhang-Rice singlet energy. The system can take advantage of this by transferring a singlet to such a site. This is approximately described by introducing a spring with a *negative* spring constant, $\kappa = -3 \text{ eV/\AA}^2$, between two O atoms on opposite sides of a Cu atom. A similar term was used to describe $\text{La}_{2-\delta}\text{Sr}_\delta\text{NiO}_4$ [47, 68]. The present work gives justification for such a spring. Figure 2.13 compares results of the shell model with and without the additional spring. Apart from the half-breathing mode, no mode is strongly softened by the new spring.² Our t - J model with phonons thus correctly softens the half-breathing mode without introducing

unphysical softening of other modes.

Finally, we comment on the coupling of the so-called B_{1g} buckling mode within our model for the electron-phonon interaction in cuprates. This optical phonon describes out-of-phase displacements of the in-plane O atoms perpendicular to the CuO_2 planes and has an energy of about 40 meV. The energy and the broadening of this phonon change upon cooling when superconductivity sets in [69,70,20], and a Fano line shape is observed in Raman scattering [70,20]. Both observations suggest an electron-phonon coupling. Also photoemission experiments have been interpreted by some authors in terms of coupling to this mode [71,72]. In our model based on a single flat CuO_2 plane, the electron-phonon interaction for the B_{1g} mode is zero to first order in the displacements for symmetry reasons. In many cuprates, however, the environment of a CuO_2 plane is asymmetric. $\text{YBa}_2\text{Cu}_3\text{O}_{7-\delta}$, for instance, has Ba^{2+} ions on one side and Y^{3+} ions on the other side [73]. The resulting electric field perpendicular to the CuO_2 plane leads to a coupling of doped holes in planar O- p orbitals to the B_{1g} phonon [73].

As the analysis in this section has shown, only the (half-)breathing modes couple strongly in the present t - J model with electron-phonon interaction which was derived using screened Coulomb interactions assumed to be appropriate for moderately doped cuprates. We will see in the next chapter, however, that the modulation of the electrostatic potential in the much more weakly screened undoped system leads to additional coupling of other modes.

2.5 Summary

We have solved the t - J model with electron-phonon interaction derived in Chap. 1 using exact diagonalization of small clusters to specifically study the effects of this coupling on the (half-)breathing modes in cuprates.

We find that the experimentally observed anomalously strong softening of the half-breathing mode upon doping is successfully described. Not only the doping dependence but also the \mathbf{q} dependence agrees well with experiment, with the half-breathing mode being softened more strongly than the breathing mode. By studying the phonon self-energy, we can also assess the broadening of the phonon spectral func-

²This spring model appropriately softens the breathing mode but softens a mode with $\epsilon_{\text{O}\hat{\mathbf{x}}/2}^{\hat{\mathbf{x}}/2} = -\epsilon_{\text{O}\hat{\mathbf{y}}/2}^{\hat{\mathbf{y}}/2} = 1/\sqrt{2}$ and $\mathbf{q} = \pi/a(1,1)$ too strongly. However, such a mode does not couple strongly in our t - J model with phonons.

tions and find qualitative agreement of our calculated widths with the experimental results.

In order to investigate the importance of strong correlations for these results, we have also considered the Hartree-Fock mean-field approximation of the three-band model. A comparison with results from the t - J model shows that in this approach both the softening and the broadening of the phonons have quite different dependences on doping and phonon wavevector which are in worse agreement with experimental findings. This indicates that the explicit treatment of strong correlations and many-body effects is essential for a successful description of the phonon anomalies in cuprates.

An analysis of the different coupling mechanisms shows that the on-site coupling due to the modulation of the p - d hopping dominates. In view of this result, other approaches to the problem are critically discussed. We also investigate the importance of non-linear contributions to the electron-phonon interaction. Calculations for a simple plaquette model indicate that they should not be neglected a priori but are difficult to treat consistently in a full lattice model.

We find that our model does not lead to strong coupling to phonon modes other than the (half-)breathing modes. In this context, it is interesting to discuss whether the latter could be relevant for superconductivity in the high- T_c cuprates. Roughly speaking, the coupling to the (half-)breathing modes becomes stronger with increasing $|\mathbf{q}|$. Such a \mathbf{q} dependence, however, has been found to be unfavorable for d -wave superconductivity in Eliashberg-like theories [74].

Chapter 3

Polaronic effects in undoped cuprates

3.1 Introduction

Angle-resolved photoemission spectroscopy (ARPES) experiments have found evidence for strong electron-phonon interaction and polaron physics in many materials like quasi-one-dimensional conductors [75, 76], the manganites [77], or the undoped high- T_c cuprates [26, 27] which we focus on in this work.

Figure 3.1a shows the ARPES spectrum of undoped $\text{Ca}_2\text{CuO}_2\text{Cl}_2$ at the top of the band ($\mathbf{k} = (\pi/(2a), \pi/(2a))$). The spectrum has a broad feature centered at A with the onset at B. The dispersions of A and B are shown in Fig. 3.1b. The dispersion of A agrees well with that of the quasi-particle in the extended t - J model [78]. Therefore, feature A has often been identified as the quasi-particle peak which is strongly broadened by some unknown mechanism as the t - J model predicts a much smaller width.

Shen *et al.* [26] pointed out, however, that the peak does not have a Lorentzian line shape as expected for a life-time broadening but is rather Gaussian (cf. Fig. 3.1a). Also, one would expect a very small width for the quasi-particle at the top of the valence band of an insulator as there is no phase space for decay by creating electron-hole pairs. As shown in Fig. 3.1b, the value of the chemical potential varies in this insulator from sample to sample probably due to different pinning by impurities. But the fact that it always is at least about 0.45 eV above feature A led to the interpretation of the spectra in terms of self-trapping of polarons due to strong coupling to bosons [26]. In this picture, with increasing strength of the electron-boson coupling a

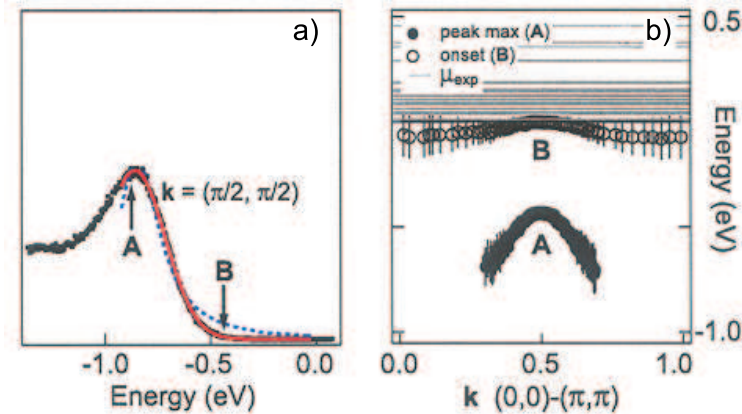


Figure 3.1: a) ARPES spectrum of undoped $\text{Ca}_2\text{CuO}_2\text{Cl}_2$ for $\mathbf{k} = (\pi/(2a), \pi/(2a))$ together with fits to a Gaussian (solid red curve) and a Lorentzian (dashed blue curve). The maximum of the broad feature is denoted by A and its onset by B. b) Dispersion of A and B along the nodal direction as well as the different values of the chemical potential for a large number of samples (after Shen *et al.* [26]).

crossover occurs from quasi-particles which are weakly coupled to bosons to polarons which are trapped due to strong interaction with the bosons. The weight and dispersion of the corresponding quasi-particle peak in ARPES spectra become strongly suppressed. This points to feature B representing the true quasi-particle peak which explains why the chemical potential is never found below B as this marks the top of the band in the new interpretation. Feature A instead is then seen as an incoherent boson side band which is expected to have a Gaussian-like shape. Furthermore, the width of the broad peak is found to have an appreciable temperature dependence providing further support to the interpretation in terms of coupling to bosons [27]. Similar ARPES spectra have been measured also for undoped La_2CuO_4 [79]. Figure 3.2 shows data taken at 20 K along the nodal direction. Again, a broad side band at a binding energy of about 0.5 eV shows up.

Some approaches to purely electronic models like the t - J model and the Hubbard model predict the quasi-particle weight Z to be zero in the undoped system [80, 81], possibly allowing for the interpretation of the broad peak seen in experimental ARPES spectra of undoped cuprates in terms of an incoherent contribution to the spectrum due to electron-electron interaction. Whereas a vanishing Z is also found in the paramagnetic phase of the dynamical mean-field approximation [7] of the half-filled Hubbard model in the limit of large on-site Coulomb repulsion, a finite quasi-particle weight is obtained in the more appropriate antiferromagnetic phase [82].

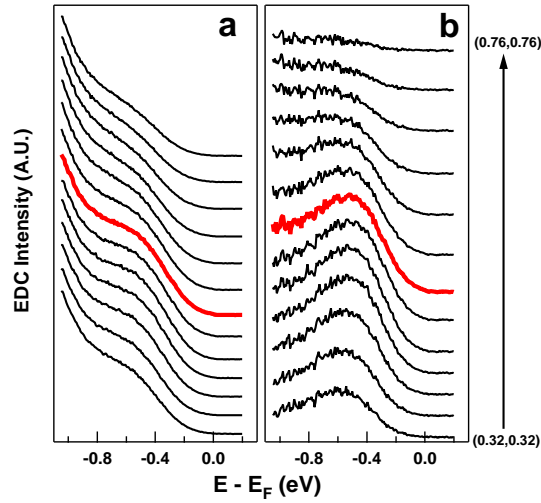


Figure 3.2: a) ARPES spectra of La_2CuO_4 along the $(0,0)$ - $(\pi/a,\pi/a)$ nodal direction. The corresponding momentum runs from $(0.32,0.32)\pi/a$ to $(0.76,0.76)\pi/a$, as indicated by the arrow. b) To highlight the momentum dependence, a "background" given by a spectrum near $(\pi/a,\pi/a)$ was subtracted from the spectra. The bold curves correspond to a momentum near $(\pi/(2a),\pi/(2a))$ (after Ref. [79]).

Exact diagonalization of t - J clusters with up to 32 sites [83,84] and quantum Monte Carlo simulations of systems with up to 32×32 sites [85,86] also give a finite Z which does not appear to vanish with increasing cluster size. These essentially exact findings suggest that the experimental results for undoped cuprates which indicate $Z \approx 0$ are inconsistent with a purely electronic model and that coupling to bosons is needed to obtain basically zero quasi-particle weight. This raises the question whether these bosons can be identified with phonons.

As already mentioned, the dispersion of the broad feature matches the quasi-particle dispersion calculated in purely electronic models. This seems surprising since the side band is thought to originate from a strong electron-boson coupling. Similar observations in the manganites [77] and quasi-one-dimensional conductors [75,76] have been interpreted in analogy with a single electron coupled to harmonic oscillators [87] and a related sum rule for the first spectral moment. With respect to the manganites, also the picture of the photohole seeing a *frozen* lattice has been used [88]. Numerical calculations [89] of the ARPES spectra for an undoped t - J model with coupling of doped holes to optical phonons indeed showed broad features tracing the dispersion of the quasi-particles in the original t - J model.

In this chapter, we want to investigate whether the polaronic behavior observed

in undoped cuprates can be explained in terms of strong electron-phonon coupling. First, we calculate the electron-phonon coupling for undoped La_2CuO_4 using a shell model. We find that the coupling is sufficiently strong to give self-trapped polarons. Next, we consider the theory for ARPES spectra in an adiabatic approximation. It explains why for undoped systems the electron-phonon interaction just leads to a broadening of spectra calculated without electron-phonon coupling and does not change the dispersion. In addition, it allows for the development of an efficient method for calculating ARPES spectra from undoped systems with many phonon modes and at finite temperature. Calculations with the coupling derived for La_2CuO_4 give side band widths which are in good agreement with experiment. The dependence of the width on the binding energy and on the temperature is analyzed.

3.2 Electron-phonon coupling in undoped cuprates

In this section, we calculate the electron-phonon coupling to a single hole added to an undoped system, e.g. in a photoemission experiment. The electron-phonon interaction derived in Chap. 1 takes into account that lattice vibrations modulate both the p - d hopping amplitude and the level energies in the three-band model of a CuO_2 plane. It is assumed, however, that due to screening of the Coulomb interaction only the displacements of the nearest-neighbor ions influence the energy of the orbitals. This may be appropriate for the doping ranges considered in the discussion of the anomalous softening of the half-breathing mode in Chap. 2. But as screening is much less effective in the insulating undoped cuprates, the coupling due to the modulation of the electrostatic potential must be reconsidered for these systems.

Because of the long-range nature of the Coulomb interaction, we cannot restrict the calculations to a CuO_2 plane but contributions from all ions in the full lattice have to be included. We therefore use a shell model [16,15] that successfully describes phonon dispersions in several cuprates. In this model, each atom is represented by a core and a shell coupled by a spring. The charges on the cores and shells of all atoms interact via the long-range Coulomb interaction. Screening is only provided by the ionic polarizations when the shells are displaced against the atomic cores. In addition, there are short-range interactions acting only between shells which are described by Born-Mayer and van der Waals potentials.

Within the shell model, the electrostatic potential at \mathbf{r} is given by

$$V(\mathbf{r}) = \frac{e}{4\pi\epsilon_0} \sum_{ik\alpha} \frac{Q_{k\alpha}}{|\mathbf{R}_{ik\alpha} - \mathbf{r}|}, \quad (3.1)$$

where ϵ_0 is the vacuum permittivity. The sum runs over all unit cells labeled by i , the atoms in each unit cell labeled by k , and core and shell of each atom labeled by $\alpha = c, s$, respectively. Cores and shells with charges $\mathcal{Q}_{k\alpha}$ (in units of the elementary charge $e > 0$) are located at $\mathbf{R}_{ik\alpha} = \mathbf{R}_i + \mathbf{r}_k + \mathbf{u}_{ik\alpha}$ where \mathbf{r}_k gives the equilibrium position within the unit cell at \mathbf{R}_i and $\mathbf{u}_{ik\alpha}$ is the displacement due to lattice vibrations. In the undistorted lattice, the centers of the core and the shell of an atom are located at the same position but a lattice vibration can displace them differently.

Adding a hole to the shell of the atom k in the unit cell i then increases the Coulomb energy by

$$\Delta E_{ik} = e V(\mathbf{R}_i + \mathbf{r}_k) = \frac{e^2}{4\pi\epsilon_0} \sum'_{i'k'\alpha} \frac{\mathcal{Q}_{k'\alpha}}{|\mathbf{R}_{i'} - \mathbf{R}_i + \mathbf{r}_{k'} - \mathbf{r}_k + \mathbf{u}_{i'k'\alpha} - \mathbf{u}_{iks}|}, \quad (3.2)$$

where the prime on the summation symbol indicates that the divergent contribution for $(i'k'\alpha) = (iks)$ is not included in the sum. If we expand ΔE_{ik} in the displacements, the contribution linear in $\mathbf{u}_{ik\alpha}$ is given by

$$\Delta E_{ik}^{(1)} = -\frac{e^2}{4\pi\epsilon_0} \sum'_{jk'\alpha} \frac{\mathcal{Q}_{k'\alpha}}{|\mathbf{R}_j + \mathbf{r}_{k'} - \mathbf{r}_k|^3} (\mathbf{R}_j + \mathbf{r}_{k'} - \mathbf{r}_k) \cdot (\mathbf{u}_{jk\alpha} - \mathbf{u}_{iks}), \quad (3.3)$$

where we changed to summing over $\mathbf{R}_j = \mathbf{R}_{i'} + \mathbf{R}_i$ with the prime on the summation symbol now indicating that terms with $(jk') = (0k)$ are excluded (for $\mathbf{R}_0 = \mathbf{0}$).

In terms of phonon creation and annihilation operators, the displacements are given by

$$\mathbf{u}_{ik\alpha} = \sum_{\mathbf{q}\nu} \sqrt{\frac{\hbar}{2N'\omega_{\mathbf{q}\nu}}} \mathbf{E}_{\mathbf{q}\nu}^{(k\alpha)} (b_{\mathbf{q}\nu} + b_{\mathbf{q}\nu}^\dagger) e^{i\mathbf{q}\cdot(\mathbf{R}_i + \mathbf{r}_k)}, \quad (3.4)$$

where the core polarization vectors $\mathbf{E}_{\mathbf{q}\nu}^{(k\alpha)}$ in the shell model for a phonon mode of branch ν with wavevector \mathbf{q} and frequency $\omega_{\mathbf{q}\nu}$ are obtained from solving

$$\omega_{\mathbf{q}\nu}^2 M \mathbf{E}_{\mathbf{q}\nu}^{(kc)} = [(R + ZCZ) - (T + ZCY)(S + YCY)^{-1}(T^T + YCZ)] \mathbf{E}_{\mathbf{q}\nu}^{(kc)}. \quad (3.5)$$

M, Z, Y, C, R, S, T are matrices describing the atomic masses, the charges of ions and shells, the Coulomb interaction, and the short-range interactions, see e.g. Ref. [90] for more details. The shell polarization vectors are then determined by

$$\mathbf{E}_{\mathbf{q}\nu}^{(ks)} = [1 - (S + YCY)^{-1}(T^T + YCZ)] \mathbf{E}_{\mathbf{q}\nu}^{(kc)}. \quad (3.6)$$

Using Eqs. (3.3) and (3.4), we arrive at the following linear electron-phonon coupling due to the modulation of the electrostatic potential in the shell model:

$$H_{\text{ep}} = \sum_{ik} \Delta E_{ik}^{(1)} n_{ik}^h = \frac{1}{\sqrt{N'}} \sum_{ik} \sum_{\mathbf{q}\nu} g_{\mathbf{q}\nu}^{(k)} n_{ik}^h (b_{\mathbf{q}\nu} + b_{\mathbf{q}\nu}^\dagger) e^{i\mathbf{q}\cdot(\mathbf{R}_i + \mathbf{r}_k)}, \quad (3.7)$$

with

$$g_{\mathbf{q}\nu}^{(k)} = -\sqrt{\frac{\hbar}{2\omega_{\mathbf{q}\nu}}} \frac{e^2}{4\pi\epsilon_0} \sum'_{jk'\alpha} \frac{Q_{k'\alpha}}{|\mathbf{R}_j + \mathbf{r}_{k'} - \mathbf{r}_k|^3} (\mathbf{R}_j + \mathbf{r}_{k'} - \mathbf{r}_k) \cdot (\mathbf{E}_{\mathbf{q}\nu}^{(k'\alpha)} e^{i\mathbf{q}\cdot\mathbf{R}_j} - \mathbf{E}_{\mathbf{q}\nu}^{(ks)} e^{i\mathbf{q}\cdot(\mathbf{r}_{k'} - \mathbf{r}_k)}). \quad (3.8)$$

The primed summation does not include terms with $(jk') = (ik)$. n_{ik}^h measures doped holes in the shell of atom k in the unit cell i . N' is the total number of unit cells in the three-dimensional lattice.

We use the t - J model to describe the electronic degrees of freedom in the CuO_2 planes, i.e., we assume that doped holes form Zhang-Rice singlets with the spins of Cu - d holes. In a first approximation, the additional charge is distributed symmetrically on the four neighboring O - p orbitals [29]. If we write the electron-phonon interaction in the t - J model as

$$H_{\text{ep}} = \frac{1}{\sqrt{N'}} \sum_{\mathbf{q}\nu i} g_{\mathbf{q}\nu} (1 - n_i) (b_{\mathbf{q}\nu} + b_{\mathbf{q}\nu}^\dagger) e^{i\mathbf{q}\cdot\mathbf{R}_i}, \quad (3.9)$$

we therefore assume that the contribution $\tilde{g}_{\mathbf{q}\nu}$ to the coupling constant $g_{\mathbf{q}\nu}$ from the modulation of the electrostatic potential is given by the average over the couplings $g_{\mathbf{q}\nu}^{(k)}$ at the four O sites surrounding a Cu atom,

$$\tilde{g}_{\mathbf{q}\nu} = \frac{1}{2} (g_{\mathbf{q}\nu}^{(\text{O}_x)} \cos(q_x a/2) + g_{\mathbf{q}\nu}^{(\text{O}_y)} \cos(q_y a/2)). \quad (3.10)$$

Equation (3.9) is an on-site coupling to empty sites representing singlets in the t - J model with \mathbf{R}_i referring to plaquette sites in a CuO_2 plane. O_x and O_y in Eq. (3.10) refer to the two O atoms in the unit cell that are part of the CuO_2 plane.

The remaining contribution to the coupling ($g_{\mathbf{q}\nu} - \tilde{g}_{\mathbf{q}\nu}$) is calculated from the modulation of the on-site energy corrections for Cu - d holes and singlets in the t - J model as obtained from the three-band model with phonon-modulated p - d hopping and charge-transfer energy. The smaller off-site-diagonal coupling is neglected (cf. the discussion in Sec. 2.4.1). Using Eqs. (1.108)-(1.111) derived in Chap. 1, we have

$$g_{\mathbf{q}\nu} - \tilde{g}_{\mathbf{q}\nu} = \left[-i \sqrt{\frac{\hbar}{2\omega_{\mathbf{q}\nu}}} 4\lambda^2 t_{pd}^2 \left. \frac{dt_{pd}}{dr} \right|_0 \left(\frac{2}{U - \Delta_{pd}} + \frac{1}{\Delta_{pd}} \right) \sum_{\delta=x,y} (\mathbf{E}_{\mathbf{q}\nu}^{(\text{O}_{\delta c})} \cdot \hat{\boldsymbol{\delta}}) \sin(q_\delta a/2) + 4\lambda^2 t_{pd}^2 \left(\frac{1}{\Delta_{pd}^2} - \frac{2}{(U - \Delta_{pd})^2} \right) (\tilde{g}_{\mathbf{q}\nu} - g_{\mathbf{q}\nu}^{(\text{Cu})}) \right], \quad (3.11)$$

where the coupling constants $\tilde{g}_{\mathbf{q}\nu}$ and $g_{\mathbf{q}\nu}^{(\text{Cu})}$ appear in the second line because we use the modulated electrostatic potential obtained from the shell model instead of

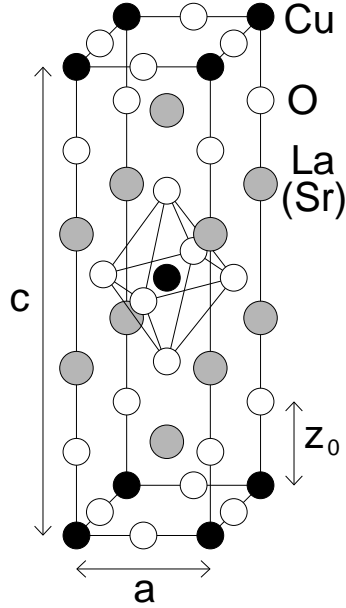


Figure 3.3: Crystal structure of $\text{La}_{2-\delta}\text{Sr}_\delta\text{CuO}_4$ (body-centered tetragonal phase).

the screened level modulations $\Delta\varepsilon_i^d$ and $\Delta\varepsilon_{i\delta}^p$ from Eqs. (1.31) and (1.32) in the contribution corresponding to $A^{(\varepsilon)}(\mathbf{q}, \nu)$ (Eq. (1.111)). The first term in $A^{(\varepsilon)}(\mathbf{q}, \nu)$ is not included because the direct coupling from the modulation of the level energies is already taken into account by Eq. (3.10).

We have implemented the shell model of Chaplot *et al.* [16, 15] for undoped La_2CuO_4 and use it to obtain the frequencies and polarization vectors of the phonon modes in this material. These are needed to calculate the electron-phonon coupling using Eqs. (3.8), (3.10), and (3.11). The phonon frequencies are in very good agreement with experimental results and, since the shell model describes neutron scattering intensities well, the eigenvectors are also believed to be accurate [17]. The summation in Eq. (3.8) is performed using the Ewald technique [91, 92] that is also needed for the Coulomb sums in the shell model, Eq. (3.6). The shell model calculations are done on a $(30)^3$ mesh in \mathbf{q} space using the high-temperature tetragonal structure from Ref. [16, 15] (cf. Fig. 3.3) but similar results are obtained for the low-temperature orthorhombic structure.

Introducing the dimensionless coupling constant $\lambda \equiv 2 \sum_{\mathbf{q}\nu} |g_{\mathbf{q}\nu}|^2 / (8t\hbar\omega_{\mathbf{q}\nu}N')$, we obtain $\lambda = 1.2^1$ for $t = 0.4$ eV. The criterion for the crossover to self-trapped polarons in the Holstein- t - J model is $\lambda > \lambda_c = 0.4$ [89]. If the next-nearest-neighbor hopping integral t' is taken into account, λ_c should increase. The coupling derived for undoped

¹The finite number of mesh points leads to an underestimate of λ by about 3% for a $(30)^3$ mesh.

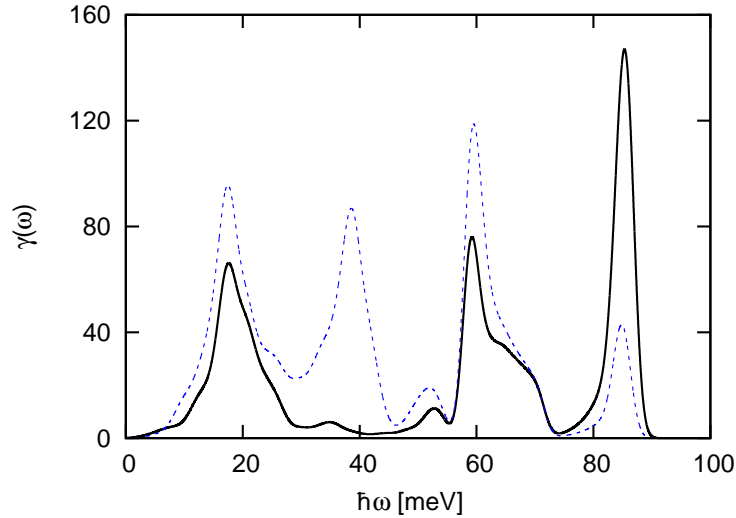


Figure 3.4: Spectral distribution of the coupling to singlets (full line) and to holes in non-bonding O- p orbitals (dashed line). A Gaussian broadening (FWHM=3 meV) was used.

La_2CuO_4 should, nevertheless, be strong enough to lead to self-trapped polarons in terms of which the experimental observations can be interpreted.

Figure 3.4 shows the spectral distribution $\gamma(\omega) \equiv \sum_{\mathbf{q}\nu} |g_{\mathbf{q}\nu}|^2 / (\hbar\omega_{\mathbf{q}\nu} N') \delta(\hbar\omega - \hbar\omega_{\mathbf{q}\nu})$ of our coupling (full line). An analysis of the polarization vectors of the coupling phonon modes shows that the peak around 20 meV can be attributed to modes involving mainly La whereas the spectral weight at 60-70 meV is mostly due to vibrations of the apical O. The peak around 85 meV is caused by the planar O (half-)breathing mode. The latter couples predominantly via the modulation of the on-site energy corrections in the t - J model. We find that the main contribution to the corresponding coupling in Eq. (3.11) still comes from the modulation of t_{pd} as discussed in Sec. 2.4.1 for the doped system. The coupling to the other modes, however, basically originates from the modulation of the electrostatic potential.

As an example, we discuss the modes involving displacements of apical oxygens perpendicular to the CuO_2 planes in a simple model framework. They give the main contribution to $\gamma(\omega)$ in the 60-70 meV energy range. If we assume that $q_{\parallel} = |(q_x, q_y)|$ is small, it is a good approximation to replace the individual ionic charges (which we do not separate into core and shell charges in this context) by homogeneously charged planes perpendicular to the c axis. From the apical oxygens with charge Q_O , we obtain two planes per unit cell with the charge density $\sigma = Q_O/a^2$ at the positions $z_{ns} = nc/2 + sz_0$ where n labels CuO_2 planes and $s = \pm$ indicates whether we refer

to oxygen ions above or below a CuO_2 plane (cf. Fig. 3.3). They give rise to the following electrostatic potential in the CuO_2 plane at $z = 0$:

$$V(z=0) = \frac{2\pi\sigma}{4\pi\epsilon_0} \frac{1}{q_{\parallel}} \sum_{n=-\infty}^{\infty} \sum_{s=\pm} e^{-q_{\parallel}|z_{ns}|}. \quad (3.12)$$

If we assume that only the apical oxygens move along the z direction with amplitude u , we can derive from Eq. (3.12) that the corresponding coupling is proportional to

$$\begin{aligned} \left. \frac{\partial V_{\text{in/out}}}{\partial u}(z=0) \right|_{u=0} &= \frac{2\pi\sigma}{4\pi\epsilon_0} \left[\frac{e^{-q_{\parallel}z_0} \pm e^{q_{\parallel}z_0} e^{(iq_z - q_{\parallel})c/2}}{1 - e^{(iq_z - q_{\parallel})c/2}} + \frac{\mp e^{-q_{\parallel}z_0} - e^{q_{\parallel}z_0} e^{-(iq_z + q_{\parallel})c/2}}{1 - e^{-(iq_z + q_{\parallel})c/2}} \right] \\ &\approx \frac{2\pi\sigma}{4\pi\epsilon_0} \times \begin{cases} \frac{8i}{c} \frac{1}{q_z} & \text{in-phase} \\ 2 & \text{out-of-phase} \end{cases} \quad \text{for } q_{\parallel} = 0, q_z \rightarrow 0. \quad (3.13) \end{aligned}$$

Here, we distinguish between two possible displacement patterns of the apical oxygens moving either in or out of phase within the same unit cell. The phase shift between adjacent unit cells along the z direction is determined by q_z . In the second line of Eq. (3.13), we consider the special case of $q_{\parallel} = 0$ and small q_z . We find that the in-phase mode has a $1/q_z$ divergence which can be attributed to the long-range nature of the unscreened Coulomb interaction in the undoped system. This divergence is integrable in three-dimensional \mathbf{q} space as it becomes suppressed for non-zero q_{\parallel} .

The energy dependence of the coupling shown in Fig. 3.4 agrees qualitatively with the observation of fine structures in the electron self-energy of $\text{La}_{2-\delta}\text{Sr}_{\delta}\text{CuO}_4$ [93] except for the calculation not giving appreciable coupling around 40 meV. This could be due to surface effects or distortions due to doping [94, 95, 96]. Such effects would be missing in our calculation which is performed for an ideal La_2CuO_4 structure. For comparison, the dashed line in Fig. 3.4 shows the spectral distribution of the coupling to holes in individual non-bonding O- p orbitals where we assume that the coupling constant is given directly by $g_{\mathbf{q}\nu}^{(\text{O}x)}$ or $g_{\mathbf{q}\nu}^{(\text{O}y)}$.

To discuss the \mathbf{q} dependence of the coupling, we sum $|g_{\mathbf{q}\nu}|^2$ over all modes and the phonon momentum q_z perpendicular to the CuO_2 planes. Generally speaking, the coupling increases with decreasing $|(q_x, q_y)|$. As exemplified by our simplified discussion of the apical oxygen modes, the modulation of the electrostatic potential can give rise to large couplings for small momenta. Some individual modes show different behavior, e.g. the coupling to the O (half-)breathing mode peaks around $(\pi/a, \pi/a)$.

3.3 Adiabatic approximation

We now introduce an adiabatic approximation for calculating (inverse) photoemission spectra which forms the basis for the work presented in the rest of this chapter. We consider a system that is modeled by the following Hamiltonian:

$$H = H_{\text{el}} + H_{\text{ph}} + H_{\text{ep}}. \quad (3.14)$$

H_{el} (H_{ph}) describes the purely electronic (phononic) part of the model whereas the interaction between electrons and phonons is given by H_{ep} .

The phonons are assumed to be harmonic in the absence of electron-phonon interaction, and the system is taken to be translationally invariant, so that we can write:

$$H_{\text{ph}} = \sum_{\mathbf{q}\nu} \frac{1}{2} (\Pi_{\mathbf{q}\nu} \Pi_{-\mathbf{q}\nu} + \omega_{\mathbf{q}\nu}^2 Q_{\mathbf{q}\nu} Q_{-\mathbf{q}\nu}). \quad (3.15)$$

Here, an individual phonon mode with frequency $\omega_{\mathbf{q}\nu}$ has wavevector \mathbf{q} and belongs to branch ν . Its generalized coordinate and momentum are denoted by $Q_{\mathbf{q}\nu}$ and $\Pi_{\mathbf{q}\nu}$.

The electron-phonon interaction couples electronic degrees of freedom to the phonon coordinates $Q_{\mathbf{q}\nu} = \sqrt{\hbar/(2\omega_{\mathbf{q}\nu})}(b_{\mathbf{q}\nu} + b_{-\mathbf{q}\nu}^\dagger)$. We assume that this interaction vanishes for a certain electronic filling of the system which we will refer to as undoped in the following. The completely empty or completely filled Holstein or Holstein- t - J model are examples for such undoped systems, see sections B.3 and B.4.

In addition, we assume that the phonon frequencies are small compared to the electronic energy scales defined by H_{el} . This justifies an adiabatic approximation [97], and we can first consider only $H_{\text{el}} + H_{\text{ep}}$ treating the phonon coordinates $Q_{\mathbf{q}\nu}$ in H_{ep} as c-numbers, i.e., as instantaneous parameters for the electronic problem. We denote the corresponding eigenstates and eigenvalues by $|E_m^{N_e}(\mathbf{Q})\rangle$ and $E_m^{N_e}(\mathbf{Q})$ which are labeled by the number of electrons N_e and other quantum numbers m . We use \mathbf{Q} as a shorthand notation for the set of phonon coordinates. The phonon eigenfunctions are then obtained by solving

$$\left(\sum_{\mathbf{q}\nu} \frac{1}{2} \Pi_{\mathbf{q}\nu} \Pi_{-\mathbf{q}\nu} + V_m^{N_e}(\mathbf{Q}) \right) \phi_{mn}^{N_e}(\mathbf{Q}) = \varepsilon_{mn}^{N_e} \phi_{mn}^{N_e}(\mathbf{Q}), \quad (3.16)$$

a Schrödinger equation with the effective potential

$$V_m^{N_e}(\mathbf{Q}) = E_m^{N_e}(\mathbf{Q}) + \sum_{\mathbf{q}\nu} \frac{1}{2} \omega_{\mathbf{q}\nu}^2 Q_{\mathbf{q}\nu} Q_{-\mathbf{q}\nu}. \quad (3.17)$$

The eigenenergies are $\varepsilon_{mn}^{N_e}$ where n stands for suitable phonon quantum numbers. The eigenstates of H are $\langle \mathbf{Q} | \varepsilon_{mn}^{N_e} \rangle = \phi_{mn}^{N_e}(\mathbf{Q}) | E_m^{N_e}(\mathbf{Q}) \rangle$ in our approximation, i.e., we assume that the electronic states $| E_m^{N_e}(\mathbf{Q}) \rangle$ do not mix.

The ground state in a system with N_e electrons is then given by $\langle \mathbf{Q} | \varepsilon_{00}^{N_e} \rangle = \phi_{00}^{N_e}(\mathbf{Q}) | E_0^{N_e}(\mathbf{Q}) \rangle$ with eigenenergy $\varepsilon_{00}^{N_e}$. In case of an undoped system with N_e^0 electrons, there is no electron-phonon interaction; the product ansatz for $\langle \mathbf{Q} | \varepsilon_{00}^{N_e} \rangle$ becomes exact, and the phonon wavefunction just corresponds to the ground state of H_{ph} :

$$\phi_{00}^{N_e^0}(\mathbf{Q}) = \prod_{\mathbf{q}\nu} \left(\frac{\omega_{\mathbf{q}\nu}}{\hbar\pi} \right)^{1/4} \exp \left(-\frac{\omega_{\mathbf{q}\nu} Q_{\mathbf{q}\nu}^2}{2\hbar} \right). \quad (3.18)$$

The electronic ground state and its eigenenergy are then independent of \mathbf{Q} , and $\varepsilon_{00}^{N_e^0} = E_0^{N_e^0} + \sum_{\mathbf{q}\nu} \hbar\omega_{\mathbf{q}\nu}/2$.

We now do (inverse) photoemission at zero temperature by destroying (creating) an electron with momentum \mathbf{k} and spin σ in the ground state of a system with N_e electrons. Within the adiabatic approximation, this can be described by considering the following Green's function:

$$\begin{aligned} G_{\mathbf{k}\sigma}^{N_e, \mp}(z) &= \langle \varepsilon_{00}^{N_e} | \psi^\dagger \frac{1}{z - \hbar^{-1}(H - \varepsilon_{00}^{N_e})} \psi | \varepsilon_{00}^{N_e} \rangle \\ &= \int d\mathbf{Q} \int d\mathbf{Q}' \phi_{00}^{N_e*}(\mathbf{Q}) \langle E_0^{N_e}(\mathbf{Q}) | \psi^\dagger \langle \mathbf{Q} | \frac{1}{z - \hbar^{-1}(H - \varepsilon_{00}^{N_e})} | \mathbf{Q}' \rangle \psi | E_0^{N_e}(\mathbf{Q}') \rangle \phi_{00}^{N_e}(\mathbf{Q}'), \end{aligned} \quad (3.19)$$

where $\psi = c_{\mathbf{k}\sigma}^{(\dagger)}$ and $\int d\mathbf{Q} = \prod_{\mathbf{q}\nu} \int dQ_{\mathbf{q}\nu}$.

We proceed in analogy to Ref. [98] and neglect the kinetic energy of the phonons in H in the resolvent in Eq. (3.19). The remaining $\mathcal{H}(\mathbf{Q})$ is diagonal in the phonon coordinates \mathbf{Q} , and one half of the integrations in Eq. (3.19) can be eliminated. This leads to the following approximation for the Green's function [98]:

$$\tilde{G}_{\mathbf{k}\sigma}^{N_e, \mp}(z) = \int d\mathbf{Q} |\phi_{00}^{N_e}(\mathbf{Q})|^2 g_{\mathbf{k}\sigma}^{N_e, \mp}(\tilde{z}_{\mathbf{Q}}(z), \mathbf{Q}), \quad (3.20)$$

where

$$g_{\mathbf{k}\sigma}^{N_e, \mp}(\tilde{z}_{\mathbf{Q}}(z), \mathbf{Q}) = \langle E_0^{N_e}(\mathbf{Q}) | \psi^\dagger \frac{1}{\tilde{z}_{\mathbf{Q}}(z) - \hbar^{-1}(\mathcal{H}(\mathbf{Q}) - \varepsilon_{00}^{N_e})} \psi | E_0^{N_e}(\mathbf{Q}) \rangle \quad (3.21)$$

and

$$\tilde{z}_{\mathbf{Q}}(z) = z + \hbar^{-1}(V_0^{N_e}(\mathbf{Q}) - \varepsilon_{00}^{N_e}). \quad (3.22)$$

Finally, the corresponding spectral function is given by

$$\tilde{A}_{\mathbf{k}\sigma}^{N_e, \mp}(\omega) = -\frac{1}{\pi} \text{Im} \tilde{G}_{\mathbf{k}\sigma}^{N_e, \mp}(\omega + i0^+) = \int d\mathbf{Q} |\phi_{00}^{N_e}(\mathbf{Q})|^2 \rho_{\mathbf{k}\sigma}^{N_e, \mp}(\omega, \mathbf{Q}), \quad (3.23)$$

where

$$\rho_{\mathbf{k}\sigma}^{N_e, \mp}(\omega, \mathbf{Q}) = \sum_m |\langle E_m^{N_e, \mp}(\mathbf{Q}) | \psi | E_0^{N_e}(\mathbf{Q}) \rangle|^2 \delta(\omega - \hbar^{-1}(V_m^{N_e, \mp}(\mathbf{Q}) - V_0^{N_e}(\mathbf{Q}))) \quad (3.24)$$

after expanding $\psi | E_0^{N_e}(\mathbf{Q}) \rangle$ in the adiabatic electronic basis states $| E_m^{N_e, \mp}(\mathbf{Q}) \rangle$. We used that $\langle E_m^{N_e, \mp}(\mathbf{Q}) | \mathcal{H}(\mathbf{Q}) | E_m^{N_e, \mp}(\mathbf{Q}) \rangle = V_m^{N_e, \mp}(\mathbf{Q})$. The replacement of the energy of the initial state $\varepsilon_{00}^{N_e}$ by the corresponding effective potential $V_0^{N_e}(\mathbf{Q})$ in the denominator of the ARPES Green's function according to Eq. (3.22) results in our approximation becoming exact in the limit of vanishing electron-phonon coupling. Furthermore, we find numerically that it also leads to spectra which have the same first moment as the exact solution.

A slightly more refined version of the adiabatic approximation for (inverse) photoemission spectra which can be directly related to the Franck-Condon principle known from molecular physics is given in App. B together with some instructive examples and a comparison to the diagrammatic Monte Carlo method used in Ref. [89].

In the following, we focus on using the present version of the adiabatic approximation to explain the dispersion of incoherent spectral features in ARPES spectra of undoped cuprates and to develop an efficient numerical method for calculating these spectra.

3.3.1 Dispersion of incoherent spectral features

Equations (3.23) and (3.24) turn out to be the key formula for interpreting ARPES spectra of undoped systems. To see this, we observe that $\rho_{\mathbf{k}\sigma}^{N_e, \mp}(\omega, \mathbf{Q})$ is the spectral function of the system without electron-phonon interaction for a given lattice distortion \mathbf{Q} . If we assume that $V_0^{N_e}(\mathbf{Q})$ has a non-degenerate absolute minimum at \mathbf{Q}_{\min} , the corresponding ground-state phonon wavefunction will be localized around this point in coordinate space. If we approximate $|\phi_{00}^{N_e}(\mathbf{Q})|^2 \approx \delta(\mathbf{Q} - \mathbf{Q}_{\min})$, we find that the spectrum corresponds to the spectrum one obtains for the system with a *frozen* distortion \mathbf{Q}_{\min} in which there is no electron-phonon interaction. Analogously, in case of more than one (quasi-)degenerate minima of $V_0^{N_e}(\mathbf{Q})$, we have to use the (weighted) superposition of the spectra corresponding to the respective distortions. If we take into account the finite width of $|\phi_{00}^{N_e}(\mathbf{Q})|^2$, it follows from Eq. (3.23) that the spectral features are broadened due to the \mathbf{Q} dependence of $V_m^{N_e, \mp}(\mathbf{Q}) - V_0^{N_e}(\mathbf{Q})$.

This analysis leads to an important conclusion for ARPES spectra of undoped materials. As there is no electron-phonon interaction in the initial state for these systems, we have $\mathbf{Q}_{\min} = 0$ and $|\phi_{00}^{N_e}(\mathbf{Q})|^2$ is a Gaussian centered around \mathbf{Q}_{\min} (cf.

Eq. (3.18)). Consequently, the spectrum is just the broadened spectrum of the same system without electron-phonon interaction ($H_{\text{ep}} = 0$). If we take into account only the leading linear \mathbf{Q} dependence of $V_m^{N_e \mp 1}(\mathbf{Q}) - V_0^{N_e}(\mathbf{Q})$, the broadening is exactly Gaussian. The broadened peak in the low-binding-energy part of the spectrum for the system with electron-phonon interaction is located at the position of the ($H_{\text{ep}} = 0$)-quasi-particle peak, and its \mathbf{k} dependence therefore exactly traces the quasi-particle dispersion of the purely electronic model. This explains the findings mentioned at the beginning of this chapter. Even in a system with strong electron-phonon interaction, ARPES spectra can show an incoherent broad peak that has the same dispersion as the quasi-particle in the ($H_{\text{ep}} = 0$)-system if there is no electron-phonon interaction in the initial state as for photoemission from undoped systems. This allows statements about the spectrum for $H_{\text{ep}} \neq 0$ from the knowledge of the ($H_{\text{ep}} = 0$)-spectrum.

For the doped system, \mathbf{Q}_{min} is typically non-zero if the electron-phonon interaction is strong. The spectrum $\rho_{\mathbf{k}\sigma}^{N_e, \mp}(\omega, \mathbf{Q}_{\text{min}})$ can then be very different from the spectrum for $\mathbf{Q} = 0$. Therefore, even if the ($H_{\text{ep}} = 0$)-spectrum is known, in general no information about the spectrum of the system with electron-phonon interaction can be deduced. In this context, we note that there may be several degenerate minima at $\mathbf{Q}_{\text{min}} \neq 0$ such that the ground state has an undistorted lattice in the sense of a vanishing expectation value of \mathbf{Q} . The spectrum for $H_{\text{ep}} \neq 0$, nevertheless, corresponds to a superposition of the spectra for \mathbf{Q} -values around the minima $\mathbf{Q}_{\text{min}} \neq 0$.

It is interesting to compare to a discussion of the problem in terms of a sum rule concerning the first moment (center of gravity) of the spectrum. For the undoped system with N_e^0 electrons that has no phonons excited in the initial state, one easily shows that the first moment of the (inverse) photoemission spectrum does not depend on the (linear) electron-phonon interaction. Therefore, the center of gravity of the spectrum does not change when the electron-phonon coupling is turned on. If in the absence of electron-phonon interaction $A_{\mathbf{k}\sigma}^{N_e^0, \mp}(\omega)$ has only one peak for a given \mathbf{k} , e.g. if there is only one band and no electron-electron interaction, the center of gravity equals the position of the quasi-particle peak. Because of the sum rule, we then expect just a broadening but no shift of the quasi-particle peak upon switching on the electron-phonon interaction. In case of electrons interacting with each other, however, already for systems without electron-phonon interaction $A_{\mathbf{k}\sigma}^{N_e^0, \mp}(\omega)$ usually has several peaks for a given \mathbf{k} and the first moment does not correspond to the quasi-particle energy. Then, the sum rule is not able to tell us how the individual peaks are influenced by the electron-phonon interaction and cannot be used to argue for prominent features in the spectrum dispersing approximately like the quasi-particles

in the system without phonons.

3.3.2 Extension to finite temperatures

The adiabatic approximation for the (inverse) photoemission spectrum at zero temperature, Eqs. (3.23) and (3.24), can be extended to finite temperatures T for undoped systems ($N_e = N_e^0$). Instead of calculating the expectation value with respect to the ground state in the expression for the Green's function, Eq. (3.19), we now have to take an ensemble average:

$$\begin{aligned} G_{\mathbf{k}\sigma}^{N_e^0, \mp}(z, T) &= \frac{1}{Z} \sum_{mn} e^{-\beta \varepsilon_{mn}^{N_e^0}} \langle \varepsilon_{mn}^{N_e^0} | \psi^\dagger \frac{1}{z - \hbar^{-1}(H - \varepsilon_{mn}^{N_e^0})} \psi | \varepsilon_{mn}^{N_e^0} \rangle \\ &\approx \frac{1}{Z'} \sum_n e^{-\beta \varepsilon_{0n}^{N_e^0}} \langle \varepsilon_{0n}^{N_e^0} | \psi^\dagger \frac{1}{z - \hbar^{-1}(H - \varepsilon_{0n}^{N_e^0})} \psi | \varepsilon_{0n}^{N_e^0} \rangle, \end{aligned} \quad (3.25)$$

where $\beta = (k_B T)^{-1}$, $Z = \sum_{mn} e^{-\beta \varepsilon_{mn}^{N_e^0}}$, and $Z' = \sum_n e^{-\beta \varepsilon_{0n}^{N_e^0}}$. In the second line of Eq. (3.25), we assume that both the phonon frequencies and the temperature are small compared to typical electronic energies. Then we can neglect electronic excitations and consider only all possible phonon excitations in the electronic ground state. In analogy to Eq. (3.23), the spectral function of $G_{\mathbf{k}\sigma}^{N_e^0, \mp}(z, T)$ is then given by

$$\tilde{A}_{\mathbf{k}\sigma}^{N_e^0, \mp}(\omega, T) = \int d\mathbf{Q} \sum_n P_n |\phi_{0n}^{N_e^0}(\mathbf{Q})|^2 \rho_{\mathbf{k}\sigma}^{N_e^0, \mp}(\omega, \mathbf{Q}), \quad (3.26)$$

where $\rho_{\mathbf{k}\sigma}^{N_e^0, \mp}(\omega, \mathbf{Q})$ is again defined by Eq. (3.24). The squared modulus of the ground-state phonon wavefunction is replaced by a weighted average of the squared modulus of the phonon wavefunctions for the effective potential corresponding to the electronic ground state but with arbitrary phonon occupation numbers $n = \{n_{\mathbf{q}\nu}\}$,

$$|\phi_{0n}^{N_e^0}(\mathbf{Q})|^2 = \prod_{\mathbf{q}\nu} \sqrt{\frac{\omega_{\mathbf{q}\nu}}{\hbar\pi}} \frac{1}{n_{\mathbf{q}\nu}! 2^{n_{\mathbf{q}\nu}}} \exp\left(-\frac{\omega_{\mathbf{q}\nu} Q_{\mathbf{q}\nu}^2}{\hbar}\right) \left[H_{n_{\mathbf{q}\nu}} \left(\sqrt{\omega_{\mathbf{q}\nu}/\hbar} Q_{\mathbf{q}\nu} \right) \right]^2. \quad (3.27)$$

As there is no electron-phonon interaction in the undoped system, these are simply free phonon wavefunctions [99]. The respective eigenenergies are given by

$$\varepsilon_{0n}^{N_e^0} = E_0^{N_e^0} + \sum_{\mathbf{q}\nu} \hbar \omega_{\mathbf{q}\nu} \left(n_{\mathbf{q}\nu} + \frac{1}{2} \right), \quad (3.28)$$

and the weighting factor is

$$P_n = \frac{1}{Z'} e^{-\beta \varepsilon_{0n}^{N_e^0}} = \prod_{\mathbf{q}\nu} (1 - e^{-\beta \hbar \omega_{\mathbf{q}\nu}}) e^{-\beta n_{\mathbf{q}\nu} \hbar \omega_{\mathbf{q}\nu}}. \quad (3.29)$$

Using the integral representation [99] of the Hermite polynomials in Eq. (3.27),

$$H_n(x) = \frac{2^n}{\pi} \int_{-\infty}^{\infty} dy (x + iy)^n e^{-y^2}, \quad (3.30)$$

one finds

$$\begin{aligned} \sum_n P_n |\phi_{0n}^{N_e^0}(\mathbf{Q})|^2 &= \prod_{\mathbf{q}\nu} (1 - e^{-\beta\hbar\omega_{\mathbf{q}\nu}}) \sqrt{\frac{\omega_{\mathbf{q}\nu}}{\hbar\pi^{3/2}}} \int_{-\infty}^{\infty} dy \int_{-\infty}^{\infty} dy' \times \\ &\times \exp \left[-\frac{\omega_{\mathbf{q}\nu} Q_{\mathbf{q}\nu}^2}{\hbar} - 2e^{-\beta\hbar\omega_{\mathbf{q}\nu}} \left(\sqrt{\frac{\omega_{\mathbf{q}\nu}}{\hbar}} Q_{\mathbf{q}\nu} + iy \right) \left(\sqrt{\frac{\omega_{\mathbf{q}\nu}}{\hbar}} Q_{\mathbf{q}\nu} + iy' \right) - y^2 - y'^2 \right] \\ &= \prod_{\mathbf{q}\nu} \sqrt{\frac{\omega_{\mathbf{q}\nu}}{\hbar\pi(2n_{\mathbf{q}\nu}^B(T) + 1)}} \exp \left(-\frac{\omega_{\mathbf{q}\nu} Q_{\mathbf{q}\nu}^2}{\hbar(2n_{\mathbf{q}\nu}^B(T) + 1)} \right). \end{aligned} \quad (3.31)$$

First, after inserting Eqs. (3.27), (3.29), and (3.30) the summations $\sum_n = \prod_{\mathbf{q}\nu} \sum_{n_{\mathbf{q}\nu}=0}^{\infty}$ can be done. Then, by twice completing the square in the exponential, the definite integrals can be performed leading to the final result in terms of the Bose-Einstein distribution $n_{\mathbf{q}\nu}^B(T) = (\exp(\hbar\omega_{\mathbf{q}\nu}/(k_B T)) - 1)^{-1}$. A comparison of Eq. (3.31) with the squared modulus of the ground-state phonon wavefunction from Eq. (3.18) shows that also at finite temperatures the spectrum in the adiabatic approximation is obtained from averaging electronic spectra for distorted lattices with a Gaussian weighting function. The temperature dependence is solely via the temperature-dependent width of the Gaussian.

3.3.3 Computational method

The adiabatic approximation for (inverse) photoemission spectra in undoped systems is not only the key for the understanding of the dispersion of incoherent spectral features as discussed in Sec. 3.3.1. It also forms the basis for a method to efficiently calculate such spectra. A Monte Carlo approach is used to perform the integral over the space of phonon coordinates in Eq. (3.26). The factor $\sum_n P_n |\phi_{0n}^{N_e^0}(\mathbf{Q})|^2$ (Eq. (3.31)) in the integrand is a Gaussian function with respect to \mathbf{Q} and serves as a weighting function. In practice, one therefore samples the remaining factor $\rho_{\mathbf{k}\sigma}^{N_e^0, \mp}(\omega, \mathbf{Q})$ in the integrand by picking random phonon coordinates with a Gaussian distribution corresponding to $\sum_n P_n |\phi_{0n}^{N_e^0}(\mathbf{Q})|^2$.² The final spectrum is then obtained from an arithmetic average of a large number of thus sampled spectra.

²This can be implemented e.g. using the Box-Muller method [100] that only requires a standard random number generator with uniform distribution on a finite interval.

The main advantage of this method is that its applicability does not depend on the strength of the electron-phonon coupling. Each sampled $\rho_{\mathbf{k}\sigma}^{N_e^0, \mp}(\omega, \mathbf{Q})$ only requires the calculation of a purely electronic problem. Its parameters are adiabatically modulated by the electron-phonon interaction depending on the respective lattice distortion but no dynamic phonons are included. If we use exact diagonalization to solve a given model, the explicit inclusion of phonons would require in practice a truncation of the Hilbert space as discussed in Sec. 2.2. The stronger the electron-phonon coupling, the more phonons would have to be included to achieve converged results. Due to the limited memory available, this usually prevents calculations for strong coupling. Instead, our method only requires enough resources to repeatedly solve the electronic part of the problem irrespective of the electron-phonon coupling strength.

Also, with our method a large number of phonon modes can be included in the calculation. This only increases the dimension of the space of phonon coordinates but brings about no essential complication as we use Monte Carlo sampling for the integration. If the modes are treated dynamically, however, the size of the Hilbert space grows with their number which is therefore quite restricted due to memory limitations.

As discussed in App. B, the spectra obtained within the adiabatic approximation do not show the fine structure from individual phonon satellites but rather give an envelope of the exact spectra. In many cases, however, this constitutes no serious limitation of the method since the fine structure is often not resolved in experiment due to limited resolution and because modes with different frequencies are involved leading to the overlap of fine structures with different spacings between peaks.

Calculation of the binding energy

So far, we have measured the energy of spectral features relative to the energy of the initial state. Experimental spectra, however, are usually plotted against the energy difference with respect to the chemical potential (or the band edge in insulators), the so-called binding energy. In our calculations, we can define a corresponding binding energy by measuring energies relative to the energy of the final state lowest in energy, i.e., the minimum of the effective potential $V_0^{N_e \mp 1}(\mathbf{Q})$.

We use two methods to find this minimum.

- We search for it in \mathbf{Q} space using simulated annealing based on the Metropolis algorithm [101].

- We use an iterative method [102]. The minimum of $V_0^{N_e \mp 1}(\mathbf{Q})$ corresponds to the ground-state energy E_0 in the ($N_e \mp 1$ electron)-sector of the adiabatic Hamiltonian $\mathcal{H}(\mathbf{Q})$ which differs from H by the neglect of the kinetic energy of the phonons. Therefore, using the Hellmann-Feynman theorem one has

$$\left. \frac{\partial E_0}{\partial Q_{q\nu}} \right|_{\mathbf{Q}_{\min}} = \left. \frac{\partial \langle E_0 | \mathcal{H}(\mathbf{Q}) | E_0 \rangle}{\partial Q_{q\nu}} \right|_{\mathbf{Q}_{\min}} = \langle E_0 | \left. \frac{\partial \mathcal{H}(\mathbf{Q})}{\partial Q_{q\nu}} \right|_{\mathbf{Q}_{\min}} | E_0 \rangle = 0 \quad \forall \mathbf{q}, \nu. \quad (3.32)$$

From this, an expression for the phonon coordinates \mathbf{Q}_{\min} at the minimum in terms of ground-state expectation values can be obtained which can be used for an iterative procedure. First, one calculates the electronic ground state for a given distortion. Then, using the expression derived from Eq. (3.32), new phonon coordinates are obtained. This is iterated until convergence is achieved.

Both methods require the repeated solution of the electronic problem for fixed phonon coordinates. The iterative method works faster than the simulated annealing algorithm. But Eq. (3.32) can be fulfilled also by meta-stable states different from the ground state. By comparing with results from simulated annealing and varying the initial lattice distortion which starts the iteration, we can, however, cross-check that we have found the true ground-state energy.

We note that the ARPES spectra calculated using the adiabatic approximation from Eqs. (3.23) and (3.24) are not bound on the low-energy side. This is a consequence of replacing the reference energy in the denominator of the ARPES Green's function according to Eq. (3.22). But in order to be able to define the position of the true quasi-particle that marks the band edge needed to define a binding energy, a lower bound is necessary. This could be naturally achieved by skipping the redefinition of z in Eq. (3.22). Although the spectra then would have an incorrect first moment, the position of the true quasi-particle would now be defined in a physical way by the minimum of the effective potential $V_0^{N_e \mp 1}(\mathbf{Q})$ of the final state lowest in energy that we used above to introduce a binding energy.

3.4 ARPES spectra for undoped La_2CuO_4

In this section, we use the method described in the previous section to calculate ARPES spectra for undoped La_2CuO_4 taking into account the electron-phonon interaction derived in Sec. 3.2.

The electronic system is described by the two-dimensional t - J model, Eq. (1.87), which was derived in Sec. 1.4 as an effective low-energy model for the electronic

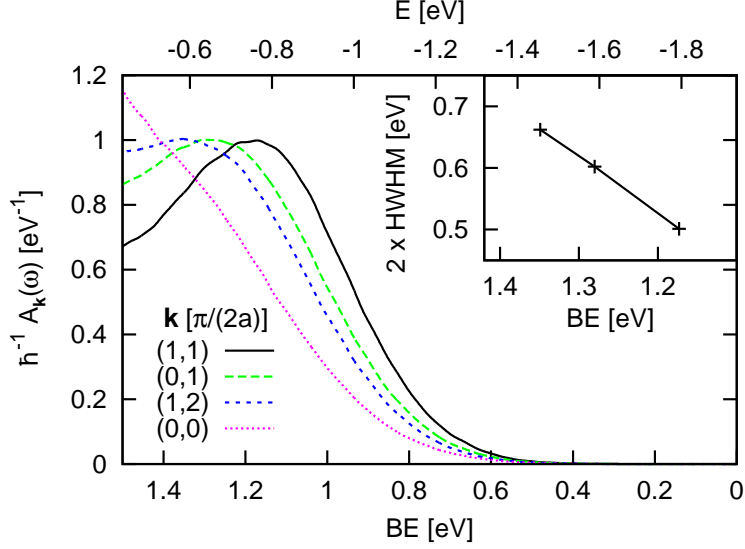


Figure 3.5: ARPES spectra for the undoped system at $T = 0$ for different \mathbf{k} normalized to the height of the phonon side band. The lower abscissa shows binding energies (BE) and the upper abscissa the energies of the final states corresponding to the spectral features. The inset shows the dependence of the width of the phonon side band on its binding energy. The width of the (0,0) spectrum is poorly defined and not shown.

degrees of freedom in the cuprates. We choose typical parameters $t = 0.4$ eV and $J = 0.3 t$. This is complemented by the electron-phonon interaction Eq. (3.9) derived in Sec. 3.2 that modifies the on-site energies and hoppings depending on the actual lattice distortion \mathbf{Q} . As the electronic model is purely two-dimensional, the dependence of the coupling on the z -component q_z of the phonon wavevector is unimportant. For given q_x, q_y, ν , we therefore use a single mode with effective coupling $g_{\text{eff}} = \sqrt{\sum_{q_z} |g_{q_z}|^2}$ and frequency $\omega_{\text{eff}} = g_{\text{eff}}^2 / \sum_{q_z} (|g_{q_z}|^2 / \omega_{q_z})$. This reduces the number of phonon momenta from $N' = (30)^3$ to $(30)^2$. Each sampled $\rho_{\mathbf{k}}(\mathbf{Q}, \omega)$ is calculated by solving $H_{t-J} + H_{\text{ep}}$ on a 4×4 cluster with periodic boundary conditions using exact diagonalization. The couplings for the $N = 16$ available momenta in this two-dimensional problem are obtained from coarse-graining those calculated on the 30×30 mesh.

We calculate $A_{\mathbf{k}}(\omega, T = 0)$ for different values of \mathbf{k} as shown in the main part of Fig. 3.5. For each spectrum, $5 \cdot 10^4$ samples are used. The poles in the sampled spectra are broadened by Gaussians with a FWHM of 33 meV. The spectra show a broad phonon side band which disperses like the quasi-particle in the t - J model

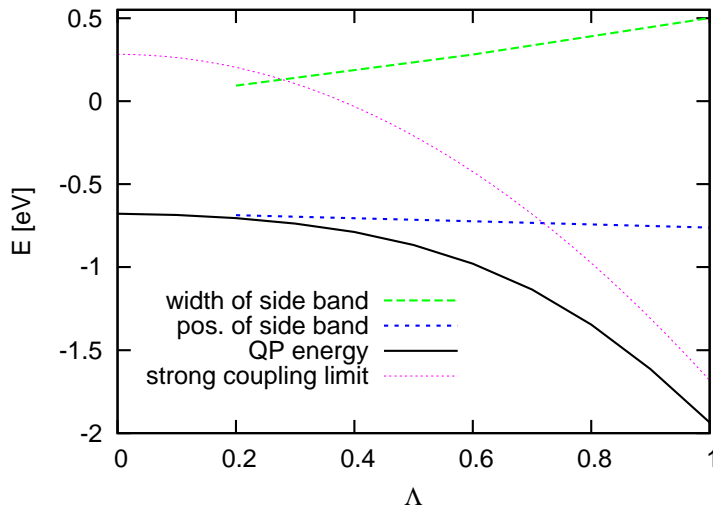


Figure 3.6: Width and position of the phonon side band and the position of the quasi-particle peak as a function of the relative coupling strength Λ for $\mathbf{k} = (\pi/(2a), \pi/(2a))$.

without phonons, as was found in Ref. [89]. As shown in Sec. 3.3.1, this can be understood easily within our adiabatic approximation. The true quasi-particle peak is almost completely suppressed in weight and dispersion and determines the energy zero on the lower abscissa in Fig. 3.5. The half-width at half maximum (HWHM) of the side band is determined on the low-binding-energy side. We obtain a width of $2 \times \text{HWHM} = 0.5$ eV for $\mathbf{k} = (\pi/(2a), \pi/(2a))$, in good agreement with the corresponding experimental result 0.48 eV (cf. bold curves in Fig. 3.2).

Width and position of the phonon side band as well as the position of the quasi-particle peak are shown in Fig. 3.6 as a function of the relative coupling strength Λ (substituting $\Lambda g_{\mathbf{q}\nu}$ for $g_{\mathbf{q}\nu}$ in Eq. (3.9)) for $\mathbf{k} = (\pi/(2a), \pi/(2a))$ at $T = 0$. For small Λ , the position of the quasi-particle peak starts out at the energy obtained in the t - J model without phonons and approaches asymptotically the curve given by $-\sum_{\mathbf{q}\nu} \Lambda^2 |g_{\mathbf{q}\nu}|^2 / (\hbar\omega_{\mathbf{q}\nu} N') + \text{const.}$ for stronger couplings. A fully localized hole obtains this energy gain from the interaction with phonons (the additional constant depends on the definition of the energy offset). The position of the phonon side band shows only a weak linear dependence on Λ . The energy difference to the position of the true quasi-particle peak determines the binding energy. The value of almost 1.2 eV at full coupling is larger than the experimental value of about 0.5 eV (cf. Fig. 3.2). Since the binding energy depends strongly on doping, a possible explanation for this discrepancy could be that the experimental samples were actually lightly doped. Our

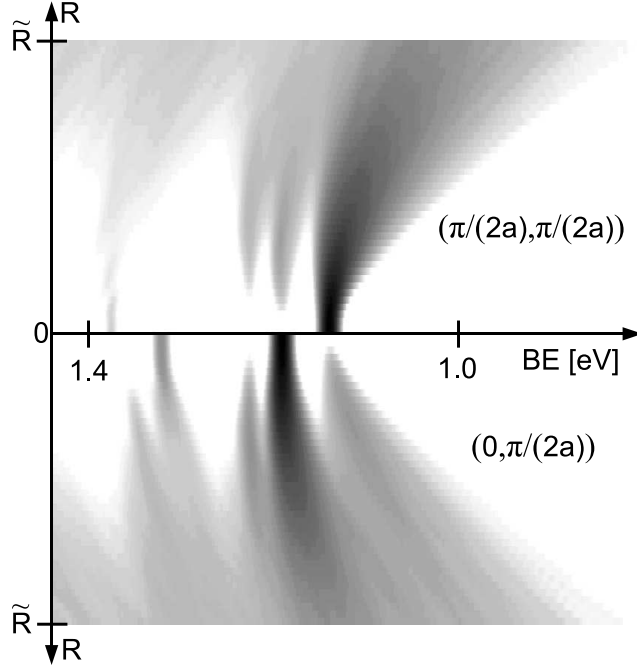


Figure 3.7: Contributions to the spectra with $\mathbf{k} = (\pi/(2a), \pi/(2a))$ and $\mathbf{k} = (0, \pi/(2a))$ at $T = 0$ for varying R . Higher spectral weight is represented by darker shading. The abscissa shows binding energies (BE). Coupling to $\mathbf{q} = (0, 0)$ modes is not included.

shell model calculation could also overestimate the coupling strength. As seen in Fig. 3.6, the binding energy of the side band has a much stronger dependence on Λ than the width. For $\Lambda = 0.8$, e.g., one would find a width of about 0.4 eV and a binding energy of about 0.6 eV, both quantities being in reasonable agreement with experimental values. As $\lambda \propto \Lambda^2$, this would reduce the dimensionless coupling constant to $\lambda = 0.75$. Such a reduction could be due to a slight underestimate of the screening in the shell model or an overestimate of the coupling to breathing phonons. Still, the coupling constant would remain considerably larger than the critical value $\lambda_c = 0.4$ [89] for the crossover to self-trapped polarons in the Holstein- t - J model.

The inset in Fig. 3.5 shows that the width of the phonon side band increases roughly linearly with its binding energy. This trend has also been found experimentally for weakly doped $\text{Ca}_{2-\delta}\text{Na}_\delta\text{CuO}_2\text{Cl}_2$ [26]. To understand this, we introduce rescaled phonon coordinates $R_{\mathbf{q}\nu} = \sqrt{\omega_{\mathbf{q}\nu}/(\hbar(2n_{\mathbf{q}\nu}(T) + 1))}Q_{\mathbf{q}\nu}$. The weighting function in Eq. (3.31) then becomes invariant under rotations in \mathbf{R} space, and Eq. (3.26) can be expressed as a sampling over directions for fixed $R = |\mathbf{R}|$ followed by an

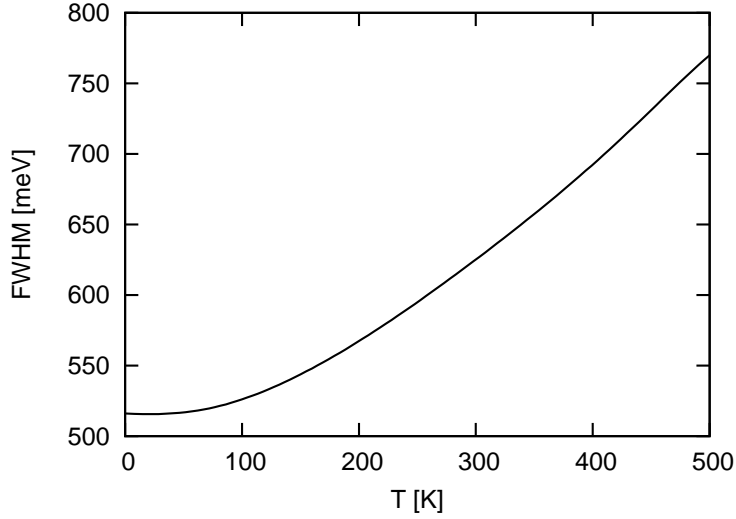


Figure 3.8: Temperature dependence of the width of the phonon side band in the $\mathbf{k} = (\pi/(2a), \pi/(2a))$ ARPES spectrum for the undoped system. The width is determined as the FWHM of a Gaussian fitted to the low binding energy side of the peak. The curve shown is an interpolation between the calculated data points.

integration over R . If the \mathbf{R} space has dimension d , the R -integral contains a factor $R^{d-1}e^{-R^2}$ which peaks strongly at $\tilde{R} \equiv \sqrt{(d-1)/2}$. Figure 3.7 shows how the contributions to the spectrum evolve with increasing R up to \tilde{R} . Poles in the sampled spectra were broadened by Gaussians with a FWHM of 11 meV. In the figure, the coupling to the $\mathbf{q} = (0, 0)$ modes is not included since it contributes the same broadening for all \mathbf{k} . We focus on peaks to the right, at the lowest binding energies. For $R = 0$, which corresponds to zero electron-phonon coupling, the spectrum for $\mathbf{k} = (\pi/(2a), \pi/(2a))$ has a peak at smaller binding energy than for $\mathbf{k} = (0, \pi/(2a))$. As R increases and the electron-phonon coupling is switched on, both peaks are broadened. This is due to the repulsion from higher states, which increases with R , but is different for different directions of \mathbf{R} . For the peak with the lowest binding energy, this broadening is largest since all the other states repel the corresponding state in the same direction. Figure 3.5 shows, however, the opposite trend for the width of the phonon side band in the final spectra due to the following opposing effect which dominates. For $R \neq 0$, spectral weight also appears at energies with no peaks in the $R = 0$ spectra; the system is distorted and the electronic momentum \mathbf{k} is not conserved. For instance, in case of $\mathbf{k} = (0, \pi/(2a))$, a peak of increasing width and weight appears at the energy of the main peak in the $\mathbf{k} = (\pi/(2a), \pi/(2a))$ spectrum.

At $R = \tilde{R}$, these side bands have more or less merged with the main peak and effectively add to its width. For $\mathbf{k} = (\pi/(2a), \pi/(2a))$, there is no such extra contribution for lower binding energies whereas for $\mathbf{k} = (0, \pi/(2a))$ the width is increased by one side band. There are more and more side bands on the low binding energy side of the main peak as the binding energy of the main peak increases which increases the width of the resulting broad peak on the low binding energy side.

Finally, we have studied the temperature dependence of the width of the phonon side band. From Eq. (3.31), it follows that the T dependence is determined by Bose factors. The phonon frequencies then set the temperature scale for strong variations in the width. For $\mathbf{k} = (\pi/(2a), \pi/(2a))$, it increases from 515 meV FWHM³ at $T = 0$ to 560 meV at $T = 200$ K and 680 meV at $T = 400$ K for our model of La_2CuO_4 . Such a T dependence is in qualitative agreement with the experimental results of Shen *et al.* [27] for $\text{Ca}_2\text{CuO}_2\text{Cl}_2$, supporting the interpretation that the side band broadening originates from electron-phonon coupling.

3.5 Summary and discussion

To summarize, we have shown that the polaronic features in ARPES spectra of La_2CuO_4 and other undoped cuprates can be attributed to strong coupling between the photo hole and phonons. This electron-phonon coupling is due to the modulation of the electrostatic potential and of the Zhang-Rice singlet energy and was found to be strong enough to induce self-trapped polarons. Based on an adiabatic approximation, we have developed a description of (inverse) photoemission spectra which explains why the dispersion of the phonon side band in undoped systems matches that of purely electronic calculations. In addition, it leads to an efficient method for obtaining ARPES spectra in undoped compounds. We have used it to show that with the derived coupling there is good agreement with experimental results. The dependence of the width of the broad phonon side band on binding energy and temperature has also been discussed. Our results show the importance of electron-phonon coupling for the physics of undoped cuprates.

Despite the successful description of the undoped system, there are several open questions concerning what happens upon doping which we discuss in the following. The doping dependence of ARPES spectra has been investigated e.g. in Ref. [103] for

³Here we use the FWHM of a Gaussian fitted to the low binding energy side of the peak which leads to a slight difference compared to the $T = 0$ width obtained earlier from twice the HWHM taken directly from the spectrum.

$\text{La}_{2-\delta}\text{Sr}_\delta\text{CuO}_4$ over a large range of dopings δ . Along the nodal direction, a broad side band and no quasi-particle peak is seen in the undoped system like in Fig. 3.2. But already for dopings as small as $\delta = 0.03$, a quasi-particle peak can be discerned. As one expects a strong suppression of the quasi-particle weight in a system of self-trapped polarons, this indicates that polaronic behavior in this sense is quickly lost upon doping. In general, we expect the electron-phonon coupling to become weaker upon doping as the doped charge carriers lead to a stronger screening of the interaction from the modulation of the electrostatic potential. We found in Sec. 3.2 that the coupling in the undoped system is considerably stronger than what is required for the crossover to self-trapped polarons. But it is conceivable that also this criterion changes upon doping. An increase seems likely as antiferromagnetic correlations become weaker which appear to help the formation of polarons [89,104,105,106]. At low doping, the quasi-particle weight is small and there is still much weight in the energy range of the side band suggesting that electron-phonon interaction remains important also in the doped system. Similar results are obtained for $\text{Ca}_{2-\delta}\text{Na}_\delta\text{CuO}_2\text{Cl}_2$ [26] although the quasi-particle peak is less clearly visible for small dopings.

In this context, it is interesting that for finite doping the nodal quasi-particle dispersion in $\text{Ca}_{2-\delta}\text{Na}_\delta\text{CuO}_2\text{Cl}_2$ is found [26] to be relatively large, although it is still about a factor of two smaller than expected from band structure calculations [107,58] assuming a simple emptying of the band. Furthermore, the position of the broad side band remains almost unchanged upon doping suggesting only a small variation of the binding energy. Usually, one assumes that a small value of Z leads to a very small dispersion as observed in the undoped system (cf. the dispersion of feature B in Fig. 3.1b). A large dispersion could result, however, if the electron self-energy has a strong \mathbf{k} dependence. It remains unclear why the binding energy of the side band shows only little change upon doping as if the electron-phonon interaction would not become weaker.

Chapter 4

Property-dependent apparent electron-phonon interaction

4.1 Introduction

The quasi-particle dispersions derived from ARPES experiments on cuprates quite universally show a kink feature at an energy of about 70 meV when the electronic wavevector is chosen along the nodal direction ($\mathbf{k} \propto (\xi, \xi)$). Typical examples taken from Lanzara *et al.* [25] are shown in Fig. 4.1. These results can be interpreted assuming that the electronic quasi-particles couple to a bosonic mode with an energy corresponding to the kink energy. In Ref. [25], the oxygen half-breathing mode has been proposed as a likely candidate for the coupling boson, and a coupling constant $\lambda \approx 1$ was derived from the change of the slope. The half-breathing phonon has the appropriate energy, and its anomalously strong softening and broadening upon doping which was discussed extensively in Chap. 2 further support this interpretation. Using measured values of the (half-)breathing phonon width [18] and a calculated density of states [107] in a formula by Allen [108, 109] (Eq. (4.47)), one derives a coupling constant $\lambda \approx 0.1 - 0.3$ for optimally doped cuprates.

The coupling constants derived from electronic and phonon properties differ by almost an order of magnitude. This seems to indicate a problem in the interpretation of the experiments in terms of electron-phonon coupling to the half-breathing mode. These estimates of λ , however, are based on theories which assume non-interacting electrons. It is not clear how the meaning of these apparent coupling constants could change for strongly correlated materials like the cuprates. We therefore study the effect of the electron-phonon interaction on the electronic and phonon properties in

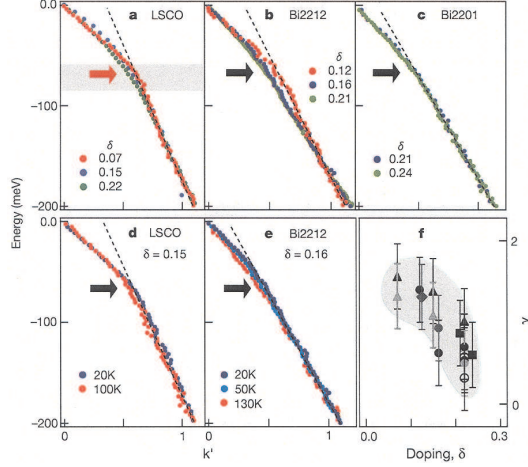


Figure 4.1: ARPES dispersions of $\text{La}_{2-\delta}\text{Sr}_\delta\text{CuO}_4$ (LSCO), $\text{Bi}_2\text{Sr}_2\text{CuO}_{6+\delta}$ (Bi2201) and $\text{Bi}_2\text{Sr}_2\text{CaCu}_2\text{O}_{8+\delta}$ (Bi2212) in the nodal direction ($\mathbf{k} \propto (\xi, \xi)$) for different dopings δ and temperatures T . The results in (a) and (b) were obtained for $T = 20$ K and in (c) for $T = 30$ K. The red arrow shows the energy of the $\mathbf{q} = (\pi/a, 0)$ half-breathing phonon and the black arrows indicate the kink energies. Panel (f) shows the change $1 + \lambda'$ of the slope at the kink (after Lanzara *et al.* [25]).

such systems. Using sum rules that we derive for both the electron and phonon self-energy, we show that for a strongly correlated system the apparent λ deduced from theories for non-interacting electrons can depend strongly on the property studied. Already Kulić and Zeyher [110] found that strong correlations greatly reduce the electron-phonon coupling in transport quantities but lead to a much smaller change in the Eliashberg function $\alpha^2F(\omega)$. Here, we demonstrate that in such systems the effects of the coupling also show up differently in electron and phonon self-energies.

We consider a doped Mott (charge transfer) insulator which has a fraction δ carriers (where δ typically is small). We find that the influence of the electron-phonon interaction on the phonon self-energy, determining its width and softening, is reduced by a factor of the order of δ compared to a system without electron-electron interaction. For the electron self-energy, determining the photoemission spectrum, there is no comparable reduction. This could explain why the λ deduced from the phonon self-energy appears to be smaller than the one deduced from photoemission, and it supports the scenario that phonons give a large contribution to structures in ARPES spectra. For similar reasons, one can speculate that there should be no reduction $\propto \delta$ in the phonon induced carrier-carrier interaction.

After defining the models used in this chapter, we start by deriving the sum rules

for the electron and phonon self-energy. In both cases, this is done for interacting and non-interacting electrons. A comparison of the different results then allows us to assess the effect of strong electronic correlations on the apparent coupling constants derived from different properties assuming non-interacting electrons. We exemplify these findings using numerical calculations. Finally, the sum rules are used to study the effect of vertex corrections in a diagrammatic treatment of electron-phonon interactions in strongly correlated systems.

4.2 Definition of models

We consider the following t - J model with phonons:

$$H = H_{t-J} + H_{\text{ep}} + H_{\text{ph}}, \quad (4.1)$$

where H_{t-J} was defined in Eq. (1.87). The electron-phonon coupling is a \mathbf{q} -dependent on-site coupling,

$$H_{\text{ep}} = \frac{1}{\sqrt{N}} \sum_{\mathbf{q}} \sum_i g_{\mathbf{q}} (n_i - 1) (b_{\mathbf{q}} + b_{-\mathbf{q}}^\dagger) e^{i\mathbf{q} \cdot \mathbf{R}_i}, \quad (4.2)$$

of doped holes to dispersive phonons described by

$$H_{\text{ph}} = \sum_{\mathbf{q}} \hbar \omega_{\mathbf{q}} b_{\mathbf{q}}^\dagger b_{\mathbf{q}}. \quad (4.3)$$

We have found in Chap. 1 that such a model can be derived as a low-energy model for a three-band model of the phonon-modulated CuO_2 planes in cuprates. For the considerations in this chapter, we neglect site-off-diagonal coupling which we found to be less important and restrict ourselves to one phonon branch. For later use, we note that as usual $\omega_{-\mathbf{q}} = \omega_{\mathbf{q}}$ and $g_{-\mathbf{q}}^* = g_{\mathbf{q}}$ is assumed.

For comparison, we also consider a similar model with electrons that do not interact with each other:

$$H_{\text{non-int}} = H_{\text{el}} + H_{\text{ep}} + H_{\text{ph}}. \quad (4.4)$$

Whereas the electronic part was described in Eq. (4.1) by the strongly correlated t - J model, we now assume non-interacting electrons with the dispersion $\varepsilon_{\mathbf{k}}$ and

$$H_{\text{el}} = \sum_{\mathbf{k}\sigma} \varepsilon_{\mathbf{k}} c_{\mathbf{k}\sigma}^\dagger c_{\mathbf{k}\sigma}. \quad (4.5)$$

H_{ep} and H_{ph} are defined like in Eqs. (4.2) and (4.3). For later use, we also give H_{ep} in a pure wavevector representation:

$$H_{\text{ep}} = \frac{1}{\sqrt{N}} \sum_{\mathbf{k}\sigma} \sum_{\mathbf{q}} g_{\mathbf{q}} c_{\mathbf{k}+\mathbf{q}\sigma}^{\dagger} c_{\mathbf{k}\sigma} (b_{\mathbf{q}} + b_{-\mathbf{q}}^{\dagger}) - \sqrt{N} g_{(0,0)} (b_{(0,0)} + b_{(0,0)}^{\dagger}). \quad (4.6)$$

Electron and phonon self-energies describe the effects of the interactions on electrons and phonons, respectively. We now derive sum rules for their imaginary parts that allow for a discussion of the interplay between electron-electron and electron-phonon interaction.

4.3 Sum rule for phonon self-energy

We first consider the phonon self-energy. Using the notation of App. C and setting $A^{\dagger} = B = b_{\mathbf{q}} + b_{-\mathbf{q}}^{\dagger}$ and $\epsilon = -1$, we define the phonon Green's function by

$$D^{\alpha}(\mathbf{q}, \omega) = \langle\langle b_{\mathbf{q}}^{\dagger} + b_{-\mathbf{q}}; b_{\mathbf{q}} + b_{-\mathbf{q}}^{\dagger} \rangle\rangle_{\omega}^{\alpha}, \quad (4.7)$$

where $\alpha \in \{\text{ret}, \text{adv}, \text{c}\}$. The phonon self-energy $\Pi^{\alpha}(\mathbf{q}, \omega)$ is defined by Dyson's equation,

$$[D^{\alpha}(\mathbf{q}, \omega)]^{-1} = [D_0^{\alpha}(\mathbf{q}, \omega)]^{-1} - \Pi^{\alpha}(\mathbf{q}, \omega), \quad (4.8)$$

with the free phonon Green's function

$$D_0^{\alpha}(\mathbf{q}, \omega) = \frac{2\omega_{\mathbf{q}}}{\omega^2 - \omega_{\mathbf{q}}^2 + i0^+ f^{\alpha}(\omega)}, \quad \text{where} \quad f^{\alpha}(\omega) = \begin{cases} \pm\omega & \text{for } \alpha = \text{ret/adv}, \\ 1 & \text{for } \alpha = \text{c}. \end{cases} \quad (4.9)$$

$D_0^{\alpha}(\mathbf{q}, \omega)$ is easily obtained as the phonon Green's function for $H_{\text{ep}} = 0$ from its equation of motion in Eq. (C.5).

Using the equation of motion for the full phonon Green's function, we can derive a useful expression for the phonon self-energy. From the first line in Eq. (C.5), one obtains:

$$\omega D^{\alpha}(\mathbf{q}, \omega) = \omega_{\mathbf{q}} \langle\langle b_{-\mathbf{q}} - b_{\mathbf{q}}^{\dagger}; b_{\mathbf{q}} + b_{-\mathbf{q}}^{\dagger} \rangle\rangle_{\omega}^{\alpha}. \quad (4.10)$$

Analogously, the equation of motion for the Green's function on the right hand side of Eq. (4.10) gives:

$$\omega \langle\langle b_{-\mathbf{q}} - b_{\mathbf{q}}^{\dagger}; b_{\mathbf{q}} + b_{-\mathbf{q}}^{\dagger} \rangle\rangle_{\omega}^{\alpha} = 2 + \omega_{\mathbf{q}} D^{\alpha}(\mathbf{q}, \omega) + \frac{2g_{\mathbf{q}}}{\hbar\sqrt{N}} \langle\langle \rho_{-\mathbf{q}}; b_{\mathbf{q}} + b_{-\mathbf{q}}^{\dagger} \rangle\rangle_{\omega}^{\alpha}, \quad (4.11)$$

with the charge density operator $\rho_{\mathbf{q}}$ defined by Eq. (2.31). It is convenient to use the second line in Eq. (C.5) to obtain the equation of motion for the Green's function in the last term of Eq. (4.11):

$$\omega \langle\langle \rho_{-\mathbf{q}}; b_{\mathbf{q}} + b_{-\mathbf{q}}^\dagger \rangle\rangle_\omega^\alpha = -\omega_{\mathbf{q}} \langle\langle \rho_{-\mathbf{q}}; b_{\mathbf{q}} - b_{-\mathbf{q}}^\dagger \rangle\rangle_\omega^\alpha. \quad (4.12)$$

Similarly,

$$\omega \langle\langle \rho_{-\mathbf{q}}; b_{\mathbf{q}} - b_{-\mathbf{q}}^\dagger \rangle\rangle_\omega^\alpha = -\omega_{\mathbf{q}} \langle\langle \rho_{-\mathbf{q}}; b_{\mathbf{q}} + b_{-\mathbf{q}}^\dagger \rangle\rangle_\omega^\alpha - \frac{2g_{-\mathbf{q}}}{\hbar\sqrt{N}} \langle\langle \rho_{-\mathbf{q}}; \rho_{\mathbf{q}} \rangle\rangle_\omega^\alpha. \quad (4.13)$$

From Eqs. (4.10) and (4.11), one has

$$\omega^2 D^\alpha(\mathbf{q}, \omega) = \omega_{\mathbf{q}} \left(2 + \omega_{\mathbf{q}} D^\alpha(\mathbf{q}, \omega) + \frac{2g_{\mathbf{q}}}{\hbar\sqrt{N}} \langle\langle \rho_{-\mathbf{q}}; b_{\mathbf{q}} + b_{-\mathbf{q}}^\dagger \rangle\rangle_\omega^\alpha \right), \quad (4.14)$$

and Eqs. (4.12) and (4.13) give

$$\omega^2 \langle\langle \rho_{-\mathbf{q}}; b_{\mathbf{q}} + b_{-\mathbf{q}}^\dagger \rangle\rangle_\omega^\alpha = -\omega_{\mathbf{q}} \left(-\omega_{\mathbf{q}} \langle\langle \rho_{-\mathbf{q}}; b_{\mathbf{q}} + b_{-\mathbf{q}}^\dagger \rangle\rangle_\omega^\alpha - \frac{2g_{-\mathbf{q}}}{\hbar\sqrt{N}} \langle\langle \rho_{-\mathbf{q}}; \rho_{\mathbf{q}} \rangle\rangle_\omega^\alpha \right). \quad (4.15)$$

Combining these two equations, we obtain

$$D^\alpha(\mathbf{q}, \omega) = D_0^\alpha(\mathbf{q}, \omega) + \frac{|g_{\mathbf{q}}|^2}{\hbar^2 N} D_0^\alpha(\mathbf{q}, \omega) \chi^\alpha(\mathbf{q}, \omega) D_0^\alpha(\mathbf{q}, \omega), \quad (4.16)$$

where we defined the charge response function

$$\chi^\alpha(\mathbf{q}, \omega) = \langle\langle \rho_{-\mathbf{q}}; \rho_{\mathbf{q}} \rangle\rangle_\omega^\alpha. \quad (4.17)$$

Inserting into Eq. (4.16) Dyson's equation from Eq. 4.8, we arrive at the final result:

$$\Pi^\alpha(\mathbf{q}, \omega) = \frac{|g_{\mathbf{q}}|^2 / (\hbar^2 N) \chi^\alpha(\mathbf{q}, \omega)}{1 + |g_{\mathbf{q}}|^2 / (\hbar^2 N) \chi^\alpha(\mathbf{q}, \omega) D_0^\alpha(\mathbf{q}, \omega)}. \quad (4.18)$$

Integrating the modulus of the imaginary part of the charge response function over all frequencies and summing over all wavevectors except for $\mathbf{q}=(0,0)$, one finds using Eqs. (C.7) and (C.8):

$$\begin{aligned} \sum_{\mathbf{q} \neq (0,0)} \int_{-\infty}^{\infty} d\omega |\text{Im} \chi^\alpha(\mathbf{q}, \omega)| &= 2\pi \sum_{\mathbf{q} \neq (0,0)} \langle 0 | \rho_{-\mathbf{q}} \rho_{\mathbf{q}} | 0 \rangle \\ &= 2\pi \sum_{\mathbf{q} \neq (0,0)} \sum_{ij} e^{i\mathbf{q} \cdot (\mathbf{R}_i - \mathbf{R}_j)} \langle 0 | n_i n_j | 0 \rangle \\ &= 2\pi \sum_{\mathbf{q}} \sum_{ij} e^{i\mathbf{q} \cdot (\mathbf{R}_i - \mathbf{R}_j)} \langle 0 | n_i n_j | 0 \rangle - 2\pi \sum_{ij} \langle 0 | n_i n_j | 0 \rangle \\ &= 2\pi N \langle 0 | \sum_i n_i^2 | 0 \rangle - 2\pi \langle 0 | (\sum_i n_i)^2 | 0 \rangle. \end{aligned} \quad (4.19)$$

4.3.1 Interacting electrons

If we describe the electrons by the strongly correlated model of Eq. (4.1), the constraint that sites cannot be doubly occupied (implying $n_i^2 = n_i$) allows for the following evaluation of the last line in Eq. (4.19):

$$\sum_{\mathbf{q} \neq (0,0)} \int_{-\infty}^{\infty} d\omega |\text{Im } \chi^\alpha(\mathbf{q}, \omega)| = 2\pi N \langle 0 | \sum_i n_i | 0 \rangle - 2\pi \langle 0 | (\sum_i n_i)^2 | 0 \rangle = 2\pi \delta(1 - \delta) N^2, \quad (4.20)$$

where δ is the doping defined as the number of doped holes per site. We have arrived at a sum rule for the charge response function that was already pointed out by Khaliullin and Horsch [34]:

$$\frac{1}{\pi N} \sum_{\mathbf{q} \neq (0,0)} \int_{-\infty}^{\infty} d\omega |\text{Im } \chi^\alpha(\mathbf{q}, \omega)| = 2\delta(1 - \delta) N. \quad (4.21)$$

According to Eq. (4.21), $\chi^\alpha(\mathbf{q}, \omega)$ becomes small for small doping which we are interested in. Therefore, the denominator in Eq. (4.18) is not very different from 1 and we can approximate $\Pi^\alpha(\mathbf{q}, \omega) \approx |g_{\mathbf{q}}|^2 / (\hbar^2 N) \chi^\alpha(\mathbf{q}, \omega)$. From Eq. (4.21), we then obtain the following approximate sum rule for the phonon self-energy:

$$\frac{1}{\pi N} \sum_{\mathbf{q} \neq (0,0)} \frac{\hbar^2}{|g_{\mathbf{q}}|^2} \int_{-\infty}^{\infty} d\omega |\text{Im } \Pi^\alpha(\mathbf{q}, \omega)| \approx 2\delta(1 - \delta). \quad (4.22)$$

4.3.2 Non-interacting electrons

If we consider non-interacting electrons described by $H_{\text{non-int}}$ from Eq. (4.4) and assume a system without spin polarization, the last line in Eq. (4.19) can be evaluated as follows:

$$\begin{aligned} \sum_{\mathbf{q} \neq (0,0)} \int_{-\infty}^{\infty} d\omega |\text{Im } \chi^\alpha(\mathbf{q}, \omega)| &= \\ &= 2\pi N \langle 0 | \sum_i (n_i + 2n_{i\uparrow}n_{i\downarrow}) | 0 \rangle - 2\pi \langle 0 | (\sum_i n_i)^2 | 0 \rangle \\ &= 2\pi N (2nN + 2n^2N) - (2nN)^2 = 4\pi N^2 n(1 - n), \end{aligned} \quad (4.23)$$

where n is the number of electrons per site and spin. If we assume not too strong couplings $|g_{\mathbf{q}}|^2$ such that the denominator in Eq. (4.18) can be approximated by 1, the sum rule for the modulus of the imaginary part of the phonon self-energy analogous

to Eq. (4.22) is given by

$$\begin{aligned} \frac{1}{\pi N} \sum_{\mathbf{q} \neq (0,0)} \frac{\hbar^2}{|g_{\mathbf{q}}|^2} \int_{-\infty}^{\infty} d\omega |\text{Im} \Pi^{\alpha}(\mathbf{q}, \omega)| &\approx 4n(1-n) \\ &\approx 1 \quad \text{for } n \approx \frac{1}{2}. \end{aligned} \quad (4.24)$$

In the second line, we assumed an approximately half-filled band which should be compared to the weakly doped t - J model.

4.3.3 Discussion

Comparing the sum rules for interacting and non-interacting electrons, Eqs. (4.22) and (4.24), shows that in the interacting case the phonon self-energy is suppressed by a factor $2\delta(1-\delta)$ compared to the result for non-interacting electrons. The electron-electron interaction therefore strongly reduces the effects of the electron-phonon interaction on phonons at low doping. The electron density is rearranged in response to the excitation of a phonon, and this rearrangement acts back on the phonon, contributing to the width and energy shift of the phonon. The system can respond to the perturbation of a phonon by transferring doped holes (Zhang-Rice singlets) to sites with a low on-site energy for singlets in the distorted lattice in order to lower its total energy. If there are few singlets, i.e., δ is small, the response of the system is weak and the phonon self-energy is small. Since typically $\delta \approx 0.1$, this drastically reduces the phonon softening and width due to the creation of electron-hole pairs. This is a direct effect of the strong correlation which allows us to neglect double occupancy of sites in case of interacting electrons.

4.4 Sum rule for electron self-energy

4.4.1 Interacting electrons

We now derive a sum rule for the electron self-energy and start again with the case of electrons interacting with each other. The one-electron Green's function $G_{\sigma}(\mathbf{k}, z) = \langle\langle \tilde{c}_{\mathbf{k}\sigma}; \tilde{c}_{\mathbf{k}\sigma}^{\dagger} \rangle\rangle_z$ in the undoped t - J model is given in terms of its spectral density $A_{\sigma}(\mathbf{k}, \omega) = -\text{Im} G_{\sigma}(\mathbf{k}, \omega + i0^+)/\pi$ by

$$G_{\sigma}(\mathbf{k}, z) = \int_{-\infty}^{\infty} d\omega \frac{A_{\sigma}(\mathbf{k}, \omega)}{z - \omega}. \quad (4.25)$$

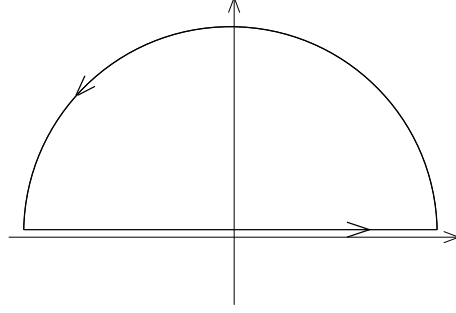


Figure 4.2: Contour in the upper half-plane of complex frequencies z for the integral over $\Sigma_\sigma(\mathbf{k}, z)$ in Eq. (4.32). It is a closed semicircle with radius R , positions on the arc are characterized by the angle φ measured against the positive real axis.

Expanding the denominator of Eq. (4.25) in powers of $1/z$, one obtains

$$G_\sigma(\mathbf{k}, z) = \sum_{m=0}^{\infty} \frac{M_{\mathbf{k}\sigma}^{(m)}}{z^{m+1}}, \quad (4.26)$$

where the moments of the spectral density are defined by

$$M_{\mathbf{k}\sigma}^{(m)} = \int_{-\infty}^{\infty} d\omega \omega^m A_\sigma(\mathbf{k}, \omega). \quad (4.27)$$

On the other hand, in terms of the electron self-energy $\Sigma_\sigma(\mathbf{k}, z)$, we have

$$G_\sigma(\mathbf{k}, z) = \frac{a_{\mathbf{k}\sigma}}{z - \hbar^{-1}\varepsilon_{\mathbf{k}\sigma} - \Sigma_\sigma(\mathbf{k}, z)}, \quad (4.28)$$

where $a_{\mathbf{k}\sigma}$ is a weight factor. We assume that any constant energy shift is absorbed in the bare dispersion $\varepsilon_{\mathbf{k}\sigma}$ such that the self-energy has a $1/z$ expansion of the form

$$\Sigma_\sigma(\mathbf{k}, z) = \frac{b_{\mathbf{k}\sigma}}{z} + \mathcal{O}(z^{-2}). \quad (4.29)$$

As we have $A_\sigma(\mathbf{k}, \omega) \geq 0$ for the real spectral density, it follows from Eq. (4.25) that $G_\sigma(\mathbf{k}, z)$ can be zero only for z on the real axis. Therefore, according to Eq. (4.28), $\Sigma_\sigma(\mathbf{k}, z)$ has no poles in both the upper and the lower half-plane away from the real axis and the integral along the contour in Fig. 4.2 vanishes. Then, using Eq. (4.29),

$$\int_{-R}^R d\omega \Sigma_\sigma(\mathbf{k}, \omega + i0^+) + \int_0^\pi i R e^{i\varphi} d\varphi \frac{b_{\mathbf{k}\sigma}}{R e^{i\varphi}} + \mathcal{O}(R^{-1}) = 0, \quad (4.30)$$

and for $R \rightarrow \infty$

$$b_{\mathbf{k}\sigma} = -\frac{1}{\pi} \int_{-\infty}^{\infty} d\omega \operatorname{Im} \Sigma_\sigma(\mathbf{k}, \omega + i0^+). \quad (4.31)$$

If we compare the $1/z$ expansion of Eq. (4.28),

$$G_\sigma(\mathbf{k}, z) = \frac{a_{\mathbf{k}\sigma}}{z} + \frac{a_{\mathbf{k}\sigma}\hbar^{-1}\varepsilon_{\mathbf{k}\sigma}}{z^2} + \frac{a_{\mathbf{k}\sigma}(\hbar^{-2}\varepsilon_{\mathbf{k}\sigma}^2 + b_{\mathbf{k}\sigma})}{z^3} + \mathcal{O}(z^{-4}), \quad (4.32)$$

with Eq. (4.26), we find

$$b_{\mathbf{k}\sigma} = \frac{M_{\mathbf{k}\sigma}^{(2)}}{M_{\mathbf{k}\sigma}^{(0)}} - \left(\frac{M_{\mathbf{k}\sigma}^{(1)}}{M_{\mathbf{k}\sigma}^{(0)}} \right)^2. \quad (4.33)$$

Let $|\Phi\rangle$ be the ground state of the undoped t - J model with phonons. Because of the constraint forbidding double occupancy of sites, only photoemission is possible. Therefore, the spectral density can be written as

$$A_\sigma(\mathbf{k}, \omega) = \sum_n |\langle n | \tilde{c}_{\mathbf{k}\sigma} | \Phi \rangle|^2 \delta(\omega + \hbar^{-1} E_n) \quad (4.34)$$

summing over all eigenstates $|n\rangle$ of H in the one-hole sector (their eigenenergies being E_n). Here, we measure energies such that $E_0 = \langle \Phi | H | \Phi \rangle = 0$. From Eq. (4.34), one derives the following formula for the moments of the spectral density defined in Eq. (4.27):

$$\hbar^m M_{\mathbf{k}\sigma}^{(m)} = \sum_n E_n^m |\langle n | \tilde{c}_{\mathbf{k}\sigma} | \Phi \rangle|^2 = \langle \Phi | \tilde{c}_{\mathbf{k}\sigma}^\dagger H^m \tilde{c}_{\mathbf{k}\sigma} | \Phi \rangle. \quad (4.35)$$

We now evaluate Eq. (4.35) for $m = 0, 1, 2$. First,

$$\begin{aligned} M_{\mathbf{k}\sigma}^{(0)} &= \langle \Phi | \tilde{c}_{\mathbf{k}\sigma}^\dagger \tilde{c}_{\mathbf{k}\sigma} | \Phi \rangle = \frac{1}{N} \sum_{ij} e^{i\mathbf{k}\cdot(\mathbf{R}_i - \mathbf{R}_j)} \langle \Phi | \tilde{c}_{j\sigma}^\dagger \tilde{c}_{i\sigma} | \Phi \rangle \\ &= \frac{1}{N} \sum_i \langle \Phi | \tilde{c}_{i\sigma}^\dagger \tilde{c}_{i\sigma} | \Phi \rangle = \frac{N_\sigma}{N}. \end{aligned} \quad (4.36)$$

In the second line, we used the fact that we must have $j = i$ as $|\Phi\rangle$ describes the undoped system. N_σ gives the number of electrons with spin σ in the undoped system. Next,

$$\hbar M_{\mathbf{k}\sigma}^{(1)} = \langle \Phi | \tilde{c}_{\mathbf{k}\sigma}^\dagger H \tilde{c}_{\mathbf{k}\sigma} | \Phi \rangle = \langle \Phi | \tilde{c}_{\mathbf{k}\sigma}^\dagger H_{t-J} \tilde{c}_{\mathbf{k}\sigma} | \Phi \rangle. \quad (4.37)$$

It was used that $\langle \Phi | \tilde{c}_{\mathbf{k}\sigma}^\dagger H_{\text{ep}} \tilde{c}_{\mathbf{k}\sigma} | \Phi \rangle = 0$ and $H_{\text{ph}} \tilde{c}_{\mathbf{k}\sigma} | \Phi \rangle = 0$ as there are no phonons in the ground state of the undoped system. Similarly, $\langle \Phi | \tilde{c}_{\mathbf{k}\sigma}^\dagger H_{t-J} H_{\text{ep}} \tilde{c}_{\mathbf{k}\sigma} | \Phi \rangle = 0$, and

$$\hbar^2 M_{\mathbf{k}\sigma}^{(2)} = \langle \Phi | \tilde{c}_{\mathbf{k}\sigma}^\dagger H^2 \tilde{c}_{\mathbf{k}\sigma} | \Phi \rangle = \langle \Phi | \tilde{c}_{\mathbf{k}\sigma}^\dagger (H_{t-J}^2 + H_{\text{ep}}^2) \tilde{c}_{\mathbf{k}\sigma} | \Phi \rangle. \quad (4.38)$$

One finds

$$\begin{aligned} \langle \Phi | \tilde{c}_{\mathbf{k}\sigma}^\dagger H_{\text{ep}}^2 \tilde{c}_{\mathbf{k}\sigma} | \Phi \rangle &= \frac{1}{N^2} \sum_{ij} e^{i\mathbf{k}\cdot(\mathbf{R}_i - \mathbf{R}_j)} \langle \Phi | \tilde{c}_{j\sigma}^\dagger \sum_{\mathbf{q}} \sum_{\mathbf{q}'} \sum_{l,l'} g_{\mathbf{q}} g_{\mathbf{q}'} (n_l - 1) \\ &\quad \times (n_{l'} - 1) (b_{\mathbf{q}} + b_{-\mathbf{q}}^\dagger) (b_{\mathbf{q}'} + b_{-\mathbf{q}'}^\dagger) e^{i(\mathbf{q}\cdot\mathbf{R}_l + \mathbf{q}'\cdot\mathbf{R}_{l'})} \tilde{c}_{i\sigma} | \Phi \rangle \end{aligned} \quad (4.39)$$

$$\begin{aligned}
&= \frac{1}{N^2} \sum_{ij} e^{i\mathbf{k}\cdot(\mathbf{R}_i-\mathbf{R}_j)} \langle \Phi | \tilde{c}_{j\sigma}^\dagger \sum_{\mathbf{q}} g_{\mathbf{q}} g_{-\mathbf{q}} \tilde{c}_{i\sigma} | \Phi \rangle \\
&= \frac{N_\sigma}{N^2} \sum_{\mathbf{q}} |g_{\mathbf{q}}|^2.
\end{aligned}$$

First, it was used that there are no phonons in $|\Phi\rangle$ which requires $\mathbf{q}' = -\mathbf{q}$ and that $(n_l - 1)(n_{l'} - 1)\tilde{c}_{i\sigma}|\Phi\rangle = \delta_{il}\delta_{i'l'}\tilde{c}_{i\sigma}|\Phi\rangle$. In the last step, we proceeded like in Eq. (4.36).

Inserting these results into Eq. (4.33), we have

$$\hbar^2 b_{\mathbf{k}\sigma} = \frac{N}{N_\sigma} \langle \Phi | \tilde{c}_{\mathbf{k}\sigma}^\dagger H_{t-J}^2 \tilde{c}_{\mathbf{k}\sigma} | \Phi \rangle - \left(\frac{N}{N_\sigma} \langle \Phi | \tilde{c}_{\mathbf{k}\sigma}^\dagger H_{t-J} \tilde{c}_{\mathbf{k}\sigma} | \Phi \rangle \right)^2 + \frac{1}{N} \sum_{\mathbf{q}} |g_{\mathbf{q}}|^2. \quad (4.40)$$

If we had considered the same system without electron-phonon interaction, i.e., $H_{\text{ep}} \equiv 0$, the result would have differed only by the disappearance of the third term in Eq. (4.40). So, if we define $\Sigma_\sigma^{\text{ep}}(\mathbf{k}, z)$ as the difference between the self-energies for the system with and without electron-phonon interaction, we arrive at the following sum rule for its spectral density:

$$-\frac{\hbar^2}{\pi} \int_{-\infty}^0 d\omega \text{Im} \Sigma_\sigma^{\text{ep}}(\mathbf{k}, \omega + i0^+) = \frac{1}{N} \sum_{\mathbf{q}} |g_{\mathbf{q}}|^2 \equiv \bar{g}^2. \quad (4.41)$$

The integration can be limited to negative energies as only photoemission is possible from the undoped system. It is interesting to note that the result depends neither on the wavevector \mathbf{k} nor the spin σ of the hole created in the photoemission process. It is also independent of the electronic parameters t and J .

4.4.2 Non-interacting electrons

Next, we consider the electron self-energy for non-interacting electrons. To lowest order in the electron-phonon coupling, the (causal) electron self-energy is given by

$$(i\Sigma^c(\mathbf{k}, \omega)) = \sum_{\mathbf{q}} \frac{|g_{\mathbf{q}}|^2}{\hbar^2 N} \frac{1}{2\pi} \int_{-\infty}^{\infty} d\omega' (iD_0^c(\mathbf{q}, \omega')) (iG_0^c(\mathbf{k} + \mathbf{q}, \omega + \omega')), \quad (4.42)$$

with the free phonon Green's function from Eq. (4.9) and the free electron Green's function

$$G_0^c(\mathbf{k}, \omega) = \frac{1}{\omega - \hbar^{-1}\varepsilon_{\mathbf{k}} + i0_{\mathbf{k}}}, \quad (4.43)$$

where

$$0_{\mathbf{k}} = \begin{cases} 0^+ & \text{if } |\mathbf{k}| > k_F, \\ -0^+ & \text{if } |\mathbf{k}| < k_F. \end{cases} \quad (4.44)$$

The integrand in Eq. (4.42) has four terms of which two vanish after the integration as both poles are in one half-plane and the contour can be closed in the other one. The remaining two contributions are easily evaluated and lead to [111]

$$\Sigma^c(\mathbf{k}, \omega) = \sum_{\mathbf{q}} \frac{|g_{\mathbf{q}}|^2}{\hbar^2 N} \left\{ \frac{\Theta(|\mathbf{k} + \mathbf{q}| - k_F)}{\omega - \hbar^{-1}\varepsilon_{\mathbf{k}+\mathbf{q}} - \omega_{\mathbf{q}} + i0^+} + \frac{\Theta(k_F - |\mathbf{k} + \mathbf{q}|)}{\omega - \hbar^{-1}\varepsilon_{\mathbf{k}+\mathbf{q}} + \omega_{\mathbf{q}} - i0^+} \right\}. \quad (4.45)$$

Therefore,

$$\begin{aligned} \frac{\hbar^2}{\pi} \int_{-\infty}^{\infty} d\omega |\text{Im } \Sigma^c(\mathbf{k}, \omega)| &= \sum_{\mathbf{q}} \frac{|g_{\mathbf{q}}|^2}{N} (\Theta(|\mathbf{k} + \mathbf{q}| - k_F) + \Theta(k_F - |\mathbf{k} + \mathbf{q}|)) \\ &= \frac{1}{N} \sum_{\mathbf{q}} |g_{\mathbf{q}}|^2 = \bar{g}^2. \end{aligned} \quad (4.46)$$

4.4.3 Discussion

A comparison of the lowest order result for non-interacting electrons, Eq. (4.46), with Eq. (4.41) shows that the electron-phonon contribution to the electron self-energy in the undoped t - J model has a similar sum rule. In contrast to the phonon self-energy, there is no strong reduction at low doping in the strongly correlated system.

This result can be understood if we notice that a singlet with the wavevector \mathbf{k} , created in a photoemission experiment, can easily be scattered by phonons to other states $\mathbf{k} + \mathbf{q}$ since only a fraction $(1 - \delta)$ of these are occupied by other singlets. We therefore expect a strong effect of the electron-phonon interaction on photoemission spectra also for a finite but small δ .

Whereas the sum rule for non-interacting electrons was derived only to lowest order in the coupling \bar{g}^2 and higher order corrections are expected to become important for stronger coupling, the result for interacting electrons is valid for arbitrary coupling strengths. Interestingly, the right hand side of Eq. (4.41) remains proportional to \bar{g}^2 even for large \bar{g} .

From the arguments above, it follows that the phonon-induced attractive carrier-carrier interaction should also be effective at low doping since for small δ the carriers (singlets) can scatter each other via phonons with few restrictions. This may be helpful for superconductivity. In particular, it should be possible to have a strong phonon-induced carrier-carrier interaction without the corresponding phonon going soft.

4.5 Apparent coupling strengths

The dimensionless electron-phonon coupling constant λ is often calculated from phonon and electron properties using standard expressions derived in the framework of theories for non-interacting electrons. A formula by Allen [108, 109] relates the line width $\gamma = 2\hbar \text{Im} \Pi(\mathbf{q}, \omega_{\text{ph}})$ of a phonon with frequency ω_{ph} to the coupling constant,

$$\lambda^{\Pi} = \frac{\gamma}{2\pi\hbar^2\omega_{\text{ph}}^2 N(0)}, \quad (4.47)$$

where $N(0)$ is the electron density of states per spin and we label λ by Π to emphasize that it is calculated from a phonon property determined by the phonon self-energy. Assuming a constant electronic density of states, a phonon energy which is small compared to the electronic band width, and not too strong coupling, one easily finds from a Kramers-Kronig relation that Eq. (4.47) can also be expressed in terms of the phonon softening $\Delta\omega_{\text{ph}} = \text{Re} \Pi(\mathbf{q}, \omega_{\text{ph}})$,

$$\lambda^{\Pi} = -\alpha \frac{\Delta\omega_{\text{ph}}}{\omega_{\text{ph}}^0}, \quad (4.48)$$

with the prefactor α being of order 1 and ω_{ph}^0 denoting the bare phonon frequency. On the other hand, a standard definition of the coupling constant is based on the electron self-energy,

$$\lambda^{\Sigma} = - \left. \frac{d\text{Re} \Sigma^{\text{ep}}(\omega + i0^+)}{d\omega} \right|_{\omega=0} = -\frac{1}{\pi} \mathcal{P} \int_{-\infty}^{\infty} d\omega \frac{\text{Im} \Sigma^{\text{ep}}(\omega + i0^+)}{\omega^2}, \quad (4.49)$$

where now λ is labeled by Σ to show that it is deduced from electronic properties.

The definitions in Eqs. (4.47), (4.48), and (4.49) are chosen such that they all give the same value for the coupling constant in a system of non-interacting electrons. If instead we consider a strongly correlated system with interacting electrons, we have to take into account the results of Secs. 4.3 and 4.4. We found from sum rules that at low doping the integrated spectral weight of the phonon self-energy is reduced $\propto \delta$ due to strong correlations. As there is no such reduction in the corresponding sum rule for the electron self-energy, the calculation of apparent coupling constants using Eqs. (4.47), (4.48), and (4.49) in a system of interacting electrons in general leads to different results depending on whether one considers phonon or electron properties. From the sum rules, one expects $\lambda^{\Pi}/\lambda^{\Sigma} = c\delta$ where $c \approx 2 - 4$ depends on the precise frequency dependence of the self-energies.

In this context, we remark on a notable aspect concerning the experimental extraction of λ^{Σ} . While originally the apparent coupling for the electron self-energy

$\lambda^\Sigma \approx 1$ was estimated from photoemission experiments, later work assigned a substantial part of this coupling to lower-lying phonons [93] bringing λ^Σ and λ^Π for the (half-)breathing phonon into better agreement. The observed kink in the photoemission spectrum can, however, substantially underestimate λ^Σ in Eq. (4.49). Let the electron self-energy $\Sigma(\omega) = -(\lambda^{\text{el}} + \lambda^\Sigma)\omega$ for small $|\omega|$ and $\Sigma(\omega) = -\lambda^{\text{el}}\omega$ for large $|\omega|$ where λ^Σ is due to the phonon of interest and λ^{el} is due to other effects. Then, the observed change of the slope at the kink is determined by $1 + \lambda^\Sigma/(1 + \lambda^{\text{el}}) < 1 + \lambda^\Sigma$ where $(1 + \lambda^\Sigma + \lambda^{\text{el}}) = Z^{-1}$, the inverse quasi-particle weight, can be a large number. This suggests that λ^Σ is substantially larger than λ^Π .

4.6 Numerical results

To illustrate the results of the previous sections, we study the t - J model with phonons from Eq. (4.1) and solve it numerically using exact diagonalization. We consider a finite cluster with 4×3 sites and periodic boundary conditions. We use the parameters $t = 0.47$ eV and $J/t = 0.3$. The entire (half-)breathing phonon branch is included. The electron-phonon interaction is given by the on-site coupling derived in Chap. 1. The Hilbert space is limited by only allowing for states which have a maximum of P phonons, where typically $P = 7$. The calculational details have already been described in Sec. 2.2.

Ideally, one would like to calculate λ^Σ as in experiment from the change of the slope in the quasi-particle dispersions around the kink which one expects to see at energies of the order of the phonon energies. For the small clusters which can be studied in exact diagonalization, however, this approach is not possible due to the few available \mathbf{k} -points for which photoemission spectra can be calculated. Instead, we focus directly on the electron self-energy. As detailed in App. A, the spectral function $A(\mathbf{k}, \omega)$ is calculated using exact diagonalization. The Green's function is then obtained from a Kramers-Kronig transformation. Finally, $\Sigma(\mathbf{k}, \omega)$ is obtained by inverting Eq. (4.28). From that, λ^Σ can be calculated using Eq. (4.49).

In a similar way, we determine the phonon self-energy $\Pi(\mathbf{q}, \omega)$ from the phonon spectral function. Then, λ^Π can be obtained using Eq. (4.47) or Eq. (4.48). As already discussed in Sec. 2.2.1, the width of the phonon peak can be extracted more reliably from the imaginary part of the phonon self-energy than from the phonon spectral function directly. But because of the small size of the cluster, there are few many-electron states with energies of the order of the phonon energies. This complicates the extraction of phonon widths even in the approach which uses the phonon self-

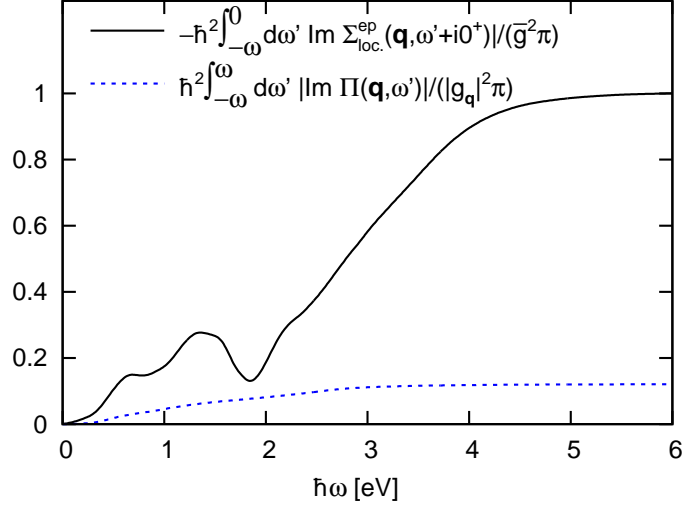


Figure 4.3: Frequency integrals over the imaginary parts of the phonon self-energy for $\mathbf{q} = (\pi/a, 0)$ and the electron-phonon contribution to the \mathbf{k} -averaged (local) electron self-energy. The results are divided by the coupling constants and were obtained for a 4×3 cluster with periodic boundary conditions. Π was calculated for $\delta = 1/12$ and $\Sigma_{\text{loc}}^{\text{ep}}$ for $\delta = 0$. The self-energies were given a 0.2 eV (FWHM) Lorentzian broadening. The figure illustrates how these quantities converge to approximately $2\delta \approx 0.17$ (Eq. (4.22)) and unity (Eq. (4.41)) for the phonon and electron self-energy, respectively.

energy because there are only a few peaks contributing to its spectral density. To extenuate this problem, we use a phonon energy larger than the experimental values for our numerical example. We increase the bare phonon energy to $\hbar\omega_{\text{ph}}^0 = 0.5$ eV. This requires a corresponding increase in the coupling constants. We have chosen a multiplying factor of 3.4 which leads to an apparent electron-phonon coupling strength of the order seen experimentally.¹

Figure 4.3 shows the frequency integrals of the imaginary parts of the phonon self-energy for the system with one doped hole and the electron-phonon contribution to the electron self-energy for the undoped system as a function of the upper limit ω . The limit $\omega \rightarrow \infty$ corresponds to the sum rules from Eqs. (4.22) and (4.41). To obtain dimensionless quantities, the coupling constants have been divided out. In this example, the phonon self-energy is calculated for $\mathbf{q} = (\pi/a, 0)$ and the electron-

¹We expect that keeping $g_{\mathbf{q}}^2/\omega_{\text{ph}}$ fixed when changing ω_{ph} leads to an unchanged λ . We have multiplied the $g_{\mathbf{q}}$ rescaled in this way by an additional factor of $\sqrt{2}$. Deducing λ from the phonon width then gives a value comparable to what is obtained from experiment.

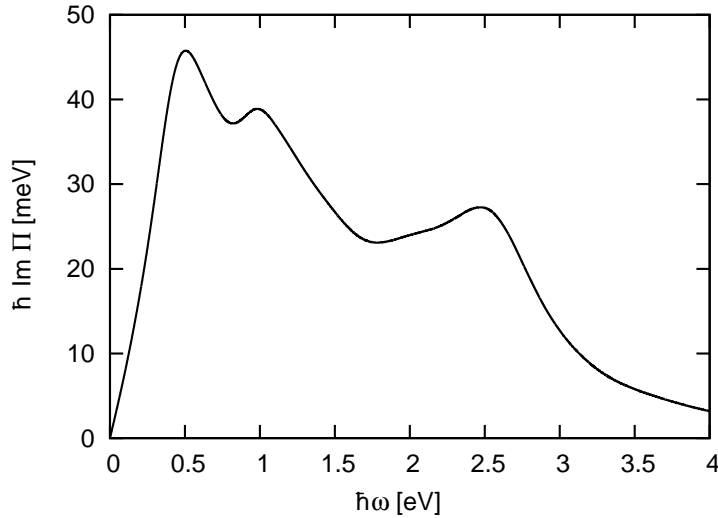


Figure 4.4: $\text{Im } \Pi(\mathbf{q}, \omega)$ of the 4×3 cluster for $\mathbf{q} = (\pi/a, 0)$ and $\delta = 1/12$. The self-energy has been given a Lorentzian broadening of 0.4 eV.

phonon contribution to the electron self-energy has been averaged over all electronic wavevectors but similar results are obtained for other choices. The figure illustrates the large ratio, $\approx 2\delta$, of the sum rules. The sum rule in Eq. (4.21) applies to an average over $\mathbf{q} \neq \mathbf{0}$ of χ , but we found that it is also rather accurate for $\Pi/g_{\mathbf{q}}^2$ for an individual value of \mathbf{q} , as is illustrated in Fig. 4.3. The reason is that the denominator in Eq. (4.18) is not very important for the coupling strengths used here and that the sum rule for an individual \mathbf{q} is not very different from the average over \mathbf{q} .

Figure 4.4 shows the broadened $\text{Im } \Pi(\mathbf{q}, \omega)$ for $\mathbf{q} = (\pi/a, 0)$. The broadening (0.4 eV FWHM) was chosen in such a way that the fine structures due to the finite cluster size were removed and the expected behavior $\text{Im } \Pi(\mathbf{q}, \omega) \propto \omega$ for small ω was obtained. The phonon is softened to $\hbar\omega_{\text{ph}} = 0.4$ eV due to the electron-phonon interaction. For this frequency, we obtain the FWHM of the phonon as $\gamma = 0.08$ eV. This result depends on the broadening of $\text{Im } \Pi(\mathbf{q}, \omega)$ and values differing by $\pm 30\%$ could be obtained for other reasonable broadenings. Based on the width of $\text{Im } \Pi(\mathbf{q}, \omega)$, we estimate an electronic density of states $N(0) \approx 0.5$ states per eV and spin and calculate an apparent electron-phonon coupling constant $\lambda^{\text{II}} = 0.2$ from Eq. (4.47). From the phonon softening $\Delta\omega_{\text{ph}}/\omega_{\text{ph}}^0 = 0.2$, we obtain a similar result for λ^{II} using Eq. (4.48).

We emphasize again as in Sec. 2.2.1 the difference between this approach which uses the broadened imaginary part of the phonon self-energy and an approach where

the phonon spectral function is broadened until a smooth spectrum is obtained. The latter method leads to an additional width of the peaks. For the present system, such a large broadening would be required that no meaningful results could be extracted. The broadening of $\text{Im } \Pi(\mathbf{q}, \omega)$, on the other hand, does not generally add to the width of the phonon spectral function since it essentially only distributes the contributions to $\text{Im } \Pi(\mathbf{q}, \omega)$ more uniformly along the energy axis.

We can also extract an apparent electron-phonon coupling constant from the electron self-energy using Eq. (4.49). This leads to $\lambda^\Sigma = 0.6$. As can be seen from Fig. 4.3, the imaginary part of the electron-phonon contribution to the electron self-energy is small for $|\hbar\omega| < \hbar\omega_{\text{ph}} = 0.4$ eV. For this frequency range, we find that $\text{Re } \Sigma(\mathbf{k}, \omega) \approx \lambda^\Sigma \omega$. Although calculated for a small cluster, the electron self-energy therefore shows the characteristic features of a self-energy due to electron-phonon interaction. λ^Σ is about a factor of $1/(c\delta)$ larger than λ^Π with $c = 4$. Therefore, our numerical example confirms the expectation in Sec. 4.5 that the different effect of strong correlations on the phonon and electron self-energy seen in the sum rules also manifests itself in the apparent coupling constants which are more directly linked to experimental observables like the phonon width and softening or the change of the slope around the kink in ARPES quasi-particle dispersions.

4.7 Effect of vertex corrections

The sum rules for the phonon and electron self-energies derived in this chapter can also be used to judge the importance of vertex corrections in a diagrammatic treatment of electron-phonon interactions in strongly correlated systems. In this context, the electronic degrees of freedom are often described by the two-dimensional Hubbard model:

$$H_{\text{H}} = \varepsilon_{\text{H}} \sum_{i\sigma} n_{i\sigma} + t_{\text{H}} \sum_{\langle ij \rangle \sigma} \left(c_{i\sigma}^\dagger c_{j\sigma} + \text{H.c.} \right) + U_{\text{H}} \sum_i n_{i\uparrow} n_{i\downarrow}. \quad (4.50)$$

Here, $c_{i\sigma}^\dagger$ creates an electron with spin σ on site i of a square lattice and $n_{i\sigma} = c_{i\sigma}^\dagger c_{i\sigma}$. ε_{H} is the level energy, t_{H} is the hopping amplitude between nearest-neighbor sites $\langle ij \rangle$, and U_{H} is the Coulomb repulsion between two electrons on the same site. In the limit of large U_{H} , states with doubly occupied states can be projected out. If certain terms are neglected [112], the resulting effective low-energy model takes the form of the t - J model (Eq. (1.87)).

It is then interesting to ask how electron-phonon interactions are influenced by the Coulomb interaction U_{H} . Using the language of diagrammatic perturbation theory,

this can happen via dressing of Green's functions [106] or corrections to the vertex functions [113, 114]. Huang *et al.* [113] as well as Koch and Zeyher [114] studied the effect of U_H on an effective vertex function in the static limit and found a suppression. According to Ref. [113], this suppression is, however, reduced for large U_H and small phonon wavevectors \mathbf{q} . Also the electron and phonon self-energies depend on vertex functions appearing in integrals over internal momenta and frequencies. With exact sum rules for these self-energies at hand, we can extract information about the effect of vertex corrections on the electron-phonon interaction which in the following we assume to be of the form defined in Eq. (4.2).

4.7.1 Electron self-energy

We first discuss how the electron self-energy of the undoped t - J model can be related to that of the half-filled Hubbard model in the limit of large U_H . We start by noting that the spectral function $A_{t-J}(\mathbf{k}, \omega)$ of the one-electron Green's function in the undoped t - J model is zero on the inverse photoemissions side ($\omega > 0$) because of suppressed double occupancy. Assuming that the Hubbard model has an identical photoemission spectrum (apart from a trivial energy shift of the order of $U_H/2$), the spectral function in the electron-hole symmetric model ($\varepsilon_H = -U_H/2$) is given by

$$A_H(\mathbf{k}, \omega) \approx A_{t-J}(\mathbf{k}, \hbar^{-1}U_H/2 + \omega) + A_{t-J}(-\mathbf{k}, \hbar^{-1}U_H/2 - \omega), \quad (4.51)$$

where the energy shift $U_H/2$ can have errors of the order of t_H . In both models, the one-electron Green's function $G(\mathbf{k}, z)$ can be defined in terms of either the spectral function $A(\mathbf{k}, \omega)$ or the electron self-energy $\Sigma(\mathbf{k}, \omega)$:

$$G(\mathbf{k}, z) = \int_{-\infty}^{\infty} d\omega \frac{A(\mathbf{k}, \omega)}{z - \omega} = \frac{a}{z - \Sigma(\mathbf{k}, z)}. \quad (4.52)$$

Here, z is a complex frequency and the weight a equals 1 and 1/2 for the Hubbard model and the t - J model, respectively. Using Eqs. (4.51) and (4.52), the self-energy $\Sigma_H(\mathbf{k}, z)$ of the Hubbard model and that of the t - J model, $\Sigma_{t-J}(\mathbf{k}, z)$, can be directly related, and we find for large U_H and $\hbar z \approx U_H/2$:

$$\Sigma_H(\mathbf{k}, z) \approx 2\Sigma_{t-J}(\mathbf{k}, \hbar^{-1}U_H/2 + z) + \frac{U_H^2}{4\hbar^2 z}. \quad (4.53)$$

Again, we allow for errors of the order of t_H in the energy argument of $\Sigma_{t-J}(\mathbf{k}, \hbar^{-1}U_H/2 + z)$ and the position of the pole at $z = 0$. This can lead to errors of the same order in $\text{Re } \Sigma_H(\mathbf{k}, z)$ around $\hbar z \approx -U_H/2$. But apart from such small relative shifts, the

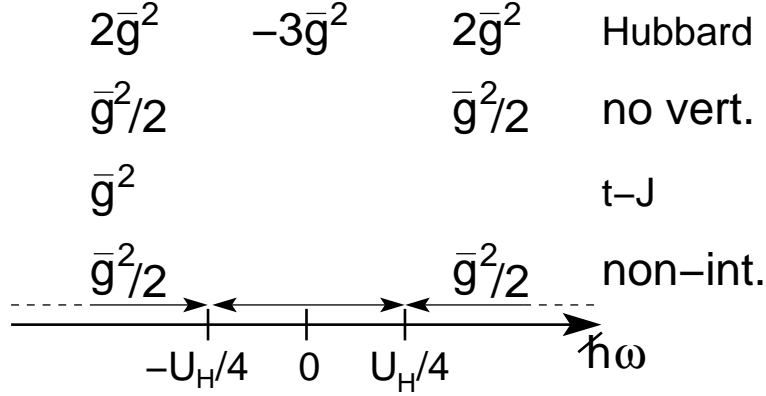


Figure 4.5: Weights obtained by integrating $-\hbar \text{Im} \Sigma^{\text{ep}}(\mathbf{k}, \omega + i0^+)/\pi$ over different energy ranges indicated by the arrows for the half-filled Hubbard model and the undoped t - J model, the latter shifted by $-U_{\text{H}}/2$. Also shown are the results for the Hubbard model without vertex corrections (“no vert.”) and for non-interacting electrons (“non-int.”, the \mathbf{k} -averaged photoemission and inverse photoemission spectra are shifted by $-U_{\text{H}}/2$ and $U_{\text{H}}/2$, respectively).

imaginary parts of the self-energies are related very accurately by a factor of two in this energy range. The pole strengths are the same in both models since

$$1 - \left. \frac{d\Sigma_{\text{H}}(\mathbf{k}, z)}{dz} \right|_{z \approx -\hbar^{-1}U_{\text{H}}/2} \approx 2 \left[1 - \left. \frac{d\Sigma_{t-J}(\mathbf{k}, \hbar^{-1}U_{\text{H}}/2 + z)}{dz} \right|_{z \approx -\hbar^{-1}U_{\text{H}}/2} \right] \quad (4.54)$$

which compensates for the different values of a in the definition of the Green’s function, Eq. (4.52).

Using Eq. (4.53), the sum rule in Eq. (4.41) for the difference between the self-energies with and without electron-phonon interaction in the undoped t - J model can be rewritten as a corresponding sum rule for the self-energies in the half-filled Hubbard model with large U_{H} :

$$-\frac{\hbar^2}{\pi} \int_{-\infty}^{-\hbar^{-1}U_{\text{H}}/4} d\omega \text{Im} \Sigma_{\text{H}}^{\text{ep}}(\mathbf{k}, \omega + i0^+) = 2\bar{g}^2. \quad (4.55)$$

We integrate up to $-\hbar^{-1}U_{\text{H}}/4$ to include the full photoemission spectrum which is located at energies of the order of $-U_{\text{H}}/2$ (we assume $\bar{g}^2/|t_{\text{H}}| \ll U_{\text{H}}$). It follows from particle-hole symmetry that the same contribution is obtained by integrating from $\hbar^{-1}U_{\text{H}}/4$ to infinity. In addition, by considering moments of the spectral density, a sum rule for integrating over all frequencies can be derived in complete analogy to Sec. 4.4.1:

$$-\frac{\hbar^2}{\pi} \int_{-\infty}^{\infty} d\omega \text{Im} \Sigma_{\text{H}}^{\text{ep}}(\mathbf{k}, \omega + i0^+) = \bar{g}^2. \quad (4.56)$$

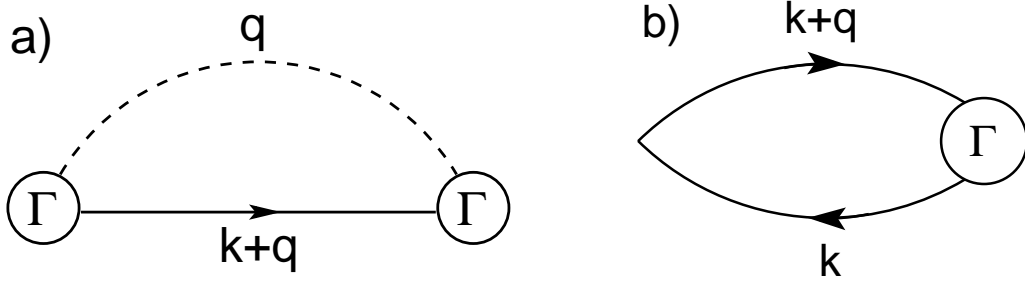


Figure 4.6: Lowest-order (in $g_{\mathbf{q}}^2$) diagrams for a) the electron-phonon contribution to the electron self-energy and b) the phonon self-energy. Full and dashed lines represent dressed electron and phonon Green's functions, respectively, and circles symbolize vertex functions times the electron-phonon coupling $g_{\mathbf{q}}$. For the electron-phonon contribution to the electron self-energy, there are also other diagrams $\propto g_{\mathbf{q}}^2$.

This implies that $\Sigma_{\text{H}}^{\text{ep}}(\mathbf{k}, z)$ has a contribution $-3\bar{g}^2$ to its spectral weight close to $\omega = 0$. The negative value results because the electron-phonon coupling slightly reduces the pole strength of a pole in this energy range which has a large weight ($\approx (U_{\text{H}}/2)^2$) already for $\bar{g} = 0$. The different sum rule results are summarized schematically in Fig. 4.5. We also include the result for non-interacting electrons ($U = 0$) where we consider the lowest order diagram like in Sec. 4.4.2. After averaging over \mathbf{k} , we obtain separate sum rules for photoemission and inverse photoemission parts where the contribution in the energy range for photoemission ($\bar{g}^2/2$) is a factor four smaller than in the Hubbard model with large U_{H} .

We now study the electron-phonon contribution to the electron self-energy in a diagrammatic approach. An important contribution to lowest order in the electron-phonon coupling comes from the diagram in Fig. 4.6a:

$$(i\Sigma_{\text{H}}^{\text{c}}(\mathbf{k}, \omega)) = \sum_{\mathbf{q}} \frac{|g_{\mathbf{q}}|^2}{\hbar^2 N} \frac{1}{2\pi} \int_{-\infty}^{\infty} d\omega' \Gamma(k, q) (iG_{\text{H}}^{\text{c}}(k+q)) (iD^{\text{c}}(q)) \Gamma(k+q, -q). \quad (4.57)$$

On the right hand side, k and q stand for (\mathbf{k}, ω) and (\mathbf{q}, ω') , respectively. G_{H}^{c} and D^{c} are (causal) electron and phonon Green's functions, respectively, dressed by the Coulomb interaction. The vertex function $\Gamma(k, q)$ corresponds to the sum of all irreducible vertex contributions (neglecting vertex corrections due to the electron-phonon interaction). k (q) stands for the incoming electron (phonon) momentum and frequency. We now evaluate Eq. (4.57) neglecting vertex corrections, i.e., replacing $g_{\mathbf{q}}\Gamma(k, q)$ by $g_{\mathbf{q}}$, to investigate their importance. As will be discussed in more detail in the next section, in the limit of large U_{H} the phonon Green's function remains

undressed in the half-filled Hubbard model and we can use the free phonon Green's function from Eq. (4.9). The electron Green's function, however, is assumed to be fully dressed. Expressing it in terms of its spectral function, we arrive at the following result analogous to Eq. (4.45):

$$\Sigma_{\text{H,no vert.}}^{\text{c}}(\mathbf{k}, \omega) = \sum_{\mathbf{q}} \frac{|g_{\mathbf{q}}|^2}{\hbar^2 N} \left\{ \int_{-\infty}^0 d\omega'' \frac{A_{\text{H}}(\mathbf{k} + \mathbf{q}, \omega'')}{\omega - \omega'' + \omega_{\mathbf{q}} - i0^+} + \int_0^{\infty} d\omega'' \frac{A_{\text{H}}(\mathbf{k} + \mathbf{q}, \omega'')}{\omega - \omega'' - \omega_{\mathbf{q}} + i0^+} \right\}. \quad (4.58)$$

It allows us to easily obtain a sum rule over the photoemission energy range:

$$\begin{aligned} -\frac{\hbar^2}{\pi} \int_{-\infty}^{-\hbar^{-1}U_{\text{H}}/4} d\omega \operatorname{Im} \Sigma_{\text{H,no vert.}}^{\text{c}}(\mathbf{k}, \omega + i0^+) &= \frac{1}{N} \sum_{\mathbf{q}} |g_{\mathbf{q}}|^2 \int_{-\infty}^{-\hbar^{-1}U_{\text{H}}/4} d\omega A_{\text{H}}(\mathbf{k} + \mathbf{q}, \omega) \\ &= \frac{1}{2} \bar{g}^2. \end{aligned} \quad (4.59)$$

Here, we used that in the half-filled Hubbard model with large U_{H} integrating the spectral function for a given spin over the lower Hubbard band gives one half. Comparing to Eq. (4.55), we find that the use of Eq. (4.57) and the neglect of vertex corrections underestimates the exact sum rule by a factor of four.

4.7.2 Phonon self-energy and charge response function

We now study the charge response function $\chi(\mathbf{q}, \omega)$ defined in Eq. (4.17) because, according to Eq. (4.18), the phonon self-energy is proportional to it to lowest order in the electron-phonon coupling. In the Hubbard model and for $\mathbf{q} \neq (0, 0)$, it is described entirely by the diagram in Fig. 4.6b:

$$(i\chi_{\text{H}}^{\text{c}}(\mathbf{q}, \omega)) = -2 \sum_{\mathbf{k}} \frac{1}{2\pi} \int_{-\infty}^{\infty} d\omega' (iG_{\text{H}}^{\text{c}}(k + q))(iG_{\text{H}}^{\text{c}}(k))\Gamma(k + q, -q). \quad (4.60)$$

We consider a system doped (with respect to the half-filled system) with a fraction δ holes per site in the limit of large U_{H} . The \mathbf{k} -averaged photoemission spectrum for a given spin integrates to $(1 - \delta)/2$. As before, we assume that this spectrum agrees with that of the t - J model. It extends over an energy range which is equal to or smaller than the width of the lower Hubbard band, $W = \mathcal{O}(t_{\text{H}}) \ll U_{\text{H}}$. The probability in inverse photoemission of adding an electron to an unoccupied site is δ . With a probability of $(1 - \delta)/2$, an electron with given spin can be added to a site already occupied by another electron, but this contributes to the inverse photoemission spectrum at an energy which is about U_{H} higher (assuming that U_{H} is so large that any transfer of

spectral weight between the two contributions can be neglected). When we evaluate Eq. (4.60) neglecting vertex corrections ($\Gamma(k+q, -q) \rightarrow 1$) and integrate the spectral function of the \mathbf{q} -averaged $\chi_{\text{H}}^{\text{c}}(\mathbf{q}, \omega)$ over the energy range $|\hbar\omega| \leq W$ that includes all excitations within the lower Hubbard band but excludes those between upper and lower Hubbard band, one easily finds using the above considerations that

$$\frac{1}{\pi N} \sum_{\mathbf{q}} \int_{-\hbar^{-1}W}^{\hbar^{-1}W} d\omega |\text{Im} \chi_{\text{H, no vert.}}^{\text{c}}(\mathbf{q}, \omega)| = 2\delta(1 - \delta)N. \quad (4.61)$$

Although vertex corrections have been neglected, this agrees with the sum rule in Eq. (4.21) which was derived for the t - J model. It is, however, important to use dressed Green's functions in the calculation of $\chi_{\text{H}}^{\text{c}}(\mathbf{q}, \omega)$. Otherwise, on the right hand side of Eq. (4.61), δ would have been replaced by $(1 + \delta)/2$ leading to a strong disagreement with Eq. (4.21). Using exact diagonalization of finite clusters and, since we assume U_{H} to be large, considering the t - J model, we have found numerically that already for individual phonon wavevectors \mathbf{q} the integrated spectral weight of the charge response function defined in Eq. (4.60) depends only weakly (typically less than 10%) on whether vertex corrections are included or not, as long as fully dressed Green's functions are used.

For the half-filled Hubbard model, there are no contributions to $\text{Im} \chi_{\text{H, no vert.}}^{\text{c}}(\mathbf{q}, \omega)$ for $|\hbar\omega| \ll U_{\text{H}}$. In order to investigate the importance of vertex corrections, we therefore focus on contributions for $|\hbar\omega| \approx U_{\text{H}}$. If $|\text{Im} \chi_{\text{H, no vert.}}^{\text{c}}(\mathbf{q}, \omega)|/(\pi N)$ is integrated over all frequencies, we obtain unity. Alternatively, we can consider the exact result by using Eq. (2.30) which equally applies to the Hubbard model. For $U_{\text{H}} \gg |t_{\text{H}}|$, the ground state of the half-filled system has exactly one electron per site to lowest order in $t_{\text{H}}/U_{\text{H}}$. Therefore, applying the charge density operator $\rho_{\mathbf{q}}$ (with $\mathbf{q} \neq (0, 0)$) to the ground state $|0\rangle$, one obtains zero to this order. It then follows from Eq. (2.30) that the sum rule for $|\text{Im} \chi(\mathbf{q}, \omega)|$ (integrating over all frequencies) is also zero to lowest order in $t_{\text{H}}/U_{\text{H}}$. The result without vertex corrections, unity, is in strong disagreement with this exact result and demonstrates the importance of including vertex corrections in this case.

4.7.3 Example: two-site Hubbard model

To demonstrate our results on the importance of vertex corrections with an explicit example, we consider the half-filled two-site Hubbard model:

$$H_{\text{H}} = -\frac{U_{\text{H}}}{2} \sum_{\sigma} (n_{1\sigma} + n_{2\sigma}) + t_{\text{H}} \sum_{\sigma} \left(c_{1\sigma}^{\dagger} c_{2\sigma} + \text{H.c.} \right) + U_{\text{H}} (n_{1\uparrow} n_{1\downarrow} + n_{2\uparrow} n_{2\downarrow}). \quad (4.62)$$

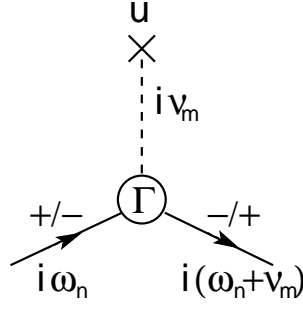


Figure 4.7: Diagrammatic representation of $G_A(i\omega_n, \pm; \nu_m)$ (Eq. (4.64)) within linear response to the external perturbation denoted by the dashed line proportional to the phonon amplitude u . The solid lines represent one-electron Green's functions dressed by the Coulomb interaction. The $q = \pi$ phonon induces transitions between bonding and anti-bonding electronic states.

We add an electron-phonon coupling of the form of Eq. (4.2). We only keep the $q = \pi$ phonon that couples bonding and antibonding states. With $c_{\pm\sigma} = (c_{1\sigma} \pm c_{2\sigma})/\sqrt{2}$ we then have

$$H_{\text{ep}} = g \sum_{\sigma} (c_{+\sigma}^{\dagger} c_{-\sigma} + c_{-\sigma}^{\dagger} c_{+\sigma}) (b + b^{\dagger}). \quad (4.63)$$

The discarded $q = 0$ phonon couples to the total number of electrons and does not lead to excitations of the electronic system (cf. Sec. B.3 for a discussion of its rather trivial effects in the context of the two-site Holstein model).

Following Ref. [113], we calculate the vertex function using a linear-response technique which includes all vertex corrections due to the Coulomb interaction. We employ the Matsubara finite-temperature formalism and replace the electron-phonon interaction in Eq. (4.63) by the external perturbation H'_{ep} , where $b + b^{\dagger}$ has been substituted by the (imaginary) time-dependent phonon amplitude $ue^{-i\nu_m\tau}$. In its presence, one evaluates an anomalous one-electron Green's function defined by

$$G_A(i\omega_n, \pm; i\nu_m) = - \int_0^{\hbar\beta} d\tau e^{i(\omega_n + \nu_m)\tau} \langle T_{\tau} c_{\mp\sigma}(\tau) c_{\pm\sigma}^{\dagger}(0) \rangle_{H+H'_{\text{ep}}}. \quad (4.64)$$

Here, the temperature T enters via $\beta = (k_B T)^{-1}$ and $\omega_n = (2\pi n + 1)/\beta$ and $\nu_m = 2\pi m/\beta$ are fermionic and bosonic Matsubara frequencies, respectively. $\langle \dots \rangle$ denotes an average over the grand canonical ensemble and T_{τ} is a time ordering operator, both defined in a standard way. $G_A(i\omega_n, \pm; \nu_m)$ can be represented by the diagram in Fig. 4.7 from which it follows that the vertex function can be expressed as

$$g \Gamma(i\omega_n, \pm; i\nu_m) = \lim_{u \rightarrow 0} \frac{1}{u} \frac{G_A(i\omega_n, \pm; \nu_m)}{G(i(\omega_n + \nu_m), \mp) G(i\omega_n, \pm)}, \quad (4.65)$$

where $G(i\omega_n, \pm)$ is the one-electron Green's function fully dressed by the Coulomb interaction. As only the linear-response contribution from the perturbation by the phonon field is considered, the vertex function comprises only all contributions due to the Coulomb interaction. After a straightforward calculation which can be found in App. D, we obtain the following result for the vertex function in the limit of large U_H/t_H and zero temperature ($\beta \rightarrow \infty$):

$$\Gamma(\omega, +; \omega') = \Gamma(\omega + \omega', -; -\omega') = \frac{\hbar\omega(\hbar\omega + \hbar\omega') + \hbar\omega't_H + (U_H/2)^2}{(\hbar\omega + t_H)(\hbar\omega + \hbar\omega' - t_H)}, \quad (4.66)$$

where various terms of higher order in t_H/U_H have been neglected and frequencies are real after analytic continuation from the imaginary axis. Here, $\Gamma(\omega, +; \omega')$ is the vertex function for an incoming electron in the bonding orbital (+) with the frequency ω scattered by a $q = \pi$ phonon with frequency ω' into the antibonding orbital (-) with the frequency $\omega + \omega'$.

Using this result for the vertex function, we can calculate the diagram in Fig. 4.6a according to Eq. (4.57). In the limit of large U_H , we find poles with weight $2g^2$ both at $\hbar\omega \approx -U_H/2$ and at $\hbar\omega \approx U_H/2$. Therefore, the sum rule for integrating over the photoemission energy range in Eq. (4.55) and the corresponding one for the inverse photoemission part are exactly fulfilled. Without vertex corrections, these sum rules are underestimated by a factor of four, cf. Eq. (4.59). This can be understood by noting that for electronic energies in the range of the lower and upper Hubbard band, $|\hbar\omega| \approx U_H/2$, it follows from Eq. (4.66) that

$$\Gamma(|\omega| \approx \hbar^{-1}U_H/2, +; \omega_{\text{ph}}) \approx 2 \quad (4.67)$$

when the phonon energy $\hbar\omega_{\text{ph}}$ is assumed to be small compared to U_H . Therefore, including vertex corrections effectively increases the weight of poles around $|\hbar\omega| \approx U_H/2$ by a factor $\Gamma^2 = 4$. In addition, the self-energy calculated using vertex corrections also has poles at $\hbar\omega = t_H - \hbar\omega_{\text{ph}}$ and $\hbar\omega = -t_H$, the latter being a double pole. Except for a different sign, to leading order in U_H they give the same contribution, $\mp g^2(U_H/2)^2/(2t_H - \hbar\omega_{\text{ph}})^2$, to the integral over the spectral function of the self-energy. The sum of the two contributions, however, is not zero, but one finds that it equals $-3g^2$ taking into account also terms which involve lower powers of U_H . Therefore, also the sum rule over all frequencies in Eq. (4.56) is fulfilled.

We also study the charge response function in the two-site Hubbard model with electron-phonon interaction. Because of the small system size, it is uninteresting to study the sum rule in Eq. (4.61) at finite doping. Already after doping one hole with

respect to the half-filled system, the remaining single electron is no longer subjected to the Coulomb interaction. But we consider the effect of vertex corrections in the half-filled two-site model in the limit of large U_H . In agreement with our general conclusions at the end of Sec. 4.7.2, we find that the charge response function has poles at $\hbar\omega \approx \pm U_H$ with weight 1/2, respectively, if the diagram in Fig. 4.6b is calculated neglecting vertex corrections. Only when the vertex function from Eq. (4.66) is used in Eq. (4.60), $\chi_H(\mathbf{q}, \omega)$ vanishes to lowest order in t_H/U_H . This is the correct result as can be easily argued using Eq. (2.30).

4.7.4 Discussion

We find that in strongly correlated systems it is crucial to include vertex corrections in the calculation of the electron-phonon contribution to the electron self-energy in order to fulfill the sum rule over the photoemission energy range. Without vertex corrections, this sum rule is violated by a factor of four. On the other hand, the sum rule for the charge response function, closely related to the phonon self-energy, can be obtained correctly even when vertex corrections are neglected, as long as properly dressed Green's functions are used. This does not rule out, however, that the energy dependence of the phonon self-energy could be substantially influenced by vertex corrections. Interestingly, vertex corrections are again essential in the undoped half-filled system where they result in a strong suppression of the phonon self-energy needed to fulfill a sum rule over the full frequency range. Also the study of vertex corrections shows that in strongly correlated systems the effect of electron-phonon interaction can be very different depending on which property is affected.

4.8 Summary

To summarize, we find that in strongly correlated systems the apparent strength λ of the electron-phonon coupling crucially depends on the property of interest. For the t - J model with phonons and a fraction δ carriers, sum rules for the imaginary parts of the electron and phonon self-energies show a reduction proportional to δ for the phonon but not the electron case. This suggests that the apparent λ deduced from phonon widths and softenings is reduced by such a factor while there is no reduction in the electron self-energy. These conclusions are confirmed by a numerical example. Our results provide support for phonons being essential for kinks seen in photoemission. Similar arguments suggest that the phonon induced interaction

between the carriers is not reduced by a factor of δ which may be of importance for superconductivity. The sum rules can also be used to study the effect of vertex corrections in the context of a diagrammatic approach to the Hubbard model which can be related to the t - J model in the limit of large Coulomb interaction. We find also in this context that it depends on the property studied whether it is crucial to include them in order to obtain correct results in the sense of fulfilling sum rules.

Conclusions

In this thesis, we have studied electron-phonon coupling in strongly correlated materials. While we have focused specifically on the cuprate high-temperature superconductors, we have also identified general effects arising from the interplay between electron-phonon and electron-electron interactions. Emphasis has been put on treating both on an equal footing by explicitly including strong correlations in our calculations and considerations.

In the first chapter, the t - J model with electron-phonon interaction has been derived as an effective low-energy model for the description of electronic and lattice degrees of freedom in the CuO_2 planes common to all cuprates. For an undistorted lattice, the t - J model is obtained from the initial three-band model by projecting out states with high energy within the framework of degenerate perturbation theory. In order to include the effects of lattice vibrations, we have discussed how they modulate the on-site level energies of Cu- d and O- p orbitals as well as the hopping amplitude between them. By suitably generalizing the procedure to the distorted lattice, we have obtained an effective model which contains electron-phonon interaction. The phonons couple to both the effective on-site energies and the effective hoppings in the t - J model. As we can use physical arguments to estimate the modulation of the parameters in the three-band model, we arrive at realistic coefficients for the site-diagonal and the site-off-diagonal coupling in the effective model and do not have to make ad hoc assumptions about which coupling mechanism dominates. The large energy gain of the Zhang-Rice singlets formed by doped holes gives just an uninteresting energy shift in the undistorted lattice, but when it is modulated by phonons it leads to a large coupling constant for the on-site electron-phonon interaction.

On the basis of this effective model, we then discussed in the second chapter how the electron-phonon coupling affects the phonon modes in their properties. We focused on the planar oxygen half-breathing mode which in experiment shows an anomalously strong softening upon doping. Our calculations were performed using exact diagonalization of small clusters leading to unbiased results except for finite-

size effects. We have found that the softening increases upon doping and for phonon wavevectors closer to the zone boundary in agreement with experiment. Also the weaker softening of the breathing mode at not too large dopings is described correctly. We have used Dyson's equation to study the phonon self-energy directly. This allows for a more reliable assessment of the line broadening due to electron-phonon coupling than from the phonon spectral function itself. The calculated widths were found in qualitative agreement with experimental values.

For comparison, we have also considered the Hartree-Fock mean-field approximation of the three-band model which does not explicitly include strong correlations. Despite the softening of the half-breathing mode being similar to the one obtained from exact diagonalization of the t - J model with phonons in a certain small doping range, we have found a much weaker doping dependence which is in disagreement with experimental findings. The same is true for the breathing mode being more strongly softened than the half-breathing mode in the Hartree-Fock approximation as well as for the considerably smaller estimates of the phonon widths. We can therefore conclude that a correct description of these phonon anomalies requires us to take into account strong electronic correlations explicitly. On the one hand, associated many-body effects give rise to a large energy gain of the Zhang-Rice singlets which enters the electron-phonon coupling. On the other hand, they cause a strong suppression of the charge response at low dopings that leads to the pronounced doping dependence. This effect of strong correlations was discussed from a more general point of view also in the last chapter.

Furthermore, we have analyzed the importance of different coupling mechanisms and found that the modulation of the effective on-site energies gives the largest contribution due to the energy gain of the Zhang-Rice singlets being the largest energy scale in the problem. Both t and J are rather small in this respect which results in a much weaker site-off-diagonal coupling via charge and spin degrees of freedom. The electron-phonon interaction predominantly originates from the modulation of the p - d hopping amplitude, but because of interference effects it is important to take into account also the coupling arising from the screened Coulomb interaction. Within our model, there is only strong coupling to the (half-)breathing mode. A rough estimate of non-linear contributions to the electron-phonon coupling showed that in principle they should not be discarded from the start like it is usually the case. Their contribution is not necessarily very small but difficult to incorporate consistently into the model.

In the subsequent third chapter, we turned to the polaronic behavior observed in

photoemission spectra of undoped cuprates. Again, the model derived in the beginning of the thesis served as a starting point for the description of these compounds. But because of much weaker screening, the electron-phonon coupling induced by the modulation of the level energies of Cu-*d* and O-*p* orbitals in the three-band model needed to be reconsidered. Using an established shell model for the description of the phonon modes in undoped La₂CuO₄, we have calculated the modulation of the electrostatic potential at individual sites from which the electron-phonon interaction can be derived. This gives a considerable contribution to the total coupling in addition to that of the (half-)breathing mode arising from the modulation of the *p-d* hopping. In this context, modes involving apical oxygens that move perpendicular to the CuO₂ planes play an important role. The overall coupling was found to be clearly strong enough to induce the formation of self-trapped polarons in the undoped cuprates which supports the interpretation of the experimental observations in terms of electron-phonon interaction. Strong correlations are crucial for lowering the critical coupling strength needed for the crossover into this regime.

We have developed a theoretical description of (inverse) photoemission spectra that is based on an adiabatic approximation. It allowed us to understand why the phonon side band in undoped systems disperses according to predictions made by purely electronic models. We found this to be basically due to the absence of electron-phonon coupling in the initial state. Our adiabatic approximation proved to be also very suitable for use as an efficient calculational method. Lattice degrees of freedom need not be dynamically included, rather a Monte Carlo integration over phonon coordinates is performed which parameterize electronic problems in distorted lattices. Together with the fact that also the temperature dependence is easily implemented, this leads to a powerful method. We employed it to calculate angle-resolved photoemission spectra of undoped La₂CuO₄ using our calculated coupling and taking into account all 21 phonon modes. Strong correlations are included explicitly as the electronic problem is solved by exact diagonalization. The obtained width and binding energy of the phonon side band are in good agreement with experimental results. We have found only a moderate temperature dependence and a systematic increase of the width with increasing binding energy which again can be understood in the framework of our adiabatic approximation.

In the final chapter, we have investigated more generally how the effects of electron-phonon interaction can be modified by the presence of strong electronic correlations. We have derived sum rules for the phonon self-energy and the electron-phonon contribution to the electron self-energy, both for the strongly correlated *t-J* model with

on-site coupling to phonons and for non-interacting electrons in an approximately half-filled band. For the phonon self-energy, a strong suppression due to strong correlations has been found at low doping which is related to the lack of doped charge carriers available to the system for a response to perturbations by lattice distortions. In contrast, the total spectral weight of the part of the electron self-energy which is due to the electron-phonon interaction remains basically unaltered when we change from non-interacting to interacting electrons. Roughly speaking, already a single doped charge carrier can be effectively scattered by phonons. The coupling constants deduced from electronic and phononic properties of strongly correlated systems then differ in a similar way if one relies on the theoretical framework developed for non-interacting electrons. As confirmed by a numerical example, the apparent coupling constants in strongly correlated systems can therefore depend crucially on which property one is actually studying.

We have used these sum rules also to investigate the importance of vertex corrections to the electron-phonon interaction in a diagrammatic study of strongly correlated systems with phonons. We specifically considered the Hubbard model in the limit of large on-site Coulomb interaction for which it becomes closely related to the t - J model. We have found that it is essential to include vertex corrections in the calculation of the electron-phonon contribution to the electron self-energy in order to obtain a correct sum rule over the photoemission energy range. The suppression of the phonon self-energy at low dopings, however, can be obtained correctly also if vertex corrections are neglected although they are again needed to arrive at a proper sum rule in the undoped system when integrating over all frequencies. These results which demonstrate once more peculiarities of the electron-phonon interaction in strongly correlated systems were illustrated using a two-site model for which analytical results can be obtained.

The work presented in this thesis shows that electron-phonon interaction in strongly correlated materials like the cuprates can lead to substantially different effects than expected from the study of non-interacting electrons. If the interplay between different interactions is properly taken into account, a variety of phenomena caused by the electron-phonon coupling in high-temperature superconductors, like the anomalous softening of the half-breathing mode or polaronic features in the photoemission spectra of undoped compounds, can be successfully understood within the model framework developed in this work.

Zusammenfassung

In der vorliegenden Arbeit wird die Wechselwirkung zwischen Elektronen und Phononen in stark korrelierten Systemen untersucht. Es werden im Speziellen die Hochtemperatur-Supraleiter aus der Familie der Kuprate betrachtet. Darüber hinaus gelangen wir zu allgemeineren Schlussfolgerungen über das Zusammenspiel von Elektron-Phonon- und Elektron-Elektron-Wechselwirkungen. Indem starke Korrelationen explizit in unsere Berechnungen und Überlegungen miteinbezogen werden, wird eine gleichberechtigte Behandlung beider Wechselwirkungen sichergestellt.

Im ersten Kapitel wird das t - J -Modell mit Elektron-Phonon-Wechselwirkung hergeleitet, das bei niedrigen Energien ein effektives Modell zur Beschreibung der elektronischen und Gitter-Freiheitsgrade in den allen Kupraten gemeinsamen CuO_2 -Ebenen darstellt. Im Falle eines statischen Gitters, in dem alle Ionen ihre Gleichgewichtspeditionen einnehmen, ergibt sich das t - J -Modell aus dem umfassenderen Dreibandmodell, indem Zustände mit hoher Energie im Rahmen einer Störungstheorie für entartete Zustände herausprojiziert werden. Gitterschwingungen werden durch ihre Modulation der Parameter im Dreibandmodell, d.h. der lokalen Energien von Cu- d - und O- p -Orbitalen und der Hüpfamplitude zwischen diesen, miteinbezogen. Durch Verallgemeinerung der zuvor benutzten Methode auf ein Gitter mit schwingenden Ionen erhalten wir ein effektives Modell, welches Elektron-Phonon-Wechselwirkung beinhaltet. Die Phononen koppeln im t - J -Modell sowohl an die effektiven lokalen Energien als auch an die effektiven Hüpfsterme. Da physikalische Argumente verwendet werden können, um die Modulation der Parameter im Dreibandmodell abzuschätzen, führt dies zu realistischen Koeffizienten für die ortsdigonale und die ortsnebendiagonale Kopplung im effektiven Modell, und es müssen keine Ad-hoc-Annahmen darüber gemacht werden, welcher Kopplungsmechanismus dominiert. Der große Energiegewinn der von dotierten Löchern gebildeten Zhang-Rice-Singletts gibt für ein statisches Gitter nur eine uninteressante Energieverschiebung. Aber bei Modulation durch Phononen kann er eine große Kopplungskonstante für die lokale Elektron-Phonon-Wechselwirkung bewirken.

Auf der Basis dieses effektiven Modells wird im zweiten Kapitel diskutiert, wie die Elektron-Phonon-Kopplung die Schwingungsmoden in ihren Eigenschaften beeinflusst. Wir konzentrieren uns auf die Sauerstoff-Halbatmungsmode, die im Experiment eine anomal starke Erweichung bei Dotierung zeigt. Die Berechnungen werden mittels exakter Diagonalisierung von kleinen Clustern durchgeführt, was zu unvoreingenommenen Ergebnissen führt, wenn man von Effekten absieht, die von der endlichen Größe der Systeme herrühren. Es zeigt sich in Übereinstimmung mit den Experimenten, dass die Erweichung mit der Dotierung und für Phonon-Wellenvektoren, die näher an der Zonengrenze liegen, zunimmt. Auch die schwächere Erweichung der Atmungsmode bei nicht zu starker Dotierung wird korrekt beschrieben. Mittels der Dyson-Gleichung wird die Phonon-Selbstenergie direkt untersucht. Dies erlaubt eine verlässlichere Abschätzung der Linienverbreiterung aufgrund von Elektron-Phonon-Kopplung, als wenn man von der Phonon-Spektralfunktion selbst ausgeht. Die erhaltenen Verbreiterungen stimmen qualitativ mit experimentell gefundenen Werten überein.

Zum Vergleich betrachten wir auch die Hartree-Fock-Molekularfeldnäherung des Dreibandmodells, die starke Korrelationen nicht explizit berücksichtigt. Obwohl die Erweichung der Halbatmungsmode in einem kleinen Dotierungsbereich derjenigen ähnelt, die durch exakte Diagonalisierung des t - J -Modells mit Phononen erhalten wird, zeigt sich eine viel schwächere Dotierungsabhängigkeit, die nicht mit den experimentellen Befunden übereinstimmt. Dasselbe gilt für die Atmungsmode, die in der Hartree-Fock-Näherung stärker als die Halbatmungsmode erweicht wird, sowie die beträchtlich kleineren Schätzwerte für die Linienverbreiterungen. Dies führt zu der Schlussfolgerung, dass eine korrekte Beschreibung dieser Phonon-Anomalien eine ausdrückliche Berücksichtigung der starken elektronischen Korrelationen erfordert. Einerseits führen Vielteilcheneffekte zu einem großen Energiegewinn der Zhang-Rice-Singletts, der in die Elektron-Phonon-Kopplung eingeht. Andererseits verursachen sie bei niedrigen Dotierungen eine starke Unterdrückung der Ladungsdichte-Suszeptibilität, die zu der ausgeprägten Dotierungsabhängigkeit führt. Das letzte Kapitel geht allgemeiner auf diese Auswirkung von starken Korrelationen ein.

Darüber hinaus wird die Bedeutung verschiedener Kopplungsmechanismen analysiert. Es zeigt sich, dass die Modulation der effektiven lokalen Energien den größten Beitrag liefert, da der Energiegewinn der Zhang-Rice-Singletts die größte Energieskala in dem Problem darstellt. Sowohl t als auch J sind in dieser Hinsicht eher klein, was zu einer viel schwächeren ortsnebendiagonalen Kopplung über Ladungs- und Spinfreiheitsgrade führt. Die Elektron-Phonon-Wechselwirkung rührt im We-

sentlichen von der Modulation der p - d -Hüpfamplitude her, aber aufgrund von Interferenzeffekten sollte auch die Kopplung berücksichtigt werden, die durch die abgeschirmte Coulomb-Wechselwirkung entsteht. In unserem Modell koppelt nur die (Halb-)Atmungsmode stark. Eine grobe Abschätzung der nichtlinearen Beiträge zur Elektron-Phonon-Kopplung zeigt, dass diese im Prinzip nicht von vornherein vernachlässigt werden sollten, wie dies üblicherweise geschieht. Ihr Beitrag ist nicht notwendigerweise sehr klein, aber es ist schwierig, ihn konsistent in das Modell aufzunehmen.

Das dritte Kapitel wendet sich dem polaronischen Verhalten zu, das in den Photoemissionsspektren undotierter Kuprate beobachtet wird. Wieder dient das anfangs abgeleitete Modell als Ausgangspunkt für die Beschreibung dieser Systeme. Aber wegen viel schwächerer Abschirmung muss die Elektron-Phonon-Kopplung, die durch die Modulation der lokalen Energien von Cu- d - und O- p -Orbitalen im Dreibandmodell hervorgerufen wird, neu untersucht werden. Mittels eines etablierten Schalenmodells zur Beschreibung der Schwingungsmoden in undotiertem La_2CuO_4 wird die Modulation des elektrostatischen Potentials berechnet. Diese liefert einen beträchtlichen Beitrag zur Elektron-Phonon-Kopplung zusätzlich zur Kopplung der (Halb-)Atmungsmode über die Modulation der p - d -Hüpfamplitude. In diesem Zusammenhang spielen Moden mit sich senkrecht zu den CuO_2 -Ebenen bewegendem apikalen Sauerstoffionen eine wichtige Rolle. Insgesamt zeigt sich, dass die Kopplung eindeutig stark genug ist, um zur Bildung von Polaronen in den undotierten Kupraten zu führen. Dies unterstützt die Interpretation der experimentellen Beobachtungen durch die Elektron-Phonon-Wechselwirkung. Starke Korrelationen sind entscheidend, um die kritische Kopplungsstärke für den Übergang in dieses Regime herabzusetzen.

Wir entwickeln eine theoretische Beschreibung von (inversen) Photoemissionsspektren, die auf einer adiabatischen Näherung basiert. Sie hilft zu verstehen, warum das Phonon-Seitenband in undotierten Systemen eine Dispersion zeigt, die Vorhersagen von rein elektronischen Modellen entspricht. Es zeigt sich, dass dies im Wesentlichen auf das Fehlen von Elektron-Phonon-Wechselwirkung im Anfangszustand zurückzuführen ist. Unsere adiabatische Näherung erweist sich gleichzeitig als geeigneter Ausgangspunkt für eine effiziente Rechenmethode. Gitterfreiheitsgrade müssen nicht dynamisch miteinbezogen werden, vielmehr wird eine Monte-Carlo-Integration über Phonon-Koordinaten durchgeführt, die elektronische Probleme in verzerrten Gittern parametrisieren. Zusammen mit der Tatsache, dass auch die Temperaturabhängigkeit leicht erhalten werden kann, führt dies zu einer leistungsstarken Methode. Sie wird verwendet, um winkelaufgelöste Photoemissionsspektren von undotiertem La_2CuO_4 für die errechnete Kopplung zu berechnen, wobei alle 21 Schwingungsmoden berück-

sichtigt werden. Starke Korrelationen werden explizit berücksichtigt, da das elektronische Problem durch exakte Diagonalisierung gelöst wird. Die erhaltene Breite und Bindungsenergie des Phonon-Seitenbands stimmen gut mit experimentellen Ergebnissen überein. Die Temperaturabhängigkeit ist moderat. Die Breite wächst systematisch mit zunehmender Bindungsenergie, was erneut im Rahmen unserer adiabatischen Näherung verstanden werden kann.

Im letzten Kapitel wird untersucht, wie allgemein Auswirkungen der Elektron-Phonon-Wechselwirkung durch das Vorhandensein starker elektronischer Korrelationen verändert werden können. Wir leiten Summenregeln für die Phonon-Selbstenergie und den Elektron-Phonon-Beitrag zur Elektron-Selbstenergie ab, sowohl für das stark korrelierte t - J -Modell mit lokaler Kopplung an Phononen als auch für nicht wechselwirkende Elektronen in einem ungefähr halbgefüllten Band. Bei der Phonon-Selbstenergie findet sich bei niedriger Dotierung eine starke Unterdrückung, da dem System nur wenige dotierte Ladungsträger zur Verfügung stehen, um auf Störungen durch Gitterverzerrungen zu reagieren. Im Gegensatz dazu bleibt das Gesamtspektalgewicht des von der Elektron-Phonon-Wechselwirkung herrührenden Anteils der Elektron-Selbstenergie praktisch unverändert, wenn wir von nicht wechselwirkenden zu wechselwirkenden Elektronen übergehen. Denn bereits ein einzelner dotierter Ladungsträger kann effektiv durch Phononen gestreut werden. Die Kopplungskonstanten, die von elektronischen und phononischen Eigenschaften stark korrelierter Systeme abgeleitet werden, unterscheiden sich daher in ähnlicher Weise, wenn Theorien benutzt werden, die für nicht wechselwirkende Elektronen entwickelt wurden. Wie durch ein numerisches Beispiel bestätigt wird, können die scheinbaren Kopplungskonstanten in stark korrelierten Systemen deshalb sehr davon abhängen, welche Eigenschaft im Einzelnen betrachtet wird.

Diese Summenregeln werden auch benutzt, um bei einer Untersuchung von stark korrelierten Systemen mit Phononen anhand von Diagrammen die Bedeutung von Vertexkorrekturen zur Elektron-Phonon-Wechselwirkung zu erforschen. Wir betrachten das Hubbard-Modell im Grenzfall großer lokaler Coulomb-Wechselwirkung, für den es in engem Zusammenhang mit dem t - J -Modell steht. Es zeigt sich, dass Vertexkorrekturen bei der Berechnung des Elektron-Phonon-Beitrags zur Elektron-Selbstenergie unverzichtbar sind, um eine korrekte Summenregel im Bereich der Photoemissionsenergien zu erhalten. Die Unterdrückung der Phonon-Selbstenergie bei niedrigen Dotierungen ergibt sich jedoch auch bei Vernachlässigung der Vertexkorrekturen in korrekter Weise. Allerdings werden sie benötigt, um zu einer richtigen Summenregel im undotierten System zu gelangen, wenn über alle Frequenzen integriert wird. Die

Ergebnisse, die erneut Besonderheiten der Elektron-Phonon-Wechselwirkung in stark korrelierten Systemen aufzeigen, werden anhand eines einfachen Modells veranschaulicht, das analytisch behandelt werden kann.

Die in dieser Arbeit vorgestellten Ergebnisse zeigen, dass die Elektron-Phonon-Wechselwirkung in stark korrelierten Systemen wie den Kupraten zu Effekten führen kann, die sich deutlich von denen unterscheiden, die man für nicht wechselwirkende Elektronen erwarten würde. Falls das Zusammenspiel der verschiedenen Wechselwirkungen korrekt berücksichtigt wird, kann eine Vielzahl von Erscheinungen wie die anomale Erweichung der Halbatmungsmode oder die polaronischen Merkmale in den Photoemissionsspektren undotierter Systeme, die durch die Elektron-Phonon-Kopplung in Hochtemperatur-Supraleitern hervorgerufen werden, erfolgreich im Rahmen der hier entwickelten Modelle verstanden werden.

Appendix A

Exact diagonalization

A.1 Calculation of ground state

The exact diagonalization or Lanczos method can be used to calculate the ground state and dynamical properties of a given Hamiltonian. A new basis is constructed iteratively with respect to which the Hamiltonian becomes a tridiagonal matrix.

To obtain the ground state, one starts out with an almost arbitrary state $|v_0\rangle$ in the Hilbert space of the problem. The only requirement is that there is finite overlap of this state with the ground state $|E_0\rangle$. Therefore, the initial state $|v_0\rangle$ is usually chosen randomly. By applying the Hamiltonian on it and subtracting the projection over $|v_0\rangle$, we define a new state

$$|v_1\rangle = H|v_0\rangle - \frac{\langle v_0|H|v_0\rangle}{\langle v_0|v_0\rangle}|v_0\rangle \quad (\text{A.1})$$

which is orthogonal to the initial state. Similarly, we construct another state

$$|v_2\rangle = H|v_1\rangle - \frac{\langle v_1|H|v_1\rangle}{\langle v_1|v_1\rangle}|v_1\rangle - \frac{\langle v_1|v_1\rangle}{\langle v_0|v_0\rangle}|v_0\rangle \quad (\text{A.2})$$

that is orthogonal to both $|v_0\rangle$ and $|v_1\rangle$. Generalizing, a new orthogonal basis is defined recursively by

$$|v_{n+1}\rangle = H|v_n\rangle - a_n|v_1\rangle - b_n^2|v_{n-1}\rangle, \quad (\text{A.3})$$

where

$$a_n = \frac{\langle v_n|H|v_n\rangle}{\langle v_n|v_n\rangle}, \quad b_n^2 = \frac{\langle v_n|v_n\rangle}{\langle v_{n-1}|v_{n-1}\rangle}, \quad (\text{A.4})$$

$n = 0, 1, 2, \dots$, and $b_0 = 0$, $|v_{-1}\rangle = 0$. The Hamiltonian matrix in this basis is tridiagonal, its non-zero elements are given by

$$\langle v_n | H | v_n \rangle = a_n, \quad \langle v_n | H | v_{n-1} \rangle = \langle v_{n-1} | H | v_n \rangle = b_n. \quad (\text{A.5})$$

It is easily diagonalized using standard numerical routines. Because of numerical rounding errors, the set $\{|v_n\rangle\}_{n=0}^N$ becomes linearly dependent already after a relatively small number N of iterations. But the method still gives accurate results for the ground state and its eigenenergy.

A.2 Calculation of spectral functions

The Lanczos method can also be used to calculate dynamical properties of a Hamiltonian, specifically the spectral functions at zero temperature of correlation functions of the form

$$I_{\hat{O}}(\omega) = -\frac{1}{\pi} \text{Im} \langle E_0 | \hat{O}^\dagger \frac{1}{\omega - \hbar^{-1}(H - E_0) + i0^+} \hat{O} | E_0 \rangle. \quad (\text{A.6})$$

It can be shown [83] that by choosing

$$|v_0\rangle = \frac{\hat{O} | E_0 \rangle}{\sqrt{\langle E_0 | \hat{O}^\dagger \hat{O} | E_0 \rangle}} \quad (\text{A.7})$$

instead of a random state as the starting state in the iterative construction of the basis $\{|v_n\rangle\}$ defined in Eq. (A.3) that leads to a tridiagonal Hamiltonian matrix, one obtains the spectral function of Eq. (A.6) in the following form after diagonalizing the tridiagonal Hamiltonian matrix:

$$I_{\hat{O}}(\omega) = \langle E_0 | \hat{O}^\dagger \hat{O} | E_0 \rangle \sum_n |c_{0n}|^2 \delta(\omega - \hbar^{-1}(E_n - E_0)). \quad (\text{A.8})$$

It consists of a sum of δ -functions whose position is determined by the eigenvalues E_n and whose weight is proportional to the squared modulus of the first component of the corresponding eigenvector, $|c_{0n}|^2$.

For example, the one-electron Green's function $G(z) = \langle\langle c ; c^\dagger \rangle\rangle_z$ has the spectral function

$$A(\omega) = S_{cc^\dagger}(\omega) = I_c(\omega) + I_c(-\omega). \quad (\text{A.9})$$

Here, c^\dagger creates an electron (with certain quantum numbers not shown here) and we use the notation of App. C.

A.3 Calculation of self-energies

As described in the previous section, the spectral function of an one-electron Green's function can be obtained using exact diagonalization as a sum of weighted δ -functions,

$$A(\omega) = \sum_n p_n \delta(\omega - \omega_n). \quad (\text{A.10})$$

Both p_n and ω_n are real and $p_n > 0$. The corresponding Green's function

$$G(z) = \sum_n \frac{p_n}{z - \omega_n} \quad (\text{A.11})$$

is a rational function with simple poles at ω_n . One easily sees that $G(z)$ has simple zeros at $\tilde{\omega}_m$, each located between a pair of neighboring poles, and $dG(z)/dz|_{\tilde{\omega}_m} < 0$. $G(z)$ can also be written in terms of the self-energy $\Sigma(z)$,

$$G(z) = \frac{a}{z - \hbar^{-1}\varepsilon - \Sigma(z)}, \quad (\text{A.12})$$

where $a = \sum_n p_n$ and $\varepsilon = \hbar \sum_n p_n \omega_n / a$ if we assume that $\Sigma(z) = b/z + \mathcal{O}(z^{-2})$. Therefore,

$$\Sigma(z) = z - \hbar^{-1}\varepsilon - \frac{a}{G(z)}, \quad (\text{A.13})$$

and it follows that $\Sigma(z)$ has simple poles at the zeros of $G(z)$ allowing for an expansion into partial fractions,

$$\Sigma(z) = \sum_m \frac{R_m}{z - \tilde{\omega}_m}. \quad (\text{A.14})$$

The weights are given by the residues at the poles of $\Sigma(z)$,

$$\begin{aligned} R_m &= \lim_{z \rightarrow \tilde{\omega}_m} (z - \tilde{\omega}_m) \Sigma(z) = \lim_{z \rightarrow \tilde{\omega}_m} \frac{-a}{(G(z) - G(\tilde{\omega}_m))/(z - \tilde{\omega}_m)} \\ &= -a \left[\frac{dG(z)}{dz} \Big|_{\tilde{\omega}_m} \right]^{-1}. \end{aligned} \quad (\text{A.15})$$

This leads to the final result

$$\Sigma(z) = - \sum_m \left[\frac{dG(z)}{dz} \Big|_{\tilde{\omega}_m} \right]^{-1} \frac{a}{z - \tilde{\omega}_m}. \quad (\text{A.16})$$

In case of a phonon Green's function we have

$$\begin{aligned} D(z) &= \sum_n p_n \left(\frac{1}{z - \omega_n} - \frac{1}{z + \omega_n} \right) \\ &= \frac{2\Omega}{z^2 - \Omega^2 - 2\Omega\Pi(z)}, \end{aligned} \quad (\text{A.17})$$

where both p_n and ω_n are real and larger than zero. $\Omega = \sum_n p_n \omega_n$ is the bare phonon frequency if the phonon self-energy $\Pi(z) = c/z + \mathcal{O}(z^{-2})$. Analogously to Eq. (A.13), one has

$$\Pi(z) = \frac{z^2 - \Omega^2}{2\Omega} - \frac{1}{D(z)}. \quad (\text{A.18})$$

So,

$$\Pi(z) = - \sum_m \left[\left. \frac{dD(z)}{dz} \right|_{\tilde{\omega}_m} \right]^{-1} \left(\frac{1}{z - \tilde{\omega}_m} - \frac{1}{z + \tilde{\omega}_m} \right), \quad (\text{A.19})$$

where the real frequencies $\tilde{\omega}_m > 0$ correspond to the zeros of $D(z)$ on the positive real axis.

Appendix B

Adiabatic approximation revisited

In this appendix, we discuss in more detail the adiabatic approximation for (inverse) photoemission spectra introduced in Chap. 3. We first present a slightly more refined version. Then, we consider several basic examples that illustrate the virtues and limitations of the method. Finally, we compare with a different approach for calculating spectra which is based on a diagrammatic Monte Carlo method.

B.1 Improved version

An improvement over the approximation made in Sec. 3.3 can be achieved by also including the kinetic energy of the phonons in the Hamiltonian appearing in the resolvent in Eq. (3.19). Then, $\psi|E_0^{N_e}(\mathbf{Q})\rangle$ must be expanded with respect to both electronic and phononic basis functions in the adiabatic approximation. From this, one obtains the following expression for the spectral function:

$$A_{\mathbf{k}\sigma}^{N_e, \mp}(\omega) = \sum_{m,n} \delta(\omega - \hbar^{-1}(\varepsilon_{mn}^{N_e \mp 1} - \varepsilon_{00}^{N_e})) \times \quad (\text{B.1})$$
$$\times \left| \int d\mathbf{Q} \langle E_m^{N_e \mp 1}(\mathbf{Q}) | \psi | E_0^{N_e}(\mathbf{Q}) \rangle \phi_{mn}^{N_e \mp 1}(\mathbf{Q}) \phi_{00}^{N_e}(\mathbf{Q}) \right|^2.$$

This version requires the solution of Eq. (3.16) to obtain the phonon eigenfunctions and eigenenergies. Compared to the result from Eqs. (3.23) and (3.24), it is therefore much less suited for the development of an efficient calculational method. Nevertheless, as Eq. (B.1) leads to spectra with individual phonon satellites that are bound from the low-energy side, it can be used to judge from a basic example like in Sec. B.3 the quality of the simpler version which gives only an unbound envelope function. It also allows for a better discussion of the underlying physical mechanisms.

We start the analysis of Eq. (B.1) by noting that each eigenstate of H in the $(N_e \mp 1)$ -electron sector represents a possible final state. It contributes to the spectrum at its eigenenergy (shifted by the ground-state energy of the system with N_e electrons). The intensity is proportional to the squared overlap of the final and the initial state (the ground state of the system with N_e electrons plus an additional hole or electron). Two conditions must be fulfilled for this overlap to be large.¹

- As the initial phonon wavefunction $\phi_{00}^{N_e}(\mathbf{Q})$ is localized around the minimum \mathbf{Q}_{\min} of $V_0^{N_e}(\mathbf{Q})$ and has no nodes, the final phonon wavefunction $\phi_{mn}^{N_e \mp 1}(\mathbf{Q})$ must have a large and slowly varying amplitude in this region, too. This is the case for final states with energies $\varepsilon_{mn}^{N_e \mp 1} \approx V_m^{N_e \mp 1}(\mathbf{Q}_{\min})$. For smaller energies, the region around \mathbf{Q}_{\min} is classically forbidden and the amplitude of the final phonon wavefunction becomes exponentially suppressed whereas for larger energies the kinetic energy increases and the wavefunction oscillates faster. In both cases, the integrated overlap of initial and final phonon wavefunction becomes smaller again.
- The electronic matrix element $\langle E_m^{N_e \mp 1}(\mathbf{Q}) | \psi | E_0^{N_e}(\mathbf{Q}) \rangle$ must be large around \mathbf{Q}_{\min} . It is sufficient to consider its value only in this region as the initial phonon wavefunction is small elsewhere.

Because the electrons have a much smaller mass than the nuclei, the electronic states vary much more slowly as a function of \mathbf{Q} than the phonon wavefunctions. Using the mean value theorem, we can therefore approximate Eq. (B.1) by

$$A_{\mathbf{k}\sigma}^{N_e, \mp}(\omega) \approx \sum_{m,n} \delta(\omega - \hbar^{-1}(\varepsilon_{mn}^{N_e \mp 1} - \varepsilon_{00}^{N_e})) \times \quad (\text{B.2})$$

$$\times \left| \langle E_m^{N_e \mp 1}(\mathbf{Q}_{\min}) | \psi | E_0^{N_e}(\mathbf{Q}_{\min}) \rangle \right|^2 \times \left| \int d\mathbf{Q} \phi_{mn}^{N_e \mp 1}(\mathbf{Q}) \phi_{00}^{N_e}(\mathbf{Q}) \right|^2.$$

The last factor in Eq. (B.2) also appears in the discussion of the Franck-Condon principle in molecular physics (cf. Ref. [115]) for radiative transitions from vibrational levels of one electronic state to vibrational levels of another electronic state. It states that the intensity of a transition depends not only on the electronic matrix element at the equilibrium position of the nuclei in the initial state but also on the overlap integral of the vibrational wavefunctions.

¹In the following discussion, we assume a non-degenerate minimum of $V_0^{N_e}(\mathbf{Q})$ for simplicity. The arguments can be easily generalized to the case of (quasi-)degenerate minima.

Altogether, this leads to the following picture: For a system without electron-phonon interaction but with a given lattice distortion \mathbf{Q}_{\min} , the spectrum consists of δ -functions at the energies $E_m^{N_e \mp 1}(\mathbf{Q}_{\min})$. If the electron-phonon interaction is switched on, spectral features with large intensities appear at similar energies and with similar relative weight but they are broadened by phonon sidebands. The dispersion and weight of the true quasi-particle, however, can be strongly altered by the electron-phonon interaction. In general, the effective phonon potential $V_0^{N_e \mp 1}(\mathbf{Q})$ corresponding to the electronic ground state in the system with $N_e \mp 1$ electrons has minima at $\mathbf{Q} \neq \mathbf{Q}_{\min}$. The ground-state phonon wavefunction $\phi_{00}^{N_e \mp 1}(\mathbf{Q})$ is localized around these minima. Consequently, there is only little overlap with the phonon wavefunction in the initial state which peaks around \mathbf{Q}_{\min} , and in the spectrum the peak lowest in binding energy has only very small weight.

B.2 Core hole problem

The model of a single electronic level (*core* level) coupled to a phonon mode serves as our most elementary example. Choosing the level energy as energy zero and neglecting the phonon zero-point energy, it is described by the Hamiltonian

$$H = \hbar\omega_{\text{ph}}b^\dagger b + g(1 - n)(b + b^\dagger). \quad (\text{B.3})$$

The phonons of energy $\hbar\omega_{\text{ph}}$ are created by b^\dagger and couple to the core hole with the coupling strength g . If the level, whose occupancy is measured by $n = c^\dagger c$, is filled with an electron, there is no electron-phonon interaction. We choose this state, $|\Phi\rangle = c^\dagger|0\rangle$, as the initial state for photoemission. The possible final states are described by

$$H_{\text{final}} = \hbar\omega_{\text{ph}}b^\dagger b + g(b + b^\dagger). \quad (\text{B.4})$$

Equation B.4 can be diagonalized by the unitary Lang-Firsov transformation [116] which in our case corresponds to introducing shifted phonon operators

$$\tilde{b} = b + \frac{g}{\hbar\omega_{\text{ph}}}. \quad (\text{B.5})$$

The transformed Hamiltonian for the final states

$$\tilde{H}_{\text{final}} = \hbar\omega_{\text{ph}}\tilde{b}^\dagger\tilde{b} - \frac{g^2}{\hbar\omega_{\text{ph}}} \quad (\text{B.6})$$

has the eigenstates

$$|\tilde{m}\rangle = \frac{1}{\sqrt{m!}}(\tilde{b}^\dagger)^m|\tilde{0}\rangle \quad (\text{B.7})$$

with eigenenergies

$$E_m = m\hbar\omega_{\text{ph}} - \frac{g^2}{\hbar\omega_{\text{ph}}}. \quad (\text{B.8})$$

One therefore obtains the following photoemission spectrum:

$$A^-(\omega) = \sum_{m=0}^{\infty} |\langle \tilde{m} | c | \Phi \rangle|^2 \delta(\omega - m\omega_{\text{ph}} + g^2/(\hbar^2\omega_{\text{ph}})). \quad (\text{B.9})$$

Using

$$\langle \tilde{m} | c | \Phi \rangle = \frac{1}{\sqrt{m!}} \langle \tilde{0} | (b + g/(\hbar\omega_{\text{ph}}))^m | 0 \rangle = \frac{1}{\sqrt{m!}} \left(\frac{g}{\hbar\omega_{\text{ph}}} \right)^m \langle \tilde{0} | 0 \rangle, \quad (\text{B.10})$$

we find

$$\begin{aligned} A^-(\omega) &= |\langle \tilde{0} | 0 \rangle|^2 \sum_{m=0}^{\infty} \frac{1}{m!} \left(\frac{g}{\hbar\omega_{\text{ph}}} \right)^{2m} \delta(\omega - m\omega_{\text{ph}} + g^2/(\hbar^2\omega_{\text{ph}})) \\ &= e^{-(g/(\hbar\omega_{\text{ph}}))^2} \sum_{m=0}^{\infty} \frac{1}{m!} \left(\frac{g}{\hbar\omega_{\text{ph}}} \right)^{2m} \delta(\omega - m\omega_{\text{ph}} + g^2/(\hbar^2\omega_{\text{ph}})). \end{aligned} \quad (\text{B.11})$$

The last line follows from the normalization of $A^-(\omega)$. The spectrum consists of a quasi-particle peak at $\omega = -g^2/(\hbar^2\omega_{\text{ph}})$ with phonon side peaks and weights given by a Poisson distribution which in the limit of large $(g/(\hbar\omega_{\text{ph}}))^2$ becomes Gaussian with a width proportional to g :

$$A^-(\omega) \rightarrow \frac{\hbar}{g\sqrt{2\pi}} e^{-\hbar^2\omega^2/(2g^2)} \quad \text{for } (g/(\hbar\omega_{\text{ph}}))^2 \rightarrow \infty. \quad (\text{B.12})$$

Furthermore, one easily finds that the first moment of $A^-(\omega)$ is always zero.

We now compare the exact result to the adiabatic approximation introduced in Eqs. (3.20)-(3.24) where we neglect the kinetic energy of the phonons in the Hamiltonian appearing in the denominator of the photoemission Green's function:

$$H \approx -\frac{\omega_{\text{ph}}}{2} + \frac{1}{2}\omega_{\text{ph}}^2 Q^2 + g\sqrt{\frac{2\omega_{\text{ph}}}{\hbar}} Q(1-n) \equiv \mathcal{H}(Q). \quad (\text{B.13})$$

The energy of the initial state that serves as reference energy in this denominator is replaced by the effective potential for the initial state which equals the free phonon potential $\omega_{\text{ph}}^2 Q^2/2$. We arrive at the following approximation for the spectral function:

$$\tilde{A}^-(\omega) = \sqrt{\frac{\omega_{\text{ph}}}{\hbar\pi}} \int dQ e^{-\omega_{\text{ph}} Q^2/\hbar} \delta(\omega - \hbar^{-3/2} g \sqrt{2\omega_{\text{ph}}} Q) = \frac{\hbar}{g\sqrt{2\pi}} e^{-\hbar^2\omega^2/(2g^2)}. \quad (\text{B.14})$$

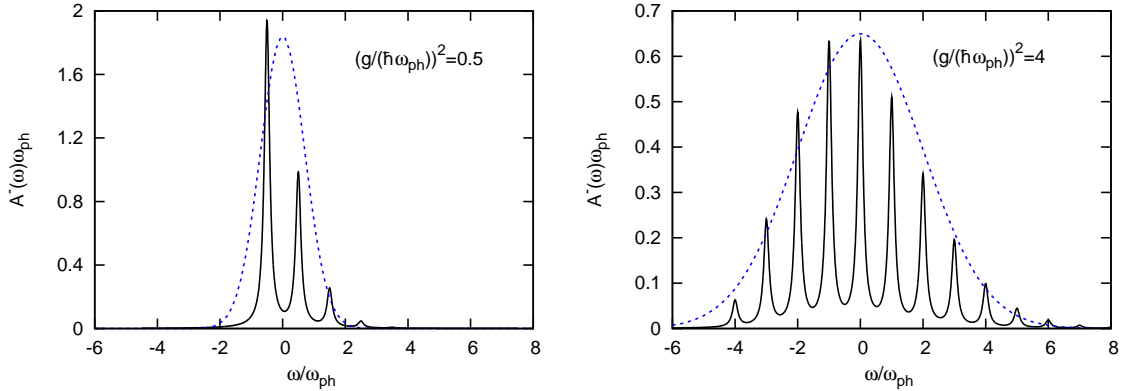


Figure B.1: Photoemission spectra $A^-(\omega)$ for removing the electron of an isolated level coupled to phonons for small (left panel) and large coupling (right panel). The solid lines give the exact result (including a Lorentzian broadening with $\text{FWHM} = 0.1\hbar\omega_{\text{ph}}$) and the dashed lines show the (rescaled) adiabatic approximation.

This is the Gaussian envelope function which the exact result converges to in the strong coupling limit, see Eq. (B.12). Like the exact spectrum, it has a vanishing first spectral moment.

In Fig. B.1, we compare the exact result, Eq. (B.11), with the adiabatic approximation from Eq. (B.14) for two different coupling strengths. For weak electron-phonon coupling like in the left panel with $(g/(\hbar\omega_{\text{ph}}))^2 = 0.05$, one obtains a leading low-energy (quasi-particle) peak with a few phonon satellites in the exact spectrum. In case of strong coupling, the weight of the quasi-particle peak becomes very small and the spectrum is dominated by the satellites (cf. right panel of Fig. B.1 where $(g/(\hbar\omega_{\text{ph}}))^2 = 4$). The spectra calculated within the adiabatic approximation correspond to approximate envelope functions and do not resolve the fine structure of the individual phonon satellites. In contrast to the exact spectra, there is no lower bound to the spectral weight in our approximation. Therefore, spectral weight can be found also below the exact quasi-particle energy. The discrepancies becomes less important for larger couplings when the quasi-particle weight diminishes and the approximate spectrum converges to the exact envelope function as expected from Eq. (B.12).

B.3 Holstein model

As a second example, we consider the two-site Holstein model [117] for which the electronic part of the Hamiltonian just contains hopping between the two sites with

amplitude t :

$$H_{\text{el}} = -t \sum_{\sigma} (c_{1\sigma}^{\dagger} c_{2\sigma} + c_{2\sigma}^{\dagger} c_{1\sigma}), \quad (\text{B.15})$$

where $c_{i\sigma}^{\dagger}$ creates an electron with spin σ on site i . The electrons are coupled to local phonons with frequency ω_{ph} as described by

$$H_{\text{ep}} = g \sum_{i\sigma} \sqrt{\frac{2\omega_{\text{ph}}}{\hbar}} Q_i c_{i\sigma}^{\dagger} c_{i\sigma} \quad (\text{B.16})$$

with the generalized phonon coordinates Q_i and the coupling constant g . Switching to symmetric (+) and antisymmetric (-) combinations of the electron and phonon operators,

$$c_{\pm\sigma} = \frac{1}{\sqrt{2}}(c_{1\sigma} \pm c_{2\sigma}), \quad (\text{B.17})$$

$$Q_{\pm} = \frac{1}{\sqrt{2}}(Q_1 \pm Q_2), \quad (\text{B.18})$$

we have

$$H_{\text{el}} = \sum_{\sigma} (-t c_{+\sigma}^{\dagger} c_{+\sigma} + t c_{-\sigma}^{\dagger} c_{-\sigma}) \quad (\text{B.19})$$

and

$$H_{\text{ep}} = g \sqrt{\frac{\omega_{\text{ph}}}{\hbar}} \sum_{\sigma} [Q_+ (c_{+\sigma}^{\dagger} c_{+\sigma} + c_{-\sigma}^{\dagger} c_{-\sigma}) + Q_- (c_{+\sigma}^{\dagger} c_{-\sigma} + c_{-\sigma}^{\dagger} c_{+\sigma})]. \quad (\text{B.20})$$

The symmetric phonon mode couples to the total number of electrons, N_e . We can therefore write $H = H_1 + H_2$, where

$$H_1 = N_e \frac{g}{2} \sqrt{\frac{2\omega_{\text{ph}}}{\hbar}} Q_+ + \frac{1}{2} (\Pi_+^2 + \omega_{\text{ph}}^2 Q_+^2) \quad (\text{B.21})$$

can be solved exactly analogously to the core hole problem in the previous section. The spectral function $A_{k\sigma}^{N_e, \mp(2)}(\omega)$ (here $k \in \{+, -\}$) that one obtains for H_2 needs to be convoluted simply by the known result for H_1 ,

$$A^{N_e, \mp(1)}(\omega) = e^{-\alpha} \sum_{l=0}^{\infty} \frac{\alpha^l}{l!} \delta(\omega + (1 \mp 2N_e)\alpha\omega_{\text{ph}} - l\omega_{\text{ph}}), \quad (\text{B.22})$$

where $\alpha = (g/(\hbar\omega_{\text{ph}}))^2/2$, in order to get $A_{k\sigma}^{N_e, \mp}(\omega)$ as defined in Eq. (B.1). We will therefore restrict our discussion to $A_{k\sigma}^{N_e, \mp(2)}(\omega)$ in the following. We calculate the inverse photoemission spectrum for creating an electron in both the empty (undoped)

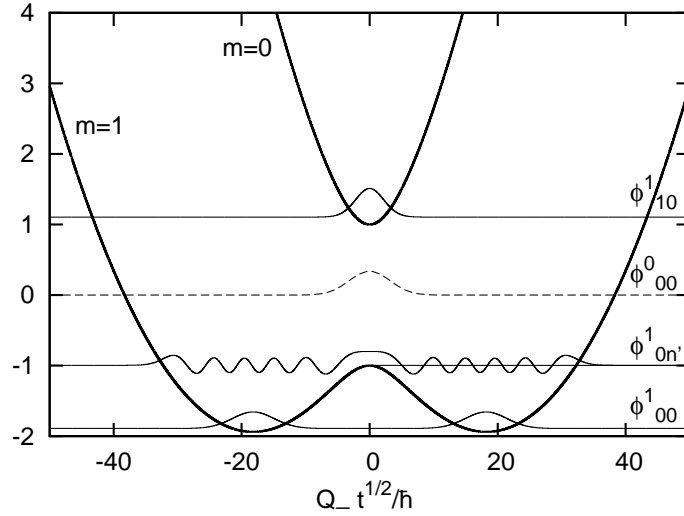


Figure B.2: Effective potentials $V_m^1(Q_-)/t$ in the two-site Holstein model with one electron as functions of the phonon coordinate $Q_- \sqrt{t}/\hbar$ for $\hbar\omega_{\text{ph}}/t = 0.1$, $g/t = 0.6$. Some selected phonon wavefunctions (no scale shown for amplitude, offset by eigenenergies) are also shown, see text.

system and the system that already contains an electron of opposite spin. There is then only one phonon coordinate Q_- in H_2 which we treat as a parameter in solving the part of H_2 originating from $H_{\text{el}} + H_{\text{ep}}$. In the one-electron sector, one obtains the two eigenenergies

$$E_{0/1}^{N_e=1} = \mp \sqrt{t^2 + \hbar^{-1}\omega_{\text{ph}}g^2Q_-^2} \quad (\text{B.23})$$

whereas there are four eigenenergies in case of two electrons with opposite spin:

$$E_{0/3}^{N_e=2} = \mp 2\sqrt{t^2 + \hbar^{-1}\omega_{\text{ph}}g^2Q_-^2}, \quad E_{1/2}^{N_e=2} = 0. \quad (\text{B.24})$$

For numerical calculations, we choose $\hbar\omega_{\text{ph}}/t = 0.1$ and $g/t = 0.6$. As $\hbar\omega_{\text{ph}}/t$ is small, our adiabatic approximation is justified. The effective potentials one obtains by adding the harmonic potential $\omega_{\text{ph}}^2 Q_-^2/2$ to the eigenenergies in Eq. (B.23) are shown in Fig. B.2.

We first consider the approximation when the kinetic energy of the phonons is neglected in the resolvent of the Hamiltonian and for which the spectral function is given by Eq. (3.23). The neglected terms are proportional to ω_{ph} so we cannot expect to resolve fine structure in the spectra on that order. But the approximation still describes the overall broadening correctly on a larger scale proportional to $\sqrt{\omega_{\text{ph}}}$ [98]. The phonon wavefunction in the initial state is known exactly for the undoped system,

see Eq. (3.18). Here

$$\phi_{00}^{N_e^0=0}(Q_-) = \left(\frac{\omega_{\text{ph}}}{\hbar\pi}\right)^{1/4} \exp\left(\frac{-\omega_{\text{ph}}Q_-^2}{2\hbar}\right). \quad (\text{B.25})$$

In the system with one electron, the lowest effective potential $V_0^{N_e=1}(Q_-)$ has two minima at $\bar{Q}_{a/b}$ around which we can treat it as a harmonic potential with the renormalized phonon frequency $\bar{\omega} = \sqrt{(\partial^2 V_0^{N_e=1}/\partial Q_-^2)|_{\bar{Q}_{a/b}}}$. This leads to the approximation

$$\phi_{00}^{N_e=1}(Q_-) \approx \frac{1}{\sqrt{2}} \sum_{l=a,b} \left(\frac{\bar{\omega}}{\hbar\pi}\right)^{1/4} \exp\left(-\frac{\bar{\omega}(Q_- - \bar{Q}_l)^2}{2\hbar}\right). \quad (\text{B.26})$$

Following Ref. [98], we can expand the argument of the δ -functions in Eq. (3.23) up to first order in Q_- around $\bar{Q}_{a/b}$. If we further assume that the electronic matrix elements vary only weakly around $\bar{Q}_{a/b}$, the integration over Q_- in Eq. (3.23) can be eliminated and we obtain the following result:

$$\tilde{A}_{k\sigma}^{N_e=1,+}(2)(\omega) \approx \sum_m |\langle E_m^2 | c_{k\sigma}^\dagger | E_0^1 \rangle|^2 \Big|_{\bar{Q}_{a/b}} \sqrt{\frac{\hbar\bar{\omega}}{\pi b_m^2}} e^{-\frac{\bar{\omega}}{\hbar b_m^2}(\hbar\omega - a_m)^2}, \quad (\text{B.27})$$

where $a_m = V_m^2|_{\bar{Q}_{a/b}} - V_0^1|_{\bar{Q}_{a/b}}$ and $b_m = (\partial V_m^2/\partial Q_-)|_{\bar{Q}_{a/b}}$. This approximation is shown in Fig. B.3 for $k = 0$ together with the spectrum obtained from exact diagonalization. The agreement with the Gaussian line shape predicted by Eq. (B.27) is very good. Only to resolve the fine structure on a scale given by the phonon frequency ω_{ph} , one has to go beyond the present approximation. As indicated schematically by the arrows in Fig. B.4, the spectrum can indeed be understood as the spectrum of electrons in a system without electron-phonon interaction but a given distortion $\bar{Q}_{a/b}$. The broadening is due to the finite width of the phonon wavefunction in the initial state. There is no structure in the spectrum arising from the highest effective potential as the corresponding electronic matrix element is negligibly small.

In the case of inverse photoemission from the empty system, the phonon wavefunction in the initial state is localized around $Q_- = 0$. The slope of both effective potentials $V_{m=0,1}^{N_e=1}(Q_-)$ vanishes at this point. An approximation analogous to Eq. (B.27) would therefore result in $\tilde{A}_{k\sigma}^{N_e^0=0,+}(2)(\omega) = \rho_{k\sigma}^{N_e^0=0,+}(\omega, Q_- = 0)$, i.e., the unbroadened spectrum of the undistorted system without electron-phonon interaction. If we evaluate Eq. (3.23) without any further approximation, we obtain the spectra shown in Fig. B.5. The comparison with results from exact diagonalization shows that this approximation cannot reproduce the fine structure and for $k = +$ does not

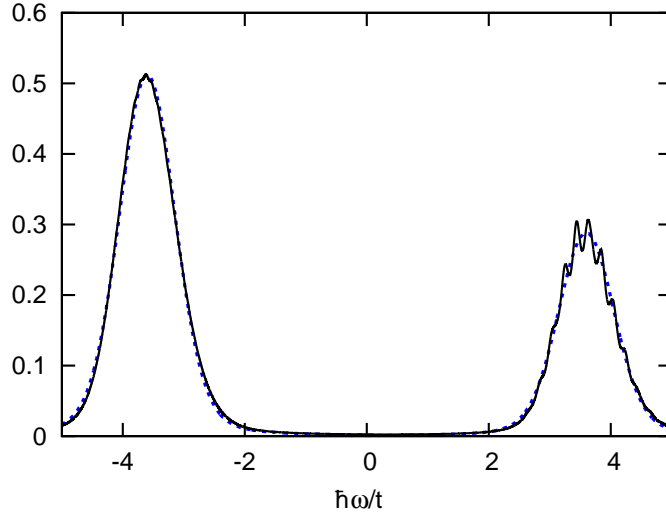


Figure B.3: Spectrum for adding an electron to a two-site Holstein model with one electron of opposite spin ($\hbar\omega_{\text{ph}}/t = 0.1$, $g/t = 0.6$). The approximation $\tilde{A}_{(k=0)\sigma}^{N_e=1,+^{(2)}}(\omega)t/\hbar$ (Eq. (B.27)) is shown as dashed line together with the spectrum obtained from exact diagonalization (full line). Both spectra have been convoluted with a Lorentzian (FWHM=0.1 t).

give spectral weight above $\hbar\omega/t = -1$ (except from broadening), but it still gives the right order of magnitude for the broadening of the peaks.

In order to understand also details of the spectra, we have to use the improved version of our adiabatic approximation from Eq. (B.1). One has to solve Eq. (3.16) for each effective potential to obtain the phonon eigenfunctions needed in Eq. (B.1). The resulting inverse photoemission spectra for creating an electron with momentum $k = +$ or $k = -$ in the empty system are shown in Fig. B.6. They are practically indistinguishable from those we obtained using exact diagonalization. This shows that the adiabatic approximation works very well for the chosen parameters. For the electronic matrix element in Eq. (B.1), one needs the Q_- -dependent electronic eigenstates corresponding to the eigenenergies in Eq. (B.23):

$$|E_{0/1}^{N_e=1}\rangle = \mathcal{N}_{0/1} \left(\left(t \pm \sqrt{t^2 + \hbar^{-1}\omega_{\text{ph}}g^2Q_{\pi}^2} \right) |+\rangle - \sqrt{\hbar^{-1}\omega_{\text{ph}}gQ_{\pi}} |-\rangle \right) \quad (\text{B.28})$$

with

$$\mathcal{N}_m = \frac{(\text{sign}(Q_{\pi}))^m}{\sqrt{(t + (-1)^m \sqrt{t^2 + \hbar^{-1}\omega_{\text{ph}}g^2Q_{\pi}^2})^2 + \hbar^{-1}\omega_{\text{ph}}g^2Q_{\pi}^2}}, \quad (\text{B.29})$$

where $|+\rangle$ and $|-\rangle$ denote the $k = +$ and $k = -$ one-electron states and $m = 0, 1$.

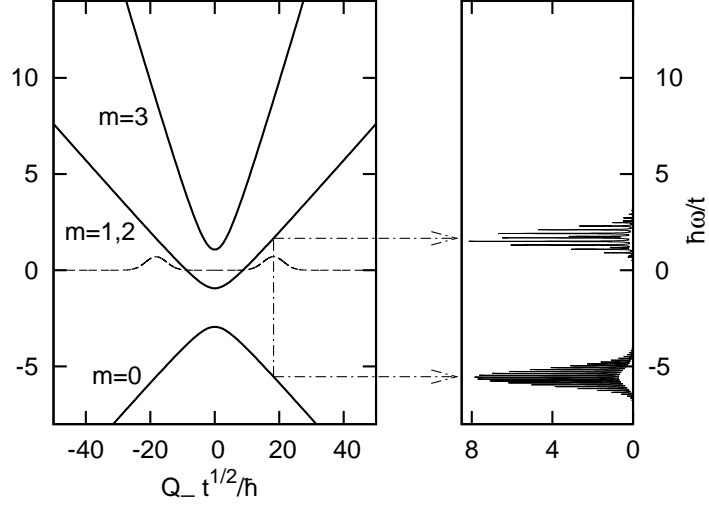


Figure B.4: Left panel: Effective potentials $(V_m^2(Q_-) - V_0^1(Q_-) + V_0^1(Q_-)|_{\bar{Q}_{a/b}})/t$ for the two-site Holstein model with two electrons with opposite spin as functions of the phonon coordinate $Q_- \sqrt{t}/\hbar$ for $\hbar\omega_{\text{ph}}/t = 0.1$, $g/t = 0.6$ and phonon wavefunction $\phi_{00}^{N_e=1}$ (dashed line, no scale shown for amplitude). Right panel: $A_{(k=0)\sigma}^{N_e=1,+ (2)}(\omega)t/\hbar$ rotated by 90° .

Let us consider e.g. the case where we create an electron with momentum $k = +$ in the empty system. The initial electronic state is then $|+\rangle$. The initial state's phonon wavefunction $\phi_{00}^{N_e^0=0}$ (dashed line in Fig. B.2) is a bell-shaped Gaussian centered around $Q_- = 0$. This effectively limits the integration over Q_- in Eq. (B.1) to a small region around the origin. Here, $|E_0^{N_e=1}\rangle \approx |+\rangle$ and $|E_1^{N_e=1}\rangle \approx |-\rangle$. Therefore, the relevant electronic matrix element in this example is $\langle E_0^{N_e=1}|+\rangle$. It has even parity with respect to Q_- . So, according to Eq. (B.1), final states with the electronic configuration $|E_0^{N_e=1}\rangle$ and a corresponding even-parity phonon wavefunction $\phi_{0n}^{N_e=1}$ that strongly overlaps with $\phi_{00}^{N_e^0=0}$ give rise to large spectral intensity. We show in Fig. B.2 the even-parity phonon wavefunction $\phi_{0n'}^{N_e=1}$ with the largest overlap offset along the ordinate by its eigenenergy. It has a sizable and slowly varying amplitude around $Q_- = 0$ because its eigenenergy is close to the local value of the effective potential which at $Q_- = 0$ equals the $(k = +)$ -eigenenergy $-t$ of the system without electron-phonon interaction. Therefore, the peak with largest weight appears around this energy in the spectrum (solid line in Fig. B.6). The side peaks arise from final states with even-parity phonon wavefunctions with lower or higher eigenenergies whose overlap with $\phi_{00}^{N_e^0=0}$ decreases. Figure B.2 also shows the even

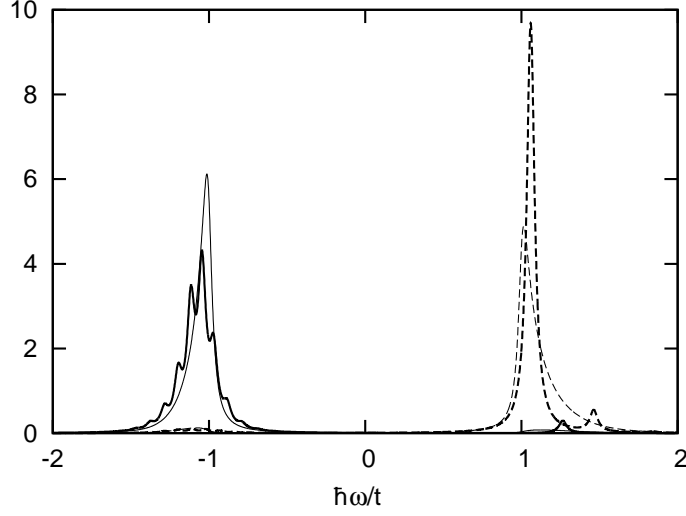


Figure B.5: Spectra for adding an electron to an empty two-site Holstein model ($\hbar\omega_{\text{ph}}/t = 0.1$, $g/t = 0.6$). The approximation $\tilde{A}_{k\sigma}^{N_e^0=0,+^{(2)}}(\omega)t/\hbar$ (Eq. (3.23), thin lines) and results from exact diagonalization (bold lines) are shown for both $k = +$ (solid lines) and $k = -$ (dashed lines). All spectra include a Lorentzian broadening (FWHM=0.06 t).

parity ground-state phonon wavefunction $\phi_{00}^{N_e=1}$ in the double-well potential. Clearly, its overlap with $\phi_{00}^{N_e=0}$ is very small leading to a strongly suppressed quasi-particle peak in $A_{(k=+)\sigma}^{N_e^0=0,+^{(2)}}$.

If, on the other hand, an electron with momentum $k = -$ is created in the empty state, one finds using similar arguments as before that final states leading to a large spectral intensity must have the electronic configuration $|E_1^{N_e=1}\rangle$. Their phonon wavefunction $\phi_{1n}^{N_e=1}$ must strongly overlap with $\phi_{00}^{N_e=0}$ and be of even-parity. In this case, the lowest-energy phonon wavefunction $\phi_{10}^{N_e=1}$ in the upper effective potential (shown in Fig. B.2) has the largest overlap because its eigenenergy is closest to $E_1^{N_e=1}(Q_- = 0) = +t$. Therefore, $A_{k=+,\sigma}^{N_e^0=0,+^{(2)}}(\omega)$ (dashed line in Fig. B.6) shows a prominent peak at $\hbar\omega \approx +t$.

As $\langle E_1^{N_e=1}|+\rangle$ ($\langle E_0^{N_e=1}|-\rangle$) only vanishes completely at $Q_- = 0$, the spectrum for $k = +$ ($k = -$) also shows weak structures around $\hbar\omega = +t$ ($\hbar\omega = -t$) where the coupling is now to phonon wavefunctions of odd parity. The density of coupling phonon states is different around $\hbar\omega = -t$ and $\hbar\omega = +t$. For example, the fact that the upper effective potential has a minimum around $Q_- = 0$ results in an asymmetric shape of $A_{k\sigma}^{N_e^0,+^{(2)}}(\omega)$ around $\hbar\omega = +t$ as no phonon eigenstates in this effective

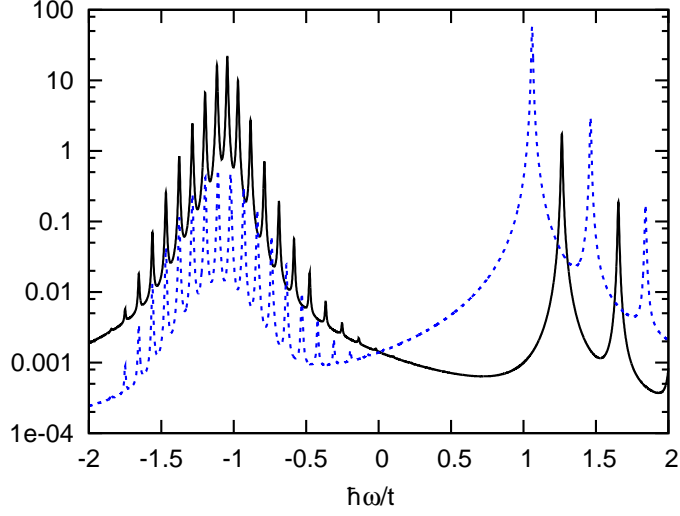


Figure B.6: Spectra $A_{k\sigma}^{N_e^0=0,+^{(2)}}(\omega)t/\hbar$ for adding an electron to an empty two-site Holstein model ($\hbar\omega_{\text{ph}}/t = 0.1$, $g/t = 0.6$) as given by Eq. (B.1). The spectra for both $k = +$ (solid line) and $k = -$ (dashed line) are shown with a Lorentzian broadening (FWHM=0.01 t). Observe the logarithmic intensity scale.

potential can have eigenenergies below $+t$.

B.4 t - J model with phonons

As another example, we study the one-dimensional N -site Holstein- t - J model with lattice constant a and periodic boundary conditions. This model also includes electron-electron interactions. The electronic part of H is given by the usual t - J Hamiltonian defined in Eq. (1.87). As in the Holstein model, we consider an interaction with dispersionless phonons where the coupling is now to empty sites (holes) labeled by j :

$$H_{\text{ep}} = \frac{g}{\sqrt{N}} \sum_{qj} \sqrt{\frac{2\omega_{\text{ph}}}{\hbar}} Q_q (1 - n_j) e^{iqja}. \quad (\text{B.30})$$

We use generalized phonon coordinates Q_q which are labeled by the phonon wavevector q . The system with one electron per site corresponds to the undoped case where the electron-phonon interaction vanishes. Again, the ($q = 0$)-phonon mode can be treated separately, the only difference being that the coupling is now proportional to the total number of empty sites N_{h} , not to the total number of electrons N_{e} .

For numerical calculations, we consider a 4-site system with $J/t = 0.3$, $\hbar\omega_{\text{ph}}/t = 0.1$, and $g/t = 0.8$. The photoemission spectra for destroying an electron with mo-

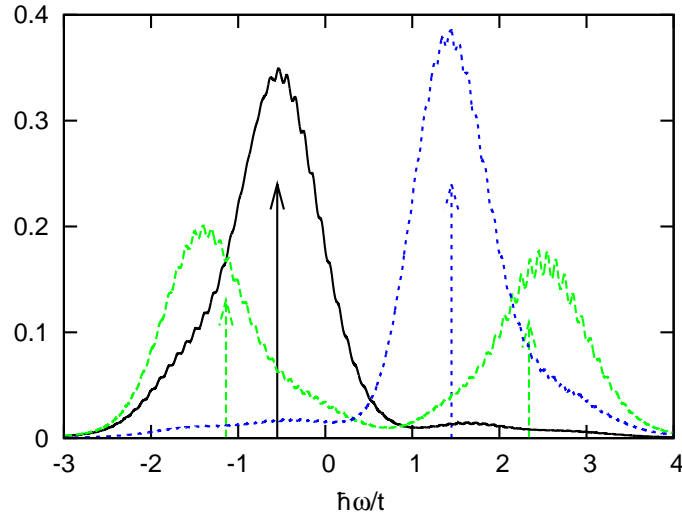


Figure B.7: Spectral functions $A_{k\sigma}^{N_h^0=0,-}(\omega)t/\hbar$ for creating a hole in the undoped 4-site Holstein- t - J model ($J/t = 0.3$, $\hbar\omega_{\text{ph}}/t = 0.1$, $g/t = 0.8$). $k = 0$: solid line, $k = \pm\pi/(2a)$: dashed line, $k = \pi/a$: dotted line (Lorentzian broadening: $\text{FWHM}=0.01t$). Arrows show positions and weights of corresponding peaks for $g = 0$.

momentum k and spin σ were obtained using exact diagonalization with up to 200 phonons per basis state for solving the problem without the ($q = 0$)-mode and subsequent convolution with $A^{N_h^0=0,-(1)}(\omega)$ (Eq. (B.22) with $N_h = 0$ instead of N_e). The results are displayed in Fig. B.7 together with arrows indicating the peaks in the corresponding spectra for $g = 0$. Without electron-phonon interaction, there is only one peak both for $k = 0$ (at -0.55) as well as for $k = \pi/a$ (at 1.45). For $k = \pm\pi/(2a)$, the spectrum has two peaks at -1.139 and 2.339 as a result of the electron-electron interaction.

Again, the dispersion found in the system without electron-phonon interaction is traced quite accurately by a broad peak in the case of strong electron-phonon coupling. The spectrum for $k = \pm\pi/(2a)$ also illustrates our comments at the end of Sec. 3.3.1 on the sum rule concerning the first spectral moment. Since the spectrum has two peaks for $k = \pm\pi/(2a)$, the sum rule cannot tell us how the peaks are broadened. Many other spectra would also have been consistent with the sum rule, e.g. spectra where the peaks are shifted. The arguments based on the adiabatic approximation, however, show that both peaks should be broadened with their individual center of gravity remaining roughly unchanged in agreement with the exact calculations.

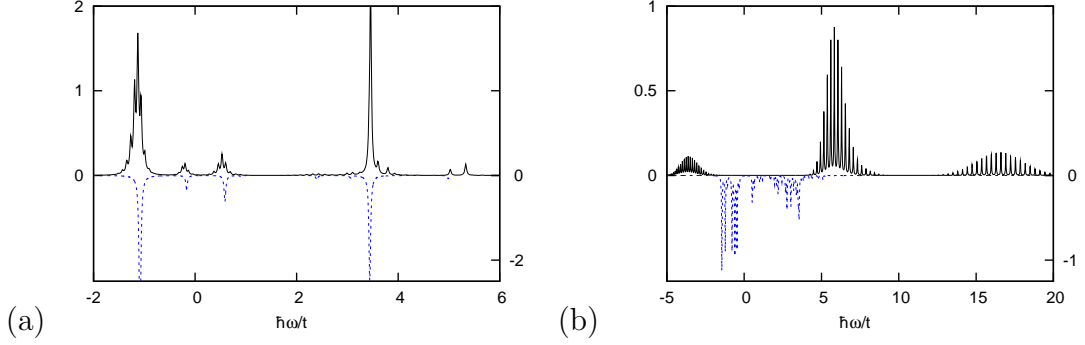


Figure B.8: Photoemission spectra ($\mathbf{k} = (3, 1)\pi/(5a)$) for the 10-site t - J model with one interacting phonon mode ($J/t = 0.4$, $\hbar\omega_{\text{ph}}/t = 0.1$, $g_{(\pi/a, \pi/a)}/t = 1.6$): (a) from the undoped system, (b) from the 10%-doped system. The corresponding spectra for systems without electron-phonon interaction are shown by dashed lines with their amplitude flipped for clarity. A Lorentzian broadening of $\text{FWHM} = 0.04t$ has been applied.

Next, we consider the t - J model in two dimensions on a tilted 10-site square cluster with periodic boundary conditions. To simplify calculations, we assume that the electron-phonon interaction is described by Eq. (B.30) but with a \mathbf{q} -dependent coupling constant $g_{\mathbf{q}}$. In the following, we choose $g_{(\pi/a, \pi/a)}/t = 1.6$ and $g_{\mathbf{q}} = 0$ for all other $\mathbf{q} \neq (\pi/a, \pi/a)$ so that effectively there is only one phonon mode that interacts with the electrons. The other parameters are $J/t = 0.4$, and $\hbar\omega_{\text{ph}}/t = 0.1$. Figure B.8 shows the photoemission spectra for $\mathbf{k} = (3, 1)\pi/(5a)$ from both the undoped (Fig. B.8(a)) and the 10%-doped system (Fig. B.8(b)). The electron-phonon interaction has been switched on and off (solid line vs. dashed line with flipped amplitude).

The spectra from the undoped system confirm again our conclusions from Sec. 3.3.1. The electron-phonon interaction basically broadens the structures in the original spectrum. This includes the quasi-particle peak at low binding energies. In contrast, the spectrum from the doped system changes quite differently when the electron-phonon interaction is switched on. Although the spectrum again develops several broad features, they cannot be related anymore in a simple way to the structures in the spectrum found without electron-phonon interaction. We have also varied \mathbf{k} and found that the dispersion of the broad features is different from the quasi-particle dispersion in the system without electron-phonon interaction. According to Eq. (3.23), the spectra rather correspond to broadened versions of spectra one would obtain in a

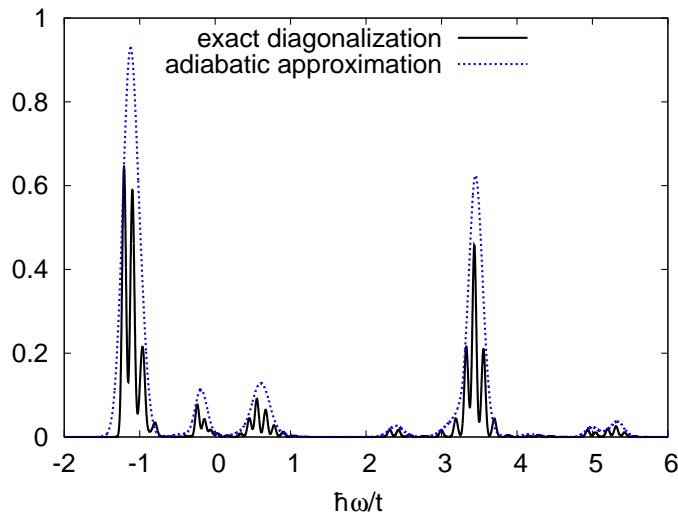


Figure B.9: Photoemission spectrum ($\mathbf{k} = (3, 1)\pi/(5a)$) for the undoped Holstein- t - J model on the 10-site tilted square cluster with periodic boundary conditions and $J/t = 0.4$, $\hbar\omega_{\text{ph}}/t = 0.1$, $g/t = \sqrt{0.05}$ following Ref. [118]. The full line is obtained from exact diagonalization, the dotted line using the adiabatic approximation (10^4 samples). In both cases, a Gaussian broadening ($\text{FWHM}=0.6\hbar\omega_{\text{ph}}$) has been applied.

purely electronic but distorted system.

Finally, we consider photoemission from the undoped Holstein- t - J model on the 10-site tilted square cluster with periodic boundary conditions. The parameters ($\mathbf{k} = (3, 1)\pi/(5a)$, $J/t = 0.4$, $\hbar\omega_{\text{ph}}/t = 0.1$, $g/t = \sqrt{0.05}$) are chosen such that we can compare with results in Fig. 1 of Ref. [118] where this problem was studied using exact diagonalization. The corresponding spectrum is shown in Fig. B.9 together with our adiabatic approximation (Eqs. (3.23) and (3.24)). Also for this more complex problem, the approximate spectrum is in good agreement with the exact result. Except for the fine structure of individual phonon satellites, the distribution of spectral weight is reproduced quite well.

B.5 Comparison with diagrammatic Monte Carlo method

ARPES spectra for the undoped two-dimensional Holstein- t - J model have also been calculated in Ref. [89] for a system in the thermodynamic limit using a diagrammatic Monte Carlo (DMC) method. The standard spin-wave approximation is introduced

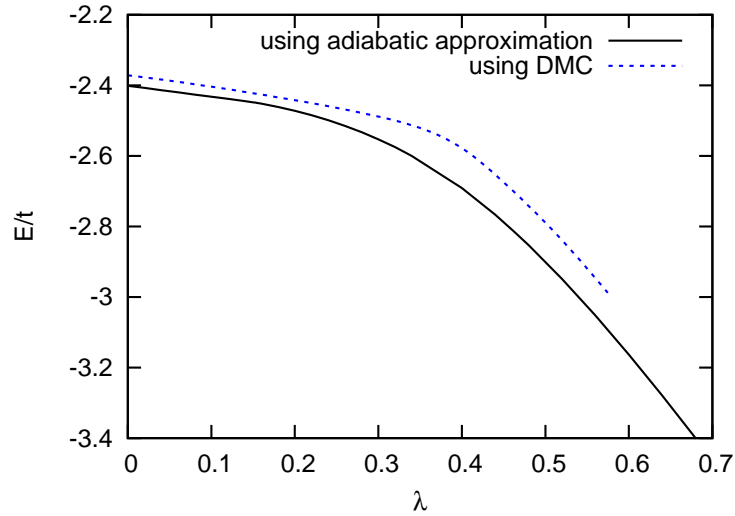


Figure B.10: Ground-state energy of the Holstein- t - J model with one hole as function of the coupling constant λ using the adiabatic approximation (solid line) and the DMC method (dashed line, after Fig. 2 in Ref. [89]). The parameters used are given in the main text.

and diagrams with a magnon propagator being crossed by magnon or phonon lines are neglected. In this section, we compare a few of the thus obtained results with corresponding calculations based on exact diagonalization of finite clusters and our adiabatic approximation.

The dashed line in Fig. B.10 shows the ground-state energy of the Holstein- t - J model ($J/t = 0.3$, $\hbar\omega_{\text{ph}}/t = 0.1$) with one hole as a function of the dimensionless coupling constant $\lambda = 2g^2/(8t\hbar\omega_{\text{ph}})$ as obtained with the DMC method in Ref. [89]. The energy is measured with respect to the ground-state energy of the system with one hole for $t = 0$ and $\lambda = 0$. One finds an approximately linear dependence on λ for both small and large coupling with a change of slope around the critical coupling $\lambda_c \approx 0.38$ above which the polarons become self-trapped. The solid line in Fig. B.10 shows the corresponding result obtained within the adiabatic approximation using the iterative method described in Sec. 3.3.3 on a 4×4 square cluster with periodic boundary conditions. Comparing with the DMC result, we find that the adiabatic approximation gives slightly lower ground-state energies. The approximately linear behavior for small and large λ is reproduced with very similar slopes. Despite a more washed-out transition, linear fits to the curve for small and large coupling still cross at $\lambda \approx 0.4$, i.e., also in the adiabatic approximation the crossover to self-trapped polarons occurs around a critical coupling similar to that found with the

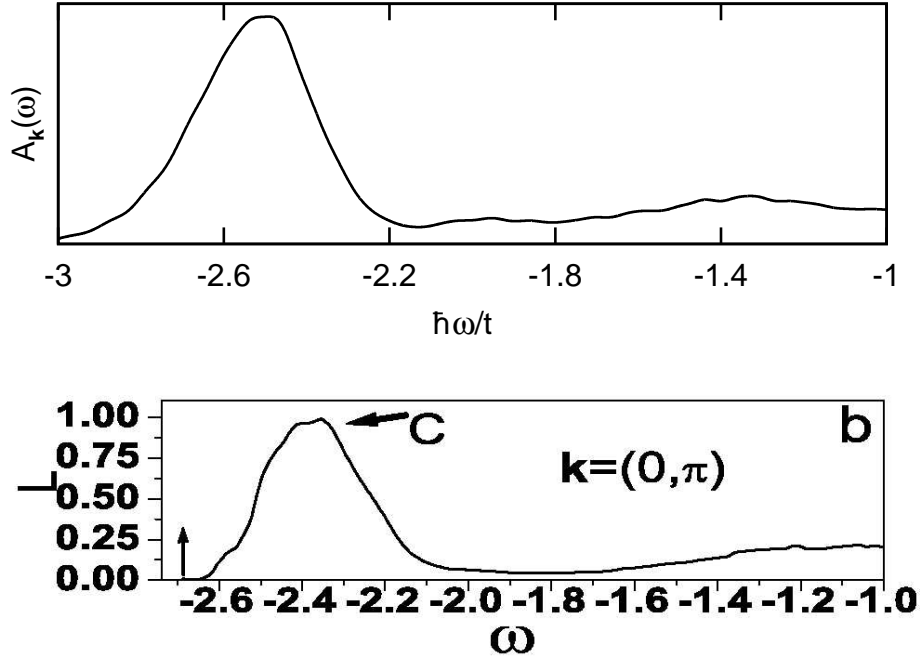


Figure B.11: Comparison of the $\mathbf{k} = (\pi/a, 0)$ ARPES spectra from the undoped Holstein- t - J model obtained using the adiabatic approximation (upper panel) and DMC (lower panel, extracted from Fig. 3 in Ref. [89] where \hbar , a , and t have been set to unity). See main text for parameters used.

DMC method. Furthermore, as detailed in Sec. 3.3.3 the ground-state energy of the system with one hole also defines the position of the quasi-particle peak in ARPES spectra from the undoped system needed to measure binding energies.

In Fig. B.11, we compare the $\mathbf{k} = (\pi/a, 0)$ ARPES spectra from the undoped Holstein- t - J model obtained using the two methods. The chosen coupling $\lambda = 0.46$ ($g/t = 0.43$) is large enough to cause self-trapping of the polaronic quasi-particles. The DMC result from Ref. [89] reproduced in the lower panel of Fig. B.11 shows a broad phonon side band in the lower energy part whereas the quasi-particle peak whose position is indicated by the arrow is strongly suppressed in weight. The upper panel shows the corresponding spectrum obtained using our adiabatic approximation on a 20-site tilted square cluster (448 samples, each broadened by a Gaussian with a FWHM of $0.6\hbar\omega_{\text{ph}}$). The two results agree quite well. We obtain similar widths of the phonon side band (one finds a FWHM of $0.33t$ in the adiabatic approximation and $0.29t$ using the DMC method). In the adiabatic approximation, some spectral weight is spread below the actual quasi-particle energy because there is no lower bound to

the spectrum in this approximation (cf. Sec. 3.3.3).

Summarizing, we find that our method of calculating (binding) energies and ARPES spectra in the adiabatic approximation using finite clusters gives results which are in good agreement with those from the DMC method which makes no adiabatic approximation and works in the thermodynamic limit.

Appendix C

Green's function formalism

Following Ref. [111], we define double-time Green's functions at zero temperature assuming that the Hamiltonian does not depend explicitly on time ($\partial H/\partial t = 0$).

Retarded Green's function:

$$G_{AB}^{\text{ret}}(t-t') \equiv \langle\langle A(t); B(t') \rangle\rangle^{\text{ret}} = -i\Theta(t-t')\langle 0|[A(t), B(t')]_{-\epsilon}|0\rangle. \quad (\text{C.1})$$

Advanced Green's function:

$$G_{AB}^{\text{adv}}(t-t') \equiv \langle\langle A(t); B(t') \rangle\rangle^{\text{adv}} = i\Theta(t'-t)\langle 0|[A(t), B(t')]_{-\epsilon}|0\rangle. \quad (\text{C.2})$$

Causal Green's function:

$$\begin{aligned} G_{AB}^{\text{c}}(t-t') &\equiv \langle\langle A(t); B(t') \rangle\rangle^{\text{c}} \\ &= -i(\Theta(t-t')\langle 0|A(t)B(t')|0\rangle + \epsilon\Theta(t'-t)\langle 0|B(t')A(t)|0\rangle). \end{aligned} \quad (\text{C.3})$$

Here, $[A, B]_{\epsilon} = AB - \epsilon BA$, and we use $\epsilon = -1$ ($+1$) if A and B are fermionic (bosonic) operators. The Heisenberg representation is used for the operators in the definitions of the Green's functions. The ground state of the system is denoted by $|0\rangle$.

The energy-dependent Green's functions are defined using a Fourier transformation:

$$G_{AB}^{\alpha}(\omega) \equiv \langle\langle A; B \rangle\rangle_{\omega}^{\alpha} = \frac{1}{2\pi} \int_{-\infty}^{\infty} d\omega' G_{AB}^{\alpha}(t-t') e^{i\omega(t-t')}, \quad (\text{C.4})$$

where $\alpha \in \{\text{ret}, \text{adv}, \text{c}\}$. All three Green's functions have the same equation of motion,

$$\begin{aligned} \omega G_{AB}^{\alpha}(\omega) &= \langle[A, B]_{-\epsilon}\rangle + \hbar^{-1} \langle\langle [A, H]_{-}; B \rangle\rangle_{\omega}^{\alpha} \\ &= \langle[A, B]_{-\epsilon}\rangle - \hbar^{-1} \langle\langle A; [B, H]_{-} \rangle\rangle_{\omega}^{\alpha}, \end{aligned} \quad (\text{C.5})$$

but different boundary conditions must be met by the individual time-dependent Green's functions which reflect themselves in different analytical behavior of $G_{AB}^\alpha(\omega)$ in the complex ω plane.

Defining the spectral density

$$S_{AB}(t, t') \equiv \frac{1}{2\pi} \langle [A(t), B(t')]_{-\epsilon} \rangle, \quad (\text{C.6})$$

both the retarded and the advanced Green's function can be written in terms of its Fourier transform:

$$\begin{aligned} G_{AB}^{\text{ret/adv}}(\omega) &= \int d\omega' \frac{S_{AB}(\omega')}{\omega - \omega' \pm i0^+} \\ &= \sum_m \left(\frac{\langle 0|A|m\rangle\langle m|B|0\rangle}{\omega - \hbar^{-1}(E_m - E_0) \pm i0^+} - \epsilon \frac{\langle 0|B|m\rangle\langle m|A|0\rangle}{\omega + \hbar^{-1}(E_m - E_0) \pm i0^+} \right). \end{aligned} \quad (\text{C.7})$$

In the second line, an explicit expression is given using a complete set of eigenstates $|m\rangle$ of the Hamiltonian with eigenenergies E_m . E_0 is the ground-state energy. The corresponding expression for the causal Green's function is

$$G_{AB}^c(\omega) = \sum_m \left(\frac{\langle 0|A|m\rangle\langle m|B|0\rangle}{\omega - \hbar^{-1}(E_m - E_0) + i0^+} - \epsilon \frac{\langle 0|B|m\rangle\langle m|A|0\rangle}{\omega + \hbar^{-1}(E_m - E_0) - i0^+} \right). \quad (\text{C.8})$$

The retarded (advanced) Green's function can be analytically continued into the upper (lower) half-plane of complex energies. We can view them as two branches of a Green's function in the complex z plane which has a cut along the real axis:

$$G_{AB}(z) \equiv \langle\langle A; B \rangle\rangle_z = \int d\omega \frac{S_{AB}(\omega)}{z - \omega} = \begin{cases} G_{AB}^{\text{ret}}(z) & \text{if } \text{Im } z > 0, \\ G_{AB}^{\text{adv}}(z) & \text{if } \text{Im } z < 0. \end{cases} \quad (\text{C.9})$$

Finally, it follows from Eq. (C.7) that

$$\begin{aligned} S_{AB}(\omega) &= \mp \frac{1}{\pi} \text{Im } G_{AB}^{\text{ret/adv}}(\omega) \\ &= \sum_m \left(\langle 0|A|m\rangle\langle m|B|0\rangle \delta(\omega - \hbar^{-1}(E_m - E_0)) \right. \\ &\quad \left. - \epsilon \langle 0|B|m\rangle\langle m|A|0\rangle \delta(\omega + \hbar^{-1}(E_m - E_0)) \right). \end{aligned} \quad (\text{C.10})$$

Appendix D

Vertex function in the two-site Hubbard model with phonons

In order to derive the vertex function in the two-site Hubbard model with phonons (Eqs. (4.62) and (4.63)) according to Eq. (4.65), we first calculate the one-electron Green's function

$$G(i\omega_n, \pm) = -Z^{-1} \int_0^{\hbar\beta} d\tau e^{i\omega_n\tau} \sum_m e^{-\beta E_m} \langle m | c_{\pm\sigma}(\tau) c_{\pm\sigma}^\dagger | m \rangle \quad (\text{D.1})$$

in the half-filled system, i.e., the chemical potential is set to zero for our electron-hole symmetric model. $Z = \sum_m e^{-\beta E_m}$ is the partition function, $c_{\pm\sigma}(\tau) = e^{H_H\tau/\hbar} c_{\pm\sigma} e^{-H_H\tau/\hbar}$, and we sum over all eigenstates $|m\rangle$ of H_H which are listed in Tab. D.1 together with their eigenenergies E_m and the required matrix elements. We assume U_H to be large and neglect contributions to the eigenstates of order t_H/U_H . Also the eigenenergies are evaluated in the limit of large U_H . We are interested in the limit of zero temperature. For $\beta \rightarrow \infty$, $Z \rightarrow \exp(-\beta E_{2a})$ and only the matrix elements from $|2a\rangle$ and $|1+; -\sigma\rangle$ contribute:

$$G(i\omega_n, \pm) \rightarrow \frac{1}{2} \left[\frac{\hbar}{\hbar i\omega_n - U_H/2 \pm t - 4t_H^2/U_H} + \frac{\hbar}{\hbar i\omega_n + U_H/2 \pm t + 4t_H^2/U_H} \right]. \quad (\text{D.2})$$

Next, we calculate the anomalous one-electron Green's function G_A defined in Eq. (4.64). For our purposes, it is sufficient to calculate only the leading linear response of G_A to H'_{ep} :

$$G_A(i\omega_n, +; i\nu_m) = \int_0^{\hbar\beta} d\tau e^{i(\omega_n + \nu_m)\tau} \int_0^{\hbar\beta} d\tau' e^{-i\nu_m\tau'} \sum_m \langle m | T_\tau H'_{\text{ep}}(\tau') c_{-\sigma}(\tau) c_{+\sigma}^\dagger | m \rangle, \quad (\text{D.3})$$

eigenstate $ m\rangle$	eigenenergy E_m	$\langle m c_{+\sigma}(\tau)c_{+\sigma}^\dagger m\rangle$
$ 0\rangle$	$E_0 = 0$	$\exp((E_0 - E_{1+})\tau)$
$ 1+; \sigma'\rangle = c_{+\sigma'}^\dagger 0\rangle$	$E_{1+} = -U_H/2 + t_H$	$\delta_{\sigma, -\sigma'} [\exp((E_{1+} - E_{2a})\tau) + \exp((E_{1+} - E_{2f})\tau)]/2$
$ 1-; \sigma\rangle = c_{-\sigma}^\dagger 0\rangle$	$E_{1-} = -U_H/2 - t_H$	$\exp((E_{1-} - E_{2c})\tau)$
$ 1-; -\sigma\rangle = c_{-(-\sigma)}^\dagger 0\rangle$	$E_{1-} = -U_H/2 - t_H$	$\frac{1}{2} [\exp((E_{1-} - E_{2b})\tau) + \exp((E_{1-} - E_{2e})\tau)]$
$ 2a\rangle \approx \frac{1}{\sqrt{2}}(c_{+\uparrow}^\dagger c_{+\downarrow}^\dagger - c_{-\uparrow}^\dagger c_{-\downarrow}^\dagger) 0\rangle$	$E_{2a} \approx -U_H - 4t_H^2/U_H$	$\frac{1}{2} \exp((E_{2a} - E_{3+})\tau)$
$ 2b\rangle = \frac{1}{\sqrt{2}}(c_{+\uparrow}^\dagger c_{-\downarrow}^\dagger - c_{-\uparrow}^\dagger c_{+\downarrow}^\dagger) 0\rangle$	$E_{2b} = -U_H$	$\frac{1}{2} \exp((E_{2b} - E_{3-})\tau)$
$ 2c\rangle = c_{+\uparrow}^\dagger c_{-\uparrow}^\dagger 0\rangle$	$E_{2c} = -U_H$	$\delta_{\sigma, \downarrow} \exp((E_{2c} - E_{3+})\tau)$
$ 2d\rangle = c_{+\downarrow}^\dagger c_{-\downarrow}^\dagger 0\rangle$	$E_{2d} = -U_H$	$\delta_{\sigma, \uparrow} \exp((E_{2d} - E_{3-})\tau)$
$ 2e\rangle = \frac{1}{\sqrt{2}}(c_{+\uparrow}^\dagger c_{-\downarrow}^\dagger + c_{-\uparrow}^\dagger c_{+\downarrow}^\dagger) 0\rangle$	$E_{2e} = 0$	$\frac{1}{2} \exp((E_{2e} - E_{3-})\tau)$
$ 2f\rangle \approx \frac{1}{\sqrt{2}}(c_{+\uparrow}^\dagger c_{+\downarrow}^\dagger + c_{-\uparrow}^\dagger c_{-\downarrow}^\dagger) 0\rangle$	$E_{2f} \approx 4t_H^2/U_H$	$\frac{1}{2} \exp((E_{2f} - E_{3+})\tau)$
$ 3+; \sigma'\rangle = c_{+\sigma'}^\dagger c_{-\uparrow}^\dagger c_{-\downarrow}^\dagger 0\rangle$	$E_{3+} = -U_H/2 - t_H$	$\delta_{\sigma, -\sigma'} \exp((E_{3+} - E_4)\tau)$
$ 3-; \sigma'\rangle = c_{-\sigma'}^\dagger c_{+\uparrow}^\dagger c_{+\downarrow}^\dagger 0\rangle$	$E_{3-} = -U_H/2 + t_H$	0
$ 4\rangle = c_{+\uparrow}^\dagger c_{+\downarrow}^\dagger c_{-\uparrow}^\dagger c_{-\downarrow}^\dagger 0\rangle$	$E_4 = 0$	0

Table D.1: Eigenstates and eigenenergies of the two-site Hubbard model together with the matrix elements needed for the calculation of the one-electron Green's function $G(i\omega_n, +)$ in the limit of large U_H .

where

$$\langle m|T_\tau H'_{\text{ep}}(\tau')c_{-\sigma}(\tau)c_{+\sigma}^\dagger|m\rangle = gu \sum_{s=\pm} \sum_{\sigma'} \langle m|T_\tau c_{(-s)\sigma'}^\dagger(\tau' + 0^+)c_{s\sigma'}(\tau')c_{-\sigma}(\tau)c_{+\sigma}^\dagger|m\rangle. \quad (\text{D.4})$$

Analogous to the one-electron Green's function, one finds that in the limit $\beta \rightarrow \infty$ only $|2a\rangle$ and $|1+; -\sigma\rangle$ give non-vanishing contributions. The respective matrix elements are

$$\langle 2a|T_\tau H'_{\text{ep}}(\tau')c_{-\sigma}(\tau)c_{+\sigma}^\dagger|2a\rangle = \Theta(\tau - \tau') \frac{gu}{2} \exp(\tau(E_{2a} - E_{3-})) \exp(\tau'(E_{3-} - E_{3+})), \quad (\text{D.5})$$

$$\begin{aligned} \langle 1+; -\sigma|T_\tau H'_{\text{ep}}(\tau')c_{-\sigma}(\tau)c_{+\sigma}^\dagger|1+; -\sigma\rangle \\ = \Theta(\tau' - \tau) \frac{gu}{2} \exp(\tau E_{1-}) [\exp(-\tau E_{2d}) - \exp(-\tau E_{2a})] \exp(\tau'(E_{1+} - E_{1-})). \end{aligned} \quad (\text{D.6})$$

Using these results in Eq. (D.3), we obtain

$$G_A(i\omega_n, \pm; i\nu_m) \rightarrow \frac{gu}{2} \left[\frac{\hbar}{(\hbar i\omega_n + U_H/2 \pm t + 4t_H^2/U_H)(\hbar i(\omega_n + \nu_m) + U_H/2 \mp t + 4t_H^2/U_H)} + \frac{\hbar}{(\hbar i\omega_n - U_H/2 \pm t - 4t_H^2/U_H)(\hbar i(\omega_n + \nu_m) - U_H/2 \mp t - 4t_H^2/U_H)} \right]. \quad (\text{D.7})$$

The vertex function is finally obtained by inserting the results in Eqs. (D.2) and (D.7) into Eq. (4.65):

$$\Gamma(i\omega_n, \pm; i\nu_m) \rightarrow \frac{\hbar^2 i\omega_n i(\omega_n + \nu_m) \pm \hbar i\nu_m t_H + (U_H/2)^2 + 4t_H^2 - t_H^2 + (4t_H^2/U_H)^2}{(\hbar i\omega_n \pm t_H)(\hbar i(\omega_n + \nu_m) \mp t_H)}. \quad (\text{D.8})$$

This leads to the expression in Eq. (4.66) after analytic continuation ($i\omega_n \rightarrow \omega$, $i\nu_m \rightarrow \omega'$) and the neglect of terms of higher order in t_H/U_H .

Bibliography

- [1] G. Grimvall, *The Electron-phonon Interaction in Metals* (North Holland, Amsterdam, 1981). 11
- [2] J. Bardeen, L. N. Cooper, and J. R. Schrieffer, *Phys. Rev.* **108**, 1175 (1957). 11
- [3] A. B. Migdal, *Zh. Eksp. Teor. Fiz.* **34**, 1438 (1958), [*Sov. Phys. JETP* **7**, 996 (1958)]. 11
- [4] G. M. Eliashberg, *Zh. Eksp. Teor. Fiz.* **38**, 966 (1960), [*Sov. Phys. JETP* **11**, 696 (1960)]. 11
- [5] G. M. Eliashberg, *Zh. Eksp. Teor. Fiz.* **39**, 1437 (1960), [*Sov. Phys. JETP* **12**, 1000 (1960)]. 11
- [6] O. Gunnarsson, *Rev. Mod. Phys.* **69**, 575 (1997). 11
- [7] A. Georges, G. Kotliar, W. Krauth, and M. Rozenberg, *Rev. Mod. Phys.* **68**, 13 (1996). 11, 76
- [8] J. E. Han, O. Gunnarsson, and V. H. Crespi, *Phys. Rev. Lett.* **90**, 167006 (2003). 11
- [9] J. G. Bednorz and K. A. Müller, *Z. Phys. B* **64**, 189 (1986). 12
- [10] M. K. Wu, J. R. Ashburn, C. J. Torng, P. H. Hor, R. L. Meng, L. Gao, Z. J. Huang, Y. Q. Wang, and C. W. Chu, *Phys. Rev. Lett.* **58**, 908 (1987). 12
- [11] B. Batlogg, R. J. Cava, A. Jayaraman, R. B. v. Dover, G. A. Kourouklis, S. Sunshine, D. W. Murphy, L. W. Rupp, H. S. Chen, A. White, K. T. Short, A. M. Muzsca, and E. A. Rietman, *Phys. Rev. Lett.* **58**, 2333 (1987). 12
- [12] S. Y. Savrasov and O. K. Andersen, *Phys. Rev. Lett.* **77**, 4430 (1996). 12, 49

-
- [13] T. Timusk and B. Statt, Rep. Prog. Phys. **62**, 61 (1999). 12
- [14] M. Gurvitch and A. T. Fiory, Phys. Rev. Lett. **59**, 1337 (1987). 12
- [15] L. Pintschovius, N. Pyka, W. Reichardt, A. Y. Rumiantsev, N. L. Mitrofanov, A. S. Ivanov, G. Collin, and P. Bourges, Physica C **185-189**, 156 (1991). 13, 39, 43, 47, 72, 78, 81
- [16] S. L. Chaplot, W. Reichardt, L. Pintschovius, and N. Pyka, Phys. Rev. B **52**, 7230 (1995). 13, 39, 40, 43, 47, 72, 78, 81
- [17] L. Pintschovius and W. Reichardt, in *Neutron Scattering in Layered Copper-Oxide Superconductors*, Vol. 20 of *Physics and Chemistry of Materials with Low Dimensional Structures*, edited by A. Furrer (Kluwer Academic, Dordrecht, 1998), p. 165. 13, 39, 40, 46, 48, 81
- [18] L. Pintschovius and M. Braden, Phys. Rev. B **60**, R15039 (1999). 13, 39, 45, 46, 47, 99
- [19] R. J. McQueeney, Y. Petrov, T. Egami, M. Yethiraj, G. Shirane, and Y. Endoh, Phys. Rev. Lett. **82**, 628 (1999). 13, 39
- [20] C. Thomsen, M. Cardona, B. Gegenheimer, R. Liu, and A. Simon, Phys. Rev. B **37**, 9860 (1988). 13, 73
- [21] B. Friedl, C. Thomsen, and M. Cardona, Phys. Rev. Lett. **65**, 915 (1990). 13
- [22] E. Altendorf, X. K. Chen, J. C. Irwin, R. Liang, and W. N. Hardy, Phys. Rev. B **47**, 8140 (1993). 13
- [23] T. Schneider and H. Keller, Phys. Rev. Lett. **86**, 4899 (2001). 13
- [24] A. Damascelli, Z. Hussain, and Z.-X. Shen, Rev. Mod. Phys. **75**, 473 (2003). 13
- [25] A. Lanzara, P. V. Bogdanov, X. J. Zhou, S. A. Keller, D. L. Feng, E. D. Lu, T. Yoshida, H. Eisaki, A. Fujimori, K. Kishio, J.-I. Shimoyama, T. Noda, S. Uchida, Z. Hussain, and Z.-X. Shen, Nature **412**, 510 (2001). 13, 99, 100
- [26] K. M. Shen, F. Ronning, D. H. Lu, W. S. Lee, N. J. C. Ingle, W. Meevasana, F. Baumberger, A. Damascelli, N. P. Armitage, L. L. Miller, Y. Kohsaka, M. Azuma, M. Takano, H. Takagi, and Z.-X. Shen, Phys. Rev. Lett. **93**, 267002 (2004). 13, 75, 76, 94, 97

-
- [27] K. M. Shen, F. Ronning, W. Meevasana, D. H. Lu, N. J. C. Ingle, F. Baumberger, W. S. Lee, L. L. Miller, Y. Kohsaka, M. Azuma, M. Takano, H. Takagi, and Z.-X. Shen, unpublished. 13, 75, 76, 96
- [28] V. J. Emery, Phys. Rev. Lett. **58**, 2794 (1987). 15, 16
- [29] F. C. Zhang and T. M. Rice, Phys. Rev. Lett. **37**, 3759 (1988). 15, 24, 31, 80
- [30] K. J. v. Szczepanski and K. W. Becker, Z. Phys. B **89**, 327 (1992). 16, 21, 67, 68
- [31] S. Ishihara and N. Nagaosa, Phys. Rev. B **69**, 144520 (2004). 16, 67
- [32] F. J. Ohkawa, Phys. Rev. B **70**, 184514 (2004). 16, 68
- [33] O. Jepsen, private communication. 20
- [34] G. Khaliullin and P. Horsch, Phys. Rev. B **54**, R9600 (1996). 21, 60, 67, 104
- [35] G. Khaliullin and P. Horsch, Physica C **282-287**, 1751 (1997). 21, 60, 67
- [36] P. Horsch, G. Khaliullin, and V. Oudovenko, Physica C **341**, 117 (2000). 21, 60, 67
- [37] P.-O. Löwdin, J. Math. Phys. **3**, 969 (1962). 22, 23
- [38] E. Müller-Hartmann and A. Reischl, Eur. Phys. J. B **28**, 173 (2002). 25, 43
- [39] O. Rösch and O. Gunnarsson, Phys. Rev. Lett. **92**, 146403 (2004). 37
- [40] L. Pintschovius, phys. stat. sol. (b) **242**, 30 (2005). 39, 41, 48, 49, 55
- [41] W. Reichardt, J. Low Temp. Phys. **105**, 807 (1996). 39
- [42] M. Braden and L. Pintschovius, J. Low Temp. Phys. **105**, 813 (1996). 39
- [43] R. J. McQueeney, J. L. Sarro, P. G. Pagliuso, P. W. Stephens, and R. Osborn, Phys. Rev. Lett. **87**, 077001 (2001). 39
- [44] L. Pintschovius, W. Reichardt, M. Kläser, T. Wolf, and H. v. Löhneysen, Phys. Rev. Lett. **89**, 037001 (2002). 39
- [45] J. H. Chung, T. Egami, R. J. McQueeney, M. Yethiraj, M. Arai, T. Yokoo, Y. Petrov, H. A. Mook, Y. Endoh, S. Tajima, C. Frost, and F. Dogan, Phys. Rev. B **67**, 014517 (2003). 39

-
- [46] H. Uchiyama, A. Q. R. Baron, S. Tsutsui, Y. Tanaka, W.-Z. Hu, A. Yamamoto, S. Tajima, and Y. Endoh, *Phys. Rev. Lett.* **92**, 197005 (2004). 39
- [47] J. M. Tranquada, K. Nakajima, M. Braden, L. Pintschovius, and R. J. McQueeney, *Phys. Rev. Lett.* **88**, 075505 (2002). 39, 72
- [48] W. Reichardt and M. Braden, *Physica B* **263-264**, 416 (1999). 39
- [49] M. Braden, W. Reichardt, S. Shiryaev, and S. N. Barilo, *Physica C* **378-381**, 89 (2002). 39
- [50] A. Weiße, H. Fehske, G. Wellein, and A. R. Bishop, *Phys. Rev. B* **62**, R747 (2000). 42
- [51] J. A. Riera, *Phys. Rev. B* **43**, 3681 (1991). 42
- [52] D. Poilblanc, *Phys. Rev. B* **44**, 9562 (1991). 42, 44
- [53] A. K. Mahan, R. M. Martin, and S. Satpathy, *Phys. Rev. B* **38**, 6650 (1988). 43
- [54] J. Zaanen, O. Jepsen, O. Gunnarsson, A. T. Paxton, O. K. Andersen, and A. Svane, *Physica C* **153-155**, 1636 (1988). 43
- [55] M. S. Hybertsen and M. Schlüter, *Phys. Rev. B* **39**, 9028 (1989). 43
- [56] J. F. Annett, R. M. Martin, A. K. McMahan, and S. Satpathy, *Phys. Rev. B* **40**, 2620 (1989). 43
- [57] M. S. Hybertsen, E. B. Stechel, M. Schluter, and D. R. Jennison, *Phys. Rev. B* **41**, 11068 (1990). 43
- [58] O. K. Andersen, A. I. Liechtenstein, O. Jepsen, and F. Paulsen, *J. Phys. Chem. Solids* **56**, 1573 (1995). 43, 54, 56, 97
- [59] J. Jaklič and P. Prelovšek, *Adv. Phys.* **49**, 1 (2000). 43
- [60] D. D. Betts, H. Q. Lin, and J. S. Flynn, *Can. J. Phys.* **77**, 353 (1999). 48
- [61] T. Fukuda, J. Mizuki, K. Ikeuchi, K. Yamada, A. Q. R. Baron, and S. Tsutsui, *Phys. Rev. B* **71**, 060501(R) (2005). 48
- [62] P. Horsch and G. Khaliullin, *Physica B* **359-361**, 620 (2005). 49, 67

-
- [63] H. Krakauer, W. E. Pickett, and R. E. Cohen, *Phys. Rev. B* **47**, 1002 (1993). 49, 61
- [64] O. K. Andersen, S. Y. Savrasov, O. Jepsen, and A. I. Liechtenstein, *J. Low Temp. Phys.* **105**, 285 (1996). 49
- [65] K.-P. Bohnen, R. Heid, and M. Krauss, *Europhys. Lett.* **64**, 104 (2003), and private communication. 49, 51, 56
- [66] W. Kohn and L. J. Sham, *Phys. Rev.* **140**, A1133 (1965). 49
- [67] O. Rösch and O. Gunnarsson, *Phys. Rev. Lett.* **93**, 237001 (2004). 61
- [68] L. Pintschovius, J. M. Bassat, P. Odier, F. Gervais, G. Chevrier, W. Reichardt, and F. Gompf, *Phys. Rev. B* **40**, 2229 (1989). 72
- [69] R. M. Macfarlane, H. Rosen, and H. Seki, *Solid State Commun.* **63**, 831 (1987). 73
- [70] S. L. Cooper, M. V. Klein, B. G. Pazol, and D. M. Rice, J. P. and Ginsberg, *Phys. Rev. B* **37**, 5920 (1988). 73
- [71] T. Cuk, F. Baumberger, D. H. Lu, N. Ingle, X. J. Zhou, H. Eisaki, N. Kaneko, Z. Hussain, T. P. Devereaux, N. Nagaosa, and Z.-X. Shen, *Phys. Rev. Lett.* **93**, 117003 (2004). 73
- [72] T. P. Devereaux, T. Cuk, Z.-X. Shen, and N. Nagaosa, *Phys. Rev. Lett.* **93**, 117004 (2004). 73
- [73] M. Opel, R. Hackl, T. P. Devereaux, A. Viroztek, A. Zawadowski, A. Erb, E. Walker, H. Berger, and L. Forro, *Phys. Rev. B* **60**, 9836 (1999). 73
- [74] N. Bulut and D. J. Scalapino, *Phys. Rev. B* **54**, 14971 (1996). 74
- [75] L. Perfetti, S. Mitrovic, G. Margaritondo, M. Grioni, L. Forró, L. Degiorgi, and H. Höchst, *Phys. Rev. B* **66**, 075107 (2002). 75, 77
- [76] L. Perfetti, H. Berger, L. Degiorgi, H. Höchst, J. Voit, G. Margaritondo, and M. Grioni, *Phys. Rev. Lett.* **87**, 216404 (2001). 75, 77
- [77] D. S. Dessau, T. Saitoh, C.-H. Park, Z.-X. Shen, P. Villella, N. Hamada, Y. Moritomo, and Y. Tokura, *Phys. Rev. Lett.* **81**, 192 (1998). 75, 77

-
- [78] T. Tohyama and S. Maekawa, *Supercond. Sci. Technol.* **13**, R17 (2000). 75
- [79] O. Rösch, O. Gunnarsson, X. J. Zhou, T. Yoshida, T. Sasagawa, A. Fujimori, Z. Hussain, Z.-X. Shen, and S. Uchida, *Phys. Rev. Lett.* **95**, 227002 (2005). 76, 77
- [80] D. N. Sheng, Y. C. Chen, and Z. Y. Wen, *Phys. Rev. Lett.* **77**, 5102 (1996). 76
- [81] A. Paramekanti, M. Randeria, and N. Trivedi, *Phys. Rev. Lett.* **87**, 217002 (2001). 76
- [82] G. Sangiovanni, private communication. 76
- [83] E. Dagotto, *Rev. Mod. Phys.* **66**, 763 (1994). 77, 136
- [84] P. W. Leung and R. J. Gooding, *Phys. Rev. B* **52**, R15711 (1995). 77
- [85] M. Brunner, F. F. Assaad, and A. Muramatsu, *Phys. Rev. B* **62**, 15480 (2000). 77
- [86] A. S. Mishchenko, N. V. Prokof'ev, and B. V. Svistunov, *Phys. Rev. B* **64**, 033101 (2001). 77
- [87] G. D. Mahan, *Many-Particle Physics*, 3rd ed. (Kluwer Academic/Plenum Publishers, New York, 2000), p. 218. 77
- [88] V. Perebeinos and P. B. Allen, *Phys. Rev. Lett.* **85**, 5178 (2000). 77
- [89] A. S. Mishchenko and N. Nagaosa, *Phys. Rev. Lett.* **93**, 036402 (2004). 77, 81, 86, 93, 94, 97, 153, 154, 155
- [90] R. A. Cowley, W. Cochran, B. N. Brockhouse, and A. D. B. Woods, *Phys. Rev.* **131**, 1030 (1963). 79
- [91] P. P. Ewald, *Ann. Phys.* **64**, 253 (1921). 81
- [92] J. M. Ziman, *Principles of the theory of solids* (Cambridge University Press, Cambridge, 1965), p. 37. 81
- [93] X. J. Zhou, J. Shi, T. Yoshida, T. Cuk, W. L. Yang, V. Brouet, J. Nakamura, N. Mannella, S. Komiyama, Y. Ando, F. Zhou, W. X. Ti, J. W. Xiong, Z. X. Zhao, T. Sasagawa, T. Kakeshita, H. Esaki, S. Uchida, A. Fujimori, Z. Zhang, E. W. Plummer, R. B. Laughlin, Z. Hussain, and Z.-X. Shen, *Phys. Rev. Lett.* **95**, 117001 (2005). 83, 111

-
- [94] A. Bianconi, N. L. Saini, A. Lanzara, M. Missori, T. Rossetti, H. Oyanagi, H. Yamaguchi, K. Oka, and T. Ito, Phys. Rev. Lett. **76**, 3412 (1996). 83
- [95] E. S. Bozin, G. H. Kwei, H. Takagi, and S. J. L. Billinge, Phys. Rev. Lett. **84**, 5856 (2000). 83
- [96] L. Tassini, F. Venturini, Q.-M. Zhang, R. Hackl, N. Kikugawa, and T. Fujita, Phys. Rev. Lett. **95**, 117002 (2005). 83
- [97] M. Born and K. Huang, *Dynamical Theory of Crystal Lattices* (Oxford University Press, London, 1954). 84
- [98] K. Schönhammer and O. Gunnarsson, Phys. Rev. B **30**, 3141 (1984). 85, 145, 146
- [99] W. Nolting, *Grundkurs Theoretische Physik 5. Quantenmechanik (Teil 1)*, 4th ed. (Vieweg, Braunschweig, 1997). 88, 89
- [100] G. E. P. Box and M. E. Muller, Ann. Math. Stat. **29**, 610 (1958). 89
- [101] N. Metropolis, A. Rosenbluth, M. Rosenbluth, A. Teller, and E. Teller, J. Chem. Phys. **21**, 1087 (1953). 90
- [102] H. Röder, H. Fehske, and H. Büttner, Phys. Rev. B **47**, 12420 (1993). 91
- [103] T. Yoshida, X. J. Zhou, T. Sasagawa, W. L. Yang, P. V. Bogdanov, A. Lanzara, Z. Hussain, T. Mizokawa, A. Fujimori, H. Eisaki, Z.-X. Shen, T. Kakeshita, and S. Uchida, Phys. Rev. Lett. **91**, 027001 (2003). 96
- [104] J. Zhong and S. H.-B., Phys. Rev. Lett. **69**, 1600 (1992). 97
- [105] H. Fehske, H. Röder, G. Wellein, and A. Mitrionis, Phys. Rev. B **51**, 16582 (1995). 97
- [106] A. Ramsak, P. Horsch, and P. Fulde, Phys. Rev. B **46**, 14305 (1992). 97, 115
- [107] L. F. Mattheiss, Phys. Rev. Lett. **58**, 1028 (1987). 97, 99
- [108] P. B. Allen, Phys. Rev. B **6**, 2577 (1972). 99, 110
- [109] P. B. Allen, Solid State Commun. **14**, 937 (1974). 99, 110
- [110] M. L. Kulić and R. Zeyher, Phys. Rev. B **49**, 4395 (1994). 100

-
- [111] W. Nolting, *Grundkurs Theoretische Physik 7. Viel-Teilchen-Theorie*, 5th ed. (Springer, Berlin, 2002). 109, 157
- [112] A. Auerbach, *Interacting electrons and quantum magnetism* (Springer, Berlin, 1994). 114
- [113] Z. B. Huang, W. Hanke, E. Arrigoni, and D. J. Scalapino, Phys. Rev. B **68**, 220507 (2003). 115, 120
- [114] E. Koch and R. Zeyher, Phys. Rev. B **70**, 094510 (2004). 115
- [115] H. Haken and H. C. Wolf, *Molekülphysik und Quantenchemie*, 3rd ed. (Springer, Berlin, 1998), p. 340. 140
- [116] I. G. Lang and Y. A. Firsov, Zh. Eksp. Teor. Fiz. **43**, 1843 (1962), [Sov. Phys. JETP **16**, 1301 (1963)]. 141
- [117] J. Ranninger and U. Thibblin, Phys. Rev. B **45**, 7730 (1992). 143
- [118] B. Bäuml, G. Wellein, and H. Fehske, Phys. Rev. B **58**, 3663 (1998). 153

List of publications

Parts of the work presented in this thesis have been published in the following articles:

1. O. Rösch and O. Gunnarsson
Electron-Phonon Interaction in the t - J Model
Phys. Rev. Lett. **92**, 146403 (2004).
2. O. Rösch and O. Gunnarsson
Apparent Electron-Phonon Interaction in Strongly Correlated Systems
Phys. Rev. Lett. **93**, 237001 (2004).
3. O. Rösch and O. Gunnarsson
Electron-phonon interaction in the three-band model
Phys. Rev. B **70**, 224518 (2004).
4. O. Rösch, J. E. Han, O. Gunnarsson, and V. Crespi
Interplay between electron-phonon and electron-electron interactions
phys. stat. sol. (b) **242**, 118 (2005).
5. O. Rösch and O. Gunnarsson
Dispersion of incoherent spectral features in systems with strong electron-phonon coupling
Eur. Phys. J. B **43**, 11 (2005).
6. O. Rösch, O. Gunnarsson, X. J. Zhou, T. Yoshida, T. Sasagawa, A. Fujimori, Z. Hussain, Z.-X. Shen, and S. Uchida
Polaronic behavior of undoped high- T_c cuprate superconductors from angle-resolved photoemission spectra
Phys. Rev. Lett. **95**, 227002 (2005).

7. O. Gunnarsson and O. Rösch,
Polaronic behaviour and electron-phonon interaction in cuprates
J. Phys.: Condens. Matter (in preparation).
8. O. Rösch and O. Gunnarsson,
Effects of vertex corrections on electron-phonon interactions
(in preparation).

Curriculum vitae

Name	Oliver Rösch
Nationality	German
Date of birth	August 6 th , 1976
Place of birth	Bietigheim-Bissingen
Marital status	Married, one child
09/1983 - 07/1987	Primary school: Grundschule in Gemmrigheim
08/1987 - 06/1996	Secondary school: Gymnasium in Besigheim
06/1996	Abitur
08/1996 - 08/1997	Civilian service at the sheltered workshop in Bietigheim-Bissingen
09/1997 - 09/1999	Physics studies at the University of Stuttgart
10/1999 - 07/2000	Physics studies at the University of Würzburg
08/2000 - 05/2001	Physics studies at the University of Stony Brook, NY, USA
05/2001	Master of Arts
06/2001 - 10/2002	Physics studies at the University of Würzburg
10/2002	Diplom (with distinction) <i>SNS contacts in electric fields</i> with Prof. Dr. Reiner Kümmel
11/2002 - 12/2005	PhD at the Max Planck Institute for Solid State Research, Stuttgart as member of the International Max Planck Research School for Advanced Materials <i>Electron-phonon interaction in strongly correlated materials</i> with Prof. Dr. Ole Krogh Andersen and Dr. Olle Gunnarsson

Acknowledgements

I would like to thank all who supported me during my PhD time in Stuttgart. Especially, I want to express my gratitude to

- Dr. Olle Gunnarsson for directing me to many interesting problems and supervising me with great care. He was always available to me for advice and valuable discussions. Working with him was both a scientific and a personal enrichment.
- Prof. Dr. Ole Krogh Andersen for giving me the opportunity to work on my PhD thesis in his department. He supported me in every respect and enabled me to travel to conferences and cooperating scientists abroad from which I profited a lot.
- Prof. Dr. Alejandro Muramatsu for undertaking the task of being coreferee.
- Prof. Dr. Jong Han for introducing me to DMFT and his kind hospitality during my one-week stay at Pennsylvania State University.
- Prof. Dr. Zhi-Xun Shen and his group for many interesting discussions during my month-long visit to Stanford University and the ongoing cooperation.
- all members of the Andersen department for the nice atmosphere and the countless conversations over coffee and Danish cookies. Special thanks to our always supportive secretary Claudia Hagemann.
- Dr. Giorgio Sangiovanni for carefully proof-reading the manuscript.
- the computer service group for providing a reliable infrastructure.
- my fellow students in the IMPRS-AM for stimulating insights into other fields. Many thanks to our coordinator Dr. Hans-Georg Libuda for his assistance.
- my wife Sabine for all her support and backing.